VOLUME 81 DECEMBER 29, 1977 NUMBER 26

JPCHAx

# THE JOURNAL OF PHYSICAL CHEMISTRY

PUBLISHED BIWEEKLY BY THE AMERICAN CHEMICAL SOCIETY

THE JOURNAL OF

# PHYSICAL CHEMISTRY



*Published by the*
**AMERICAN CHEMICAL SOCIETY**
**BOOKS AND JOURNALS DIVISION**

D. H. Michael Bowen, Director

Marjorie Laflin, Assistant to the Director

Editorial Department: Charles R. Bertsch, Head; Marianne C. Brogan, Associate Head; Joseph E. Yurvati, Assistant Editor

Magazine and Production Department: Bacil Guiley, Head

Research and Development Department: Seldon W. Terrant, Head

Advertising Office: Centcom, Ltd., 25 Sylvan Road South, Westport, Conn. 06880.



Published biweekly by the American Chemical Society at 20th and Northampton Sts., Easton, Pennsylvania 18042. Second class postage paid at Washington, D.C. and at additional mailing offices.

### Editorial Information

**Instructions for authors** are printed in the first issue of each volume. Please conform to these instructions when submitting manuscripts.

**Manuscripts for publication** should be submitted to *The Journal of Physical Chemistry*, Department of Chemistry, University of Minnesota, Minneapolis, Minn. 55455. Correspondence regarding **accepted papers and proofs** should be directed to the Editorial Department at the address below.

**Page charges** of $60.00 per page may be paid for papers published in this journal. Payment does not affect acceptance or scheduling of papers.

**Bulk reprints or photocopies** of individual articles are available. For information write to Business Operations, Books and Journals Division at the ACS Washington address.

Requests for **permission to reprint** should be directed to Permissions, Books and Journals Division at the ACS Washington address. The American Chemical Society and its Editors assume no responsibility for the statements and opinions advanced by contributors.

### Subscription and Business Information

1977 Subscription rates—including surface postage

| | U.S. | PUAS | Canada, Foreign |
|---|---|---|---|
| Member | $24.00 | $33.00 | $34.00 |
| Nonmember | 96.00 | 105.00 | 106.00 |
| Supplementary material | 15.00 | 19.00 | 20.00 |

**Air mail and air freight** rates are available from Membership & Subscription Services, at the address below.

**New and renewal subscriptions** should be sent with payment to the Office of the Controller at the ACS Washington address. **Changes of address** must include both old and new addresses with ZIP code and a recent mailing label. Send all address changes to Membership & Subscription Services. Please allow six weeks for change to become effective. **Claims for missing numbers** will not be allowed if loss was due to failure of notice of change of address to be received in the time specified: if claim is dated (a) North America—more than 90 days beyond issue date, (b) all other foreign—more than 1 year beyond issue date; or if the reason given is "missing from files". Hard copy claims are handled by Membership & Subscription Services.

**Microfiche subscriptions** are available at the same rates but are mailed first class to U.S. subscribers, air mail to the rest of the world. Direct all inquiries to Special Issues Sales, at the ACS Washington address or call (202) 872-4554. **Single issues** in hard copy and/or microfiche are available from Special Issues Sales at the ACS Washington address. Current year $4.75. Back issue rates available from Special Issues Sales. **Back volumes** are available in hard copy and/or microform. Write to Special Issues Sales at the ACS Washington address for further information. **Microfilm** editions of ACS periodical publications are available from volume 1 to the present. For further information, contact Special Issues Sales at the ACS Washington address. **Supplementary material** mentioned in the journal appears in the microfilm edition. Single copies may be ordered directly from Business Operations, Books and Journals Division, at the ACS Washington address.

| | U.S. | PUAS, Canada | Other Foreign |
|---|---|---|---|
| Microfiche | $2.50 | $3.00 | $3.50 |
| Photocopy | | | |
| 1–7 pages | 4.00 | 5.50 | 7.00 |
| 8–20 pages | 5.00 | 6.50 | 8.00 |

Orders over 20 pages are available only on microfiche, 4 × 6 in., 24X, negative, silver halide. Orders must state photocopy or microfiche if both are available. Full bibliographic citation including names of all authors and prepayment are required. Prices are subject to change.

American Chemical Society
1155 16th Street, N.W.
Washington, D.C. 20036
(202) 872-4600

Editorial Department
American Chemical Society
P.O. Box 3330
Columbus, Ohio 43210
(614) 421-6940 ext 3171

Membership & Subscription Services
American Chemical Society
P.O. Box 3337
Columbus, Ohio 43210
(614) 421-7230

**Notice to Authors last printed in the issue of January 13, 1977**

THE JOURNAL OF

# PHYSICAL CHEMISTRY

*Volume 81, Number 26 December 29, 1977*

JPCHAx 81(26) 2587–2712 (1977)

ISSN 0022-3654

## COMMUNICATIONS TO THE EDITOR



■ Supplementary and/or miniprint material for this paper is available separately (consult the masthead page for ordering information); it will also appear following the paper in the microfilm edition of this journal.

* In papers with more than one author, the asterisk indicates the name of the author to whom inquiries about the paper should be addressed.

## AUTHOR INDEX



## PUBLISHER'S NOTE

To conform to provisions of U.S. copyright law effective January 1, 1978, the American Chemical Society is instituting new procedures.

Contributors and readers will notice two changes:

(1) Authors will be required to transfer copyright to ACS by means of a simple form. The relationship between the Society and the author will remain unchanged, however, since under prior copyright law ACS has in fact been the copyright owner of individual articles.

(2) Issues published after January 1, 1978 will have a multiple-digit code at the foot of the first page of most articles. This code signifies ACS participation in the not-for-profit Copyright Clearance Center. Operation of the Center will permit libraries and other institutions to reproduce legally and without delay journal articles beyond "fair use" as described in the new law and accompanying guidelines.

Questions on the new copyright law or ACS procedures may be addressed to the Office of the Director, Books and Journals Division, American Chemical Society, 1155 16th Street, N.W., Washington, D.C. 20036. Or call (202) 872-4556 or 872-4367.

# THE JOURNAL OF

# PHYSICAL CHEMISTRY

*Volume 81*

JANUARY—JUNE 1977

PAGES 1–1342

JPCHAx 81(1–13) 1–1342 (1977)
ISSN 0022-3654

# THE JOURNAL OF PHYSICAL CHEMISTRY

*Volume 81*

JULY—DECEMBER 1977

PAGES 1343–2712

JPCHAx 81(14–26) 1343–2712 (1977)
ISSN 0022-3654

THE JOURNAL OF
PHYSICAL CHEMISTRY



VOLUME 81, NUMBER 26 DECEMBER 29, 1977

# Some Models and Calculations for the Laser Induced Decomposition of Fluorochloromethanes†

I. Oref‡ and B. S. Rabinovitch*

Department of Chemistry, University of Washington, Seattle, Washington 98195 (Received August 8, 1977)

Models for infrared laser-enhanced unimolecular decompositions are considered. Quantitative calculations are carried out for some of these models. Comparison is made with existing experimental data on the decomposition of chlorofluoromethanes. It is emphasized that some recent results and theories concerning intra- and intermolecular energy relaxation, which are valid for lower energy infrared laser excited molecule behavior, may not be transferred to the higher energy regime corresponding to reacting molecules.

## Introduction

In recent years infrared laser-induced enhancement of unimolecular chemical reactions has been reported and discussed by a number of authors.[1-7] Because of the importance of this method in effecting chemical reactions and isotope separations, a variety of theoretical models have been proposed to explain the experimental results.[2,6,7] This is understandable in view of the variability of experimental systems. Moreover, in spite of its apparent simplicity, careful and reliable results are hard to come by because of complicating side reactions and competing processes, as has been pointed out by Bauer and coworkers.[1] One model for unimolecular decomposition was given by Ambartzumian and Letokhov[2] for $SF_6$ and stipulates a single molecule multiphoton excitation into vibrationally discrete and continuous manifolds, which is due to the high density of molecular vibrational states above the $v = 3$ level of the S–F stretch.

A different model for the laser-induced unimolecular decomposition was proposed by Grunwald and co-workers[7] based on their experimental results on fluorochloromethanes. These results and conclusions are of importance for the understanding of the mechanisms of vibrational energy relaxation and have stimulated considerable interest.[6,8] In this paper we have undertaken a quantitative examination of their proposals. Grunwald and co-workers studied the infrared laser-induced unimolecular decompositions of $CCl_3F$ and $CClF_3$ at ~60 Torr[7a] and of $CHClF_2$ at various pressures.[7b] Dever and Grunwald[7a] (DG) plotted their results as logarithm of percent conversion per flash (CPF) vs. the inverse of the energy absorbed per molecule, $E_{abs}$, and obtained quasi-straight lines of form:

$$\ln \mathrm{CPF} = A - E_a/E_{abs}$$

$E_a$ appeared to be the same within experimental limits as the high pressure activation energy for the thermal decomposition of the reactants.[7] The experiments on $CHClF_2$[7b] were performed at various initial pressures of parent and inert gas. It was found for the neat reaction that ln CPF is also a linear function of $E_{abs}^{-1}$ and is independent of pressure. This behavior was interpreted[7] by DG on the basis of the following assumptions: Intermolecular energy transfer processes in the single absorbing mode (V → V) is faster than either V → T,R or intermode vibrational energy transfer (V → V′), so that a Boltzmann distribution is established in the absorbing mode (symmetric C–F stretch at 1100 $cm^{-1}$). No significant degree of intramolecular redistribution of absorbed energy among the vibrational modes of the molecule occurs during the laser pulse. Decomposition begins only after the light field is switched off. The agreement of $E_{act}$ with thermal values was interpreted as a crucial corroboration of their assumptions.

† Work supported by the National Science Foundation.

‡ On sabbatical leave from the Department of Chemistry, Technion, Haifa, Israel. The support of the U.S.–Israel Binational Fund is acknowledged.

In the following we have reexamined these results and the assumptions and conclusions based on this model. A quantitative comparison is given between the actual magnitudes of the experimental values of CPF[7] and calculated values found from several models for the processes that follow the light absorption. Some general predictions of the dependence of the experimental results on intra- and intramolecular energy transfer are made for the models employed.

## Reaction Models

Several models[7] for the distribution function of the excited molecules are assumed, corresponding to current thinking (none correspond to our view of the behavior described in ref 7). An expression for either CPF or the unimolecular rate coefficient, $k$, is then derived and compared with experiment.

A. *Single Oscillator Model (SO).* In the SO model the following assumptions[7] are adopted in order to examine their consequences (and not because they are physically realistic). During the irradiation pulse of duration ~0.1 μs, no reaction takes place; there is no V → T intermolecular energy transfer and no intramolecular energy transfer; and only efficient V–V collisional transfer occurs so that a Boltzmann population distribution is established in the single *absorbing* mode (by contrast, V → T relaxation *is* known to be very efficient at high vibrational levels of reacting polyatomic molecules in the presence of a cold bath gas).[9]

In those cases where the absorbing mode is not an important contributor to the reaction coordinate for unimolecular decomposition, it is evident that extensive internal redistribution of energy *must* precede reaction. For purposes of this model, we assume that only *after* irradiation does very fast intramolecular energy relaxation into all $n$ modes of the molecule occur. (By contrast, this relaxation *has* been shown to be operative on a much shorter time scale in unimolecular reaction systems.[10]) Unimolecular decomposition of the internally randomized excited species must take place in competition with collisional deactivation. A statistical model (RRKM) is applied to the calculation of the specific rate of decomposition at each energy.

Of the models discussed here, SO corresponds the most closely to the preferred interpretation in ref 7.

The process is written in a generalized form

$$A \xrightarrow{I} A_1^* \quad \text{(Ia)}$$

$$A_1^* \xrightarrow{\omega'} A_1^{**} \quad \text{(Ib)}$$

$$A_1^{**} \xrightarrow{\lambda} A_n^* \quad \text{(II)}$$

$$A_n^* \xrightarrow{\beta\omega} A \quad \text{(III)}$$

$$A_n^* \xrightarrow{k(E')} D \quad \text{(IV)}$$

$I$ is the exciting function; $A_i^*$ signifies excitation in $i$ internal modes; $A_1^{**}$ signifies the collision-induced (specific rate $\omega'$) Boltzmann populations of the absorbing mode levels; $\lambda$, $\omega$, and $\beta$ represent the specific rate of intramolecular relaxation, collisional frequency, and relative deactivation efficiency, respectively; $k(E')$ is the RRKM energy-dependent unimolecular rate coefficient whose value is zero for $E' < E_0$, the threshold energy; $E' = E + \langle E_{th} \rangle$, where $E$ is the energy provided by the excitation function and $\langle E_{th} \rangle$ is the average thermal energy at the initial ambient temperature at which reaction is initiated. The material conservation equation is

$$[A]_0 = \sum_{E=0}^{\infty} [A^*(E)]_0$$

where the subscript zero denotes initial concentrations before reaction. The distribution function for excited molecules is

$$[A_1^*(E)]_0\, dE_1 = [A]_0 e^{-E_1/E_{abs}}\, d(E_1/E_{abs}) \quad (1)$$

where all laser energy is allegedly distributed in one mode only, by reactions Ia and Ib, and relaxation into $n$ modes, by process II, occurs only after the laser pulse is over. The rate equations for the decay of $A_n^*(E)$ and appearance of decomposition product $D(E)$ are

$$d[A_n^*(E)]/dt = -(\beta\omega + k(E'))[A_n^*(E)] \quad (2)$$

$$d[D(E)]/dt = k(E')[A_n^*(E)] \quad (3)$$

Equation 2 was integrated between $t = 0$ and $\infty$ (in the experimental systems of interest here, there was enough time for the system to relax between pulses), and the results substituted in eq 3, which is then integrated between $t = 0$ and $\infty$ and between the threshold energy for decomposition, $E_0$, and the maximum energy which can be placed in the symmetric C–F stretch without breaking the bond, $E_{diss}$. The final expression obtained is

$$\frac{CPF}{100} = \frac{[D]}{[A]_0} = \int_{E_0}^{E_{diss}} \frac{k(E')}{\beta\omega + k(E')} e^{-E/E_{abs}}\, d(E/E_{abs}) \quad (4)$$

where subscripts on $E$ have been omitted; $k(E')$ is defined as[9]

$$k(E') = \sum_{E_{vr}^+=0}^{E^+} P(E_{vr}^+)/F_w h N^*(E') \quad (5)$$

where $N^*(E')$ is the density of vibrational states of A at $E'$; $\sum P(E^+)$ is the number of states of A with energy up to $E^+$; $E^+ = E' - E_0$; $F_W$ is a centrifugal constant; $h$ is Planck's constant.

B. *The "Plasma" Model (PM).* The basic assumption of this model is that laser energy is not confined to the C–F, absorbing mode and/or that the V → V transfer is not specific to the absorbing mode so that a Boltzmann distribution of vibrationally hot, but translationally-rotationally cold molecules is produced. This model is somewhat reminiscent of one which has been given by Breshears and Blair[11] and by Shamah and Flynn[8] at lower energies, in which efficient V → V′ energy transfer is allowed but in which a *set* of Boltzmann distributions governs the ensemble of oscillators. As discussed in section A, it does not correspond to the known experimental evidence dealing with intra- and intermolecular vibrational energy transfer, for the highly excited end of the energy spectrum corresponding to reacting polyatomics.[9,10]

The distribution function is

$$[A_n^*(E_n)]_0\, dE_n = Q_v^{-1} N(E_n) e^{-E_n/RT_{vib}}\, dE_n \quad (6)$$

$Q_v^{-1}$ is a normalizing constant and $N(E_n)$ is the density of internal states.

The expression for CPF is

$$\frac{CPF}{100} = \frac{[D]}{[A]_0} = \frac{Q_v^{-1}}{[A]_0} \int_{E_0}^{E_{diss}} \frac{N(E')k(E')}{\beta\omega + k(E')} e^{-E'/RT_{vib}}\, dE' \quad (7)$$

The vibrational temperature of the molecules was found by iterating $T_{vib}$ in eq 8, in such a way that $\langle E' \rangle = E_{abs} +$

$$\langle E' \rangle = RT_{vib} \sum_i^n \frac{x_i}{\exp x_i - 1}; \quad x_i = h\nu_i/kT_{vib} \quad (8)$$

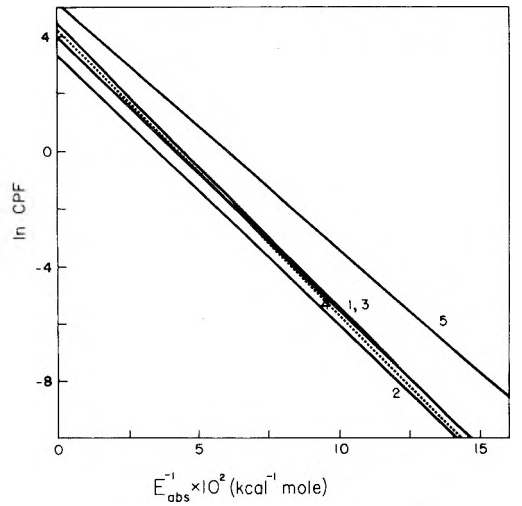


**Figure 1.** Some illustrative plots of ln CPF vs. $E_{abs}^{-1}$ for $CF_3Cl$: SO model, $\beta = 1$, $P = 60$ Torr. All values in kcal mol$^{-1}$: (1) $E_0 = 83.7$, $E_{diss} = 125$, $E_{a(calcd)} = 95.4$; (2) $E_0 = 85.8$, $E_{diss} = 125$, $E_a$(calcd) = 93.3; (3) $E_0 = 83.7$, $E_{diss} = \infty$, $E_a$(calcd) 97.3; (4) $E_0 = 85.8$, $E_{diss} = \infty$, $E_{a(calcd)} = 101.2$; (5) $E_a$(expt)[7a] = 85.8.

$\langle E_{th} \rangle$; $\langle E_{th} \rangle$ is the average thermal energy of A; the integral is over $E'$ because a distribution is established over all available vibrational energy; and the subscript $n$ has been dropped.

C. *Thermal Model (TM).* In this model, which has been widely used,[7,12] all modes of energy exchange are allowed and the system attains thermal equilibrium consistent with the total energy input. In principle, a distribution function analogous to eq 6 applies but with $T_{vib}$ replaced by $T_{th}$, the new temperature, and $E_n$ is the internal thermal energy of the molecules. In practise, consideration of this model is more involved than for a simple thermal system.

The system is not in an equilibrium state nor is it in a steady state; rather, a spatial-temporal temperature profile is established[7b] throughout the cell *beginning with the onset of irradiation.* An exact calculation of CPF calls for the integration of the nonequilibrium expression

$$-d[A]/dt = (-1)^{\alpha} \sum_j \prod_k \nu_j C_{kj} A_j T^{n_j} \exp(-E_{aj}/RT) \quad (9)$$

where A is the reactant species; $\alpha = 0$ for the disappearance of A and $\alpha = 1$ for its appearance; $\nu_j$ is the stochiometric coefficient, $A_j$ the preexponential coefficient; $n_j$ the temperature dependence, and $E_{aj}$ the activation energy, all for reaction $j$; $C_{kj}$ is species $k$ taking part in reaction $j$. The use of eq 9 is evidently subject to great difficulty. In addition to the fact that $T = f(t)$, the exact solution of eq 9 requires a knowledge of the dependence of $E_{aj}$ on temperature since $E_{aj} = g_j(T)$ if reaction $j$ is unimolecular and is not in the high pressure region.

## Results and Discussion

In the following we apply the three models which were presented above to the results reported by Grunwald and co-workers.[7] The results of the calculations based on the SO model are reported for all three compounds, $CF_3Cl$, $CFCl_3$, and $CHClF_2$, and sample calculations are reported for the other two models.

*SO Model.* Assuming that only the primary processes of C–Cl rupture for $CF_3Cl$, $Cl_2$ split-off for $CCl_3F$, and HCl elimination for $CHClF_2$ are important (no chain or back reactions), then eq 4 gives the value for CPF. Values were calculated for several choices of $E_{diss}$; those for an integration limit nominally equal to $D$(C–F) ~ 124 kcal mol$^{-1}$

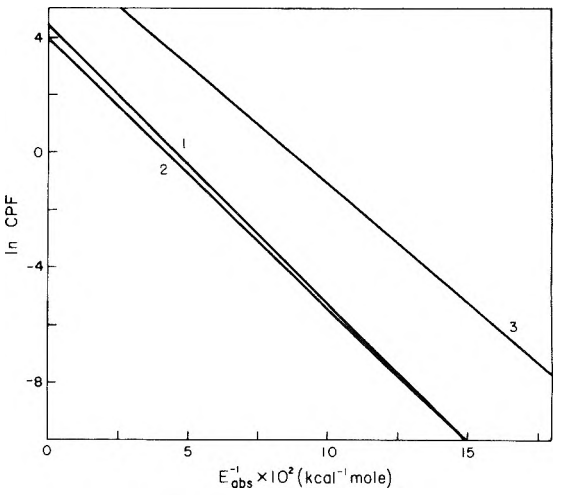


**Figure 2.** ln CPF vs. $E_{abs}^{-1}$ for $CFCl_3$: SO model, $\beta = 1$, $P = 60$ Torr. All values in kcal mol$^{-1}$: (1) $E_0 = 80.1$, $E_{diss} = \infty$, $E_a$(calcd) = 96; (2) $E_0 = 80.1$, $E_{diss} = 125$, $E_a$(calcd) = 92.9; (3) $E_a$(expt)[7a] = 81.

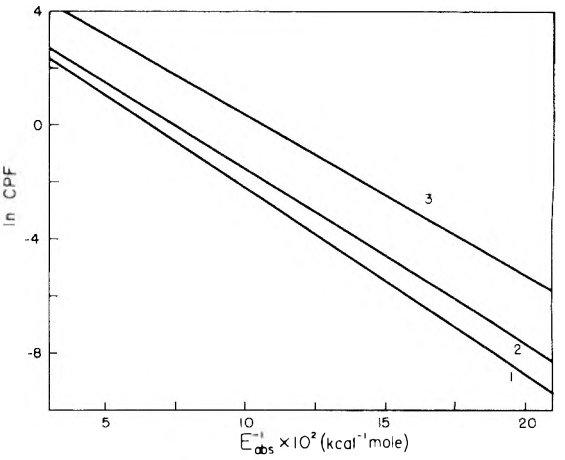


**Figure 3.** ln CPF vs. $E_{abs}^{-1}$ for $CHClF_2$: SO model, $P = 100$ Torr. Values in kcal mol$^{-1}$: (1) $E_0 = 55.5$, $E_{diss} = \infty$, $E_a$(calcd) = 65, $\beta = 1$; (2) $E_0 = 55.5$, $E_{diss} = \infty$, $E_a$(calcd) = 60, $\beta = 0.1$; (3) $E_a$(expt)[7b] = 56.

(as given in ref 7a) are the lowest, while an infinity limit is the most favorable value for attempting to reconcile the data with the model. The value $\beta = 0.5$–1 is the best estimate[9] of the correct magnitude for this system in which the translational and rotational degrees of freedom of the bath gas are at room temperature and the excited polyatomic molecules exceed 60 kcal mol$^{-1}$ in energy.

Figures 1–3 show illustrative calculations of ln CPF vs. $E_{abs}^{-1}$ (i.e., $(RT_{SO})^{-1}$) for a range of parameters. Agreement between the magnitudes of experimental and calculated values of CPF is not obtained in general. The least disagreement is found for $CClF_3$: for $\beta = 1$, and $E_{diss} = \infty$, the mean discrepancy in CPF is a factor of ~5.5; for $E_{diss}$ lowered to 125 kcal mol$^{-1}$, the factor increases to ~7.5, while for the low estimate $\beta = 0.1$, together with $E_{diss} = \infty$, the factor is ~3.5 (not shown). The greatest disagreement is found for $CCl_3F$; for $\beta = 1$ and $E_{diss} = \infty$, the mean discrepancy in CPF is a factor of ~30, increasing to ~40 for $E_{diss} = 125$ kcal.

The apparent "activation energies" found from the calculated plots in Figures 1–3 for $CF_3Cl$, $CCl_3F$, and $CHClF_2$ decomposition are, respectively, ~100, 96, and 65 kcal mol$^{-1}$, whereas $E_0$ is[7] ~86, ~81, and ~56 kcal mol$^{-1}$. However, there is no reason to expect these quantities to be coincident as proposed by DG (quite apart from any failings of the model or of the chemical mechanism discussed later). This is for the reason that the high pressure

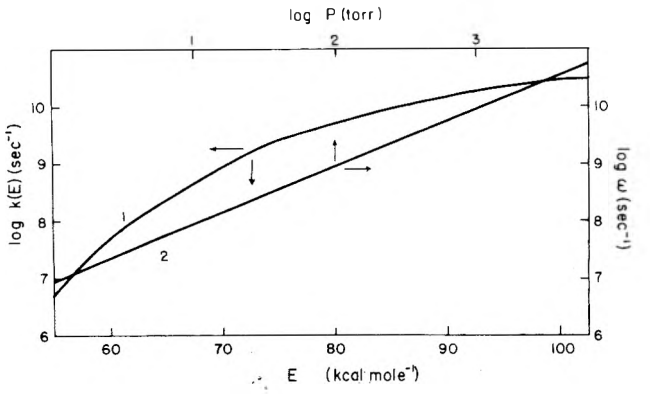


**Figure 4.** (1) log $k(E)$ vs. $E$, left and bottom coordinates for $CHClF_2$; also (2) log $P$ vs. log $\omega$, right and top coordinates.

thermal activation energy is defined with respect to the following expression

$$k_\infty = \int_{E_0}^{\infty} k(E)B(E)\,dE$$

where $B(E)$ is the Boltzmann distribution. This is not the same as the experimental form of the results; nor may CPF and $k_\infty$ be treated as equivalent.

The independence of CPF on pressure (over the range 1.6–100 Torr) which was found experimentally in the laser photodecomposition of neat $CHClF_2$, is not predicted by the SO model in which it is postulated that, *following the laser flash*, there may be competition between decomposition and deactivating collisions. Since the calculated values of $k(E)$, at energies upward of $E_0(CHClF_2) = 56$ kcal mol$^{-1}$, are $\lesssim\beta\omega$ over a significant range of the critically excited populations, collisional deactivation should play an important role. This is clearly seen from Figure 4 for the given experimental values of $P$ and $E$. Pressure independence was explained in ref 7b on the basis of the assumption that V-T,R (and, implicitly required, also, V-V') transitions, after the laser pulse is over, are inefficient, i.e., $\beta$ is very small. Since the bath gas is at room temperature, this assumption is contrary to available evidence for the efficiency of collisional deactivation of highly vibrationally excited polyatomics by a substrate bath gas.[9]

It may be noted that inclusion of back reaction in this model would lower the calculated values and increase the discrepancy.

*Plasma Model.* The calculational results for $CF_3Cl$ laser decomposition[7a] are given in Figure 5; there is no agreement with experiment. The slope of the calculated ln CPF vs. $T_{vib}^{-1}$ does indeed give back 84 kcal mol$^{-1}$ as compared with the assigned value 86 kcal mol$^{-1}$. In this case, the plot of the experimental results vs. $T_{vib}^{-1}$ has slope of ~30 kcal mol$^{-1}$. This illustrates the lack of fundamental criterion provided by the slope of such lines alone.

All other models in which $n$ is intermediate between the values used in the SO($n$ = 1) and PM models are expected to give intermediate results. Use of the model of intramolecular energy redistribution preferred by Shamah and Flynn,[8] and involving subsets of internal vibrational temperatures, would be expected to give results qualitatively or semiquantitatively similar to those calculated from the PM model on the basis of a single internal temperature.

*Thermal Model.* In this model all modes of energy exchange are allowed. However, a knowledge is required of the time evolution of the spatial temperature profile as affected by the various modes of cooling.[7b] An equilibrium temperature is not expected to be established in these

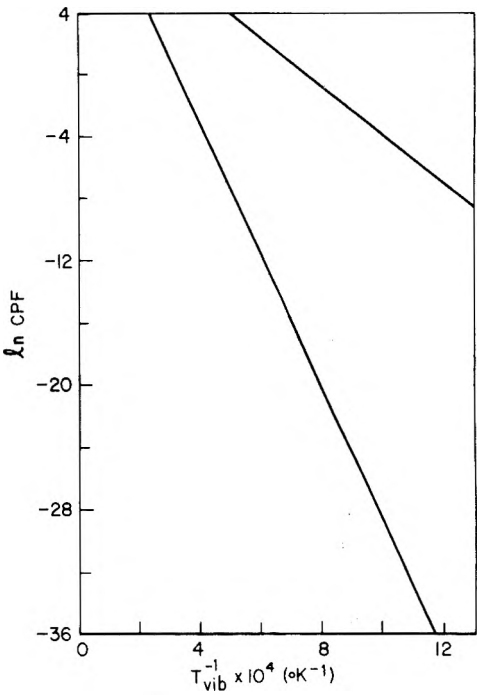


**Figure 5.** ln CPF vs. $T_{vib}^{-1}$ for $CF_3Cl$, PM model. $E_0$ = 86 kcal mol$^{-1}$: (1) $E_{a(calcd)}$ = 84.8 kcal mol$^{-1}$; (2) $E_a(expt)$[7a] = 30 kcal mol$^{-1}$.

systems. CPF is found by integrating d[A]/[A] = $-k$ d$t$. $k$ should be calculated with consideration of the fact that at high temperatures the reaction order, at a given pressure, is greater than unity. Hence, a high pressure activation energy and frequency factor should not be used, in principle.

Since the temperature profile is not known, as a practical expedient equilibrium temperatures[13] were employed, as in ref 7a, and the high pressure limiting slope was calculated. A plot of calculated values of ln $k_\infty$ vs. $T_{th}^{-1}$ for $CFCl_3$ (not presented) gives a slope of 90 kcal mol$^{-1}$. Thus, the thermal model gives almost the "right" slope for $k_\infty$. A plot of the experimental quantities ln CPF vs. $T_{th}^{-1}$ is reported[7a] to have a slope of 22 kcal mol$^{-1}$. For a thermal system $k_\infty$ is the fundamental rate quantity, and not CPF. The former has the well-known relationship to $T_{th}^{-1}$.

## Comments on the $CF_3Cl$ Chemical System

The following reaction scheme was given[7a] for the decomposition of $CF_3Cl$:

$$CClF_3^* \rightarrow CF_3 + Cl \quad (R1)$$

$$CClF_3^* \rightarrow CClF_2 + F \quad (R2)$$

$$CClF_3^* \rightarrow CF_2 + FCl \quad (R3)$$

$$CF_3 + CClF_3 \rightarrow CF_4 + CClF_2 \quad (R4)$$

$$CClF_2 + CClF_3 \rightarrow CCl_2F_2 + CF_3 \quad (R5)$$

$$2CF_3 + M \rightarrow C_2F_6 + M \quad (R6)$$

$$CF_3 + Cl + M \rightarrow CF_3Cl + M \quad (R7)$$

$$2Cl + M \rightarrow Cl_2 + M \quad (R8)$$

$$CClF_2 + CF_3 + M \rightarrow CF_3CClF_2 + M \quad (R9)$$

Reactions R2 and R3 were ruled out[7a] because of high activation energy. It can be seen that reactions R1, R4, and R5 all contribute to CPF inasmuch as $CClF_3$ disappears. Because an exact treatment of this system is impossible, we thought it of interest to see what a steady state treatment of the transient products of these reactions would predict for the temperature dependence of the product ratio $[CF_4]/[C_2F_6]$:

$$\frac{[CF_4]}{[C_2F_6]} = \frac{k_{R4}}{k_{R6}^{1/2}k_{R1}^{1/2}}[CF_3Cl]^{1/2}$$

which, with[7a] $E_4 = 20 \pm 10$ kcal/mol and $E_1 = 86 \pm 4$ kcal/mol, has the temperature dependence of $\exp(20/RT)$. This is opposite to what was found experimentally. It is of course true that this system does not follow steady state relations and this "discrepancy" is not presented as definite contradiction but only as a disquieting fact.

Clearly, the process involved here is more complicated than a single one-step decomposition and the above scheme does not account for all the behavior. There are only a few reactions in the literature which involve the $CF_3$ radical. In all cases reported where $CF_3$ was produced by photolysis of fluoroacetone,[14,15] fluoroazomethane,[15] and $CF_3I$[16] no $CF_4$ was detected and the main product was $C_2F_6$. Photolysis of pure $CF_3I$ yielded some $CF_4$ which was eliminated by admixture of inert gas.[17] Shock tube experiments on $CF_3I$ decomposition gave $CF_4$ as one of the products[18] emanating from the reaction $CF_3 + F + M \rightarrow CF_4$, the F coming from $CF_3 + M \rightarrow CF_2 + F + M$. The ratio $[CF_4]/[C_2F_6]$ showed the behavior encountered in the DG work. No F abstraction is reported for fluorochloroethane; only Cl is abstracted,[14] as in the example, $CF_2ClCFCl_2 + CF_3 \rightarrow CF_3Cl + R$. There is one case, however, for which F abstraction by $CF_3$ is reported.[19] This is the radiolysis of $CF_3I$ in the gas phase. No $C_2F_6$ was found in contrast to the other systems reported above; an explanation given by Sutcliffe[20] is that the $CF_3$ radical is produced in an excited electronic state.

Either of the two mechanisms for $CF_4$ production mentioned above call for a composite experimental value of $k$ different from that of the primary process, with consequent change in the observed activation energy.

## Conclusion

Calculations of the rate for the primary step of decomposition of $CClF_3$, $CCl_3F$, $CHClF_2$ do not agree with the values of CPF observed by DG, regardless of the model of population distribution prior to reaction. It is believed that the chemistry involved in their systems may be complicated so that no single quasi-equilibrium rate coefficient may represent the experimental results. Also, the assumptions made with regard to collisional deactivation inefficiency[9] and the rate of intramolecular energy relaxation[10] in the SO model contradict existing experimental evidence. We feel that the SO model is not supported by experiment and that further investigation is desirable. These data, we believe, do not provide a suitable basis for theoretical constructions.[6] Moreover, the assertions in the theory of ref 6b do not accord well with some aspects of experimental fact[9,10] at the high energies above reaction threshold.

*Acknowledgment.* We thank Professor E. Grunwald for communicating some unpublished results to us and thank Professor C. Steel for calling our attention to a "lost" constant in earlier calculations.

## Appendix. Molecular and Reaction Parameters

*$CF_3Cl$.* The vibration frequencies (in $cm^{-1}$) used are[21] 1210(2), 1102, 783, 560(2), 478, 356(2). The reaction coordinate was taken as the 783-$cm^{-1}$ C–Cl stretch, and the "loose" complex vibrations were changed, 560 → 400, 478 → 320 $cm^{-1}$, so as to obtain a frequency factor, log $A = 13.5$. Other parameters used are $\sigma = 5$ Å; $L^{\pm} = 1$; $\omega = 5.3 \times 10^8$ $s^{-1}$; $\beta = 1$.

*$CFCl_3$.* The vibration frequencies (in $cm^{-1}$) are[22] 1085, 846(2), 534, 400(2), 351, 245(2). The C–Cl stretch at 534 $cm^{-1}$ was taken as the reaction coordinate of the "tight" complex. Two configuration were tried for the complex but with no significant difference between them. The data which are discussed here are based on a complex where no changes were made in the molecular frequencies. The frequency factor which was obtained for this configuration is log $A = 13.6$. Additional parameters which were used are $\sigma = 5.5$ Å, $L^{\pm} = 3$. The value of $D(CCl_3\text{–}F)$ has been given as[12] 105 kcal $mol^{-1}$. The value of $D(CH_3\text{–}F) = 110$ kcal $mol^{-1}$ is given in the "Handbook of Chemistry and Physics", Vol. 46, Chemical Rubber Company, Cleveland, Ohio, 1965, p F127; $\omega = 5.3 \times 10^8$ $s^{-1}$; $\beta = 1$.

*$CHClF_2$.* The molecular frequencies (in $cm^{-1}$) are[23] 3025, 1311, 1178, 809, 595, 422, 1347, 1116, 365. The reaction coordinate was taken as the 365-$cm^{-1}$ bend and the "tight complex" vibrations were adjusted so as to obtain the appropriate frequency factor, log $A = 12.9$. The complex frequencies are (in $cm^{-1}$) 3025, 1500, 1178, 1116, 595, 500, 1600, 1000. Other parameters are $\sigma = 4.8$ Å, $L^{\pm} = 1$, $\omega = 9.0 \times 10^8$ $s^{-1}$, and $\beta = 1$.

## References and Notes

(1) (a) E. R. Lory and S. H. Bauer, *J. Phys. Chem.*, **79**, 545 (1975); (b) K.-R. Chien and S. H. Bauer, *ibid.*, **80**, 1405 (1976); (c) S. H. Bauer and K. R. Chien, *Chem. Phys. Lett.*, **45**, 529 (1977).
(2) (a) R. V. Ambartzumian and V. S. Letokhov, *Acc. Chem. Res.*, **10**, 61 (1977); (b) R. V. Ambartzumian, N. V. Chehalin, V. S. Letokhov, and E. A. Ryabov, *Chem. Phys. Lett.*, **36**, 301 (1975).
(3) F. V. Ambartzumian, N. V. Chekalin, V. S. Doljikov, V. S. Letokhov, and E. A. Ryabov, *Chem. Phys. Lett.*, **25**, 515 (1974).
(4) J. Stone, M. F. Goodman, and D. A. Dows, *Chem. Phys. Lett.*, **44**, 411 (1976).
(5) K. C. Kim and J. M. McAfee, *Chem. Phys. Lett.*, **45**, 235 (1977).
(6) (a) S. A. Rice and J. Jortner, quoted in ref 7b; (b) S. Mukamel and J. Ross, *J. Chem. Phys.*, **65**, 5235 (1977).
(7) (a) D. V. Dever and E. Grunwald, *J. Am. Chem. Soc.*, **98**, 5055 (1976); (b) E. Grunwald, K. J. Olszyna, D. F. Dever and B. Knishkowsky, private communication
(8) I. Shamah and G. Flynn, *J. Am. Chem. Soc.*, **99**, 3191 (1977).
(9) D. C. Tardy and B. S. Rabinovitch, *Chem. Rev.*, **77**, 369 (1977); G. H. Kohlmaier and B. S. Rabinovitch, *J. Chem. Phys.*, **38**, 1692, 1709 (1963).
(10) (a) L. D. Spicer and B. S. Rabinovitch, *Annu. Rev. Phys. Chem.*, **21**, 349 (1971); (b) J. D. Rynbrandt and B. S. Rabinovitch, *J. Phys. Chem.*, **75**, 2164 (1971); A. N. Ko, K. J. Chao, and B. S. Rabinovitch, *J. Chem. Phys.*, **66**, 1374 (1977).
(11) W. D. Breshears, *Chem. Phys. Lett.*, **20**, 429 (1973); W. D. Breshears and L. S. Blair, *J. Chem. Phys.*, **59**, 5824 (1973).
(12) W. M. Shaub and S. H. Bauer, *Int. J. Chem. Kinet.*, **7**, 509 (1975).
(13) Temperature calculated with use of JANAF tablets (*Natl. Stand. Ref. Data Ser., Natl. Bur. Stand.*, **No. 73** (1971)).
(14) L. M. Quick and E. Whittle, *J. Chem. Soc., Faraday Trans. 1*, **68**, 878 (1972).
(15) P. C. Kobrinsky and G. O. Pritchard, *J. Chem. Phys.*, **76**, 2196 (1972).
(16) J. N. Cape, A. C. Greig, J. M. Tedder, and J. C. Walton, *J. Chem. Soc., Faraday Trans. 1*, **71**, 592 (1975).
(17) T. Ogoaw, G. A. Carlson, and G. C. Pimentel, *J. Chem. Phys.*, **74**, 2090 (1970).
(18) A. P. Modica and S. J. Sillers, *J. Chem. Phys.*, **48**, 3283 (1968).
(19) I. McAlpine and H. Sutcliffe, *J. Phys. Chem.*, **73**, 3215 (1969).
(20) H. Sutcliffe, *Int. J. Radiat. Phys. Chem.*, **4**, 494 (1972).
(21) H. W. Thompson and R. B. Temple, *J. Chem. Soc.*, 1422 (1948).
(22) R. B. Bernstein, J. P. Zietlow, and F. F. Cleveland, *J. Chem. Phys.*, **21**, 1778 (1953).
(23) E. K. Plyler and W. S. Benedict, *J. Res. Natl. Bur. Stand.*, **47**, 212 (1951).

# Photolysis of *cis*-2-Butene at 7.1 eV

**Andrzej Więckowski[†] and Guy J. Collin***

*Département des Sciences pures, Université du Québec, Chicoutimi, Québec, Canada G7H 2B1* *(Received February 8, 1977)*

*Publication costs assisted by l'Université du Québec à Chicoutimi*

The photolysis of *cis*-2-butene (C2B) was carried out in a static system using nitrogen resonance lines at 7.10–7.11 eV (174.5–174.3 nm). The main fragmentation processes of the photoexcited $(C_4H_8)^{**}$ molecule are as follows: $C_4H_8\text{-}2^{**} \rightarrow C_4H_6 + 2H$ $(H_2)$, $\Phi = 0.40$, and $C_4H_8\text{-}2^{**} \rightarrow C_3H_5 + CH_3$, $\Phi = 0.38$. The energy partitioning between $CH_3CH{=}CH$ and $CH_3$ radicals is discussed. The excited vinylic radicals either decompose yielding acetylene, or isomerize (which is followed by allene formation), or are stabilized by collisions. The kinetics of the $(s\text{-}C_4H_9)^*$ radical decomposition provide some information on the energy distribution of the atomic hydrogen present in the studied system. The stabilization of $C_4H_8\text{-}2^{**}$ molecules and the formation of isomers are inefficient processes between 6.6 and $4 \times 10^4$ N m$^{-2}$ (0.05 and 300 Torr).

## Introduction

There have been several studies of direct photolysis of *cis*-2-butene (C2B) at different photon energies. Chesick[1] used a zinc lamp (6.01–6.12 eV) and investigated the effects of pressure on the total product yields and the product distributions. Similar experiments have been reported by Borrell et al.[2] at 6.11 and 6.70 eV (cadmium and mercury lamps, respectively). In both studies, it has been possible to quench the decomposition of photoexcited C2B molecules by the addition of foreign gases or by increasing the pressure of the reactant itself. This effect has not been observed at a higher photon energy. At 8.44 and 10.0 eV (xenon and krypton lines, respectively), Collin et al.[3] have indicated that the yields of primary products, as well as the yields of products formed from the decomposition of primary fragments, are virtually pressure independent.

Some other differences between the results obtained at low and high photon energies may be noted. At 6.70 eV, the major primary process is $C_4H_8\text{-}2^{**} \rightarrow C_4H_7 + H$ ($\beta$ splitting, ref 2) but at 8.4 and 10.0 eV, the cleavage of the two C–H bonds, yielding 1,3-butadiene, becomes more important. Moreover, the C–C break is more frequent than the C–H break when the photon energy increases.[3]

Only small differences between the fragmentation pattern at 8.4 and 10.0 eV, respectively, have been observed[3] indicating that the primary photochemical processes are unaffected by the changes in photon energy in this region. This result gives support to the same conclusions arrived at in other photochemical olefinic systems at these energies and it appears to be of general validity, except for ethylene.[4,5]

The aim of the present authors is to examine the energy region from 6.70 to 8.44 eV. One of our purposes is to study the primary photochemical processes as a function of photon energy. We also would like to show that this region is interesting from the kinetic point of view. Below 6.70 eV, due to the numerous oscillators in C2B, lifetimes are long enough to permit observation of collision stabilization. Above 8.44 eV, the excess internal energy is too high to measure the rates of the decomposition processes by the use of a collisional stabilization technique. In the intermediate region, at least the secondary processes should be accessible to kinetic analysis and some threshold energy values may be determined. A nitrogen lamp[6] has been constructed first. Further studies are under preparation.

## Experimental Section

The nitrogen lamp was built from Pyrex tubing fitted with a quartz window (1 mm thick, thermal fused quartz). In order to degas the glass walls,[7] before filling with nitrogen, the lamp was heated to 500 °C under vacuum by the use of an electrical oven. The cooling and heating of the lamp to just below the melting point of the glass did not destroy the vacuum at ca. $7 \times 10^{-4}$ N m$^{-2}$ ($5 \times 10^{-6}$ Torr). Then 50 N m$^{-2}$ of nitrogen (Matheson, Assayed Grade) was introduced and the lamp was sealed off from the vacuum line.

The emission spectrum of the lamp was taken with a 0.5-m vacuum monochromator (235 GCA/McPherson Instrument) with a 30-$\mu$m slit at a scanning speed of 5 nm/min. The 7.11 and 7.10 eV (174.3 and 174.5 nm, relative intensities 1 and 0.5, respectively) were the main lines and there were several minor contributions in the 6.36–7.51-eV region. It was estimated that the contributions to the total emission above 7.2 eV were ca. 15%, between 7.0 and 7.2 eV ca. 70%, and below 7.0 eV ca. 15%.

Ethylene actinometry was carried out; the quantity of acetylene was determined. The quantum yield of acetylene formation used in this work was equal to 0.75.[4] Good independence of the acetylene yield on photon energy in the range from 6.42 to 8.44 eV and on ethylene pressure has been reported by different laboratories.[4,8] The output of the lamp was of the order of $5 \times 10^{13}$ quanta/s. Except where otherwise indicated, the period of irradiation was 1 h.

The remaining details on the experimental and chromatographical procedure were essentially the same as described in previous studies from this laboratory.[3] Squalane (8 m), $Al_2O_3$ (3.5 m, temperature programming), and *n*-octane–porasil c (1.5 m) columns were applied in analytical runs. C2B (Philips Research grade) was used with no additional purification; the only detectable impurities were butadiene (0.0165%) and *trans*-2-butene (T2B) (0.0302%). The results described below were corrected for the presence of these impurities.

The accuracy of the quantum yields reported in this work is estimated to be better than 10%. Larger error limits apply for experiments with HI and $H_2S$ radical scavengers since the resulting quantum yields were ob-

[†] On leave from the Chemistry Department, Warsaw University, Warsaw, Poland

TABLE I: Formation of Products at 133 N m$^{-2}$ (1.0 Torr) from the Photolysis of C2B at 7.1 eV

| Products | Pure C2B | With 5% NO |
|---|---|---|
| Methane | 0.059[a] | 0.043 |
| Acetylene | 0.10 | 0.10 |
| Ethylene | 0.039 | 0.040 |
| Ethane | 0.21 | 0.00 |
| Propylene | 0.25 | 0.25 |
| Propyne | 0.025 | 0.026 |
| Allene | 0.059 | 0.058 |
| 1-Butene | 0.12[b] | 0.00 |
| 1,3-Butadiene | *c* | 0.40 |
| *n*-Butane | 0.040 | 0.00 |
| T2B | 0.086[d] | 0.01 |
| 3-Methyl-1-butene | 0.030[d] | 0.00 |
| Isopentane | 0.154 | 0.00 |
| *trans*-2-Pentene | 0.031[d] | 0.00 |
| *cis*-2-Pentene | 0.049[d] | 0.00 |

[a] Quantum yields. [b] 0.16 at 10 Torr. [c] Not measured. [d] There values are pressure independent between 0.665 and 133 N m$^{-2}$.

tained as a difference between two quantum yield values (see Results) with their own error limits. In this case, the estimated error is around 15%.

## Results

The photolysis of C2B at 7.1 eV yields a number of hydrocarbon products which, as well as their quantum yields for C2B pressure of 133 N m$^{-2}$, are summarized in Table I. Within our experimental conditions (the percentage of conversion is less than 1%), the quantities of products were found to be linear vs. irradiation time, showing that reactions with accumulated products may be ignored here. If a solid polymer was formed, it was transparent to the applied radiation since no decrease in the intensity of the light beam with the number of experiments was observed. The sulfuric or iodic species accumulated on the quartz window during the experiments with radical scavengers were easily washed off by the use of a $CCl_4$ solvent. Molecular hydrogen, if formed, was not analyzed in this work.

*NO, HI, and $H_2S$ Radical Scavengers.* At a sufficient concentration level, NO removes free radicals from the reaction environment (except hydrogen atoms and "hot" radicals) via radical–molecule reactions which give products not detectable in our analytical runs. The results for C2B pressure equal to 133 N m$^{-2}$ and 5% of NO are also presented in Table I. HI and $H_2S$ radical scavengers react with radicals via a hydrogen atom transfer forming hydrocarbons whose yields could be determined chromatographically. The quantum yields of the radicals present in the studied system were determined by subtracting the yields of the hydrocarbons formed in the presence of NO from those obtained in the experiments with HI and $H_2S$, respectively, for identical pressure and concentration conditions. The results for C2B pressure in the range 130–6650 N m$^{-2}$ and for fixed scavenger concentrations are given in Table II.

It should be added that no essential difference in quantum yield values were observed when passing from 5 to 10% of HI and from 10 to 20% of $H_2S$, respectively. The difference in the quantum yields of $C_3H_5$ radicals scavenged by HI and $H_2S$, respectively, should be noted.

*He, Xe, and C2B as Collisional Quenchers.* The addition of foreign gases (He, Xe) and the increase in the C2B pressure exhibited a varying effect on the product yields. While the yields of propylene, allene, acetylene, and ethylene essentially decreased with the increase in pressure, those of butadiene and propyne were virtually

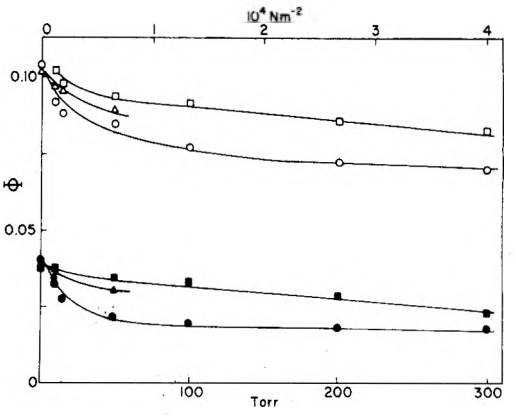


**Figure 1.** The quantum yields of acetylene (open symbols) and ethylene (solid symbols) plotted against (O, ●) C2B, (□, ■) He, and (△, ▲) Xe pressure. Added, NO, 5% of a total C2B pressure.

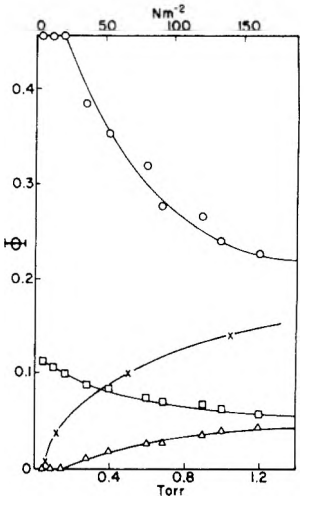


**Figure 2.** The quantum yields of (O) propylene, (□) allene, (X) isopentane, and (△) *n*-butane plotted against C2B pressure in the low pressure region.

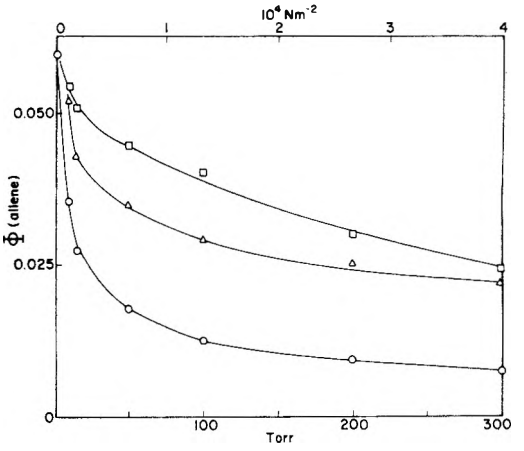


**Figure 3.** The quantum yields of allene plotted against (O) C2B, (□) He, and (△) Xe pressure. High pressure region.

unaffected. The pressure dependence of ethylene and acetylene is illustrated in Figure 1. For both products, the decrease in the quantum yields approaches the limiting values at ca. 4 × 10$^4$ N m$^{-2}$ of C2B which enables one to separate their pressure dependent and independent contributions to the total quantum yields. In the case of propylene and allene the results are more complex since, contrary to those on $C_2H_2$ and $C_2H_4$, (i) a strong falloff of the Φ vs. C2B pressure was observed below ca. 130 N m$^{-2}$ and, (ii) this was followed by a much smoother quantum yield drop in the high pressure region (Figures 2 and 3 and

TABLE II: Radical Quantum Yields Determined in Experiments with HI (10%) and $H_2S$ (20%)

| C2B press, N m$^{-2}$ | $CH_3$ | | $C_2H_3$ | | $C_2H_5$ | | $C_3H_5$ | | $C_4H_9$ |
|---|---|---|---|---|---|---|---|---|---|
| | HI | $H_2S$ | HI | $H_2S$ | HI | $H_2S$ | HI | $H_2S$ | HI |
| 133[a] | 0.90 | 0.93 | 0.021 | 0.018 | 0.008 | 0.010 | 0.26[b] | 0.20 | 0.18 |
| 1330 | 0.83 | 0.80 | 0.021 | 0.022 | 0.014 | 0.020 | 0.30 | 0.19 | 0.31 |
| 2130 | 0.75 | 0.73[c] | 0.019 | *d* | 0.023 | *d* | 0.33 | 0.24 | 0.32 |
| 6650 | 0.68 | 0.66[c] | 0.020 | *d* | 0.020 | *d* | 0.34[e] | 0.24 | 0.38[e] |

[a] 133 N m$^{-2}$ = 1 Torr. [b] This value may be underestimated since HI, by intercepting H atoms, reduces the yield of propylene formed from the ($s$-$C_4H_9$)* radicals. [c] 5% $H_2S$ concentration. [d] Not measured. [e] This value was determined with 1% of HI only. The radical quantum yields may be slightly higher than those indicated in this table.[3b]

TABLE III: Propylene Quantum Yields in Experiments with C2B and Helium Collisional Quenchers

| Total press, N m$^{-2}$ | C2B[a] | He[b] |
|---|---|---|
| 6650 | 0.042 | 0.055 |
| 13300 | 0.040 | 0.029 |
| 26600 | 0.036 | 0.019 |
| 39900 | 0.037 | 0.013 |

[a] C2B + 5% NO. [b] C2B (1 Torr) + NO (5%) + helium.

Table III). Moreover, in the latter region, the decrease in the $\Phi(C_3H_6)$ value with the increase in the helium pressure was faster than that with the increase in C2B pressure (Table III). This result is particularly important since C2B is a better collisional quencher of excited organic molecules than helium.

The increase in $n$-butane and isopentane yields concurrent with the decrease in that of propylene is also shown in Figure 2.

## Discussion

*Radicals and Their Decomposition Process.* The most important radicals in the studied system are $CH_3$, $C_3H_5$, and $C_4H_9$ (Table II). The last one is formed through the addition of a hydrogen atom to the double bond of the C2B molecule:

$$C2B + H \rightarrow s\text{-}C_4H_9^* \qquad \Delta H = -1.65 \text{ eV} \qquad (1)$$

$$C2B + H \rightarrow H_2 + C_4H_7 \qquad (2)$$

The abstraction of the hydrogen atom (process 2) competes with process 1[9,10] and the ratio of the rate constants $k_2/k_1$ given by Jennings and Cvetanović[9] is equal to 0.066. This indicates that process 1 occurs predominently in our system. However process 2 contributes to $C_4H_7$ radical formation and must be taken into account in estimating its quantum yield (see further). If not collisionally stabilized, these excited ($s$-$C_4H_9$)* radicals have enough excess energy to decompose; the decomposition–stabilization ($D$–$S$) mechanism is represented by the following reactions:[11]

$$s\text{-}C_4H_9^* \xrightarrow{D} C_3H_6 + CH_3 \qquad \Delta H = +1.09 \text{ eV} \qquad (3)$$

$$s\text{-}C_4H_9^* + M \xrightarrow{S} s\text{-}C_4H_9 + M \qquad (4)$$

As it is seen from the data given in Figure 2, below ca. 10 N m$^{-2}$, the quantum yield of propylene, formed in process 3,[18] is no longer increased with a decrease in C2B pressure. Moreover, at ca. 10 N m$^{-2}$, the yields of $n$-butane (formed by disproportionation of $s$-$C_4H_9$ radicals and other radicals present in the system studied) and isopentane (formed by combination of $s$-$C_4H_9$ and $CH_3$ radicals) are equal to zero. This proves that at ca. 10 N m$^{-2}$ the $s$-$C_4H_9$* radicals entirely decompose. If so, the quantum yield of propylene below 10 N m$^{-2}$ is equal to the maximum quantum yield of *sec*-butyl radicals formed in process 1 ($\Phi^{max}(s\text{-}C_4H_9^*)$). The value of the *sec*-butyl radical

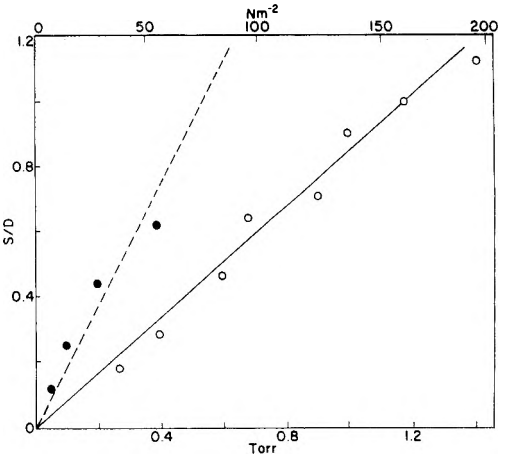


**Figure 4.** The ratio $S/D$ as a function of C2B pressure: (●) data taken from ref 11, (○) this work.

quantum yield obtained in experiments with HI scavenger at 6650 N m$^{-2}$ (Table II), after correction for the competing process:[3b]

$$H + HI \rightarrow H_2 + I \qquad (5)$$

is equal to 0.43 and agrees well with the value of $\Phi^{max}$-($s$-$C_4H_9$*) = 0.45 (Figure 2).

By definition: $D$ = $\Phi$(propylene) and $S$ = $\phi^{max}(s\text{-}C_4H_9^*)$ – $\Phi$(propylene) and the analysis of the process of *sec*-butyl radical decomposition may be carried out by the use of a $S/D$ vs. C2B pressure plot. This form of presentation is chosen in order to compare our data with those taken from Rabinovich and Diesen's work[11] on the decomposition of chemically activated *sec*-butyl radicals and this is shown in Figure 4. Since virtually thermal hydrogen atoms were used in the cited work[11] the difference in the slope of $S/D$ vs. pressure line taken from ref 11 and that obtained in this work (Figure 4) is considered as evidence that the average energy of hydrogen atoms produced in our system is higher than the energy of thermal hydrogen atoms at room temperature. Moreover, the presence of hot hydrogen atoms is indicated by the data given in Table III; above ca. 6700 N m$^{-2}$ the propylene yield ceased to decrease with increase in C2B pressure. This effect was not observed in experiments with helium (Table III). The reasonable explanation is as follows: the hot hydrogen atoms, when attaching to the double bond of C2B molecules, result in the formation of high energy and short-lived *sec*-butyl radicals. These radicals decompose before collision with a molecule of a quencher even at high pressure. "Cooled down" by the efficient helium moderator, the hydrogen atoms form $s$-$C_4H_9$* radicals of a lesser energy content and the latter species may efficiently be stabilized by any collisional quencher such as helium; (the double role of helium as a hot hydrogen moderator and as a collisional quencher of $s$-$C_4H_9$* radicals should be noted). If this interpretation is valid, a complex character for atomic hydrogen energy distribution may be

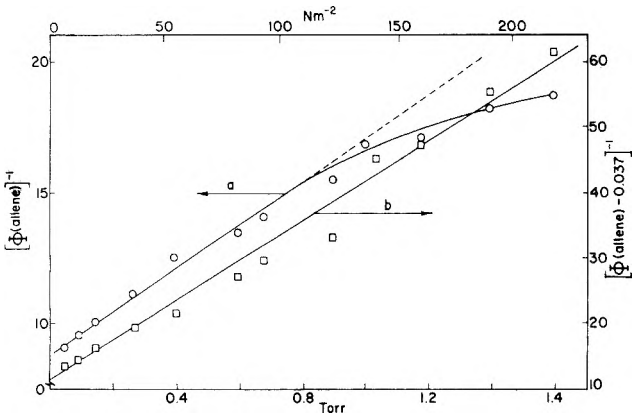


**Figure 5.** The reciprocal of the quantum yields of allene against C2B pressure (curve a, left axis) and the reciprocal of [Φ(allene) - 0.037] against C2B pressure (curve b, right axis). Low pressure region. Explanations given in the text.

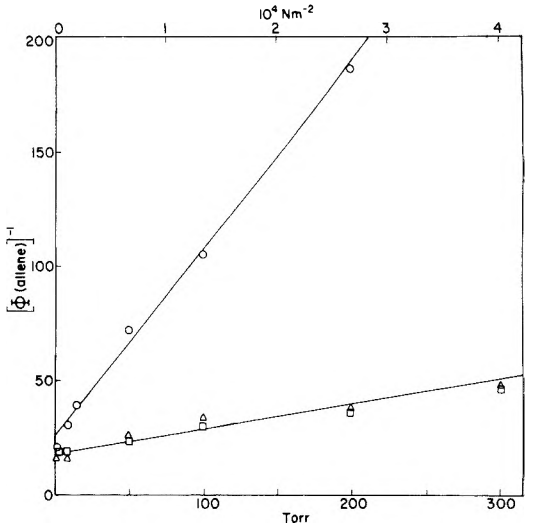


**Figure 6.** The reciprocal of the allene quantum yield against (O) C2B, (□) He, and (Δ) Xe pressure. High pressure region.

concluded. This may be due to different routes for hydrogen atom formation in the system studied (see further).

The methyl radical quantum yield decreases with an increase in pressure (Table II); between 133 and 6650 N $m^{-2}$ $\Delta\Phi(CH_3)$ is equal to 0.25. This value corresponds well with the decrease in propylene quantum yield; in this pressure region $\Delta\Phi$(propylene) = 0.21 (see data given in Figure 2, and Tables II and III). Thus, we may conclude that a decrease in $\Phi(CH_3)$ is mainly due to process 3.

$C_3H_5$ radicals formed by direct fragmentation of photoexcited C2B molecules

$$C_4H_8^{**} \rightarrow C_3H_5^* + CH_3 \qquad (6)$$

originally have a vinylic structure. The vinylic radicals may decompose or isomerize or may be stabilized by collisions provided that they have sufficient excess energy. Their decomposition may lead to the formation of acetylene according to

$$CH_3CH{=}CH^* \rightarrow CH_3 + CH{\equiv}CH \qquad (7)$$

Propyne may also be formed from $CH_3CH{=}CH$ radicals but the yield of this compound is small (Table I) and pressure independent and, as such, is not discussed here.

The isomerization of vinylic radicals leads to the allylic structure

$$CH_3CH{=}CH^* \rightarrow CH_2CHCH_2^* \qquad (8)$$

This process may be followed by the formation of allene

$$CH_2CHCH_2^* \rightarrow CH_2CCH_2 + H \qquad (9)$$

The stabilization of $C_3H_5^*$ radicals (in any isomeric form) may be expressed by the classical formula:

$$C_3H_5^* + M \rightarrow C_3H_5 + M \qquad (10)$$

The resulting (process 8) allylic radicals do not react with $H_2S$[3b,13] and the difference in the $\Phi(C_3H_5)$ values found for HI and $H_2S$ (Table II) provides a direct support for the occurence of the isomerization process. The steady-state approximation, applied for allene, yields the familiar Stern–Volmer equation described in a form convenient for lineation:

$$[\Phi(\text{allene})]^{-1} = [\Phi(C_3H_5^*)]^{-1} + [\Phi(C_3H_5^*)]^{-1}(K_{st}/K_{dec})M$$

and some important conclusions[14] come from the fact that no simple steady-state treatment covering the whole C2B pressure region may be found. The $[\Phi(\text{allene})]^{-1}$ vs. C2B pressure plot (low pressure region) is given in the Figure 5, curve a; the curvature of the Stern–Volmer plot at ca. 120 N $m^{-2}$ should be noted. This curvature may be accounted for if we assume that it reflects the partitioning of energy between two fragments formed from the photodecomposition of the C2B** molecule (process 6). As a result of such partitioning, the $C_3H_5^*$ radical is formed with a spread of internal energies which is wider than that observed in chemically activated systems (see ref 14 and references given in this work). However, at a higher C2B pressure (Figure 6), the linearity of $1/\Phi$ vs. pressure plot is apparently recovered yielding a $\Phi'(C_3H_5^*)$ value equal to 0.037 ($\Phi'$ denotes the quantum yield of high pressure $C_3H_5^*$ radicals extrapolated to zero pressure). This value has a definite physical meaning since we may assume that the low pressure allene formation process is completed at the beginning of the high pressure region scale. If so, the low pressure data may be analyzed by use of the $[\Phi(\text{allene}) - 0.037]^{-1}$ vs. C2B pressure plot (Figure 5, curve b). At is seen, the linearity of the plot is highly improved and this yields $\Phi''(C_3H_5^*)$ equal to 0.09 ($\Phi''$ denotes the quantum yield of the low pressure $C_3H_5^*$ radicals extrapolated to zero pressure). If this analytical procedure which results in two linear regions of the $\Phi^{-1}$ vs. C2B pressure plot is reliable,[15] it may be concluded that two distinct types of $C_3H_5^*$ radicals ($C_3H_5^{\ddagger\ddagger}$, $C_3H_5^{\ddagger}$) of reasonably narrow energy content are formed rather than a number of $C_3H_5^*$ radicals over a wide monotonic spread of internal energy. This is shown by the following simplified mechanism:

$$\begin{aligned} C_4H_8^{**} &\rightarrow C_3H_5^{\ddagger\ddagger} + CH_3 \\ C_4H_8^{**} &\rightarrow C_3H_5^{\ddagger} + CH_3 \end{aligned} \qquad (11)$$

The sensitivity of the Stern–Volmer plot and/or the precision of the experiments is probably too low to respond to differences in the spread of internal energies within the two types of $C_3H_5$ radicals formed in process 11.

The overall pressure material balance reveals that only 42% of the $C_3H_5$ radicals formed in process 10 may further decompose (the quantum yield of process 11 is equal to 0.38, Table IV; the sum of the values of $\Phi$(allene) and $\Phi$(acetylene) extrapolated to zero pressure, Figures 3 and 7, is equal to 0.16), the remaining $C_3H_5$ radicals may only combine with other radicals or attach to the double bond of C2B molecules. The combination processes of $C_3H_5$ and $CH_3$ radicals may partly explain the formation of *n*-butene and T2B, Table I (no attempts to look for $C_6$, $C_7$, ..., compounds were undertaken). The consistency of the kinetic analysis implies that process 9 is the rate-deter-

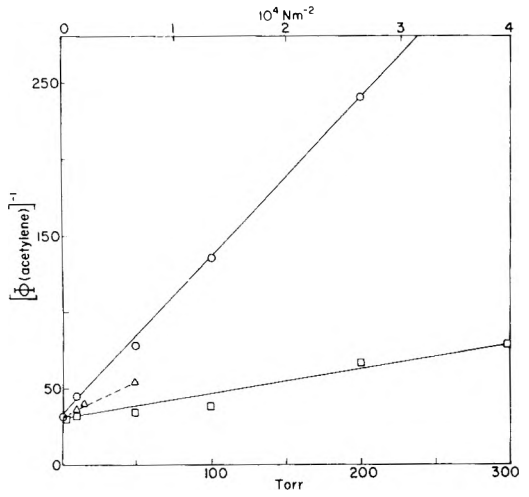


**Figure 7.** The reciprocal of the acetylene quantum yield against (○) C2B, (□) He, and (△) Xe pressure.

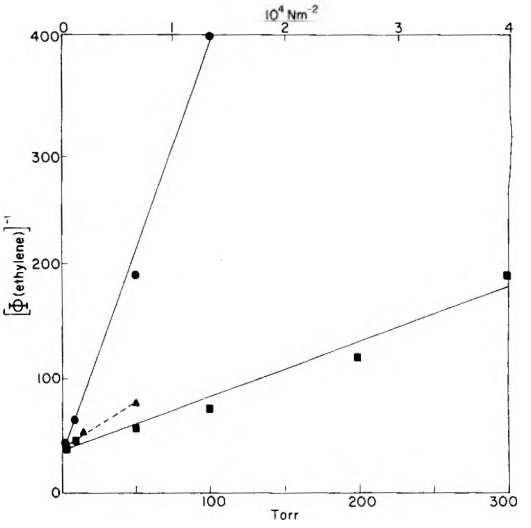


**Figure 8.** The reciprocal of the ethylene quantum yield against (●) C2B, (■) He, and (▲) Xe pressure.

mining step for allene formation, thus process 10 refers to the stabilization of allylic radicals. Since no pressure dependence on the acetylene yield in the low pressure region was found, it is concluded that only higher energized vinylic radicals are acetylene precursors.

Ethyl and vinyl radicals are formed in minor quantities (Table II). It is of interest to note the small increase of the $\Phi(C_2H_5)$ value with the increase in pressure in the 133–6650 N m$^{-2}$ region (Table II) together with a small decrease of the ethylene yield (Figure 1) suggesting the following mechanism:

$$C_4H_8^{**} \rightarrow C_2H_3 + C_2H_5^* \quad (12)$$

$$C_2H_5^* \rightarrow C_2H_4 + H \quad (13a)$$

$$C_2H_5^* + M \rightarrow C_2H_5 + M \quad (13b)$$

Stern-Volmer plots for acetylene and ethylene are shown in Figures 7 and 8, respectively[19] and some general comments on the experiments with three different collisional quenchers (He, Xe, and C2B) may be made. The results presented in Figures 4 and 6–8 provide evidence that, in the deactivation processes of excited *sec*-butyl, $C_3H_5$, and $C_2H_5$ radicals the nature of the quenchers used for the investigations plays an important role. Our results on the stabilization of $(s\text{-}C_4H_9)^*$ radicals by He and C2B are in accord with the data of Rabinovich and Diesen.[11] On the other hand, in the 6.70-eV photolysis of C2B, Borell et al.[2] have shown the similarity in quenching efficiency of such diverse collision partners as $H_2$, $CO_2$, and C2B. It should be pointed out however that the latter observation has been referred to the deactivation of primary photoexcited C2B species but not to the deactivation of the radical fragments. Since we were unable to observe the stabilization of the C2B** molecules (1,3-butadiene and propyne quantum yields were virtually pressure independent, see Results), the results of Borell et al.[2] and ours can hardly be compared. As is seen from the data given in Figure 6, the $1/\Phi$(allene) vs. He and Xe pressure experimental points, respectively, scatter around a common line indicating the identity (within the experimental error) of the noble gases acting as energy sinks. Measurable differences are observed for acetylene and ethylene formation processes (Figures 7 and 8) but due to the difficulties in chromatographic analysis of samples containing higher amounts of xenon only a small Xe pressure region was accessible to investigations. Thus, we may conclude that, contrary to the striking differences between He and C2B acting as quenchers of the excited radicals, those between He and Xe are very much smaller.

Finally, it is necessary to have a look at $C_4H_7$ radicals. These radicals in the pure system react with other free radicals by a combination–disproportionation mechanism. The combination mechanism explains the formation of the $C_5H_{10}$ compounds (Table I). There is no variation in the yield of the total $C_5H_{10}$ compounds in the low pressure region (Table I) which implies that $C_4H_7$ radicals are not allene precursors. These radicals may be formed in process 2 and to some extent via hydrogen abstraction by hot radicals, e.g.

$$CH_3^* + C2B \rightarrow CH_4 + C_4H_7 \quad (14)$$

The presence of hot $CH_3$ radicals is consistent with process 11, and with the preceding discussion. It should be noted that methane is present in the C2B system scavenged by NO (Table I).

The detachment of a hot hydrogen atom from the photoexcited molecule has previously been proposed:[1-3]

$$C_4H_8^{**} \rightarrow C_4H_7 + H^* \quad (15)$$

It is difficult to evaluate this process. Nevertheless, we may make the simple assumption that $C_4H_7$ radicals react on a statistical basis by combination with other free radicals. At 133 N m$^{-2}$ (1 Torr), the total radical quantum yield, $\Phi(R\cdot)$, is equal to $\Phi(CH_3) + \Phi(C_2H_3) + \Phi(C_2H_5) + \Phi(C_3H_5) + \Phi(H) - \Phi(C_3H_6) = 1.40$ (Tables I and II). Assuming that $\Phi(C_4H_7) \ll 1.40$, we can write

$$\Phi(CH_3)/\Phi(R\cdot) \approx \Phi(C_5H_{10})/\Phi(C_4H_7R)$$

and $\Phi(C_4H_7) \approx \Phi(C_4H_7R)$. Thus, we estimate a rough $\Phi(C_4H_7)$ value close to 0.20. Subtracting the $\Phi$(process 2) value calculated for thermal hydrogen atoms[10] and the $\Phi$(process 14) value from $\Phi(C_4H_7) = 0.20$, we obtain an estimated value for process 15: $\Phi = 0.12 \pm 0.06$.[16]

*Molecular Products and Primary Fragmentation.* At this point we wish to describe the fragmentation of the photoexcited molecule using the preceding observations and material balances (Table IV). The quantum yield of process 6 is equal to the $\Phi(C_3H_5)$ value found in the HI scavenged system at 6650 N m$^{-2}$ (Table II) increased by a quantity of 0.04 which is equal to the sum of $\Delta\Phi$(allene) and $\Delta\Phi$(acetylene) over this pressure. The quantum yields of 1,3-butadiene formed in processes 16a and 16b and propyne formed in process 18 were virtually pressure independent and these values were obtained directly from actinometry. Molecular hydrogen was not measured. Reactions 17 and 19 are proposed to take into account the formation of acetylene and ethylene, whose yields no longer

TABLE IV: Primary Decomposition Processes[a] of the Photoexcited C2B Molecules at 7.1 eV ($C2B + h\nu \rightarrow C_4H_8\text{-}2^{**}$)

| Reaction no. | $C_4H_8\text{-}2^{**} \rightarrow$ | Φ |
|---|---|---|
| 6 | $C_3H_5^* + CH_3$ | 0.38 ± 0.04 |
| 16a | $C_4H_6 + H_2$ | 0.40 ± 0.02 |
| 16b | $C_4H_6 + 2H$ | |
| 15 | $C_4H_7 + H^*$ | 0.12 ± 0.06 |
| 17 | $C_2H_2 + 2CH_3$ | 0.07 ± 0.01 |
| 12 | $C_2H_3 + C_2H_5^*$ | 0.035 ± 0.005 |
| 18 | Propyne + $CH_4$ ($CH_3$ + H) | 0.026 ± 0.005 |
| 19 | $2C_2H_4$ | 0.01 ± 0.005 |
| 20 | T2B (isomerization) | 0.012 ± 0.005 |
| | Total | 1.05 ± 0.15 |

[a] An asterisk denotes hot or excited radicals which may decompose at a low pressure (see text).

TABLE V: Fragmentation of Photoexcited C2B Molecule at Different Photon Energies

| Energy, eV | 6.7 | 7.1 | 8.4 | 10.0 |
|---|---|---|---|---|
| Ref | 2 | This work | 3 | 3 |
| Types of reactions | | | | |
| Hydrogen elimination | 0.70[a] | 0.52 | 0.47 | 0.37 |
| C-C cleavage | 0.30 | 0.51 | 0.62 | 0.63 |
| Isomerization | <0.10 | 0.01 | 0.02 | 0.02 |

[a] Primary quantum yields

decreased with the reactant pressure above ca. $5 \times 10^4$ N $m^{-2}$ (Figure 1). The isomeriztion of C2B (process 20) is a minor one; the presence of T2B in the starting material makes the analysis of this compound difficult. No pressure dependence of the T2B yield in the low pressure region was observed.

## Conclusion

At 7.1 eV, it appears that cleavage of the C-C and C-H bonds of the photoexcited C2B molecules are of equal importance. This result is consistent with the results of Borrell et al.[2] at 6.70 eV and with our previous data at 8.44 and 10.0 eV[3] (Table V). There is practically no stabilization of the primary photoexcited states in the present study contrary to what was observed at a lower energy, at 6.01–6.12 eV[1] and even at 6.7 eV.[2] Since the latter value is only 0.4 eV lower than that used for the present investigations, it may be suggested that different spectroscopic states involved in both studies[2,17] are responsible for the observed discrepancies rather than the energy difference.

*Acknowledgment.* We would thank the NRC of Canada and l'Université du Québec à Chicoutimi for their financial help throughout this work.

## References and Notes

(1) J. P. Chesick, *J. Chem. Phys.*, **45**, 3934 (1966).
(2) P. Borell and F. C. James, *Trans. Faraday Soc.*, **62**, 2452 (1966); P. Borell, P. Cashmore, A. Cervenka, and F. C. James, *J. Chim. Phys.*, 229 (1970).
(3) (a) G. J. Collin and P. Perrin, *Can. J. Chem.*, **50**, 2823 (1972); (b) G. J. Collin and K. Bukka, *J. Photochem.*, **6**, 381 (1976–1977).
(4) P. Potzinger, L. C. Glasgow, and G. Von Bünau, *Z. Naturforsch. A*, **27**, 628 (1971).
(5) G. J. Collin, *J. Chim. Phys.*, **14**, 302 (1977).
(6) D. Davis and W. Braun, *Appl. Opt.*, **7**, 2071 (1968).
(7) L. F. Loucks and R. J. Cvetanović, *J. Chem. Phys.*, **56**, 321 (1972).
(8) H. Hara and I. Tanaka, *Bull. Chem. Soc. Jpn.*, **46**, 3012 (1973).
(9) K. R. Jennings and R. J. Cvetanović, *J. Chem. Phys.*, **35**, 1233 (1961).
(10) W. E. Falconer and W. A. Sanders, *Int. J. Chem. Kinet.*, **4**, 315 (1972).
(11) B. S. Rabinovitch and R. W. Diesen, *J. Chem. Phys.*, **30**, 735 (1959).
(12) D. F. Ring and B. S. Rabinovitch, *Int. J. Chem. Kinet.*, **1**, 11 (1969).
(13) P. Ausloos, R. E. Rebbert, and S. G. Lias, *J. Photochem.*, **2**, 267 (1973–1974).
(14) W. Forst in "Theory of Unimolecular Reactions", Academic Press, New York, N.Y., 1973, Chapter 9.
(15) The reliability of this procedure is strengthened by our recent results on the photolysis of the three remaining butenes at the same photon energy: *J. Photochem.*, accepted for publication; *Can. J. Chem.*, in press. See also: J. H. Vorachek and R. D. Koob, *J. Phys. Chem.*, **74**, 4455 (1970).
(16) As remarked by one of our referees, the $k_1/k_2$ ratio varies with the energy of hydrogen atoms (see, e.g. B. G. Dzantiev and A. V. Tshishkov, *Khim. Vys. En.*, **1**, 192 (1967)). Thus, the presence of the hot hydrogen atoms in our system affects the real Φ(process 15) value. We feel, however, that within the estimated broad error limits, this energy effect may be neglected.
(17) W. M. Flicker, O. A. Mosher, and A. Kupperman, *Chem. Phys. Lett.*, **36**, 56 (1975).
(18) We ignore the possible formation of propylene by other processes, e.g., by fragmentation of the photoexcited C2B molecules: $C2B^{**} \rightarrow C_3H_6 + CH_2$. In fact, we were unable to observe a formation of derivatives of the $CH_2$ + C2B reactions such as 1,2-dimethylcyclopropane[12] even at high pressure.
(19) The analysis of Stern-Volmer plots for ethylene at 10–130 N $m^{-2}$ revealed a similar curvature as that observed for allene (Figure 5a). However, at low pressure ethylene may be formed not only in process 13a but also from *n*-butyl radicals formed via isomerization of *sec*-butyl radicals (see ref 3a). Thus, we consider that the results in the low pressure region are ambiguous and as such are not discussed here.

# Photooxidation of Isobutane by Nitrogen Dioxide at 366 nm[1]

**G. Paraskevopoulos* and R. J. Cvetanović***

*Division of Chemistry, National Research Council of Canada, Ottawa, Ontario, Canada K1A OR9* *(Received June 28, 1977)*

*Publication costs assisted by the National Research Council of Canada*

The photochemical reaction of isobutane–$NO_2$ mixtures at 366 nm has been studied in the gas phase at 25 °C with isobutane in large excess (125:1). The main reaction products are the nitro compounds of the *tert*-butyl and (to a much smaller extent) of *sec*-butyl radicals and isobutene. The minor products are 2-methylpropanal, isobutene oxide, acetone, 2-methyl-2-propanol, traces of methyl ethyl ketone, and possibly traces of methyl nitrate. The photooxidation is initiated by the ground state oxygen atoms, $O(^3P)$, from the photolysis of $NO_2$ at 366 nm, followed by their interaction with isobutane in a simple manner, i.e., by abstraction mainly of the tertiary H atom and to a smaller extent of the primary H atoms. The OH radicals thus produced abstract in their turn H atoms from isobutane. The butyl radicals formed react further with $NO_2$, NO, and $O_2$ to give the nitro compounds, nitrites, nitrates, and isobutene. Secondary attack of O atoms on isobutene is responsible for the minor products.

## Introduction

Photolysis of $NO_2$ at 366 nm is a good source of the ground state oxygen atoms, $O(^3P)$. It has been shown in this laboratory that photooxidation of simple olefins (1-butene, isobutene)[2] by $NO_2$ at this wavelength conforms to the established mechanism of $O(^3P)$ interaction with olefins when allowance is made for the presence of $NO_2$ and its secondary reactions with some of the primary products. It may therefore be expected that the $NO_2$ photooxidation at 366 nm of saturated hydrocarbons should similarly provide information on the mechanism of their reaction with $O(^3P)$ atoms. While it is generally believed[3-7] that this interaction is basically very simple, consisting simply of H atom abstraction, in some investigations of the $O(^3P)$–alkane reactions considerably more complex mechanisms have been postulated.[8-10] In the present study we have investigated the $NO_2$ photooxidation of isobutane at 366 nm. Apart from the information which it can provide on the primary interaction of $O(^3P)$ with alkanes, this reaction is also of interest from the point of view of chemical reactions in photochemical smog and also of the general mechanism of the photooxidation of hydrocarbons by $NO_2$.

## Experimental Section

The $NO_2$ was irradiated with essentially monochromatic light of 366 nm provided by a medium pressure mercury arc (Hanovia S500) and a set of two Corning (7-39 and 0-52) glass filters ($320 < \lambda < 400$ nm). The light output of the lamp operated at 2 A was constant after a warm-up period of 0.5 h.

The cylindrical photolysis cell (12 cm long, 5 cm o.d.) with plane end windows was made of Pyrex glass and had a volume of 221 mL. During experiments the cell was screened from the diffuse light of the laboratory.

The purification, storage, and transfer of the reactants were carried out in a mercury-free vacuum system in order to prevent reactions of $NO_2$ with mercury. Pressures were measured with a Bourdon gauge and a bellows gauge. The photolysis cell was connected to the mercury containing analytical system through three liquid nitrogen traps, which served to prevent mercury vapor from entering the cell. After irradiation the contents of the cell were condensed in a liquid nitrogen trap and the noncondensable gases (mainly $O_2$) were pumped-off slowly. The condensable products and excess reactants were distilled into a trap containing mercury which on warming to room temperature reacted with and removed excess $NO_2$.[2] The mixture was then distilled into a mixing bulb, provided with a high-speed magnetically driven stirrer; several aliqots could be taken from the bulb for gas chromatographic analysis.

*Analysis of the Products.* The products were analyzed by gas chromatography as follows:

The oxygenated products were measured on a 300 ft. long, 0.015 in. i.d. stainless-steel capillary column coated with dinonyl phthalate and equipped with a flame ionization detector. The column was operated at 0 °C with helium as the carrier gas. Excess isobutane and isobutene product were retained relatively little on this column and the oxygenated products were separated well. Qualitative identification was based on the retention times on this and a second column (12 ft. $\beta,\beta'$-thiodipropionitrile on Anakrom A 80/90 mesh, equipped with a flame ionization detector and operated at 30 °C) and by seeding with authentic samples. Since authentic samples of *tert*-nitroisobutane, nitroisobutane, and *tert*- and isobutyl nitrate were not available, these products were identified from peak assignments based on linear plots of the logarithms of the relative retention times against the boiling points, as described in detail elsewhere.[11] Quantitative determinations were based on peak area measurements with benzene as an internal standard. It was assumed that the molar responses (relative to benzene) of *tert*-nitroisobutane and nitroisobutane were equal to the measured responses[11] of 2-nitrobutane and 1-nitrobutane, respectively, and that those of iso- and *tert*-butyl nitrate were equal to 1-butyl nitrate.[11]

Isobutene was separated from unreacted isobutane and measured quantitatively, in the majority of the experiments, on a 12 ft. column packed with 2% squalane modified alumina; in a few experiments a 40 ft. glass column packed with 25% glycol saturated with $AgNO_3$ on firebrick was used in series with a 32 ft. glass column packed with 30% propylene carbonate on firebrick. Both columns were operated at 25 °C, with He as carrier gas and were equipped with flame ionization detectors. Isobutene was identified by its retention time and by seeding with an authentic sample. Quantitative determinations were based on peak area measurements after calibration with known mixtures.

The analytical results reported are average values for each column from two to three chromatograms. The individual differences were not larger than about 5% but,

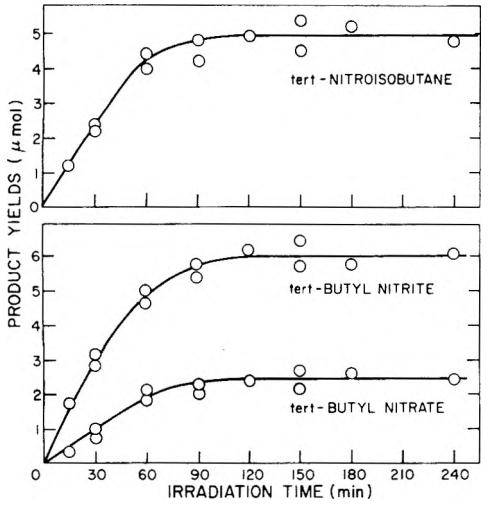


**Figure 1.** Plots of the yields of the *tert*-nitro compounds against the irradiation time.

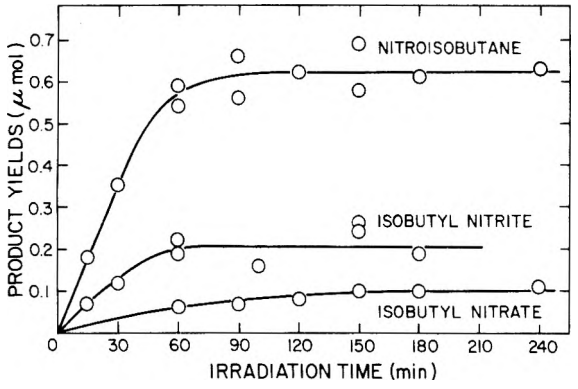


**Figure 2.** Plots of the yields of the isonitro compounds against the irradiation time.

due to the relatively small quantities of some products and the assumptions made for the molar responses of some of the products, we estimate the analytical error to be 5–10% for the more abundant products and 15–20% for the minor products.

*Materials.* The isobutane was Phillips 66 research grade, stated purity 99.98%. It was thoroughly degassed at −196 °C before each experiment. Gas chromatographic analysis showed that the isobutane contained 0.01 ± 0.001% of isobutene impurity. Nitrogen dioxide was prepared from pure dry oxygen and Matheson nitric oxide which had been passed over activated Molecular Sieve 13X to remove carbon dioxide and water. It was stored at −78 °C and was degassed before each experiment.

## Results and Discussion

Blank experiments showed no dark reaction between $NO_2$ and isobutane. Experiments were made with a constant ratio $i\text{-}C_4H_{10}/NO_2 \approx 125 \pm 1$ ($i\text{-}C_4H_{10} \approx 750$ Torr, $NO_2 \approx 6.0$ Torr) and irradiation times varying from 15 to 240 min. The major products were the nitro compounds of the *tert*-butyl radical and isobutene. The minor products were the nitro compounds of the isobutyl radical, 2-methylpropanal, isobutene oxide, acetone, 2-methyl-2-propanol, traces of methyl ethyl ketone and possibly traces of methyl nitrate. The yields of the products are plotted as functions of the irradiation time in Figures 1–4. The yields of the nitro compounds and isobutene, Figure 1–3, increase initially with time but after about 90 min level off and remain constant; this is due to complete consumption of $NO_2$ after this time. The other products, Figure 4, appear to increase slowly over a longer time.

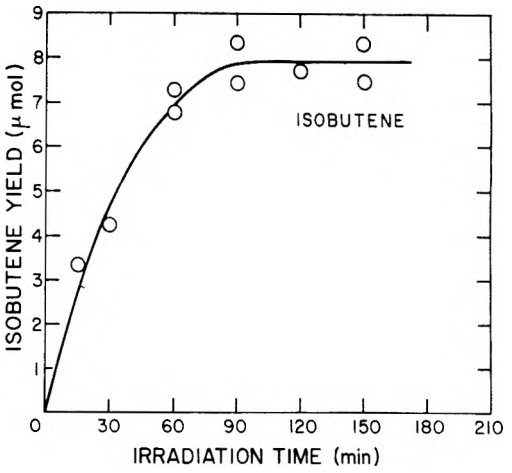


**Figure 3.** Plot of the yield of isobutene (corrected for the isobutene impurity in isobutane) against the irradiation time.

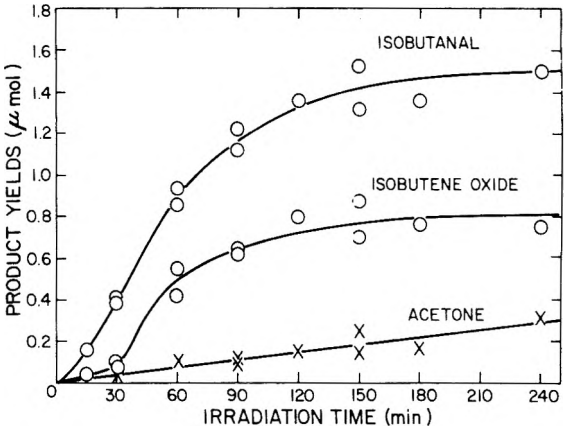


**Figure 4.** Plots of the yields of 2-methylpropanal, isobutene oxide, and acetone against the irradiation time.

The reactions leading to the products will now be considered in detail.

*Nitro Compounds.* These products and their relative yields are consistent with a mechanism in which ground state atoms $O(^3P)$ generated by photolysis of $NO_2$ react with $NO_2$ and abstract hydrogen from isobutane to form mainly *tert*-butyl radicals and to a much smaller extent isobutyl radicals, i.e.

$$NO_2 + h\nu \rightarrow O + NO \quad (1)$$

$$O + NO_2 \rightarrow O_2 + NO \quad (2)$$

$$O + (CH_3)_3CH \rightarrow \cdot OH + a(CH_3)_3C\cdot + (1-a)(CH_3)_2CHCH_2\cdot \quad (3)$$

$$\cdot OH + (CH_3)_3CH \rightarrow H_2O + b(CH_3)_3C\cdot + (1-b)(CH_3)_2CHCH_2\cdot \quad (4)$$

The *tert*- and isobutyl radicals react subsequently very fast with $NO_2$ to form nitro compounds:

$$(CH_3)_3C\cdot + NO_2 \rightarrow (CH_3)_3CNO_2 \quad (5)$$

$$\rightarrow (CH_3)_3CO\cdot + NO \quad (6)$$

$$(CH_3)_3CO\cdot + NO \rightarrow (CH_3)_3CONO \quad (7)$$

$$(CH_3)_3CO\cdot + NO_2 \rightarrow (CH_3)_3CONO_2 \quad (8)$$

The corresponding reactions of the isobutyl radicals with $NO_2$ take place to a smaller extent and are not written here explicitly. Reaction 5 was tentatively suggested by Blacet et al.[3] who found that the reaction product, condensable at −80 °C, had a mass spectrum resembling that of *tert*-nitroisobutane. This compound was also formed when a mixture of 6 Torr of $NO_2$ and 760 Torr of $i\text{-}C_4H_{10}$ was

heated at 130 °C,[3] and in the nitration of $i$-$C_4H_{10}$ with $NO_2$ or $HNO_3$ at 400 °C.[12] Although reaction 5 is exothermic and may require collisional stabilization, it would be favored by low temperatures and high pressures and, therefore, would be expected to occur readily in the present experiments at room temperature. The *tert*-butyl nitrite, however, is probably formed by reactions 6 and 7 rather than by direct association, $(CH_3)_3C\cdot + NO_2 \rightarrow (CH_3)_3C\text{-}ONO$, because the O–N bond is weaker than the C–O bond formed and, therefore, it is difficult to stabilize the *tert*-butyl nitrite in the gas phase.[12]

*Isobutene.* Appreciable amounts of isobutene were found among the products; these were a factor of 4–10 larger than the amount contained as an impurity in the isobutane reagent (0.01%) and, therefore, there is no doubt that isobutene is formed during the photolysis. Possible reactions which would form isobutene are as follows:

$$(CH_3)_3C\cdot + (CH_3)_3C\cdot \rightarrow (CH_3)_2C{=}CH_2 + i\text{-}C_4H_{10} \quad (9)$$

$$(CH_3)_3C\cdot + NO \rightarrow (CH_3)_3CNO \quad (10)$$

$$(CH_3)_3CNO \rightarrow (CH_3)_2C{=}CH_2 + HNO \quad (11)$$

The disproportionation reaction 9 is probably insignificant compared to the combination reactions 5, 6, and 10, and the combination of *tert*-butyl radicals with $O_2$ which will be discussed below. This was indicated by the failure to find the recombination product of *tert*-butyl radicals. Reactions 10 and 11 were postulated by Kraus and Calvert[13] for the formation of isobutene from *tert*-butyl radicals in the presence of NO. They found that in the absence of NO *tert*-butyl radicals formed isobutene by reaction 9, whereas in the presence of about 10 Torr of NO reactions 10 and 11 occurred exclusively and only isobutene was formed. For the present experiments too, reactions 10 and 11 are suggested as the isobutene forming reactions and perhaps also the analogous exothermic (~38 kcal/mol) reaction with $NO_2$:

$$(CH_3)_3C\cdot + NO_2 \rightarrow (CH_3)_2C{=}CH_2 + HNO_2 \quad (11')$$

for which no experimental evidence has been reported so far.

*Other Minor Products.* The minor products, 2-methylpropanal, isobutene oxide, acetone, and traces of methyl ethyl ketone and methyl nitrate, have all been identified by Sato and Cvetanović[2] to be the products of the reaction of O atoms with isobutene in the presence of $NO_2$. Since O atoms react with isobutene two to three orders of magnitude faster than with alkanes,[14] there is little doubt that in our experiments these compounds are formed in the secondary reaction of O atoms with the isobutene product. The slow thermal reaction of isobutene with $NO_2$ was ignored since the photochemical reaction is much faster and gives different products.[2] The origin of the minor products was confirmed by seeding the reaction mixture with 1.5 Torr of isobutene before irradiation. In this experiment, the yields of 2-methylpropanal and acetone, listed in Table I (last column), as well as the yields of methyl ethyl ketone and methyl nitrate, not listed, increased when isobutene was added. The observed yield of isobutene oxide increased only a little; however, isobutene oxide reacts with $NO_2$[2] and its yields are irregular and do not represent the actual amount formed.

*Effect of Added NO and $O_2$.* Although $O(^3P)$ atoms react very rapidly with $NO_2$ ($k_2 = 5.49 \times 10^9$ L mol$^{-1}$ s$^{-1}$),[15] it may be estimated[14] that for the present experimental conditions ($i$-$C_4H_{10}/NO_2 \approx 125$) the initial rates of reactions 2 and 3 are of comparable magnitude. It follows therefore that NO and $O_2$ will build up during the photolysis and will take part in secondary reactions, as for example in the isobutene forming reactions 10 and 11 mentioned above. The effects of NO and $O_2$ were assessed in experiments in which NO and $O_2$ were added to the reaction mixture before irradiation. The product yields in the absence and presence of 6.0 Torr of NO and 5.5 Torr of $O_2$ are listed in Tables I and II, respectively, for 30- and 60-min irradiations.

TABLE I: Effect of Addition of NO and Isobutene on the Product Yields

| Irradiation time, min | 30 | | 60 | | |
|---|---|---|---|---|---|
| NO added, Torr | None | 6 | None | 6 | None |
| Isobutene added, Torr | None | None | None | None | 1.55 |
| | Product yields, μmol | | | | |
| *tert*-Nitrobutane | 2.30 | 3.60 | 4.19 | 5.62 | 3.44 |
| *tert*-Butyl nitrite | 2.99 | 3.37 | 4.81 | 5.10 | 4.60 |
| *tert*-Butyl nitrate | 0.89 | 0.72 | 2.00 | 1.32 | 1.55 |
| Isonitrobutane | 0.35 | 0.37 | 0.56 | 0.56 | Trace |
| Isobutyl nitrite | 0.12 | 0.16 | 0.20 | 0.24 | Trace |
| Isobutyl nitrate | Trace | Trace | 0.06 | 0.09 | Trace |
| Isobutene[a] | 4.26 | 4.06 | 7.03 | 6.83 | Nd[b] |
| 2-Methylpropanal | 0.40 | 0.39 | 0.89 | 0.84 | 2.92 |
| Isobutene oxide | 0.09 | 0.04 | 0.50 | 0.08 | 0.60 |
| Acetone | 0.03 | 0.03 | 0.11 | 0.11 | 0.34 |

[a] The yields of isobutene are corrected for the isobutene impurity in isobutane. [b] Nd = not determined.

TABLE II: Effect of Addition of $O_2$ on the Product Yields

| Irradiation time, min | 30 | | 60 | |
|---|---|---|---|---|
| $O_2$ added, Torr | None | 5.5 | None | 5.5 |
| | Product yields, μmol | | | |
| *tert*-Nitrobutane | 2.30 | 2.16 | 4.19 | 3.59 |
| *tert*-Butyl nitrite | 2.99 | 4.73 | 4.81 | 8.97 |
| *tert*-Butyl nitrate | 0.89 | 4.93 | 2.00 | 9.50 |
| Isonitrobutane | 0.35 | 0.37 | 0.56 | 0.58 |
| Isobutyl nitrite | 0.12 | 0.31 | 0.20 | 0.51 |
| Isobutyl nitrate | Trace | 0.11 | 0.06 | 0.19 |
| Isobutene[a] | 4.26 | 3.04 | 7.03 | 4.10 |
| 2-Methylpropanal | 0.40 | 0.53 | 0.89 | 1.04 |
| Isobutene oxide | 0.09 | 0 | 0.50 | 0.22 |
| Acetone | 0.03 | 0.34 | 0.11 | 0.92 |

[a] The yields of isobutene are corrected for the isobutene impurity in isobutane.

*Addition of NO.* NO addition (6 Torr) produced only small changes in the yields of the products. These were a small overall increase of the nitro compounds (the nitroalkane and nitrite increased while the nitrate decreased slightly) and a slight decrease of isobutene and isobutene oxide. These changes are in accord with the now well-established[16-18] mechanism whereby NO disproportionates to $NO_2$ by multiple addition to alkyl radicals. In this scheme one molecule of nitrosoalkane can lead to the decomposition of several hundred molecules of NO.[17] Thus *tert*-butyl radicals take part, in addition to reactions 10 and 11, also in the reactions[18]

$$(CH_3)_3CNO + 2NO \rightarrow (CH_3)_3C\cdot + N_2 + NO_3 \quad (12)$$

$$NO_3 + NO \rightarrow 2NO_2 \quad (13)$$

This scheme predicts that with increasing NO pressure the yield of the nitrite would increase while that of the nitrate would decrease (as a result of competition between reactions 7 and 8); the yield of the nitroalkane would not be affected or, perhaps, would increase because reactions 10, 12, and 13 regenerate alkyl radicals and $NO_2$; the isobutene yield would decrease (as a result of competition between reactions 11 and 12). The data in Table I are in agreement with these predictions and also the addition of 50 Torr of NO was found to produce, at irradiation times of 30 and

90 min, a large decrease in the isobutene yield (~50–60%) while the nitrobutane yield did not change. It may be concluded, therefore, that the effect of the small amounts of NO formed in reactions 1 and 2 (in the absence of initially added NO) should be governed by the mechanism incorporating reactions 1–11.

*Addition of $O_2$.* $O_2$ addition (5.5 Torr) produced a very pronounced effect on the yields of most of the products (Table II). The nitrites and nitrates increased two- and fivefold, respectively, whereas the nitro compounds remained unaltered, acetone increased eightfold, 2-methylpropanal increased slightly, and isobutene decreased by about 30–40%.

It may be calculated[19] that the extent of the reaction

$$O + O_2 + M \rightarrow O_3 + M \quad (14)$$

is less than 1% of the reactions 2 and 3. It follows, therefore, that radical–$O_3$ reactions can be neglected. The observed effect of $O_2$ on the product yields is fully consistent with the accepted mechanism of interaction of alkyl radicals with $O_2$.[20,21] For the interaction of $t$-$C_4H_9$· with $O_2$, studied by Thomas and Calvert,[22] the following reaction steps may be written:

$$(CH_3)_3C\cdot + O_2 + M \rightarrow (CH_3)_3COO\cdot + M \quad (15)$$

$$2(CH_3)_3COO\cdot \rightarrow 2(CH_3)_3CO\cdot + O_2 \quad (16)$$

$$(CH_3)_3CO\cdot + i\text{-}C_4H_{10} \rightarrow (CH_3)_3COH + (CH_3)_3C\cdot \quad (17)$$

$$(CH_3)_3CO\cdot \rightarrow CH_3COCH_3 + CH_3\cdot \quad (18)$$

From the effects of the $O_2$ addition in Table II it may be concluded that $O_2$ formed in reaction 2 is responsible in part for the formation of the nitrites and nitrates (through reactions 15, 16, 7, and 8), of acetone (reactions 15, 16, and 18), methyl nitrate (from the $CH_3$· radicals formed in reaction 18), and 2-methyl-2-propanol (reactions 15, 16, and 17). The yields of 2-methyl-2-propanol were small and very irregular (ranging from 0.03 to 0.4 μmol). At room temperature it would be expected that reaction 17 would be favored over reaction 18 since the difference in activation energies $E_{18} - E_{17} \approx 7$ kcal/mol[23] ($E_{18} \approx 13$–17 kcal/mol[24]). However, it was shown in blank experiments that the concentration of 2-methyl-2-propanol was affected by dark reactions (2-methyl-2-propanol reacts with $NO_2$ to give mainly the nitrite, and the *tert*-butyl nitrite hydrolyzes in air to give 2-methyl-2-propanol). It is not possible, therefore, to attribute the small 2-methyl-2-propanol yields to any particular reaction.

*Photolysis of Products.* Secondary photolysis of the products by 366-nm light is not important in view of the extremely large absorption coefficient of $NO_2$[25] compared to those of the products.[25]

## Conclusions

The photolysis of $NO_2$–isobutane mixtures is a complex process, with a number of competing reactions occurring simultaneously. The presence of $NO_2$, however, offers some advantage for the elucidation of the mechanism since it can act as a trap for the free radicals initially formed and assist in their identification.

The suggested mechanism explains adequately the observed products and, at least qualitatively, their yields. There is no doubt that the oxidation is initiated by O atoms from the photolysis of $NO_2$ which react with isobutane in a simple manner, i.e., by abstracting mainly the tertiary H atom and to a much smaller extent the primary H atoms to form OH and the corresponding butyl radicals. Further attack on isobutane by the OH radicals so formed gives the same butyl radicals. The butyl radicals react fast with $NO_2$ and also, in competitive reactions, with $O_2$ and NO formed in the process to give nitro compounds, nitrites, nitrates, and isobutene. Some secondary attack of O atoms on isobutene accounts for the minor products.

The more complex mechanisms suggested for the O($^3$P)–alkane reactions,[8-10] mentioned in the Introduction, are, in our opinion, based on experimental observations under conditions in which secondary reactions are very important, i.e., where the ratio [alkane]/[O] is not sufficiently large to suppress very fast atom–radical reactions such as

$$(CH_3)_3C\cdot + O \rightarrow \text{products} \quad (19)$$

$$\cdot OH + O \rightarrow H + O_2 \quad (20)$$

This argument has been developed in more detail previously[26] in connection with the divergent views on the mechanism of the O($^3$P) reaction with acetaldehyde.

## References and Notes


(1) Issued as N.R.C.C. No. 16272.
(2) S. Sato and R. J. Cvetanović, *Can. J. Chem.*, **36**, 970 (1958).
(3) F. E. Blacet, T. C. Hall, and P. A. Leighton, *J. Am. Chem. Soc.*, **84**, 4011 (1962).
(4) H. Yamazaki and R. J. Cvetanović, *J. Chem. Phys.*, **41**, 3703 (1964).
(5) C. Papadopoulos, P. G. Ashmore, and B. J. Tyler, *Symp. (Int.) Combust. [Proc.], 13th*, 281 (1971).
(6) A. B. Harker and C. S. Burton, *Int. J. Chem. Kinet.*, **7**, 907 (1975).
(7) R. E. Huie and J. T. Herron, *Prog. React. Kinet.*, **8**, 1 (1975).
(8) (a) L. I. Avramenko, R. V. Kolesnikova, and N. L. Kuznetsova, *Izv. Akad. Nauk. SSSR, Otd. Khim. Nauk*, 620 (1963); (b) L. I. Avramenko, R. V. Kolesnikova, and G. I. Savinova, *ibid.*, 976 (1963).
(9) (a) F. J. Wright, *J. Chem. Phys.*, **38**, 950 (1963); (b) *Symp. (Int.) Combust. [Proc.], 10th*, 387 (1965).
(10) L. I. Avramenko and R. V. Kolesnikova, *Izv. Akad. Nauk. SSSR, Ser. Khim.*, 2693 (1971).
(11) G. Paraskevopoulos and R. J. Cvetanović, *J. Chromatogr.*, **25**, 479 (1966).
(12) P. Gray, *Trans. Faraday Soc.*, **51**, 1367 (1955), and references therein.
(13) J. W. Kraus and J. G. Calvert, *J. Am. Chem. Soc.*, **79**, 5921 (1957).
(14) (a) R. J. Cvetanović, *Adv. Photochem.*, **1**, 115 (1963); (b) R. J. Cvetanović and L. C. Doyle, unpublished results
(15) D. D. Davis, J. T. Herron, and R. E. Huie, *J. Chem. Phys.*, **58**, 530 (1973).
(16) J. F. Brown, *J. Am. Chem. Soc.*, **79**, 2480 (1957).
(17) M. I. Christie, C. Gilbert, and M. A. Voisey, *J. Chem. Soc.*, 3147 (1964).
(18) M. I. Christie, J. S. Frost, and M. A. Voisey, *Trans. Faraday Soc.*, **61**, 674 (1965).
(19) F. Kaufman and J. R. Kelso, *J. Chem. Phys.*, **46**, 4541 (1967).
(20) J. H. Raley, L. M. Porter, F. F. Rust, and W. E. Vaughan, *J. Am. Chem. Soc.*, **73**, 15 (1951).
(21) E. R. Bell, J. H. Raley, F. F. Rust, F. H. Seybold, and W. E. Vaughan, *Discuss. Faraday Soc.*, **10**, 242 (1951).
(22) S. S. Thomas and J. G. Calvert, *J. Am. Chem. Soc.*, **84**, 4207 (1962).
(23) J. H. T. Brook, *Trans. Faraday Soc.*, **53**, 327 (1957).
(24) (a) P. Gray and A. Williams, *Chem. Rev.*, **59**, 239 (1959); (b) L. Batt and F. R. Cruickshank, *J. Phys. Chem.*, **71**, 1836 (1967); (c) D. M. Golden, R. K. Solly, and S. W. Benson, *J. Phys. Chem.*, **75**, 1333 (1971).
(25) J. G. Calvert and J. N. Pitts, Jr., "Photochemistry", Wiley, New York, N.Y., 1966.
(26) H. E. Avery and R. J. Cvetanović, *J. Chem. Phys.*, **43**, 3727 (1965); **44**, 3150 (1966).

# The Effect of Molecular Structure on the Quenching of the Charge-Transfer Luminescence of Ruthenium(II) Complexes

**Sze-Ming Y. Huang and Harry D. Gafney***

*Department of Chemistry, City University of New York, Queens College, Flushing, New York 11367* *(Received April 18, 1977)*

*Publication costs assisted by the Research Foundation of The City University of New York*

The effect of molecular structure on the quenching of the luminescent charge-transfer state of $Ru(bpy)_3^{2+}$ and $Ru(bpic)_3^{2+}$ has been studied with eight geometric $\beta$-diketonate isomers of Co(III) and Cr(III). The isomers have identical electronic spectra, but differ in their molecular structure. The Co(III) isomers quench at essentially a diffusion-controlled limit, whereas the Cr(III) isomers quench at an order of magnitude less than the theoretical limit. The cis and trans isomers of the Co(III) complexes yield identical Stern–Volmer constants suggesting little or no discrimination during the quenching encounter. A similar lack of discrimination is found with the phenyl substituted Cr(III) complex, $Cr(bzac)_3$. With the trifluoro-substituted analogue, however, *cis*-$Cr(tfac)_3$ is ca. 40% more efficient in quenching than *trans*-$Cr(tfac)_3$.

## Introduction

The expansive growth of mechanistic inorganic photochemistry has created a demand for selective population (sensitization) and depopulation (quenching) as an aid in understanding the chemical behavior of specific excited states. Although this demand has led to an ever-increasing use of sensitization and quenching techniques with transition metal complexes, in many cases the results are ambiguous and have not led to a satisfactory understanding.[1] To a significant extent, the ambiguity with transition metal complexes arises from a lack of understanding of the factors which affect the sensitization or quenching processes. The results which have been obtained with transition metal complexes are often discussed within a framework derived from similar experiments with organic systems. Although the quantum mechanical constraints on the processes are independent of whether the system is organic or inorganic, the observed results may be dependent on several "external" factors characteristic of transition metal complexes. In principle, a number of these external factors, such as charge, nature of the ligand and/or metal, solvent, ionic strength, and molecular structure, might be expected to affect the quenching process. Elucidation of the relative importance of these effects would not only decrease the present uncertainity of many sensitization experiments, but increase our understanding of the quenching and energy transfer phenomena as well.

With the low energy donor $Ru(bpy)_3^{2+}$ (bpy denotes bipyridine), recent studies have shown that quenching by various charged metal complexes is dependent on the ionic strength and suggest a dependence on the geometry of the quencher.[2a] With donors of insufficient energy to populate ligand centered excited states, Wilkinson and Farmilo report a more pronounced dependence on the structure of the quencher due to the involvement of the ligand-field excited states of the quencher.[2b] Unlike organic systems, however, in which alkylation of the chromaphore causes little or no change in the absorption spectrum, changes in the coordination sphere of a transition metal complex causes not only the desired structural changes, but concurrent changes in the electronic structure of the complex as well. Thus a clear distinction between electronic and structural effects on the quenching rate is not currently available.

Although different in their outer structure and dipole moment, the cis and trans geometric isomers of the $\beta$-diketone complexes have identical electronic spectra.[3] These isomers thus offer a unique opportunity to study the effect of molecular structure on the quenching rate. We report the results of an investigation of the quenching of $Ru(bpy)_3^{2+}$ and $Ru(bpic)_3^{2+}$ (bpic denotes 2,2′-bi-4-picoline) by eight geometric $\beta$-diketonate isomers of Cr(III) and Co(III).

## Experimental Section

*Materials.* The ligands 1-phenyl-1,3-butanedione and 1,1,1-trifluoro-2,4-pentanedione were obtained from Eastman Kodak. The complexes tris(1-phenyl-1,3-butanedionate)cobalt(III), $Co(bzac)_3$; tris(1-phenyl-1,3-butanedionate)chromium(III), $Cr(bzac)_3$; tris(1,1,1-trifluoro-2,4-pentanedionate)cobalt(III), $Co(tfac)_3$; and tris(1,1,1-trifluoro-2,4-pentanedionate)chromium(III), $Cr(tfac)_3$, were prepared by the methods of Fay and Piper.[3] The geometric isomers were separated and purified by chromatography on a Florisil column. The electronic, infrared, and NMR spectra and melting points agreed with published data.[3]

$Ru(bpy)_3Cl_2 \cdot 6H_2O$ was obtained from J. T. Baker and used without further purification since its absorption and emission spectra agreed with published spectra.[4] $Ru(bpic)_3Cl_2 \cdot 6H_2O$ was prepared by refluxing 1.73 g (9.4 mmol) of 2,2′-bi-4-picoline (J. T. Baker) and 0.5 g (1.9 mmol) of $RuCl_3 \cdot 3H_2O$ in 200 mL of 95% ethanol. After refluxing for 16 h, the reaction mix was evaporated to dryness. The dark orange-red product was taken up in 75 mL of hot water, the unreacted bipicoline was extracted with four 25-mL portions of benzene, and NaCl was added to the aqueous solution to precipitate the product. After cooling, dark red crystals were filtered off and dried by aspiration. Absorption and emission spectra of the product were essentially identical with that of $Ru(bpy)_3^{2+}$.

*Luminescence Measurements.* Luminescence measurements were carried out at room temperature, 23–24 °C, in a Perkin-Elmer Hitachi MPF-2A emission spectrophotometer equipped with either a Hamamatsu R106 or a red sensitive Hamamatsu R818 photomultiplier. All samples were contained in quartz cuvettes equipped with degassing bulbs and degassed by three freeze–thaw cycles.

To determine the uncertainity associated with the transmission characteristics of the different cells as well as the various pairs of cell faces, the emission intensity of a degassed ethanol solution containing $10^{-4}$ M $Ru(bpy)_3^{2+}$ was measured at 588 nm. The maximum difference be-

TABLE I: Energies of the Relevant Donor and Quencher States, Stern-Volmer Quenching Constants, and Bimolecular Rate Constants

| Complex | Energy, $\mu m^{-1}$ | $K_{SV}$,[a] $M^{-1}$ | $k_b$,[b] $M^{-1}$ $s^{-1}$ | $K_{SV}$,[c] $M^{-1}$ |
|---|---|---|---|---|
| $Ru(bpy)_3^{2+}$ | 1.80 | | | |
| $Ru(bpic)_3^{2+}$ | 1.83 ± 0.03 | | | |
| *cis*-$Co(tfac)_3$ | 1.37 | 1428 ± 260 | $1.8 \times 10^9$ | 1584 ± 182 |
| *trans*-$Co(tfac)_3$ | 1.37 | 1386 ± 221 | $1.8 \times 10^9$ | 1406 ± 126 |
| *cis*-$Co(bzac)_3$ | 1.37 | 885 ± 112 | $1.1 \times 10^9$ | 792 ± 99 |
| *trans*-$Co(bzac)_3$ | 1.37 | 871 ± 115 | $1.1 \times 10^9$ | 796 ± 101 |
| *cis*-$Cr(tfac)_3$ | 1.44(1.234)[e] | 281 ± 29(199 ± 65)[d] | $3.6 \times 10^8$ | 243 ± 22 |
| *trans*-$Cr(tfac)_3$ | 1.40(1.234)[e] | 201 ± 24(200 ± 55)[d] | $2.5 \times 10^8$ | 176 ± 24 |
| *cis*-$Cr(bzac)_3$ | 1.42(1.242)[e] | 669 ± 149 | $8.5 \times 10^8$ | 486 ± 55 |
| *trans*-$Cr(bzac)_3$ | 1.42(1.242)[e] | 498 ± 63 | $6.3 \times 10^8$ | 539 ± 45 |

[a] Obtained for the quenching of $Ru(bpy)_3^{2+}$. [b] Obtained from the average $K_{SV}$ for the quenching of $Ru(bpy)_3^{2+}$ and the lifetime of $Ru(bpy)_3^{2+}$ in absolute ethanol, 790 ns. [c] Obtained for the quenching of $Ru(bpic)_3^{2+}$. [d] Measured in a 40% (by volume) formamide–ethanol solution. [e] Energy of the $^2E$ state, P. Fleischauer and P. Fleischauer, *Chem. Rev.*, **70**, 199 (1970).

tween the cells and pairs of cell faces was 18%. To minimize this uncertainity, all measurements were made with specific pairs of faces of the different cells so that the maximum uncertainity was 8.1%.

Samples containing $Ru(bpy)_3^{2+}$ were excited at 452 nm and the emission intensity monitored at 588 nm. With $Ru(bpic)_3^{2+}$, the samples were excited at 460 nm and the emission monitored at 590 nm. The observed emission intensities were corrected for trival reabsorption with previously described equations.[5] Although these equations involve approximations, it is important to realize that the absorption spectra of both isomers are identical at the excitation and emission wavelengths. Thus potential differences in the Stern–Volmer constants, $K_{SV}$, obtained with each pair of isomers are not tainted by these corrections. With the trifluoroacetylacetonate chelates, absolute ethanol was used as the solvent. The benzoylacetonate chelates, however, are only slightly soluble in ethanol and it was necessary to use 10% chloroform (by volume) in ethanol as the solvent. We have observed that chloroform solutions of $Ru(bpy)_3^{2+}$ change color from red-orange to purple when allowed to stand for 3–4 days. In 10% chloroform–ethanol solutions, however, spectra of a $10^{-4}$ M $Ru(bpy)_3^{2+}$ solution recorded periodically showed no detectable change over a 3-h period. Nor was any change in the emission intensity of the solution detected over the same time period.

To determine whether any sensitized decomposition of the quenchers occurred, a number of steady-state and flash photolysis experiments were carried out. The apparatus used in these experiments has been previously described.[6]

## Results and Discussion

Since its introduction as a photosensitizer,[7] $Ru(bpy)_3^{2+}$, has been the subject of a number of photochemical and quenching studies. In a recent extensive study, Demas and Addington have pointed out that catalytic deactivation of $*Ru(bipy)_3^{2+}$ induced by either the spin–orbit coupling or paramagnetism of a first transition series metal complex is unlikely, and quenching occurs by a bimolecular process leading to energy transfer or electron transfer.[8]

In absolute ethanol, the luminescence maxima of $Ru(bpy)_3^{2+}$ and $Ru(bpic)_3^{2+}$ are observed at 588 and 590 nm, respectively. The energies of the thermally equilibrated states, listed in Table I, were estimated by the Fleischauer–Adamson criteria applied to the short wavelength tail of the emission band.[9] The ultraviolet spectra of these Cr(III) and Co(III) isomers are dominated by intense ligand $\pi$–$\pi^*$ and charge transfer transitions.[10] The high energies, $\geq 3.0\ \mu m^{-1}$, of these states, however, suggest little involvement in the quenching of these low energy Ru(II) complexes. A number of studies have illustrated the role of lower energy ligand triplet states in intramolecular energy transfer processes.[11] A phosphorescence, characteristic of the anionic form of the ligand, is observed in the low temperature emission spectra of the corresponding alkali metal salts and the La(III) and Gd(III) complexes.[12] The maxima of the phosphorescence occurs at ca. 450 nm indicating that these states lie at energies $\geq 2.2\ \mu m^{-1}$. Thus, on energetic grounds, quenching of these low energy Ru(II) donors by an energy transfer mechanism is limited to population of the lower energy ligand-field states of these Co(III) and Cr(III) isomers. The energies of these thermally equilibrated ligand-field states, also estimated by the Fleischauer–Adamson criteria, are summarized in Table I.

The values of the $K_{SV}$'s listed in Table I were obtained from least-squares analyses of plots of $(I_0/I)_{corr}$ as a function of the concentration of the isomer. With the exception of the experiments in ethanol–water mixtures, the plots for each isomer studied were found to be linear through ca. 70% quenching. The linearity of the plots as well as difference spectra, which yielded no evidence of an association between the donor and the quencher, indicates that quenching occurs by a collisional process. As expected with uncharged quenchers, the $K_{SV}$'s were found to be independent of added electrolyte (0.01 M LiCl).

The bimolecular rate constants, $k_b$, listed in Table I are obtained from the measured $K_{SV}$ values and the radiative lifetime of $*Ru(bpy)_3^{2+}$ in deareated absolute ethanol, 790 ns.[13] Assuming the Stokes' radii and interaction radii are equal, the Einstein–Smoluchowski theory yields a theoretical limit of $5.5 \times 10^9$ $M^{-1}$ $s^{-1}$ for $k_b$ in ethanol at 25 °C.[14] The Co(III) isomers quench at slightly less than the theoretical diffusion-controlled rate and, within experimental error, yield $K_{SV}$'s which are identical. This equality, which is also observed with the slightly more hindered $Ru(bpic)_3^{2+}$ suggests little or no discrimination on the basis of molecular structure or dipole moment during the quenching encounter. Alternatively, the lack of discrimination may be due to the leveling effect of the rate of diffusion.

With the Cr(III) isomers, however, the values of $k_b$ are less than the theoretical limit suggesting that barriers exist and a number of collisions are requisite to achieve a set of requirements for quenching to occur. Under these conditions, some discrimination of the isomeric forms of $Cr(tfac)_3$ occurs, but not of the isomeric forms of $Cr(bzac)_3$. The $K_{SV}$ of *cis*-$Cr(tfac)_3$ is 1.4 ± 0.3 larger than that of the trans isomer. This difference, which is found with both donors, is frustratingly small, but is similar to that previously reported for the cis and trans isomers of Cr-

$(en)_2Cl_2^+$.[2a] The difference in the $K_{SV}$'s was not affected by the addition of an electrolyte, 0.01 M LiCl, but is dependent on the solvent medium. Although solubilities limit the solvents which could be used, a number of measurements were made in mixed solvents. Increasing the solvent dielectric constant by the addition of formamide, 40% by volume, led to an elimination of the difference. The $K_{SV}$'s of the cis and trans isomers were then identical within experimental error. Increasing the solvent dielectric by adding water to ethanol, 30% by volume, caused a substantial change in behavior. The Stern–Volmer plots were nonlinear showing a distinct upward curvature for concentrations of *cis*- or *trans*-$Cr(tfac)_3$ greater than $10^{-3}$ M. The initial slopes, less than 25% quenchng, were different, but must be judged with caution since an associative mechanism cannot be ruled out.[15]

Concealment of a potential difference in the quenching efficiency by either a thermal[16] or photochemical[17] isomerization during the preparation or measurement of the samples appears unlikely. The $K_{SV}$'s obtained from degassed samples stored in the dark for 1 h prior to measurement were within experimental error of the $K_{SV}$'s obtained from equivalent samples measured immediately after preparation and deaeration. The emission intensity of samples $10^{-3}$ M in the isomers and $10^{-4}$ M in $Ru(bpy)_3^{2+}$ (ca. 80% of the light is absorbed by $Ru(bpy)_3^{2+}$) was also found to be independent of the time of exposure, 10 min, to the exciting light of the emission spectrophotometer.

Although not conclusive, the differences in the quenching efficiencies of the Co(III) and Cr(III) complexes do suggest different quenching mechanisms. With the Cr(III) substrates, $Cr(tfac)_3$ is more efficient than $Cr(bzac)_3$. With the Co(III) substrates, the order is inverted and a number of steady state and flash photolysis experiments were carried out in an attempt to elucidate the quenching mechanism. Ethanol solutions $10^{-3}$ M in $Co(tfac)_3$ or $Co(bzac)_3$ and $10^{-4}$ M in $Ru(bpy)_3^{2+}$ were photolyzed at 452 nm, but Co(II) was not detected in the photolyte, $\phi_{Co(II)} \leq 10^{-3}$. Nor were we able to detect, following flash photolysis (250 J), a transient lasting longer than 20 $\mu$s at 675 nm, the absorption maximum of $Ru(bpy)_3^{3+}$,[18] or in the 480–550-nm region, an absorption band of $Co(acac)_2$.[19] These results are inconclusive, however, since quenching by electron transfer could be followed by a rapid reverse reaction leading to no net chemical change.[20]

Independent of the question of intimate mechanism, we find these results somewhat surprising since a bimolecular collision which involves ligand-field states might be expected, a priori, to be susceptible to structural differences. For example, the rate constant for quenching of a triplet donor by $Fe(acac)_3$ is 6.1 times larger than that of $Fe(dpm)_3$[21] when energy transfer to a ligand field state occurs, but the ratio decreases to 3.2 when energy transfer to an internal ligand state occurs. Also, the differences in the quenching efficiency of the cis and trans isomers of $Cr(en)_2X_2^+$ and $Cr(en)_2XY^+$ led to the suggestion that geometric factors play some role in determining quenching efficiency.[2a] Although this suggested structural dependence is somewhat clouded due to the differences in the electronic structure of the isomers, the importance of steric hinderence is indicated in the quenching of organic triplets by the higher efficiency of acetylacetonate complexes as compared to dipivaloylmethanate complexes.[2b,22] The difference in the quenching efficiency found with the latter complexes is substantially larger than that found in these experiments. With these geometric isomers, however, the molecular size is essentially the same and the structural difference arises from the complex as a whole. If quenching reflects a specific part of the complex, the lack of any apparent discrimination of the $Cr(bzac)_3$ isomers may reflect an extension of the "conducting ability"[23] of the ligand through the inductively coupled phenyl substituent. With the $Cr(tfac)_3$ isomers, the "conducting" region is not as extensive. A more intimate encounter would be required and the difference in the $K_{SV}$'s may reflect the differences in the molecular structure of the isomers. We doubt that the difference is due to differences in their diffusion rates. If this were the case, the similarity in the formal charge and size of the $Co(tfac)_3$ and $Cr(tfac)_3$ would suggest similar differences in the quenching efficiencies of the Co(III) isomers, yet none is observed.

Intuitively a structural dependence is expected, yet our results, at least with these Co(III) isomers and the $Cr(bzac)_3$ isomers, and those of Wilkinson[24] indicate that such a dependence can be small or nonexistant.

*Acknowledgment.* Financial support of this research from the Research Corporation and the Research Foundation of The City University of New York is gratefully acknowledged.

## References and Notes

(1) V. Balzani, L. Moggi, M. F. Manfrin, F. Bolletta, and G. S. Laurence, *Coord. Chem. Rev.*, **15**, 321 (1975), and references therein.
(2) (a) F. Bolletta, M. Mastri, L. Moggi, and V. Balzani, *J. Am. Chem. Soc.*, **95**, 7864 (1973); (b) F. Wilkinson and A. Farmilo, *J. Chem. Soc., Faraday Trans. 2*, 604 (1976).
(3) R. C. Fay and T. S. Piper, *J. Am. Chem. Soc.*, **84**, 2303 (1962); **85**, 500 (1963).
(4) J. N. Demas and G. A. Crosby, *J. Am. Chem. Soc.*, **93**, 2841 (1971).
(5) (a) J. N. Demas and A. W. Adamson, *J. Am. Chem. Soc.*, **95**, 5159 (1973); (b) G. Navon and N. Sutin, *Inorg. Chem.*, **13**, 2159 (1974).
(6) M. Katz and H. D. Gafney, *Inorg. Chem.*, submitted for publication.
(7) J. N. Demas and A. W. Adamson, *J. Am. Chem. Soc.*, **93**, 1800 (1971).
(8) J. N. Demas and J. W. Addington, *J. Am. Chem. Soc.*, **98**, 5800 (1976).
(9) P. D. Fleischauer, A. W. Adamson, and G. Satori, "Inorganic Reaction Mechanisms", Part II, J. O. Edwards, Ed., Wiley, New York, N.Y., 1972.
(10) (a) I. Hanajaki, F. Hanajaki, and S. Nagakura, *J. Chem. Phys.*, **50**, 265, 276 (1969); (b) D. W. Barnum, *J. Inorg. Nucl. Chem.*, **21**, 221 (1961).
(11) G. A. Crosby, *Mol. Cryst.*, **1**, 37 (1966), and references therein.
(12) (a) H. D. Gafney, Ph.D. Thesis, Wayne State University, 1970. (b) J. S. Brinen, F. Halverston, and J. R. Leto, *J. Chem. Phys.*, **42**, 4213 (1965); (c) G. A. Crosby, R. E. Whan, and R. M. Alire, *ibid.*, **34**, 743 (1961).
(13) J. N. Demas, private communication.
(14) J. B. Birks, "Photophysics of Aromatic Molecules", Wiley-Interscience New York, N.Y., 1970, p 312.
(15) J. N. Demas and J. W. Addington, *J. Am. Chem. Soc.*, **96**, 3663 (1974).
(16) A. Y. Girgis and R. C. Fay, *J. Am. Chem. Soc.*, **92**, 7061 (1970), and references therein.
(17) (a) R. D. Koob, J. Bensen, S. Anderson, D. Gerber, S. P. Pappas, and M. L. Morris, *Chem. Commun.*, 966 (1972); (b) H. D. Gafney, unpublished observations.
(18) C. Creutz and N. Sutin, *Proc. Natl. Acad. Sci. U.S.A.*, **72**, 2858 (1975).
(19) F. A. Cotton, and R. H. Soderberg, *Inorg. Chem.*, 3, 1 (1964).
(20) R. C. Young, F. R. Keene, and T. J. Meyer, *J. Am. Chem. Soc.*, **99**, 2468 (1977), and references therein.
(21) $Fe(dpm)_3$ designates tris(dipivaloylmethanato)iron(III).
(22) G. S. Hammond and R. P. Foss, *J. Phys. Chem.*, **68**, 3739 (1964).
(23) A. Pfiel, *J. Am. Chem. Soc.*, **93**, 5359 (1971).
(24) A. Adamczyk and F. Wilkinson, *J. Chem. Soc., Faraday Trans. 2*, **68**, 2031 (1972).

# Ionic and Neutral Species Detected by Mass Spectrometry in a Radio-Frequency Discharge of Tetrafluoroethylene

**M. J. Vasile and G. Smolinsky***

*Bell Laboratories, Murray Hill, New Jersey 07974* *(Received May 31, 1977)*

*Publication costs assisted by Bell Laboratories*

The chemistry of the radio-frequency discharge of $C_2F_4$ is dominated by the production of neutral gas phase species and polymeric deposits on the electrodes and walls of the discharge vessel. Ionic species observed in the discharge are characteristic of electron impact ionization of $C_2F_4$ and the neutral products: $C_2F_6$, $C_3F_6$, $C_3F_8$, and $C_4F_8$. In contrast to discharges of hydrocarbons, ion–molecule reactions are not a dominant feature of the $C_2F_4$ discharge. Appearance potential measurements gave direct evidence for the effusion of $CF_2$ radicals from the discharge, but not for CF or $CF_3$ radicals. At pressures above 0.1 Torr, small fragments of the polymer were sputtered and showed in the discharge as $C^+$, $CF^+$, and $CF_2^+$ ions. Sputtering of the discharge-produced polymer with xenon gave the ions $C^+$, $CF^+$, $CF_2^+$, and $CF_3^+$ by charge exchange, with no detectable buildup of the corresponding neutral fragments.

## Introduction

Organic chemical vapors are converted to polymeric material when subjected to an rf discharge. This is true whether or not the compound in question possesses unsaturated bonds. Thus polymers have been prepared from straight-chain hydrocarbons as well as from cyclic, aromatic, and unsaturated compounds. In order better to understand the chemistry of a reactive gas discharge and perhaps gain insight into the polymerization process, we had made mass-spectrometric studies of the ionic and neutral species present in discharges of vinyltrimethylsilane,[1] methane,[2] ethane,[3] ethylene,[4] acetylene,[5] and benzene.[6] In brief, the following held true for all the above compounds: The most energetic process occurred in the sheath between the plasma and rf electrode. In addition, more fragmentation into radicals and ions occurred in this region than in other places in the discharge chamber. This observation correlated with a higher rate of polymer deposition on the electrodes than on the reactor walls.[7] Moreover, low energy paths to ionization are important, i.e., radical species often were intermediates in the ionization process. For benzene,[6] isomerization to fulvene and benzvalene occurred, a process which required electron energies several volts below the first ionization level. In every case, under conditions of high plasma density where polymer formation is most rapid, molecular hydrogen was detected as an appreciable fraction of the neutral molecules along with unsaturated derivatives of the starting material. An important difference observed between the ion chemistry of saturated molecules such as methane and ethane, and the unsaturated compounds ethylene, acetylene, and benzene, was the role of $\pi$-complexed-cationic intermediates. To a large extent, the fate of these complexes determined the ion chemistry. The degree of stabilization of the complex was directly proportional to the pressure and inversely proportional to the power.

Usually glow discharge polymerization results in amorphous, clear, adherent films which are chemically inert and possess thermal stability as well as high electrical resistance. Conventionally prepared polytetrafluoroethylene (PTFE) also possesses chemical and thermal stability and high electrical resistance. No doubt, the latent advantageous properties of a glow discharge produced tetrafluoroethylene ($C_2F_4$) polymer film has stimulated the investigation of the production of such a potentially useful material.

An early study of $C_2F_4$-discharge polymers dealt with apparatus configuration and experimental parameters.[8] Infrared studies revealed the presence of carbonyl groups in the polymer. As expected there are similarities between a spectrum of PTFE and that of $C_2F_4$-glow polymer. In other work,[9] it was shown that PTFE could be easily sputtered. An argon discharge was used to initiate the sputtering process. However, after several minutes the flow of inert gas could be turned-off but the sputtering would continue, sustained, apparently by the sputter-produced ions. The infrared spectra and dynamic electrical properties of films formed from sputtered PTFE and plasma polymerized $C_2F_4$ proved to be essentially identical.[10] Plasma polymerization rates for $C_2F_4$ and ethylene were also found to be comparable.[11]

An x-ray photoelectron spectrometry (XPS) study[12] of inductively coupled, electrodeless, rf-discharge-produced $C_2F_4$ films was quite indicative of what happened during polymer deposition. Polymer films prepared in the plasma zone and down stream from this luminous region were investigated. A lower fluorine atom content and more different kinds of carbon bonding were found in films produced in the plasma zone than in films produced down stream. Down-stream films consisted mainly of $CF_3$ and $CF_2$ groups while plasma-zone films contained about equal numbers of carbon atoms bonded to three, two, one, and zero fluorine atoms, respectively. The latter films were clearly more highly cross linked. Subjection of down-stream films to an argon discharge changed the XPS results so as to look more like that gathered with plasma-zone film, i.e., cross linking was increased. The infrared spectra of the films deposited in the two regions were also different: Plasma-zone polymer presented a diffuse spectrum while down-stream films had a spectrum resembling that of PTFE. In addition, the surface tension of down-stream film was very low, a fact consistent with the XPS finding of a high $CF_3$-group concentration.

In this paper we will report on the neutral and ionic species produced from $C_2F_4$ during plasma–polymer deposition and sputtering of the deposited film with xenon. As an aid in explaining the observed ion chemistry, use will be made of the literature on the photochemistry and high pressure mass spectrometry of $C_2F_4$.

## Experimental Section

Figure 1 shows a schematic representation of the ex-

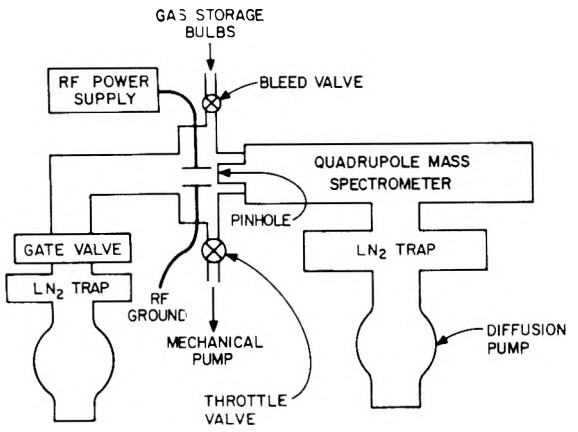


**Figure 1.** Schematic of the experimental equipment.

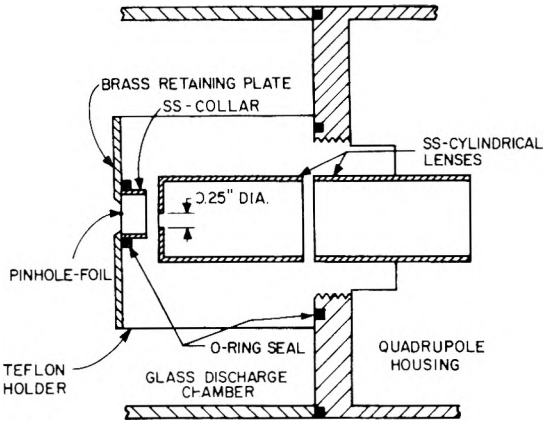


**Figure 2.** Schematic of the sampling orifice and electrostatic focusing lenses.

perimental equipment. The stainless-steel quadrupole housing was fitted with an ion gauge while the 4-in. o.d., glass-pipe discharge chamber was fitted with both an ion gauge and capacitance monometer. Viton O-rings were used to seal the glass discharge tube to the quadrupole housing. Vacua of $4 \times 10^{-9}$ and $3 \times 10^{-8}$ Torr were routinely obtained in the quadrupole housing and discharge tube, respectively. Two-inch diameter brass electrodes were mounted on the ends of 0.25-in. brass rods held in position by O-ring pressure fittings. The electrodes were freely adjustable as to spacing (maintained at about 4 cm) and distance to the sampling orifice (the face of the rf active electrode was positioned about 2 mm from the pinhole). Power from a 13.56-MHz radio-frequency generator was supplied to one of the electrodes through an impedance-matching network. The peak-to-peak (p–p) voltage on the electrodes was usually maintained at 200 V in these experiments and was monitored with an oscilloscope.

Figure 2 shows the detail of the sampling orifice and electrostatic focusing lens mounting. The electrical potential relative to ground of the pinhole assembly (retaining plate, foil, and collar) and each cylinder lens could be continuously varied over several hundred volts dc. Adjustment of the potentials was made to give a maximum ion flux or a zero ion flux if neutral species were being examined. The pinhole (0.002 in. diameter) was laser machined in a 0.001 in. nickel foil and held an axis with the quadrupole rods by means of a 2 in. o.d. polyfluorocarbon cylinder. The approximate dimensions of the SS-collar were 0.5-in. i.d. × 0.3-in. long and those of the lenses 1-in. i.d. × 1.8-in. long. The opening of the lens nearest the pinhole was closed down to 0.25-in. by means of a stainless-steel cap.

**TABLE I: Percent Ion Current from 20-eV Electron Impact on TFE and Neutrals Present in a 0.2 Torr, 200 V, p-p TFE Discharge**

| | | % of total ion current | |
|---|---|---|---|
| *m/e* | Assignment | Disch off | Disch on |
| 31 | $CF^+$ | 12.5 | 13.6 |
| 50 | $CF_2^+$ | 13.4 | 15.8 |
| 69 | $CF_3^+$ | 4.1 | 18.3 |
| 81 | $C_2F_3^+$ | 13.9 | 9.8 |
| 100 | $C_2F_4^+$ | 55 | 34.4 |
| 62 | $C_2F_2^+$ | | 1.5 |
| 93 | $C_3F_3^+$ | | 0.8 |
| 112 | $C_3F_4^+$ | | 0.8 |
| 119 | $C_2F_5^+$ | | 1.9 |
| 131 | $C_3F_5^+$ | | 2.0 |
| 143 | $C_4F_5^+$ | | 0.3 |
| 150 | $C_3F_6^+$ | | 0.6 |
| 169 | $C_3F_7^+$ | | 0.1 |

In order to remove water or other contaminants, reactant gases flowed from the storage bulbs to the bleed valve via a U-tube immersed in a suitable coolant. Commercially available tetrafluoroethylene was obtained from PCR, Inc., and contained a polymerization inhibitor, limonene. Xenon was research purity grade obtained from Matheson Gas Products.

The quadrupole mass filter and associated electronics were standard commercial products. Data collection was automated by means of A/D converters and a programmable desk-top calculator. Mass spectra were taken at a rate of about 1 amu/s. After completion of a spectrum, the mass number and associated absolute and relative peak height for each atomic mass unit above a preset background level were calculated and printed.

Before making observations with the above-described apparatus, all the inside surfaces of the reactor were coated with a plasma-polymerized tetrafluoroethylene film. This was done to avoid any possible complications in the observed species due to the interaction of the glass walls with fluorine containing species.

Neutral species identification was made by ionizing the products effusing from the discharge tube (with 20-V electrons) after the ions had been repelled. The 20-eV mass spectra of the following list of perfluoro compounds were taken on our spectrometer for the sake of instrumental consistency: ethylene, $C_2F_4$; ethane, $C_2F_6$; propene, $C_3F_6$; propane, $C_3F_8$; and cyclobutane, c-$C_4F_8$.

## Results and Discussion

A 200-V, p–p, $C_2F_4$ discharge is blue in color, with the glow filling most of the reactor volume at a pressure below 0.1 Torr. Above this pressure, the luminous region is confined to a relatively small zone surrounding the electrodes. Strong ion currents were detected over a wide pressure range, but only below 0.1 Torr was it possible to observe the primary ionic process, relatively uncontaminated with ions that were later identified as originating from a sputtering process.

*$C_2F_4$ Neutrals.* Table I shows a comparison of the mass spectra obtained from $C_2F_4$ by conventional electron impact with 20-eV electrons, and the 20-eV spectrum of the neutral species formed in a 0.21 Torr, 200-V, p–p $C_2F_4$ discharge. While there are pronounced differences, these are not inexplicable. The mass spectrum observed with the discharge on is the sum of the 20-eV spectra of the unreacted $C_2F_4$ and those of the neutral-product gases in the reactor. In contrast to discharges in hydrocarbon systems, the $C_2F_4$ discharge apparently has a high yield of gaseous products as well as polymer. The most probable of these products are hexafluoroethane ($C_2F_6$), hexa-

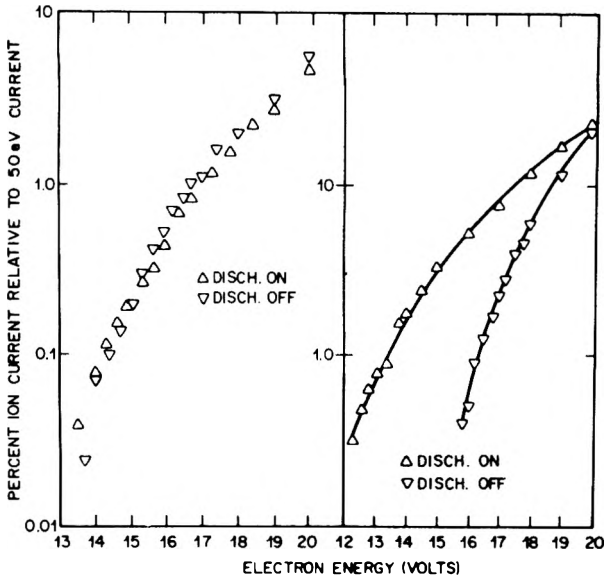


**Figure 3.** Semilogrithmic plot of the intensities of $CF^+$ (left side) and $CF_2^+$ (right side) as a function of electron energy: (△) from a 200 V, p–p, 0.2 Torr $C_2F_4$ discharge.

fluorocyclopropane (c-$C_3F_6$), hexafluoropropene ($C_3F_6$), octafluoropropane ($C_3F_8$), and octafluorocyclobutane (c-$C_4F_8$). No evidence could be found for the effusion of HF, or atomic or molecular fluorine from the discharge. The absence of the latter two species may be due to a very low steady-state concentration. Both would be expected as reaction by-products, but their rate of reactivity in the discharge environment must be very high. All of the ions observed with the discharge on, except for $C_2F_2^+$ and $C_3F_3^+$, could be accounted for with the cracking patterns of the above neutral products. The $C_2F_2^+$ ion may be the parent ion of difluoroacetylene, which is a product of the direct photolysis[13] (6.7 eV) of $C_2F_4$. Any vibrationally excited $C_3F_6$ or c-$C_3F_6$ formed by the reaction of $CF_2$ with $C_2F_4$ near the sampling point may also yield both $C_2F_2^+$ and $C_3F_3^+$. Mass spectra taken on our instrument at 50 eV showed $C_3F_3^+$ and $C_2F_2^+$ fragment ions from $C_3F_6$ at 1.5% of the total ionization. Similarly, $C_3F_3^+$ and $C_2F_2^+$ are reported in the 75-eV mass spectra[14] of c-$C_3F_6$.

The presence of the $C_3$ and $C_4$ molecules in the discharge is inferred from the following evidence: Observation of the $C_3F_6^+$ ion in the neutral spectrum (Table I) indicates the presence of $C_3F_6$ in the discharge since the parent ion is well represented in its 20-eV impact spectrum. The ratio of the intensities of the ion, $C_3F_5^+$, and parent ion taken on our instrument from a sample of $C_3F_6$ was unity. In Table I, the ratio of these intensities for the gases effusing from the discharge chamber is 3.3, indicating additional sources of the $C_3F_5^+$ ion, assumedly from c-$C_3F_6$ and c-$C_4F_8$. The parent ion from either of these compounds is essentially nonexistent; the first ion readily observed[14] being $C_3F_5^+$. The $C_3F_7^+$ ion is tantamount to $C_3F_8$, which like other saturated fluorocarbons shows no parent ion in its electron-impact spectrum. Although the linear $C_3F_8$ molecule fragments at 20 eV to a $C_2F_5^+$ ion, the ratio of the intensities of the two daughter ions, $C_2F_5^+$:$C_3F_7^+$, is only about 4:1. In Table I, the value of the intensity ratios is seen to be about 19, pointing to another source for $C_2F_5^+$, which is most certainly the $M - 19$ fragment ion from the $C_2F_6$ molecule. The latter also shows no parent ion in its 20-eV spectrum.

The literature on the photolysis of $C_2F_4$ can explain the presence of all the $C_3$ and $C_4$ molecules found in the discharge. Mercury-sensitized photolysis[15] demonstrated the low energy (4.8 eV) at which the $C_2F_4$ molecule cleaves to difluorocarbene. Chemically, the $CF_2$ radical is relatively inert,[16] but it does react with $C_2F_4$ under these conditions to give c-$C_3F_6$. Direct photolysis[13] of $C_2F_4$ with 6.7-eV (1849 nm) radiation produced high yields of each of the $C_3$ and $C_4$ molecules for which we found evidence in the discharge, as well as a high yield of $C_2F_6$. Photolysis of $C_2F_4$ always produced $C_2F_2$ and polymer as well.[13] The consistency of the results deduced by mass spectrometric examination of the gases in the discharge tube, and the results of photolysis lead to the conclusion that the neutral chemistry in the discharge tube is dominated by a few simple reactions:

$$C_2F_4 \xrightarrow{e^-} 2CF_2 \quad (1)$$

$$CF_2 + C_2F_4 \rightarrow \text{c-}C_3F_6^* \xrightarrow{M} \begin{cases} \text{c-}C_3F_6 \\ \text{n-}C_3F_6 \end{cases}$$

$$C_2F_4^* + C_2F_4 \rightarrow \text{c-}C_4F_8^* \xrightarrow{M} \text{c-}C_4F_8 \quad (2)$$

$$C_2F_4 \xrightarrow{e^-} C_2F_2 + 2F\ \{F_2\} \quad (3)$$

$$C_2F_4 \xrightarrow{e^-} C_2F_3 + F$$

$$\text{n-}C_3F_6 + F_2 \rightarrow C_3F_8 \quad (4)$$

$$C_2F_4 + F_2 \rightarrow C_2F_6 \quad (5)$$

*Radical Species.* The relative intensities of $CF^+$, $CF_2^+$, and $CF_3^+$ with the discharge on (Table I) seemed to be higher than one might expect from 20-eV ionization, and suggested radical effusion from the discharge. Therefore, an attempt was made to justify the production of these three fragment ions by calculating the fractional contribution made to the observed spectrum by each of the molecular species present in the discharge. In this way, the relative intensities of $CF^+$ and $CF_3^+$ could be accounted for, but only about 70% of the $CF_2^+$ intensity was accounted for. The excess was postulated to result from ionization of $CF_2$ radicals effusing directly from the discharge. Confirmation was obtained from a measurement of the appearance potentials under electron impact of the three fragment ions with the discharge on and off. Figures 3 and 4 show semilog plots of intensities as a function of electron energy in volts. In each case the plotted intensity was calculated relative to the intensity obtained under comparable conditions using 50-V electrons.

*$CF^+$.* The appearance potentials of the $CF^+$ ion from $C_2F_4$ or other molecular precursors found as products in the discharge are between 14 and 18 eV.[17] The ionization potential of the CF radical is between 9 and 10 eV.[18] Figure 3A shows the ionization efficiency curve of $CF^+$ with the discharge on, and the appearance potential curve of $CF^+$ from $C_2F_4$ with no discharge. These two curves are essentially the same, and hence there is no appreciable flux of CF radicals from the discharge.

*$CF_2^+$.* Figure 3B definitely shows that the ionization efficiency curve for $CF_2^+$ has a threshold value at least 3 eV lower with the discharge on than the appearance potential curve of $CF_2^+$ from $C_2F_4$ with no discharge. The ionization potential[17] of the $CF_2$ radical is 11.7 eV, and the appearance potential of $CF_2^+$ from $C_2F_4$ is 15.2 eV, a difference of 3.5 eV. The data presented in Figure 3B are in very good agreement with these values, and can be taken as direct evidence for the effusion of $CF_2$ radicals from the discharge.

*$CF_3^+$.* The energy dependence of the $CF_3^+$ ion derived from $C_2F_4$ is known to be anomolous,[19] and indeed a comparison between the ionization efficiency curve of $CF_3^+$ with the discharge on and that of $CF_3^+$ from $C_2F_4$ with the

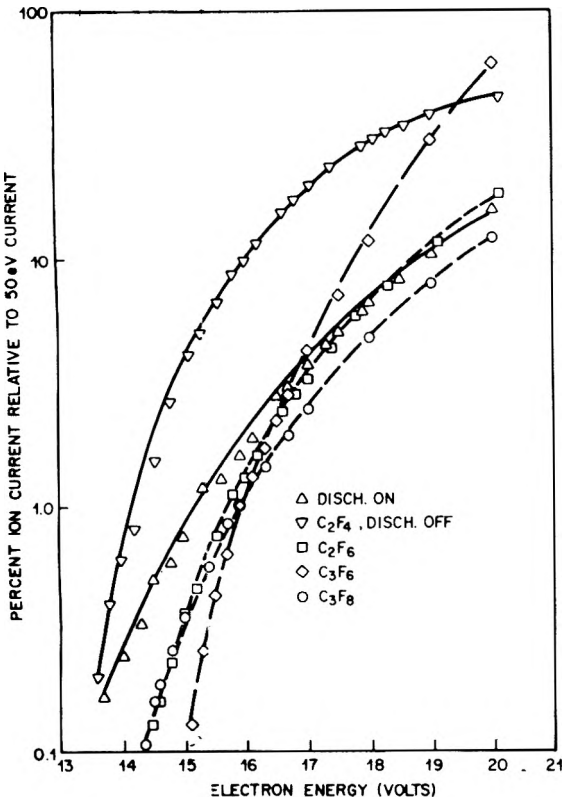


**Figure 4.** Semilogrithmic plot of the intensity of the $CF_3^+$ ion as a function of electron energy: (△) from a 200 V, p-p, 0.2 Torr discharge. The other curves are for $CF_3^+$ from several compounds in the absence of a discharge.

discharge off was not as straightforward as the $CF_2^+$ or $CF^+$ case. This is not surprising, since $CF_3^+$ is a minor component in the mass spectrum of $C_2F_4$ at any energy, while the $CF_3^+$ intensity in the mass spectra of the neutral species produced with the discharge on is large, even at 20 eV. We thus compared the ionization efficiency curves for $CF_3^+$, discharge on, to those obtained from $C_2F_6$, $C_3F_6$, and $C_3F_8$, with no discharge. Figure 4 shows that the appearance potential curve for $CF_3^+$ with the discharge on follows the curves derived from $C_2F_6$ and $C_3F_8$ at relatively high energies (17–20 eV), while below ~17 eV, the curve approaches that of $C_2F_4$ with the discharge off. The shape of the discharge-on curve is consistent with $C_2F_6$, $C_2F_6$, etc. being the principal source of $CF_3^+$ at 20-eV ionization energy, and with $C_2F_4$ being the principal source in the threshold region. The reported appearance potentials,[17] in electron volts, of $CF_3^+$ from various precursors are as follows: $C_2F_4$, 13.5–14.4; $C_2F_6$, 14.2; $C_3F_6$, 15–16; $C_3F_8$, 14.4–14.7. There is no evidence for any contribution to the $CF_3^+$ signal from $CF_3$ radicals, since no shift in the ionization efficiency curve toward the 10-eV level was found in the threshold region.

*Ion Chemistry.* The ion–molecule reactions of $C_2F_4$ and its fragment ions have been studied by high pressure mass spectrometry[20] and ion cyclotron resonance.[21] In general, the ionic reactions in this system are not rapid unless they involve fragment ions produced by high energy electron impact (e.g., $C^+$, $F^+$, $C_2F^+$, and $C_2F_2^+$). According to the high pressure mass spectrometer (HPMS) study ion–molecule reaction products are to be expected in the discharge from $CF_2^+$ and $C_2F_3^+$ with $C_2F_4$ since these ions have large rate constants and can be formed by relatively low energy (20 eV) electron impact. Similarly, ionic products can be expected from the reactions of $C_2F_4^+$ and $CF^+$, but to a lesser extent, since their rate constants are an order of magnitude lower. There are no ion–molecule reactions reported for $CF_3^+$. There is evidence that vibrational excitaton[21] of $C_2F_4^+$ plays a significant role in breaking the ion–molecule complex, $(C_4F_8^+)^*$, back into reactants.

TABLE II: Some Mass Spectra of Tetrafluoroethylene (% of Total Ion Current)

| | | High press[b] | Low | 200 V p-p Discharge | | |
|---|---|---|---|---|---|---|
| m/e[a] | Assignment | 0.06 Torr | press[c] (75 eV) | 0.02 Torr | 0.07 Torr | 0.1 Torr |
| 12 | $C^+$ | 0.33 | | | | |
| 19 | $F^+$ | 0.15 | | | | |
| 24 | $C_2^+$ | 0.10 | | | | |
| 31 | $CF^+$ | 31.4 | 29 | 4.5 | 5.4 | 12.9 |
| 43 | $C_2F^+$ | 0.06 | | | | |
| 50 | $CF_2^+$ | 1.44 | 11 | 6.3 | 8.9 | 10.3 |
| 62 | $C_2F_2^+$ | 0.08 | 0.3 | | 0.5 | 0.5 |
| 69 | $CF_3^+$ | 7.4 | 1.3 | 63 | 65 | 53 |
| 81 | $C_2F_3^+$ | 13.0 | 37 | 0.5 | 1.1 | 2.8 |
| 100 | $C_2F_4^+$ | 39.8 | 20 | 6.8 | 7.8 | 11.6 |
| 55 | $C_3F^+$ | 0.01 | | | | |
| 74 | $C_3F_2^+$ | 0.01 | | | | |
| 93 | $C_3F_3^+$ | 0.16 | | 1.2 | 1.3 | 1.9 |
| 112 | $C_3F_4^+$ | 0.05 | | 0.2 | 0.2 | .2 |
| 119 | $C_2F_5^+$ | 0.03 | | 8.7 | 4.6 | 2.4 |
| 124 | $C_4F_4^+$ | 0.01 | | 0.2 | 0.2 | 0.1 |
| 131 | $C_3F_5^+$ | 6.0 | | 5.8 | 4.8 | 2.0 |
| 143 | $C_4F_5^+$ | | | 0.2 | 0.3 | 0.3 |
| 150 | $C_3F_6^+$ | | | 0.6 | 0.6 | 0.04 |
| 162 | $C_4F_6^+$ | 0.2 | | | | 0.01 |
| 169 | $C_3F_7^+$ | 0.05 | | 0.1 | | 0.02 |
| 181 | $C_4F_7^+$ | 0.02 | | 0.1 | | 0.02 |

[a] Ions listed in the second half of the table must result from ion-molecule reactions. [b] From a high pressure mass spectrum, ref 20. [c] Reference 19.

Table II shows the ion distribution found in the HPMS study,[20] and that found by direct ion sampling of the $C_2F_4$ discharge. The latter qualitatively reproduces all but the primary ions formed by 80-eV ionization in the HPMS study, viz. $C^+$, $F^+$, $C_2^+$, and $C_2F^+$. The distribution of product ions in the two experiments is, however, somewhat different. The major discrepancy occurs in the intensity of $C_2F_5^+$, which is two orders of magnitude more abundant in the discharge. A comparison of the relative intensities of fragment ions of $C_2F_4$ in the 80-eV HPMS study[20] with the published[19] 75-eV mass spectrum shows that the high pressure spectrum is deficient in $C_2F_3^+$ and $CF_2^+$. This is to be expected, since these ions have reaction cross sections of ~18 and 52 Å$^2$, respectively. A similar comparison of the relative intensities of the fragment ions from the discharge and the 20-eV cracking pattern (Table I) shows a deficiency of $C_2F_3^+$, an overabundance of $CF_2^+$ (by about a factor of 4), and a superabundance of $CF_3^+$ (by at least two orders of magnitude). The deficiency of $C_2F_3^+$ again can be expected from the ion–molecule reactions:

$$C_2F_3^+ + C_2F_4 \rightarrow C_3F_5^+ + CF_2 \quad (6)$$

$$C_2F_3^+ + C_2F_4 \rightarrow C_3F_4^+ + CF_3 \quad (7)$$

$$C_2F_3^+ + C_2F_4 \rightarrow C_4F_6^+ + F \quad (8)$$

The overabundance of the $CF_2^+$ ion would be larger than observed (a prime source for this ion is the $CF_2$ radical population) if it were not lost, at a high rate, by charge transfer[21] to $C_2F_4$, while the overabundance of the $CF_3^+$ ion is due to the fact that it is unreactive in the present environment.

The $C_2F_4^+$ ion undergoes a slow reaction that should be favored in the discharge due to high collision frequency and subsequent loss of vibrational excitation.

$$C_2F_4^+ + C_2F_4 \rightarrow C_3F_5^+ + CF_3 \quad (9)$$

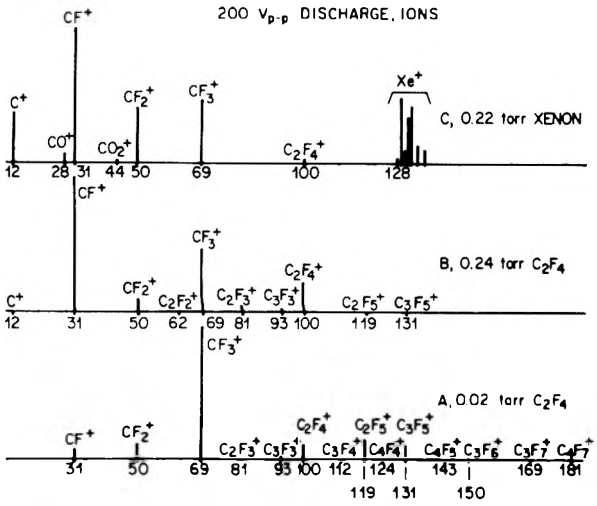


**Figure 5.** (A and B) Relative intensities of ions from a 200 V, p-p, $C_2F_4$ discharge; (C) relative intensities of ions from a 200 V, p-p, xenon discharge in the presence of $C_2F_4$-glow polymer.

If a comparison is made between the ions obtained from the neutral products of the discharge (Table I) and ions obtained by direct sampling (Table II), it can be seen that except for the greater variety of $C_4$ ions and a higher abundance of $C_3F_5^+$ in Table II, both lists exhibit similar trends. Excluding charge-exchange reactions, the only other reactions involving primary ions formed by low energy ionization in the discharge that proceed at appreciable rates[20] are (6) to (9). From this we conclude that most of the ions observed in Table II are the result of electron impact on the neutral products. This is quite a different situation from the discharges of hydrocarbon systems, in which a rich ion chemistry was observed.[2-6] Vastly different ionic species were found between direct sampling of the discharge and electron-impact induced ionization of neutral hydrocarbon products.

*Sputtering Effects.* An anomolous change was observed in the flux of the $CF^+$ ion on increasing the discharge pressure from 0.02 to 0.24 Torr (Figure 5). By calculating the ratio of the ion current of the $CF^+$ ion to that of the $m/e$ 93 ion at both pressures and then comparing these calculated values, it was found that the $CF^+$ flux increased by a factor of 10. (The mass 93 ion was used because its intensity relative to the total ion intensity remained essentially constant). Similar calculations showed a 50% decrease for the $CF_3^+$ and $CF_2^+$ ions, and a 50% increase in the $C_2F_4^+$ flux. Note also the appearance of $C^+$ at 0.24 Torr. The changes observed in $CF_2^+$, $CF_3^+$, $C_2F_4^+$, and higher mass species are consistent with a less efficient conversion of $C_2F_4$ to products. The increased pressure tends to reduce the electron energy and the result is less fragmentation of $C_2F_4$ upon ionization which is consistent with all previous discharges we have studied. The increased $CF^+$ flux and the appearance of $C^+$ are, however, quite the opposite of what would be expected. A possible cause of this effect might be sputtering of the polymer film on the electrodes.

Confirmation of this possibility was obtained by evacuating the discharge tube to a pressure of $1 \times 10^{-8}$ Torr, and back-filling with xenon to 0.22 Torr. Figure 5C shows that the ignition of the xenon discharge produces a significant ion flux of $C^+$, $CF^+$, $CF_2^+$, and $CF_3^+$. It is clear that xenon ion bombardment of the polymer film sputters small fragments of the polymer framework. These fragments are exactly the species known to be present in polymer produced in the discharge zone.[12] Electron impact ionization and charge exchange with $Xe^+$ obviously was very efficient since these fragments must have migrated to the sampling region from the electrode region. Neutral species other than xenon could not be detected at one part in $10^3$, and we conclude that no significant concentration of the neutral sputtered species develops. The ionization potentials of the sputtered fragments are given in Table III. It is seen that each species observed in Figure 5C has a lower IP than xenon except CO and $CO_2$. The appearance of these two molecular ions was unexpected, even at their low relative intensity. They are probably an effect of residual gases in the discharge tube.

**TABLE III: Reported[a] Ionization Potentials**

| Ion | $C^+$ | $CF^+$ | $CF_2^+$ | $CF_3^+$ | $C_2F_4^+$ | $CO^+$ | $CO_2^+$ | Xe |
|---|---|---|---|---|---|---|---|---|
| IP, V | 11.3 | 8.9[b] 9.6[b] | 11.7 | 10 | 10.1 | 14 | 13.8 | 12.1 |

[a] Reference 17. [b] Reference 18.

## Summary

The $C_2F_4$ discharge differs from discharges in hydrocarbon systems in that significant quantities of neutral products containing three and four carbon atoms are produced. (The only exception to this statement was found in the acetylene[5] case.) A second major difference occurs in the ionic products observed: In a $C_2F_4$ discharge, these are produced overwhelmingly by electron impact on the neutral species, rather than by ion-molecule reactions.

## References and Notes

(1) (a) M. J. Vasile and G. Smolinsky, *Int. J. Mass Spectrom. Ion Phys.*, **12**, 133 (1973); (b) G. Smolinsky and M. J. Vasile, *ibid.*, **12**, 147 (1973); (c) M. J. Vasile and G. Smolinsky, *ibid.*, **13**, 381 (1974).
(2) (a) G. Smolinsky and M. J. Vasile, *Int. J. Mass Spectrom. Ion Phys.*, **16**, 137 (1975); (b) M. J. Vasile and G. Smolinsky, *ibid.*, **18**, 179 (1975).
(3) M. J. Vasile and G. Smolinsky, *Int. J. Mass Spectrom. Ion Phys.*, **21**, 263 (1976).
(4) G. Smolinsky and M. J. Vasile, *Int. J. Mass Spectrom. Ion Phys.*, **22**, 171 (1976).
(5) M. J. Vasile and G. Smolinsky, *Int. J. Mass Spectrom. Ion Phys.*, **24**, 11 (1977).
(6) G. Smolinsky and M. J. Vasile, *Int. J. Mass Spectrom. Ion Phys.*, **24**, 311 (1977).
(7) G. Smolinsky and M. J. Vasile, *J. Macromol. Sci.-Chem.*, **A10**, 473 (1976).
(8) M. S. Lee, *Insulation/Circuits*, 33 (1971).
(9) D. T. Morrison and T. Robertson, *Thin Solid Films*, **15**, 87 (1973).
(10) J. M. Tibbitt, M. Shen, and A. T. Bell, *Thin Solid Films*, **29**, L43 (1975).
(11) H. Kobayoshi, M. Shen, and A. T. Bell, *J. Macromol. Sci.-Chem.*, **A8**, 1345 (1974).
(12) (a) D. W. Rice and D. F. O'Kane, *J. Electrochem. Soc.*, **123**, 1308 (1976); (b) D. F. O'Kane and D. W. Rice, *J. Macromol. Sci.-Chem.*, **A10**, 567 (1976).
(13) J. R. Dacy and J. G. F. Littler, *Can. J. Chem.*, **47**, 3871 (1969).
(14) C. Lifshitz and F. A. Long, *J. Phys. Chem.*, **69**, 3741 (1965).
(15) N. Cohen and J. Heicklin, *J. Chem. Phys.*, **43**, 871 (1965).
(16) J. P. Simons and A. J. Yarwood, *Nature (London)*, **192**, 943 (1961).
(17) J. L. Franklin, J. G. Dillard, H. M. Rosenstock, J. T. Herron, K. Draxl, and F. H. Field, *Natl. Stand. Ref. Data Ser., Natl. Bur. Stand.*, **No. 26** (1969).
(18) J. W. C. Johns and R. F. Barrow, *Proc. Phys. Soc. A*, **71**, 476 (1958); C. Lifshitz and F. A. Long, *J. Phys. Chem.*, **69**, 3731 (1965).
(19) C. Lifshitz and F. A. Long, *J. Phys. Chem.*, **67**, 2463 (1963).
(20) G. A. W. Derwish, A. Galli, A. Giardoni-Guidoni, and G. G. Volpi, *J. Am. Chem. Soc.*, **86**, 4563 (1964).
(21) V. G. Anicick, M. T. Bowers, R. M. O'Malley, and K. R. Jennings, *Int. J. Mass Spectrom. Ion Phys.*, **11**, 99 (1973).

# The Chlorination of Paraffin Hydrocarbons. Calculation of the Activation Energies and *A* Factors for Reactions in the Total Chlorination of Methane

**Thomas N. Bell,**

*Department of Chemistry, Simon Fraser University, Burnaby 2, British Columbia, Canada*

**Kathryn A. Perkins, and Peter G. Perkins***

*Department of Pure and Applied Chemistry, University of Strathclyde, Glasgow, G1 1XL* *(Received May 25, 1977)*

Activation energies and *A* factors for the series of gas-phase hydrogen transfer reactions $CH_{(4-x)}Cl_x + Cl\cdot$ and $CH_{(3-x)}Cl_x + HCl$ and chlorine transfer reactions $CH_{(3-x)}Cl_x + Cl_2$ and $CH_{(3-x)}Cl_{(x+1)} + Cl\cdot$ for $x = 0$, 1, 2, and 3 have been calculated using the molecular orbital-bond index (MOBI) and group contribution method. Generally satisfactory agreement is found between observed and calculated activation energies, while in certain cases the *A* factors obtained are more reliable than currently accepted estimates.

## Introduction

The chlorination of long-chain paraffin hydrocarbons is an important technical process in the manufacture of solvents and fire-resistant materials and, in this reaction, the kinetic factors controlling the positions and degree of substitution are of vital importance in determining the products. Despite this, there has been little systematic kinetic work on such reactions with hydrocarbons containing more than four carbon atoms. The variety of products which may be obtained and the possibilities for substitutional isomers, together with experimental difficulties, have combined to produce this situation. Clearly, an advance could be made if a method were available to estimate the kinetic parameters for the reactions. Such a method has been described recently[1,2] by us and in this paper, as the first part of a general theoretical investigation into the activation processes for the chlorination of paraffins, we deal with the series of reactions which bring about the total chlorination of methane. This system was chosen for the obvious reasons that it is the simplest and, moreover, kinetic parameters have been measured[3-5] or already estimated[5] for all the reactions involved.

The series of reactions studied were (a) the initiating step

$$CH_{(4-x)}Cl_x + Cl\cdot \rightarrow CH_{(3-x)}Cl_x + HCl$$

and (b) the sustaining step

$$CH_{(3-x)}Cl_x + Cl_2 \rightarrow CH_{(3-x)}Cl_{(x+1)} + Cl\cdot$$

Back reactions were also considered. Satisfactory values for the activation energies for these steps were calculated, while the *A* factors obtained are probably more accurate than those previously proposed.

## Method

The method previously described[1,2] for calculating the energies of activation for some gas-phase hydrogen transfer reactions was extended to cover the reactions of present interest. As before, the heat of atomization of each system is computed in the standard state and at 298 K at appropriate positions in the coordinate space such that the minimum enthalpy path for the reaction may be obtained. The activation enthalpy $\Delta H^{\circ\ddagger}_{298}$ is then computed from a knowledge of $\Delta H^{\circ}_{atom}$ for the initial and transition states of the system.

The enthalpies generated from these calculations are for reaction at 298 K. In order to obtain the activation enthalpy at a different reaction temperature, it is necessary to correct the value of $\Delta H^{\circ\ddagger}$ by the integrated form of Kirchoff's law, i.e.

$$\Delta H^{\circ\ddagger} = \Delta H^{\circ\ddagger}_{298} - \Delta C^{\circ}_{p(T_m)}\Delta T$$

where $\Delta T$ is the difference between the mean experimental reaction temperature and 298 K and $\Delta C^{\circ}_{p(T_m)}$ is the difference in specific heat between the activated complex and the reactants at a mean temperature, $T_m$. Values of $C^{\circ}_p$ at different temperatures for reactants were obtained from the JANAF Tables[6] and $C^{\circ}_p$ for the transition state was estimated from group contributions as described previously.[2]

The activation energy for a bimolecular reaction at the mean reaction temperature $T$ is then given by[7]

$$\Delta E^{\ddagger}_T = \Delta H^{\circ\ddagger}_T + 2RT$$

$\Delta E^{\ddagger}$ may be compared directly with experimentally determined values of the activation energy.

In addition to the activation energy, $\Delta E^{\ddagger}$, the preexponential factor, *A*, was calculated for each of the reactions studied, i.e.

$$A = \frac{e^2 kT}{h} e^{\Delta S^{\circ\ddagger}_c/R}$$

where $T$ is the mean temperature for the reaction and $\Delta S^{\circ\ddagger}_c$ is the difference in entropy between the transition state and the reactants in concentration units.

A value of $\Delta S^{\circ\ddagger}_p$ (the activation entropy in pressure units) was computed for each reaction, using values of $S^{\circ}_p$ from the literature,[6] e.g., in the activation process

$$CH_4 + Cl\cdot \rightarrow H_3C\cdots H^*\cdots Cl$$

values of $S^{\circ}_p$ are available over a range of temperature for $CH_4$ and Cl·; $S^{\circ}_p$ for the complex was estimated using the group contribution scheme.[2]

$\Delta S^{\circ\ddagger}_c$ was then computed from

$$\Delta S^{\circ\ddagger}_c = \Delta S^{\circ\ddagger}_p - (1-\gamma)R \ln R'T_m$$

where $R$ is the gas constant in J $K^{-1}$ $mol^{-1}$, $R'$ is the gas constant in L atm $K^{-1}$ $mol^{-1}$, $\gamma = 2$ (i.e., the molecularity of the reaction) and $T_m$ is the mean reaction temperature.

The basic types of reaction of interest are discussed under two heads.

TABLE I: Atom Pair Parameters

| Atom pair | Bonding parameter, kJ mol$^{-1}$ |
|---|---|
| Bonded H-Cl | 444.76 |
| "Nonbonded" H-Cl | 25.87 |
| "Nonbonded" Cl-Cl | −20.49 |
| "Nonbonded" C-Cl | 336.70 |
| Bonded C-H | 410.79-420.66 |
| "Nonbonded" C-H | 420.66 |

1. *Hydrogen Transfer Reactions.* Reactions studied here were those between a chlorine atom and the molecules $CH_4$, $CH_3Cl$, $CH_2Cl_2$, and $CHCl_3$, together with the reverse reactions.

The optimum paths for the set of reactions

$$\text{—C—H*} + \text{Cl}\cdot \rightarrow \text{—C--H*--Cl} \rightarrow \text{—C}\cdot + \text{H*Cl}$$

were obtained by calculating the heats of atomization for different geometries of the systems

$$\text{—C--H*--Cl}$$

The geometry of the group $CH_xCl_{(3-x)}$ is of importance with respect to the bond properties which have to be considered in these calculations. In the isolated molecule $CH_{(x+1)}Cl_{(3-x)}$ the geometry may be considered tetrahedral. However, the geometry of the free radical $CH_xCl_{(3-x)}$ is not established. The assumption is made in this paper that the radicals are planar, thus, in forming the transition states

$$\text{Cl—C--H*--Cl} \quad \text{H—C--H*--Cl} \quad \text{Cl—C--H*--Cl}$$
$$\text{H} \qquad\qquad \text{Cl} \qquad\qquad \text{Cl}$$

the geometry of the moiety $CH_xCl_{(3-x)}$ was assumed to change from pyramidal to planar as its C---H* length increased from 0.109 to 0.5 nm concomitantly with the H*--Cl bond length being changed from 0.5 to 0.127 nm.

The atom configuration C---H*---Cl was assumed to remain colinear throughout the reaction.

The atom pair bond energy paramters which afford the heats of atomization are listed in Table I. Those for the atom pairs C–Cl, "nonbonded" H–Cl, "nonbonded" Cl–Cl, and C–H remain the same as those used in previous work.[2] As before, the C–H parameter varies with the C–H* bond length according to whether the C–H* bond is in a planar, a "fully" pyramidal, or some intermediate environment. The parameter used for the interaction between "bonded" H and Cl atoms was taken as 444.76 kJ mol$^{-1}$.[2]

The C–Cl bonding parameter is allowed to vary with the configuration of the carbon atom, as was previously done for the corresponding C–H quantity. The value when the C–Cl is in the "fully" pyramidal situation is 336.70 kJ mol$^{-1}$.

Bond energy parameters for C–Cl relevant to the radicals $CH_2Cl\cdot$, $CHCl_2\cdot$, and $CCl_3\cdot$ can be determined from experimental heats of formation and SCF calculations on the species. Benson[7] gives experimental values for $\Delta H_f°$ at 298 K for $CH_3\cdot$ and $CCl_3\cdot$ as 142.26 and 77.40 kJ, respectively. A linear interpolation affords values of $\Delta H_f°$ for $CH_2Cl\cdot$ and $CHCl_2\cdot$ at 298 K as 120.50 and 99.16 kJ, and these values may be used to compute the value of $\Delta H°_{atom}$ for each radical. Thus, the C–Cl parameter appropriate to each species can be deduced. These are as follows: C–Cl ($CH_2Cl\cdot$), 288.65 kJ mol$^{-1}$; C–Cl ($CHCl_2\cdot$), 303.05 kJ mol$^{-1}$; C–Cl ($CCl_3\cdot$), 311.75 kJ mol$^{-1}$. It is now necessary to allow the C–Cl bond parameters to vary with the C–H* bond length. The lower limit is selected according to which radical is involved in the reaction; the higher limit, however, remains at 336.70 kJ mol$^{-1}$. Contributions to the C–Cl parameter at intermediate bond lengths stem from the parameters for the pyramidal molecule, the planar radical, and the pyramidal radical, as in the C–H case.

Current evidence on the most stable geometry of the $CCl_3$ radical[9] suggests that, while not completely planar, the radical is only slightly bent, having a structure intermediate between $CH_3$ and $CF_3$. The $CH_3$ radical has a planar geometry and it is known by calculation that the energy of reorganization from the planar to the pyramidal form is 56.41 kJ mol$^{-1}$.[2] The $CF_3$ radical, however, is known to be pyramidal and, hence, has a reorganization energy in the opposite sense. Evidence on the structure of the $CHCl_2$ radical has shown it to be planar.[10]

In these calculations we have made the assumption that the isolated radicals $CCl_3$, $CCl_2H$, and $CClH_2$ are all planar and that the bond-energy parameter for the pyramidal form is identical with that calculated for the planar form. Since the C–Cl bond indices in the two forms of $CCl_3$ differ by only 2%, this is consistent with a small reorganization energy for this radical (about 17.2 kJ mol$^{-1}$). The fraction which each of the three moieties contributes to the overall C–Cl bond-energy parameter at each C–H* bond length was assumed identical with that for the C–H parameter. Thus, at 0.16 nm where each of the three types of C–Cl bond contributes equally, the overall parameter for the C–Cl bond in $Cl_3C$– is

$$^1/_3(336.70 + 311.75 + 311.75) = 320.07 \text{ kJ mol}^{-1}$$

In calculating the $A$ factor for the process

$$CH_3\text{-H*} + Cl\cdot \rightarrow CH_3\text{---H*---Cl}$$

values of $S°_p$ at different temperatures are listed[6] for methane and the chlorine atom. Values of $S°_p$ for "bound H" and "bound Cl" in the transition state were taken as $^1/_2S°_p(H_2)$ and $^1/_2S°_p(Cl_2)$, respectively, and a value for "bound $CH_3$" was abstracted from Benson's tables.[7]

For other reactions, in order to estimate $\Delta S°^{\ddagger}$, $S°$ (bound radical) must be estimated. Thus, for example, in the process

$$CH_{(4-x)}Cl_x + Cl \rightarrow CH_{(3-x)}Cl_x\text{---H*---Cl} \qquad x = 1, 2, 3$$

$$\Delta S°^{\ddagger}_p = S°_p(CH_{(3-x)}Cl_x\text{---H*---Cl}) - S°_p(CH_{(4-x)}Cl_x) - S°_p(Cl) \quad (1)$$

$$S°_p(CH_{(3-x)}Cl_x\text{--H*---Cl}) = S°_p(CH_{(3-x)}Cl_x \text{ bound}) + S°_p(\text{H bound}) + S°_p(\text{Cl bound}) \quad (2)$$

$$S°_p(CH_{(3-x)}Cl_x \text{ bound}) = S°_p(CH_{(4-x)}Cl_x) - S°_p(\text{H bound}) \quad (3)$$

Using $S°_p(\text{H bound}) = {}^1/_2S°_p(H_2)$ and $S°_p(\text{Cl bound}) = {}^1/_2S°_p(Cl_2)$ then substitution of (3) into (2) and then into (1) yields

$$\Delta S°^{\ddagger}_p = {}^1/_2\, S°_p(Cl_2) - S°_p(Cl)$$

This means that the difference $\Delta S°^{\ddagger}_p$ between the transition state and the reactants depends only on the difference $S°_p$(Cl bound) – $S°_p$(Cl atom) at the mean temperature. Clearly, at a specific reaction temperature the $A$ factors for this series of reactions are the same.

$A$ factors were also calculated for the reverse reactions $CH_3$ + HCl and $CCl_3$ + HCl. However, no entropy data

TABLE II: C-Cl and Cl-Cl Bond Energy Parameters

| C-H* bond length in —C---H*, nm | C-Cl* bond length in —C---Cl*, nm | C-Cl parameter for $CH_2Cl\cdot$, kJ mol$^{-1}$ | C-Cl parameter for $CHCl_2\cdot$, kJ mol$^{-1}$ | C-Cl parameter for $CCl_3\cdot$, kJ mol$^{-1}$ | Cl-Cl parameter, kJ mol$^{-1}$ |
|---|---|---|---|---|---|
| 0.10 | 0.178 | 336.70 | 336.70 | 336.70 | 0 |
| 0.12 | 0.187 | 321.32 | 326.07 | 328.71 | 45.46 |
| 0.13 | 0.195 | 316.42 | 322.69 | 326.17 | 59.91 |
| 0.14 | 0.203 | 310.45 | 318.32 | 323.07 | 77.55 |
| 0.15 | 0.212 | 307.77 | 316.44 | 321.68 | 85.46 |
| 0.16 | 0.220 | 304.67 | 314.27 | 320.07 | 94.56 |
| 0.17 | 0.228 | 302.00 | 312.40 | 318.68 | 102.53 |
| 0.18 | 0.236 | 299.95 | 310.96 | 317.61 | 108.62 |
| 0.19 | 0.245 | 297.98 | 309.58 | 316.59 | 114.42 |
| 0.20 | 0.253 | 295.89 | 308.12 | 315.51 | 120.57 |
| 0.25 | 0.294 | 291.00 | 304.69 | 312.97 | 135.02 |
| 0.30 | 0.335 | 289.28 | 303.49 | 312.08 | 140.08 |
| 0.35 | 0.376 | 288.99 | 303.29 | 311.93 | 140.94 |
| 0.40 | 0.418 | 288.82 | 303.17 | 311.84 | 141.45 |
| 0.45 | 0.459 | 288.74 | 303.11 | 311.79 | 141.73 |
| 0.50 | 0.50 | 288.65 | 303.05 | 311.75 | 141.96 |

are available for the radicals $CH_2Cl$ and $CHCl_2$, so that $A$ factors for reactions involving these radicals could not be calculated.

2. *Chlorine Transfer Reactions.* Here the reactions studied were those between $Cl_2$ and the radicals $CH_3\cdot$, $CH_2Cl\cdot$, $CHCl_2\cdot$, and $CCl_3\cdot$, i.e.

$$\text{—C}\cdot + Cl_2 \rightarrow \text{—C--Cl*--Cl} \rightarrow \text{—C—Cl*} + Cl\cdot$$

The reverse reactions were also considered. The reaction path with minimum enthalpy was again calculated. The Cl-Cl bond length was varied between 0.199 (the bond length in the chlorine molecule[8]) and 0.5 nm. The latter corresponds to effectively total separation. The C-Cl* bond length was varied concomitantly between 0.5 and 0.178 nm[8] and the geometry of the >C moiety was varied from planar to pyramidal as the reactions proceeded.

The method of approach to this series, where the migrating atom is chlorine, was identical with that already described and, in general, the same bond energy parameters were used. The scaled parameters for C-H and C-Cl interactions were, however, made to depend on the length of the C-Cl* bond. Moreover, it was necessary to incorporate energy contributions from the two *mutually bonded* chlorine atoms between which the Cl-Cl distance varied. Since this had not occurred in any previous calculations, a new parameter for Cl-Cl was needed.

The quantity appropriate to $Cl_2$ was calculated from the known standard heat formation of the molecule and the Cl-Cl bond index; this yielded 141.96 kJ mol$^{-1}$. For transient stages in the reaction, it was found appropriate to vary the Cl-Cl parameter as a function of the C-Cl* bond distance. Hence, the parameter for bonded Cl-Cl* atoms was varied from its full value, 141.96 kJ mol$^{-1}$, when C-Cl was 0.5 nm (i.e., when the chlorine has no interaction with the radical) to zero when C-Cl* was 0.178 nm (i.e., as it exists in the $CH_xCl_{4-x}$ molecule). The Cl-Cl parameter was caused to change with C-Cl* bond length in a manner identical with the C-Cl parameters. Values of the Cl-Cl parameter at different C-Cl* distances are given in Table II.

The results also afford the activation energies for the back reactions, i.e.

$$\text{—C-Cl*} + Cl\cdot \rightarrow \text{—C}\cdot + Cl^*\text{-Cl}$$

The calculated change in enthalpy $\Delta H^{\circ\ddagger}_b$ was corrected for temperature as described above and the activation energy for the reverse reaction obtained.

In calculating the $A$ factors for forward complex formation

$$\text{—C}\cdot + Cl^*\text{-Cl} \rightarrow \text{—C---Cl*---Cl}$$

the relevant values of $S^\circ_p$ for the radicals $CH_3\cdot$ and $CCl_3\cdot$ were taken from JANAF tables.[6] For complex formation, $\Delta S^{\circ\ddagger}_p$ is given by

$$\Delta S^{\circ\ddagger}_p = S^\circ_p(\text{bound radical}) - S^\circ_p(\text{radical})$$

since $S^\circ_p$(bound Cl) in the transition state is assumed to be $^1/_2 S^\circ_p(Cl_2)$. No entropy data for the free radicals $CH_2Cl\cdot$ and $CHCl_2\cdot$ are available, so that no $A$ factors involving these radicals could be calculated.

It was possible to calculate $A$ factors for all four reverse (chlorine transfer) reactions, taking the values of $S^\circ_p$ for the bound radical, $CH_xCl_{(3-x)}$ as

$$S^\circ_p(CH_xCl_{(3-x)}) = S^\circ_p(CH_{(x+1)}Cl_{(3-x)}) - {}^1/_2 S^\circ_p(H_2)$$

## Results and Discussion

The activation energy and log $A$ calculated for each of the reactions are listed in Table III. The corresponding experimental quantities are also given; unless otherwise indicated, these were taken from Trotman-Dickenson and Milne's tables.[3] Each calculated value has been corrected to the median of the temperature range quoted for the particular reaction.

The two central bond lengths specifying the dimensions of the transition state are also given in Table III. It is found that, in general, the more highly substituted the carbon atom, the more compact the transition state becomes.

*Hydrogen Transfer Reactions.* The largest discrepancy between the experimental and calculated activation energies in this series occurs for the reaction $CH_4 + Cl\cdot$, although even here the difference is only ~10 kJ mol$^{-1}$. Possible reasons for this were discussed earlier.[2] In addition, it is worthy of note that the activation energy for this reaction calculated by Zavitsas and Melikian[11] is also considerably greater than the accepted experimental value. The activation energies calculated for the abstraction of hydrogen by a chlorine atom from $CH_3Cl$, $CH_2Cl_2$, and $CHCl_3$ are in good agreement with experiment.

For the reverse reactions, the RMS difference between the calculated and experimental activation energies is 6.3 kJ mol$^{-1}$. For the reaction of HCl with $CH_3\cdot$ and $CCl_3\cdot$ the

TABLE III: Arrhenius Parameters for Reactions

| Reaction | Mean reaction temp, K | Geometry of transition state, nm C-H | H-Cl | $\Delta S_p(T_m)$, J K$^{-1}$ mol$^{-1}$ | Calcd $\Delta E^{\ddagger}$, kJ mol$^{-1}$ | Calcd log $A$ | Exptl $\Delta E^{\ddagger}$, kJ mol$^{-1}$ | Exptl log $A$ |
|---|---|---|---|---|---|---|---|---|
| **Hydrogen Transfer Forward Reactions** | | | | | | | | |
| $CH_4 + Cl \rightarrow CH_3 + HCl$ | 389 | 0.158 | 0.17 | −47.9 | 26.4 | 12.77 | 16.1 | 13.42 |
| | | | | | | | 13.8 ± 0.4 | 13.5 ± 0.7 |
| $CH_3Cl + Cl \rightarrow CH_2Cl + HCl$ | 423 | 0.135 | 0.14 | −55.2 | 13.3 | 12.46 | 14.1 | 13.76 |
| | | | | | | | 12.9 | 13.5 |
| | | | | | | | 12.5 | 13.43 |
| $CH_2Cl_2 + Cl \rightarrow CHCl_2 + HCl$ | 423 | 0.125 | 0.145 | −55.2 | 15.1 | 12.46 | 13.1 | 13.4 |
| | | | | | | | 23.0 | 14.6 |
| $CHCl_3 + Cl \rightarrow CCl_3 + HCl$ | 423 | 0.125 | 0.14 | −55.2 | 13.6 | 12.46 | 14.0 | 12.84 |
| | | | | | | | 13.9 | 13.2 |
| | | | | | | | 27.2 | 14.6 |
| **Back Reactions** | | | | | | | | |
| $CH_3 + HCl \rightarrow CH_4 + Cl$ | 360 | 0.158 | 0.17 | −77.5 | 18.1 | 11.46 | 12.9 | 11.73 |
| | | | | | | | 20.9[a] | 12.0[a] |
| $CH_2Cl + HCl \rightarrow CH_3Cl + Cl$ | 400 | 0.135 | 0.14 | | 32.6 | | 34.3[a] | 12.1[a] |
| $CHCl_2 + HCl \rightarrow CH_2Cl_2 + Cl$ | 400 | 0.125 | 0.145 | | 38.2 | | 46.9[a] | 12.0[a] |
| $CCl_3 + HCl \rightarrow CHCl_3 + Cl$ | 365 | 0.125 | 0.14 | −77.2 | 42.9 | 11.18 | 47.3[d] | 11.65[d] |
| | | | | | | | 56.1[a] | 11.8[a] |
| **Chlorine Transfer Forward Reactions** | | | | | | | | |
| | | C-Cl | Cl-Cl | | | | | |
| $CH_3 + Cl_2 \rightarrow CH_3Cl + Cl$ | 365 | | | −68.2 | 6.4 | 11.65 | 9.6[a] | 12.9[a] |
| $CH_2Cl + Cl_2 \rightarrow CH_2Cl_2 + Cl$ | 365 | 0.265 | 0.20 | | 23.6 | 11.66 (est) | 12.5[a] | 12.6[a] |
| $CHCl_2 + Cl_2 \rightarrow CHCl_3 + Cl$ | 365 | 0.23 | 0.205 | | 26.5 | 11.66 (est) | 16.7[a] | 12.0[a] |
| $CCl_3 + Cl_2 \rightarrow CCl_4 + Cl$ | 365 | 0.23 | 0.21 | −67.8 | 30.4 | 11.67 | 25.1[a] | 11.74 ± 0.6[a] |
| | | | | | | | 22.2 | 12.86 |
| **Back Reactions** | | | | | | | | |
| $CH_3Cl + Cl \rightarrow CH_3 + Cl_2$ | 400 | | | −51.0 | 112.8 | 12.63 | 104.6[a] | 14.0[a,b] |
| $CH_2Cl_2 + Cl \rightarrow CH_2Cl + Cl_2$ | 400 | 0.265 | 0.20 | −47.5 | 121.0 | 12.82 | 89.5[a] | 14.0[a,b] |
| $CHCl_3 + Cl \rightarrow CHCl_2 + Cl_2$ | 400 | 0.23 | 0.205 | −38.0 | 111.2 | 13.31 | 87.9[a] | 14.0[a,b] |
| $CCl_4 + Cl \rightarrow CCl_3 + Cl_2$ | 400 | 0.23 | 0.21 | −27.4 | 100.6 | 13.87 | 83.7[c] | 14.0[c] |
| | | | | | | | 79.1[a] | 14.3[a] |

[a] Values taken from ref 5. [b] $A$ factor is assumed to be $10^{14}$. [c] Calculated from the reverse reaction. [d] Values taken from ref 4.

values given by Chiltz et al.[5] are somewhat higher than more recently determined values. It may be that their experimental activation energies for the reactions $CH_2Cl + HCl$ and $CHCl_2 + HCl$ are also in error in the same sense.

The calculated value of log $A$ for $CHCl_3 + Cl\cdot$ agrees well with experiment, whereas for the remainder of the series the calculated values are rather lower than the experimentally determined quantities. The overall root mean square error is ~0.8 in log units. The two $A$ factors which it was possible to compute for the reverse reactions show satisfactory agreement with experiment.

*Chlorine Transfer Reactions.* 1. *Forward Reactions.* The enthalpy calculations for the reaction

$$CH_3\cdot + Cl_2 \rightarrow CH_3\text{--}Cl^*\text{--}Cl \rightarrow CH_3Cl + Cl\cdot$$

indicate that the reaction path follows a steady decrease in energy from reactants to products. Hence, $\Delta H^{\circ\ddagger}$ for this reaction is computed to be zero. At a mean reaction temperature of 365 K, $\Delta E^{\ddagger}$ is thus 6.4 kJ mol$^{-1}$, to be compared with an experimental value of 9.6 kJ mol$^{-1}$.

For the reactions of $Cl_2$ with $CH_2Cl\cdot$, $CHCl_2\cdot$, and $CCl_3\cdot$, the experimental activation energies are given as 12.6, 16.7, and 25.1 kJ mol$^{-1}$, respectively. Of these, the data for the last reaction are probably the most accurate since, in this case, the measurements are not complicated by further chlorination of the products. Such phenomena generally lead to systematic errors in experimental determinations which are frequently difficult either to eliminate or estimate. However, for this most reliable case we calculate that the activation energy is 30.4 kJ mol$^{-1}$, in good agreement with experiment. The activation energies calculated for the reactions $CH_2Cl\cdot$ and $CHCl_2\cdot$ agree less well with experiment although, over the whole series, the RMS difference is only 8 kJ mol$^{-1}$.

Calculation of log $A$ was not possible for the reactions $CH_2Cl\cdot + Cl_2$ and $CHCl_2\cdot + Cl_2$, since values of $S^{\circ}_p$ are not available for the radicals $CH_2Cl\cdot$ and $CHCl_2\cdot$. However, evaluation of log $A$ at 365 K was carried out for the systems $CH_3\cdot + Cl_2$ and $CCl_3\cdot + Cl_2$, yielding values of 11.65 and 11.67, respectively. Since these two values are so close, log $A$ values for $CH_2Cl\cdot + Cl_2$ and $CHCl_2\cdot + Cl_2$ are estimated

to be 11.66 by interpolation. The agreement of the calculated and experimental values of log $A$ for $CCl_3\cdot + Cl_2$ is very satisfactory.

(2) *Back Reactions* $R-Cl + Cl \rightarrow Cl_2 + R$. The back reactions in which a chlorine atom reacts with a chlorinated methane all have higher activation energies than any of the reactions so far studied. Little experimental work has been carried out on these systems and $A$ factors have not been measured for the reaction of a chlorine atom with $CH_3Cl$, $CH_2Cl_2$, and $CHCl_3$. For the reaction $CCl_4 + Cl\cdot$ our calculated value for log $A$ is 13.87, to be compared with average experimental values of 14.15.

Taking the activation energies first, the most reliable experimental results will again be those for the fully chlorinated reactant $CCl_4$. Here, the calculated value differs from experiment by 17 kJ mol$^{-1}$.

A survey of the calculated and experimental activation energies in Table III reveals a discrepancy in the experimental results. Whereas the RMS difference between theory and experiment for the reactions of radicals with $Cl_2$ is 8 kJ mol$^{-1}$, that for the reverse reactions is $\sim$19 kJ mol$^{-1}$. This is somewhat difficult to reconcile. Since in all reactions the transition state is the same whatever the direction of reaction, we would expect the difference between the calculated and experimental activation energies to be very similar for both the forward and reverse reactions. It is, moreover, noteworthy that, for reactants in the reverse processes, the heats of formation have been accurately determined and so should not introduce further error to the values of $\Delta E^{\ddagger}_{forward}$. This discrepancy must cast some doubt on the experimental values hitherto accepted.

## References and Notes


(1) T. N. Bell and P. G. Perkins, *Nature (London)*, **256**, 300 (1975).
(2) T. N. Bell and P. G. Perkins, submitted for publication.
(3) A. F. Trotman-Dickenson and G. S. Milne, *Natl. Bur. Stand. Ref. Data Ser.* **No. 9** (1967).
(4) E. Ratajczak and A. F. Trotman-Dickenson, "Supplementary Tables of Bimolecular Gas Reactions", UWIST, Cardiff, 1969.
(5) G. Chiltz, P. Goldfinger, G. Huybrechts, G. Martens, and G. Verbeke, *Chem. Rev.*, **63**, 355 (1963).
(6) "JANAF Thermochemical Tables", Dow Chemical Co., Midland, Mich., 1965.
(7) S. W. Benson and H. E. O'Neal, *Natl. Bur. Stand., Circ.*, **No. 21** (1970).
(8) "Tables of Interatomic Distances and Configuration in Molecules and Ions", *Chem. Soc., Spec. Publ.*, **No. 11** (1958).
(9) L. J. Aarons, I. H. Hillier, and M. F. Guest, *J. Chem. Soc., Faraday Trans. 2*, **70**, 167 (1974).
(10) S. P. Mishra, G. W. Neilson, and M. C. R. Symons, *J. Chem. Soc., Faraday Trans. 2*, **69**, 1425 (1973).
(11) A. A. Zavitsas and A. A. Melikian, *J. Am. Chem. Soc.*, **97**, 2757 (1975).


# The Rate of Hydrated Electron Reaction with Neutral and Anionic Scavengers in Concentrated Salt Solutions


**E. Hankiewicz[†] and D. Schulte-Frohlinde***

*Institut für Strahlenchemie im Max-Planck-Institut für Kohlenforschung, D-4330 Mülheim/Ruhr, West Germany*


*(Received July 11, 1977) Publication costs assisted by Institut für Strahlenchemie im Max-Planck-Institut für Kohlenforschung*



The rate constants, $k_{obsd}$, of the $e_{aq}^-$ reaction with nitrobenzene, $IrCl_6^{2-}$, and $Fe(CN)_6^{3-}$ have been measured in water, and in LiCl and CsCl solutions up to a concentration of 14 M LiCl and 6 M CsCl and were found to be diffusion controlled. The viscosity of CsCl solutions is independent of CsCl concentration whereas in the case of LiCl solutions the logarithm of the viscosity decreases linearly with concentration. Since the logarithm of the rate constant, log $k_{obsd}$, with nitrobenzene decreases linearly with LiCl concentration the viscosity is the rate-determining parameter. In CsCl solutions the rate constants do not vary with salt concentration. Iridate and ferricyanide behave like neutral species at LiCl concentrations above 1 and 6 M, respectively; above these LiCl concentrations the dependence of their rate constants and that of nitrobenzene on salt concentration is the same. This is due to the formation of undissociated scavengers and the behavior described by the Smoluchowski–Debye equation at high salt concentration.


## I. Introduction

Anbar and Hart[1,2] have measured the rate constants for the reaction of the hydrated electron with several solutes (acetone, nitrous oxide, benzoate, and nitrate ions) in water and in aqueous solutions which were 12.4 M in potassium fluoride. They found that the rate constants are lower in the concentrated salt solution by a factor of 2–5 depending on the solute. It remained an open question whether a decrease of the activity coefficient of $e_{aq}^-$, a decrease of its diffusion coefficient, or a viscosity change of the salt solutions was responsible for the observed effect.

A similar decrease in the reactivity of the solvated electron was observed by Pikaev at al.[3] for the reaction of $e_{aq}^-$ with ions of transuranium elements in concentrated alkali and in carbonate solutions. These reactions were faster than diffusion controlled in contrast to the ones investigated by Anbar and Hart.[1] As a possible explanation for the decrease of the rate constants an increase of the viscosity of the solutions or capture of electrons in deeper traps was mentioned but not proved. A similar decrease was also observed for rate constants of the reactions $e_{aq}^- + e_{aq}^-$ and $e_{aq}^- + O^-$.[4]

Since concentrated aqueous salt solutions in liquid and especially in glassy states are currently under intensive investigation, we decided to study the factors which may be responsible for the decrease of the rate constant of the hydrated electron in the case of diffusion-controlled reactions. Lithium chloride was used as an added salt since the viscosity of its solutions is known and the rate of reaction of $e_{aq}^-$ with $Li^+$ is slow.

Furthermore we wanted to test whether different cations have different effects on the reaction rate constants of $e_{aq}^-$ with added scavengers, since enhancement of the rate


[†] Permanent Address: Institute of Applied Radiation Chemistry, Technical University, Wroblewskiego 15, 93-590 Lodz, Poland.

TABLE I: Rate Constants of $e_{aq}^-$ in Water and in Aqueous Solutions[h] ($k \times 10^{-10}$ $M^{-1}$ $s^{-1}$)

| | Water | | | | Salt solution | | | |
|---|---|---|---|---|---|---|---|---|
| Scavenger | (1) $k_{obsd,0}$ | (2) $k_{corr}$ | (3) $k_{diff,0} = 4\pi N r_\Sigma D_\Sigma$ | (4) $F = k_{diff,i}/k_{diff,0}$ | (5) Slope a' | (6) k' (from intercept) | (7) $r_\Sigma$, A | (8) $\gamma = k'/k_{diff,0}$ |
| $C_6H_5NO_2$ | 2.8[a] | | 2.5 ($r_\Sigma$ = 5.5 A) | | 0.063 | 2.9 | 6.4 | 1.0-1.16 |
| | 2.9[b] | | 2.7 ($r_\Sigma$ = 6.0 A) | | | | | |
| | 3.0[c] | | 2.8 ($r_\Sigma$ = 6.3 A) | | | | | |
| | 3.2[d] | | | | | | | |
| | 4.2[e] | | | | | | | |
| $Na_2IrCl_6$ | 1.7[d] | 1.23[d] | | | | | | |
| | | | 2.5 ($r_\Sigma$ = 5.5 A) | 0.52[d] | 0.063 | 2.6 | 5.7 | 1.0 |
| | | | 2.7 ($r_\Sigma$ = 6.0 A) | 0.65[d] | | | | |
| | 2.0[f] | 0.93[f] | | 0.55[f] | | | | |
| | 2.6[g] | | | | | | | |
| $K_3Fe(CN)_6$ | | 0.30[f] | 2.4 ($r_\Sigma$ = 5.5 A) | 0.19;[f] 0.19[d] | 0.063 | 2.2 | 5.0 | 0.85-0.91 |
| | 0.40[d] | 0.34[d] | 2.6 ($r_\Sigma$ = 6.0 A) | 0.27[d] | | | | |

[a] Reference 7. [b] Reference 8. [c] Reference 9. [d] This work. [e] Reference 10. [f] Reference 15. [g] Reference 16. [h] The column numbering is as follows: (1) the experimentally observed values in water; (2) values corrected for kinetic salt effect; (3) values recalculated according to the Smoluchowski equation with $D_{e_{aq}^-} = 1.96 \times 10^{-5}$ $cm^2$ $s^{-1}$,[11] $D_{C_6H_5NO_2} = 1.0 \times 10^{-5}$ $cm^2$ $s^{-1}$,[7] $D_{IrCl_6^{2-}} = 1.0 \times 10^{-5}$ $cm^2$ $s^{-1}$,[5] $D_{Fe(CN)_6^{3-}} = 0.9 \times 10^{-5}$ $cm^2$ $s^{-1}$,[15] $r_{e_{aq}^-} = 2.5$-$3.0$ A,[2,11] and 3.3 A,[12] $r_{C_6H_5NO_2} = 3.0$ A,[7] $r_{IrCl_6^{2-}} = 3.0$ A,[15] $r_{Fe(CN)_6^{3-}} = 3.0$ A.[15] (4) Values calculated according to the Smoluchowski-Debye equation with Debye correction factor $F$; (5 and 6) slope $a'$, and $k'$ value from intercept, both from empirical eq 2; (7) reaction distance from $k'$ and Smoluchowski equation; (8) parameter $\gamma$ comparing experimental $k'$ and theoretical $k_{diff,0}$ values.

constant[5] was observed in aqueous salt solutions for electron transfer reactions between two complex anions if LiCl was replaced by CsCl.

## II. Experimental Section

Nitrobenzene (Fluka, puriss, p.a. 99.5% GC), $K_3[Fe(CN)_6]$ (Merck p.a.), and $Na_2IrCl_6 \cdot 6H_2O$ (Merck p.a.), LiCl (Merck p.a.), and CsCl (Merck suprapur) were used without further purification.

The water used was triply distilled under nitrogen, from alkaline permanganate, from acid dichromate, and finally from a quartz apparatus.

The concentrations ($10^{-4}$ to $10^{-\epsilon}$ M) in water were determined spectrophotometrically using an $\epsilon$ value of 7800 $M^{-1}$ $cm^{-1}$ at $\lambda$ 268.5 nm for nitrobenzene and an $\epsilon$ value of 1050 $M^{-1}$ $cm^{-1}$ at $\lambda$ 420 nm for ferricyanide.

The pH of the solutions was adjusted to about 8 using barium hydroxide and perchloric acid. Redistilled 2-methyl-2-propanol (Merck p.a.) was added ($5 \times 10^{-3}$ to $10^{-2}$ M) to scavenge OH· radicals. Before irradiation all solutions were bubbled ~1 h with argon in order to remove oxygen. The 3-MeV van de Graaff accelerator and the remote controlled flow system used in the experiments have previously been described.[6] The dose applied was 1 krad and the measurements were carried out at room temperature, i.e. +20 °C.

The rates of reaction of the hydrated electron were determined by following the decay at the maximum of its absorption spectrum (e.g., at 720 nm in water and at 610 nm in 14 M LiCl solution).

A correction for $e_{aq}^-$ decay in the matrix itself, i.e., without $e_{aq}^-$ scavenger, was applied. The rate constant for the decay of $e_{aq}^-$ in the matrix alone was found to be ~10 and ~20% of that in solutions containing scavengers when the matrix was <6 M in LiCl and >6 M LiCl, respectively.

## III. Results

*Reaction of $e_{aq}^-$ with Nitrobenzene in Water.* Experimentally observed rate constants of $e_{aq}^-$ with nitrobenzene in water, $k_{obsd,0}$,[7,10] are summarized in column 1 of Table I. For neutral scavengers reacting with diffusion-controlled rate constants a correlation is expected between $k_{obsd,0}$ and $k_{diff}$ obtained from the Smoluchowski equation

$$k_{diff} = 4\pi N r_\Sigma D_\Sigma \quad (1)$$

where $N$ is Avogadro's number, $r_\Sigma = r_{e_{aq}^-} + r_X$ is the sum of the radii of hydrated electron and of the second reactant X and $D_\Sigma = D_{e_{aq}^-} + D_X$ is the sum of their diffusion coefficients.

Using the recently obtained diffusion coefficient for $e_{aq}^-$, $D_{e_{aq}^-} = 4.96 \times 10^{-5}$ $cm^2$ $s^{-1}$,[11] $D_{C_6H_5NO_2} = 1 \times 10^5$ $cm^2$ $s^{-1}$,[7] the published values for $r_{e_{aq}^-} = 2.5$-$3.0$ Å[2,11] and 3.3 Å,[12] and $r_{C_6H_5NO_2} = 3$ Å,[7] eq 1 leads to the rate constants (2.5-2.7) $\times 10^{10}$ and $2.8 \times 10^{10}$ $M^{-1}$ $s^{-1}$, respectively. Since these calculated values (column 3) agree with the majority of the experimental values (column 1) within the limits of experimental error (~10%), the rate of the reaction of the hydrated electron with nitrobenzene is expected to be diffusion controlled. Using $k = 3.0 \times 10^{10}$ $M^{-1}$ $s^{-1}$,[9] Hart and Anbar obtained a somewhat larger reaction distance ($r_\Sigma$ = 7.5 Å) due to using a smaller diffusion coefficient[2] for $e_{aq}^-$.

*Reaction of $e_{aq}^-$ with Nitrobenzene in Salt Solutions.* Experimentally observed rate constants of $e_{aq}^-$ with nitrobenzene in aqueous LiCl solutions, $k_{obsd,s}$, are presented in Figure 1. It was found that log $k_{obsd,s}$ depends linearly on the LiCl concentration $C$. These results can be described by the following empirical equation:

$$\log k_{obsd,s} = \log k' - a'C \quad (2)$$

with slope $a' = 0.063$ and intercept log $k'$ corresponding to $k' = 2.9 \times 10^{10}$ $M^{-1}$ $s^{-1}$ (Table I, columns 5 and 6).

This experimental result can be understood in terms of a pure viscosity effect of the added salt if it is assumed that the diffusion coefficients are inversely proportional to the viscosity of the solution as in the Stokes–Einstein equation, and that the reaction distance does not vary with LiCl concentration. The viscosity of LiCl solutions has been measured[13] and was found to obey the equation[14]

$$\log \eta_{rel} = \frac{aC}{1 - bC} \quad (3a)$$

where $\eta_{rel} = \eta_s/\eta_{H_2O}$, $\eta_s$ = viscosity of salt solutions, $\eta_{H_2O}$ = viscosity of water, $a = 0.0586$, $b = 0.0079$, and $C$ = LiCl concentration [M]. Since $bC << 1$ eq 3a simplifies to

$$\log \eta_{rel} = aC \quad (3b)$$

Combining the Stokes–Einstein equation ($D = kT/6\pi\eta r$) with the Smoluchowski equation (eq 1), using the defi-

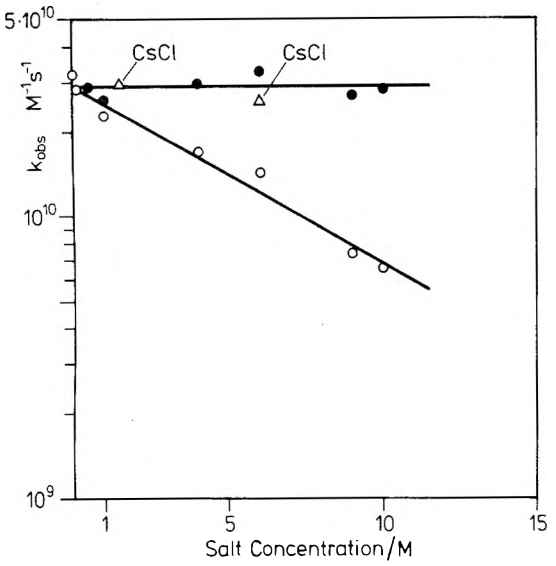


**Figure 1.** Semilogarithmic plot of the rate constants of $e_{aq}^-$ with nitrobenzene, $k_{obsd,s}$ [$M^{-1}$ $s^{-1}$], vs. alkali salt [M] concentrations: (○) $k_{obsd,s}$ = experimentally observed values in LiCl solution; (△) $k_{obsd,s}$ = experimentally observed values in CsCl solution; (●) $k_{obsd,s}\eta_{rel}$ = observed values multiplied by the relative viscosity of LiCl solution.

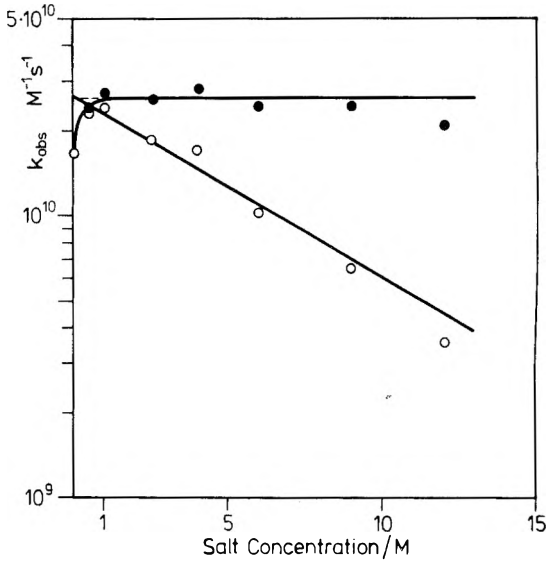


**Figure 2.** Semilogarithmic plot of the rate constants of $e_{aq}^-$ with hexachloroiridate, $k_{obsd,s}$ [$M^{-1}$ $s^{-1}$], vs. LiCl [M] concentration: (○) $k_{obsd,s}$ = experimentally observed values; (●) $k_{obsd,s}\eta_{rel}$ = observed values multiplied by the relative viscosity of the solution.

nition for $\eta_{rel}$ and using $k_{diff,0} = k_{diff}$ in water and $k_{diff,s} = k_{diff}$ in salt solution, the following results:

$$k_{diff,s} = k_{diff,0}/\eta_{rel} \quad (4)$$

After substitution of (3b) into (4) the theoretical equation, $\log k_{diff,s} = \log k_{diff,0} - aC$, is obtained with the same form as empirical eq 2. The slope $a'$ (column 7 of Table I) and $k'$ from the intercept (column 8) of the empirical equation agrees well with the corresponding theoretical values, $a = 0.0586$, and $k = (2.5\text{–}2.8)10^{10}$ (column 3). Hence $\gamma = k'/k_{diff,0}$ equals unity (column 8) and the reaction distance $r_\Sigma = 6.4$ Å (column 7), obtained from $k'$ values, agrees with the diffusion controlled one. Therefore $k_{obsd,s}$ values multiplied by the relative viscosity and plotted against LiCl concentration yield a line with zero slope and $\log k'$ as intercept. Further in agreement with the observed viscosity influence are the results with CsCl, an additive which does not change the viscosity (Figure 1) but changes the dielectric constant similar to added LiCl.

*Reaction of $e_{aq}^-$ with Iridate.* The measured rate constants of $e_{aq}^-$ with $Na_2IrCl_6$ in water, $k_{obsd,0}$,[15,16] and corrected for kinetic salt effect, $k_{corr}$, are summarized in Table I, columns 1 and 2, respectively. Our experimental value was found to be slightly higher than the value obtained by Anbar and Hart.[15]

Addition of LiCl increases the observed rate constant $k_{obsd,s}$ and a maximum value is obtained at 1 M LiCl (Figure 2). At still higher concentrations a linear decrease of $\log k_{obsd,s}$ as a function of LiCl concentration is observed (Figure 2). This linear dependence can be described using the same empirical equation (eq 2) which was used for nitrobenzene. This equation has the same form as the theoretical one assuming that only the viscosity influences the observed rate constant (see section 1b). A comparison between the parameters of the empirical equation (eq 2), $a'$ (column 5) and $k'$ (column 6), with the theoretical values $a = 0.0586$ and $k = (2.5\text{–}2.7)10^{10}$ $M^{-1}$ $s^{-1}$ (column 3) shows good agreement. Accordingly $\gamma = 1$ (column 8) and the empirical reaction distance $r_\Sigma = 5.7$ Å (column 7) equal the values calculated from the Smoluchowski equation (column 3). Hence the $k_{obsd,s}$ values multiplied with the relative viscosity give a line with zero slope and the intercept $\log k'$ (Figure 2). Thus it seems that sodium hexachloroiridate behaves as if it were neutral in LiCl solutions with concentrations ≥1 M. Since $\gamma = 1$ (column 8), and the empirical reaction distance $r_\Sigma = 5.7$ Å (column 7) equals the value calculated from the Smoluchowski equation (column 3), the reaction of $e_{aq}^-$ with sodium hexachloroiridate is diffusion controlled. Anbar and Hart[1] obtained $r_\Sigma = 8.2$ Å using $k_{corr} = 0.93 \times 10^{10}$ $M^{-1}$ $s^{-1}$, $D_{e_{aq}^-} = 4.5 \times 10^{-5}$ $cm^2$ $s^{-1}$, and the Smoluchowski–Debye equation.[2] We consider this $r_\Sigma$ value too high because the iridate is probably not completely dissociated and therefore the Debye correction is too large. Experiments with CsCl as an added salt could not be performed since $Cs_2IrCl_6$ is not sufficiently soluble.

*Reaction of $e_{aq}^-$ with Ferricyanide.* The measured rate constants of the reaction of $e_{aq}^-$ with ferricyanide in water, $k_{obsd,0}$, and corrected for salt effect, $k_{corr}$, are summarized in Table I, columns 1 and 2, respectively. The dependence of the experimentally observed rate constant $k_{obsd,s}$ on LiCl and CsCl concentration is presented in Figure 3.

Up to salt concentrations of ~0.3 M LiCl a strong increase of $k_{obsd,s}$ values is noted. Around 1 M LiCl the rate constant reaches a maximum value and then decreases on further increasing the LiCl concentration. The further decrease of $\log k_{obsd,s}$ is different from that of nitrobenzene and iridate; the plot of $\log k_{obsd,s}$ may be represented in terms of two linear parts.

The first part, in the concentration range up to ~6 M LiCl, has a slope clearly smaller than that obtained using nitrobenzene and iridate as $e_{aq}^-$ scavengers. On multiplying these $k_{obsd,s}$ values with the relative viscosity of the solution an ascending line is obtained (see Figure 3). However the second part of the observed dependence of $\log k_{obsd,s}$ for LiCl concentrations >6 M has approximately the same slope (column 5) as for nitrobenzene and iridate, in agreement with the slope of the theoretical eq 2. Also $k'$ from the empirical intercept (Table I column 6) agrees approximately with the theoretical value (column 3).

On multiplying $k_{obsd,s}$ values with the relative viscosity a line with zero slope and intercept $\log k'$ is obtained. These experimental results lead to the conclusion that at LiCl concentration >6 M potassium ferricyanide behaves like a neutral species and the decrease of $\log k_{obsd,s}$ may be explained in terms of the viscosity change of the so-

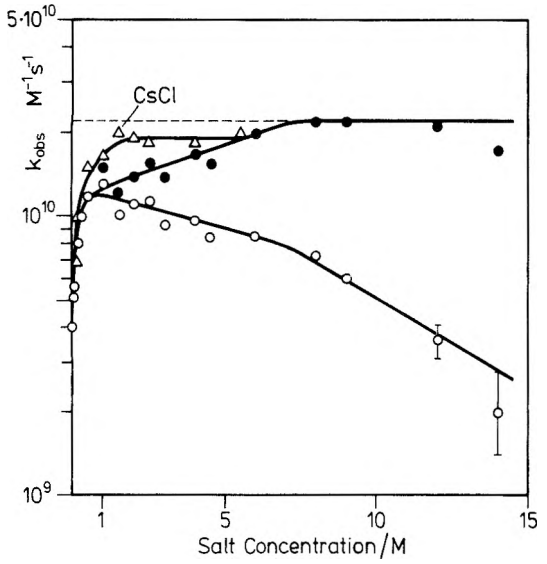


**Figure 3.** Semilogarithmic plot of the rate constants of $e_{aq}^-$ with ferricyanide, $k_{obsd,s}$ [$M^{-1}$ $s^{-1}$], as a function of alkali salt concentration $C$ [M]: (○) $k_{obsd,s}$ = experimentally observed values in LiCl solution; (△) $k_{obsd,s}$ = experimentally observed values in CsCl solution; (●) $k_{obsd,s}\eta_{rel}$ = observed values multiplied by the relative viscosity of LiCl solutions.

lution. The experimentally obtained reaction distance (column 7) agrees with that for diffusion controlled reactions (column 3) and also with $r_\Sigma$ = 6.5 Å calculated by Anbar and Hart[2] from the Smoluchowski–Debye equation using $k_{corr} = 0.30 \times 10^{10}$ $M^{-1}$ $s^{-1}$, $D_{e_{aq}^-} = 4.5 \times 10^{-5}$ $cm^2$ $s^{-1}$. Hence in agreement with earlier conclusions we find the reaction of $[Fe(CN)_6]^{3-}$ with $e_{aq}^-$ to be diffusion controlled.

When LiCl is replaced by CsCl a steeper increase of log $k_{obsd,s}$ with increasing salt concentration is observed (Figure 3). The rate constant, $k_{obsd,s}$, reaches a maximum value of $\sim 2 \times 10^{10}$ $M^{-1}$ $s^{-1}$ at about 1.5 M CsCl and does not vary further with increasing salt concentration up to approximately saturated solution at 6 M CsCl. In the range studied the viscosity of CsCl solutions is practically constant for our purpose ($\eta_{rel}$(1 M) = 0.963, $\eta_{rel}$(5 M) = 1.036).[17]

Since the plateau value for $k_{obsd,s}$ obtained in the range ~1.5–5.5 M CsCl is nearly equal to the rate constant for diffusion controlled reaction, $k_{diff,0}$, it seems that ferricyanide behaves like a neutral species in this concentration range. The measured rate constants are independent of CsCl concentration in agreement with the negligible influence of CsCl on the viscosity of the solution.

## IV. Discussion

The good agreement between measured rate constants for the reaction of $e_{aq}^-$ with nitrobenzene and the values calculated from the Smoluchowski equation (eq 1) shows this reaction to be diffusion controlled in pure water. This renders unnecessary the hypothesis that tunneling over distances larger than the encounter distance is involved in this reaction. Such effects were treated theoretically by Pilling and Rice[18] and enhancement of effective encounter distance to twice that of $r_\Sigma$ in the "normal" Smoluchowski equation was estimated for fluid solvents such as water. Larger enhancement factors were only found at very high viscosities (eightfold at $\eta = 10^{12}$ cP).

In LiCl solutions the similarly good agreement between experimental $k_{obsd}$ values and the ones calculated as $k_{diff,0}/\eta_{rel}$ (eq 4) for the nitrobenzene shows that the viscosity is the most important parameter. However, two assumptions have been made in order to arrive at this result. The first is that the reaction distance $r_\Sigma$ (from eq 1) does not vary with salt concentration.

It is known that salt addition to water causes a blue shift of the hydrated electron spectrum[2] which is explained as a result of contraction of the electron cavity. Taking the energy of the maximum of the $e_{aq}^-$ spectrum to be inversely proportional to the radius of the cavity,[2] one finds that even at 14 M LiCl where $\lambda_{max}$ is 600 nm[19] the radius $r_{e_{aq}^-}$ of the cavity is ~90% of that in pure water. Assuming that the changes of the radius of the electron cavity are analogous to the changes of its reaction radius in eq 1, a 10% change in the cavity radius is evidently insufficient to explain the about eightfold change in the rate constant when going from water to 14 M LiCl solution (Figure 1). It is not probable that the radius of nitrobenzene varies.

The second assumption is that the diffusion coefficient of $e_{aq}^-$ which constitutes 80% of $D_\Sigma$[20] is inversely proportional to the viscosity as is done in the Stokes–Einstein equation. A deviation can occur, e.g., when the hydration shell of $e_{aq}^-$ changes strongly on going from water to 14 M LiCl where fewer water molecules are available for hydration. The diffusion coefficient of $e_{aq}^-$ in LiCl solutions is not known. However, the diffusion coefficients of $Cl^-$, $Br^-$, and $I^-$ in LiCl solutions up to 4 M LiCl have been determined.[20] The results show that the viscosity determines the diffusion rate, e.g., the diffusion coefficients of these ions are inversely proportional to the viscosity.[20] All three ions behave very similarly. Since differences in size obviously do not change the diffusion pattern it is reasonable to assume that the $e_{aq}^-$ behaves like the halogen anion in this respect in agreement with the second assumption.

Furthermore it is possible that the reactivity of $e_{aq}^-$ is reduced in LiCl solutions due to changes in the reducing power. The reducing power of $e_{aq}^-$ may be changed by addition of LiCl in such a way that the reaction of $e_{aq}^-$ with nitrobenzene (or iridate or ferricyanide) is no longer diffusion controlled. However this possibility is ruled out since the difference between the standard potentials of $e_{aq}^-$ (−2.86 eV)[11] and that of nitrobenzene (−0.43 eV)[21] (hexachloroiridate (+1.02 eV) and ferricyanide (+0.34 eV)) is so large that even a 20% reduction in the reducing power of $e_{aq}^-$, as can be estimated roughly from the blue shift of the $e_{aq}^-$ absorption spectrum, cannot lead to an activation controlled reaction.

There was no indication for the formation of ion pairs, e.g., $(Li^+e_{aq}^-)$, as was found in liquids with much lower dielectric constants such as amines, ammonia, and ethers.[22]

From our experimental results for anionic scavengers of $e_{aq}^-$ it is evident (see section 2 and 3) that at sufficiently high salt concentration they behave like neutral species. The question arises as to whether the substrates behave like neutral species due to the kinetic salt effect at high salt concentration or due to the formation of undissociated salt (complex formation)[23] e.g., according to

$$2Li^+ + IrCl_6^{2-} \rightleftharpoons Li^+ + LiIrCl_6^- \rightleftharpoons Li_2IrCl_6 \qquad (5)$$

The diffusion-controlled rate constant between $e_{aq}^-$ and an ion, $k_{diff,i}$, is described by the Smoluchowski–Debye equation

$$k_{diff,i} = k_{diff,0}F \qquad (6)$$

where $F$, commonly known as the Debye correction factor, denotes the factor by which the rate constant for ions, $k_{diff,i}$, differs from that of neutral molecules, $k_{diff,0}$. This factor may be calculated as $F = Q/e^{Q-1}$ with $Q = Z_eZ_Xe^2/\epsilon kTr\Sigma$ where $Z_X$ is the charge of the ion, $\epsilon$ is the static dielectric constant of water, $k$ is Boltzmann's constant, and $r_\Sigma = r_{e_{aq}^-}$

$+ r_X$ is the sum of the two radii.

Equation 6 has been theoretically shown by Logan[24] to reduce to the Brönsted–Bjerrum equation for primary kinetic salt effect at low ionic strength. With increasing ionic strength of the solution Logan has suggested that the Debye correction factor $F$ tends to unity, i.e., the ions behave kinetically as if they were neutral. Recently Buxton et al.[25] have also suggested that in 10 M LiCl the Debye correction factor equals unity.

Since the Debye correction factor converges to unity at the same ionic strength for all ions independent of their charge[24] iridate and ferricyanide should behave similarly. However, comparison of Figures 2 and 3 shows that iridate and ferricyanide behave differently. Further differences appear between the behavior of ferricyanide in LiCl and in CsCl solutions (Figure 3). We assume that both these differences are due to the formation of undissociated salts (complex formation) the formation of which differs for different substrates.

*Acknowledgment.* One of the authors (E.H.) thanks the Alexander von Humboldt Foundation for a grant. We thank Mrs. M. Pruchova for technical assistance and Dipl.-Phys. F. Schwörer and his staff for excellent operation of the pulse radiolysis equipment.

## References and Notes

(1) M. Anbar and E. J. Hart, *J. Phys. Chem.*, **69**, 1244 (1965).
(2) E. J. Hart and M. Anbar, "The Hydrated Electron", Wiley-Interscience, New York, N.Y., 1970, p 172.
(3) A. K. Pikaev, B. G. Ershov, and I. E. Makarov, *J. Phys. Chem.*, **79**, 3026 (1975).
(4) A. K. Pikaev, T. P. Zhestikova, and G. K. Sibirskaya, *J. Phys. Chem.*, **76**, 3765 (1972).
(5) J. Holzwarth and L. Strohmaier, *Ber. Bunsenges. Phys. Chem.*, **77**, 1145 (1973).
(6) N. Getoff and F. Schwörer, *Radiat. Res.*, **41**, 1 (1970).
(7) B. Cercek, *Int. J. Radiat. Phys. Chem.*, **3**, 231 (1971).
(8) K. D. Asmus, A. Wigger, and A. Henglein, *Ber. Bunsenges. Phys. Chem.*, **70**, 862 (1966).
(9) (a) E. J. Hart, S. Gordon, and J. K. Thomas, *J. Phys. Chem.*, **68**, 1271 (1964); (b) M. Anbar and E. J. Hart, *J. Am. Chem. Soc.*, **86**, 5633 (1964).
(10) F. Barat, L. Gilles, B. Hickel, and B. Lesigne, *J. Phys. Chem.*, **77**, 1711 (1973).
(11) M. S. Matheson, "Physical Chemistry. An Advanced Treatise", Vol. VII, Academic Press, London, 1975, p 570.
(12) J. Jortner, *Radiat. Res., Suppl.*, **4**, 24 (1964).
(13) Landolt-Börnstein, "Zahlenwerte and Funktionen", Vol. 5, Springer-Verlag, Berlin, 1969.
(14) R. A. Robinson and R. H. Stokes, "Electrolyte Solutions", London, Butterworths, 1959, p 306.
(15) M. Anbar and E. J. Hart, *Adv. Chem. Ser.*, **No. 81**, **79** (1968).
(16) F. S. Dainton and R. Rumfeldt, *Proc. R. Soc. London, Ser. A*, **298**, 239 (1967).
(17) P. A. Lyons and J. F. Riley, *J. Am. Chem. Soc.*, **76**, 5216 (1954).
(18) M. J. Pilling and S. A. Rice, *J. Chem. Soc., Faraday Trans. 2*, **71**, 1563 (1975).
(19) R. J. Woods, B. Lesigne, and L. Gilles, *J. Phys. Chem.*, **79**, 2700 (1975).
(20) R. Mills, *J. Phys. Chem.*, **61**, 1631 (1957).
(21) K. Schwabe, "Polarographie und chemische Kostitution organischer Verbindungen", Akademie-Verlag, Berlin, 1957.
(22) J. W. Fletcher and W. A. Seddon, *J. Phys. Chem.*, **79**, 3055 (1975).
(23) G. V. Buxton, F. S. Dainton, and D. R. McCracken, *Trans. Faraday Soc.*, **69**, 243 (1973).
(24) S. R. Logan, *Trans. Faraday Soc.*, **62**, 3416 (1966).
(25) G. V. Buxton, F. C. R. Cattell, and F. S. Dainton, *J. Chem. Soc., Faraday Trans. 1*, **71**, 115 (1975).

# Sonoluminescence of Aqueous Solutions[1]

**C. Sehgal, R. P. Steer,* R. G. Sutherland, and R. E. Verrall**

*Department of Chemistry and Chemical Engineering, University of Saskatchewan, Saskatoon, Saskatchewan, Canada S7N OWO*

*(Received July 22, 1977)*

*Publication costs assisted by the University of Saskatchewan*

The effects of adding efficient H atom and OH radical scavengers on the spectral distribution and intensity of sonoluminescence from argon saturated aqueous solutions have been investigated. The results indicate that the emissive continuum is due to a chemiluminescent process, likely $H + OH + M \rightarrow H_2O + M + h\nu$.

## Introduction

The propagation of acoustic waves through a liquid medium is known to result in the phenomenon of acoustic cavitation. Cavitation is a three stage process consisting of the formation, growth, and collapse of gas or vapor filled bubbles suspended in the liquid phase. The presence of dissolved gas or microparticles reduces the liquid strength and hence favors the initiation of cavity formation.

In aqueous solutions the decomposition of water into H atoms and OH radicals is thought to result from either "adiabatic" heating or electrical discharge during the irreversible collapse of transient bubbles. Reactions may occur among these primary species and other reactive molecules present in the cavity, and the contents of collapsed bubbles may subsequently diffuse into solution where secondary reactions may occur. Reactions may also occur at the gas–liquid bubble interface.

The mechanism of production of luminescence from aqueous solutions subjected to ultrasonically induced cavitation has been the subject of considerable speculation since the phenomenon was first reported by Marinesco and Trillat in 1933.[2] Low resolution spectra[3] show that there are likely two contributions to the emission from water saturated with the noble gases; a broad continuum extending from about 250 nm into the near infrared with a broad maximum near 400 nm, and a second, banded component in the near UV. The latter has been assigned unequivocally to the well-known $A(^2\Sigma^+) \rightarrow X(^2\Pi)$ transition of the hydroxyl radical, while the former, which contributes the majority of the emission at high ultrasonic frequencies, has been attributed variously to black body incandescence,[4-6] bremsstrahlung,[7] and chemiluminescent $H + OH$[2,8] or ion–electron recombination[7,9] at the moment of cavity collapse. No definitive mechanism has been established for the production of either emissive component, however.

We have carried out studies of the effects of adding various radical scavengers on the spectra and intensity of

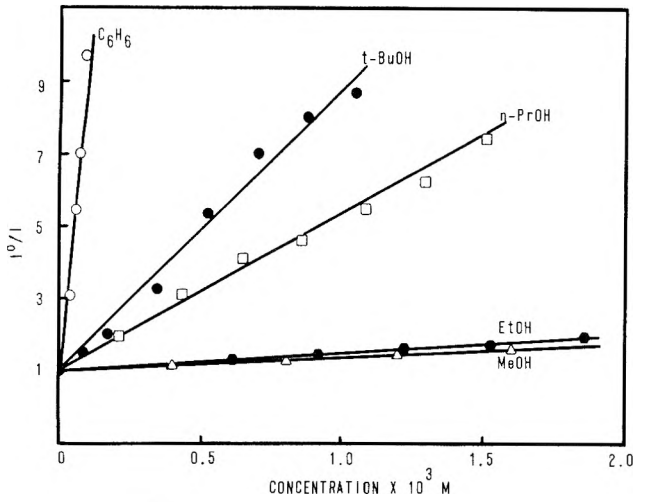


**Figure 1.** Plot of ratio of total sonoluminescence intensity in the absence of scavenger, $I^0$, to total intensity, $I$, vs. concentration of scavenger in bulk solution. The insonation frequency is 459 kHz.

emission from ultrasonically cavitated solutions with the objective of obtaining chemical evidence for the mechanism of sonoluminescence production.

## Experimental Section

Air-free argon-saturated aqueous solutions in a closed, temperature regulated ($T$ = 285 ± 2 K) system were insonated at 333 or 459 kHz using transducers and a generator previously described.[10] Sonoluminescence from the cylindrical cell was observed axially by means of a GCA/McPherson Model EU-700 grating monochromator coupled to a cooled RCA C31034A photomultiplier tube and single photon counting detection system.[11] Measured volumes of reagent grade liquid scavengers were added to the system by microsyringe injection through a specially designed inlet and were allowed to mix thoroughly with the liquid. Spectral measurements were made using first-order diffraction from the grating and intensity measurements were made with the monochromator in place using the spectrally undispersed zero order diffraction to obtain a higher signal-to-noise ratio.

## Results and Discussion

Sonoluminescence spectra of argon-saturated water obtained with 333-kHz insonation showed a strong band at 307 nm with weaker bands at 281 and 343 nm, attributable to the 0–0, 1–0, and 0–1 transitions of OH $A(^2\Sigma^+) \rightarrow X(^2\Pi)$, superimposed upon a strong continuum extending from ca. 250 to 700 nm, in agreement with previous observations.[2] The OH emission bands were almost completely buried in the continuum when 459-kHz insonation was used, as predicted,[2] and the shape of the continuum was invariant (although attenuated in intensity) with the addition of benzene and several aliphatic alcohol scavengers.

Figure 1 shows that the total sonoluminescence intensity diminishes with increasing concentration of benzene and several alcohols in a Stern–Volmer-like fashion over the 0 to 2 × $10^{-3}$ M bulk solution concentration range. The observed effects cannot be due to the suppression of cavitation by the organic component because the addition of higher concentrations of poor radical scavengers such as $CCl_4$ is known[12,13] to enhance slightly the intensity of sonoluminescence from aqueous solutions containing dissolved noble gases.

The fact that the presence of small concentrations of reactive free radical scavengers can reduce the sonoluminescence intensity to near zero is strong evidence that the emissive continuum is the result of a chemiluminescent process. If the continuum were due to "black body" radiation from incandescent collapsing bubbles, then a diminution in radiant intensity with increasing added concentration (due, for example, to a lowering of the temperature of the cavity contents) should be accompanied by a shift in the spectrum to longer wavelengths. Such is not the case and therefore cavity incandescence cannot contribute substantially to sonoluminescence.

Spectroscopic investigations[14] of $H_2$–$O_2$ flames have been shown that an emissive continuum, likely resulting from the process[15]

$$H + OH + M \rightarrow H_2O + M + h\nu$$

may be observed from the near UV through the visible region of the spectrum. The intensity of this continuum is known[16] to increase markedly relative to that of the OH $A(^2\Sigma^+) \rightarrow X(^2\Pi)$ bands with increasing pressure. It is therefore quite conceivable that, at the very high pressures encountered during bubble collapse, radiation from this source could dominate the sonoluminescence spectrum.

Chemical scavenging of either H atoms or OH radicals is therefore most likely responsible for the observed attenuation of the sonoluminescence intensity with increasing benzene or alcohol concentration. Benzene and the aliphatic alcohols are known to be efficient OH radical scavengers in aqueous solution[17] and, although Arrhenius parameters for the corresponding reactions have not been measured, estimation of these quantities by semiempirical[18] means indicates that the same should be true for the gas phase at high temperature. Bimolecular gas phase reactions of these scavengers with H atoms are also relatively rapid, having rate constants at 900 K of 1.3 × $10^7$, 9.4 × $10^7$, 1.9 × $10^8$, 8.8 × $10^8$, and 1.6 × $10^8$ $M^{-1}$ $s^{-1}$ for H + MeOH, EtOH, *n*-PrOH, *t*-BuOH, and $C_6H_6$, respectively.[19]

Quantitative correlation of the relative efficiencies of sonoluminescence attenuation with scavenging reaction rate constant is unfortunately not yet possible. Temperatures inside the collapsing bubbles are unknown. Intracavity concentrations of the scavengers are not known accurately since equilibrium vapor pressures are not established within the bubbles. Arrhenius parameters for OH + alcohol reactions in the gas phase have not been measured. Nevertheless, the efficiencies of sonoluminescence attenuation increase in the order MeOH ~ EtOH < *n*-PrOH ~ *t*-BuOH < $C_6H_6$, which, qualitatively, correlates reasonably well with the expected relative rates of H and OH scavenging at high temperature.

Further work is underway to elucidate the details of the sonoluminescence and scavenging mechanisms.

## References and Notes

(1) Financial support from the National Research Council of Canada and the University of Saskatchewan is gratefully acknowledged.
(2) M. Marinesco and J. J. Trillat, *Compt. Rend.*, **196**, 858 (1933).
(3) K. J. Taylor and P. D. Jarman, *Aust. J. Phys.*, **23**, 319 (1970).
(4) P. Gunther, E. Heim, and G. Eichkorn, *Z. Angew. Phys.*, **11**, 274 (1959).
(5) D. Srinivasan and L. V. Holroyd, *J. Appl. Phys.*, **32**, 446 (1961).
(6) B. E. Noltingk and E. A. Neppiras, *Proc. Phys. Soc. (London)*, **63**, 674 (1950).
(7) M. A. Margulis, *Sov. Phys.-Acoust.*, **15**, 135 (1969).
(8) T. K. Saksena and W. L. Nyborg, *J. Chem. Phys.*, **53**, 1722 (1970).
(9) M. Degrois and P. Baldo, *Ultrasonics*, **12**, 25 (1974).
(10) E. L. Mead, R. G. Sutherland, and R. E. Verrall, *Can. J. Chem.*, **54**, 1114 (1976).
(11) T. Oka, A. R. Knight, and R. P. Steer, *J. Chem. Phys.*, **63**, 2414 (1975).
(12) K. Negishi, *J. Phys. Soc. Jpn.*, **16**, 1450 (1961).
(13) V. Griffing, *J. Chem. Phys.*, **18**, 997 (1950).
(14) A. G. Gaydon, "The Spectroscopy of Flames", Chapman and Hall, London, 1957.
(15) P. J. Padley, *Trans. Faraday Soc.*, **56**, 449 (1960).

(16) J. Diederichsen and H. G. Wolfhard, *Proc. R. Soc. London, Ser. A*, **236**, 89 (1956).
(17) Farhataziz and A. B. Ross, *Natl. Stand. Ref. Data Ser., Natl. Bur. Stand.*, 59 (1977).
(18) S. W. Benson, "Thermochemical Kinetics", 2nd ed, Wiley, New York, N.Y., 1976.
(19) J. A. Kerr in "Comprehensive Chemical Kinetics", Vol. 18, C. H. Bamford and C. F. H. Tipper, Ed., Elsevier, Amsterdam, 1976, p 39.

# Ultrasonic Absorption in Relation to Hydrogen Bonding in Solutions of Alcohols. 2. Ultrasonic Relaxation Spectra of Solutions of Alcohols in Cyclohexane

**A. Djavanbakht,† J. Lang, and R. Zana***

*CNRS, Centre de Recherches sur les Macromolécules 6, rue Boussingault, 67083 Strasbourg, Cedex, France* *(Received March 23, 1977)*

*Publication costs assisted by CNRS*

The ultrasonic absorption of solutions of ethanol, 1-butanol, 1-octanol, 1-dodecanol, 1-hexadecanol, 3-octanol, 2-methyl-3-heptanol, and 2,4-dimethyl-3-hexanol in cyclohexane at 25 °C has been measured in the frequency range 4–250 MHz. The relaxation spectra of all of the investigated solutions could be fitted to a relaxation equation with a single relaxation frequency. The results have been interpreted on the basis of a reaction mechanism where $n$ alcohol molecules associate to give cyclic and noncyclic $n$-mers. The absorption is attributed to the perturbation by the sound waves of the association equilibrium leading to noncyclic $n$-mers. For all primary alcohols no fit to the data could be obtained for $n = 3$ but equally good fits were obtained for $n = 4$ and $n = 5$, except with 1-hexadecanol for which $n = 5$ provides the best fit. The results indicate that (1) the rate of association of alcohol molecules through H bonds is close to its diffusion-controlled limit, even for the most hindered alcohol investigated; (2) the dissociation rate constant of one alcohol molecule from a noncyclic $n$-mer is only very slightly dependent on the alcohol chain length for primary alcohols. This rate constant increases with the degree of steric hindrance, reflecting the decreased stability of noncyclic aggregates. For 2-methyl-3-heptanol the best fit to the data is obtained for $n = 3$. Likewise, the results for 2,4-dimethyl-3-hexanol appear to indicate that the association of this alcohol is essentially restricted to dimerization. Larger associated species appear to be present only in very small amount. The relation between ultrasonic absorption data and dipole moment data for octanol solutions is examined.

## I. Introduction

Infrared spectroscopy,[1-6] NMR,[7-9] vapor pressure osmometry,[8,10,11] vapor density,[11] partition coefficient,[13,14] cryoscopy,[4] dielectric constant,[15-17] relaxation,[18-20] calorimetry,[6,13,21-23] ultrasonic absorption,[24-30] and chemical kinetics[31] have been extensively used for the study of the association of alcohols in solution through H bonding. In spite of this very large number of studies an examination of the literature till about 1970 reveals considerable confusion in the understanding of the association behavior of alcohols. In the past few years, however, some concensus appears to have been reached among workers about several important features of the self-association of alcohols in nonpolar solvents such as saturated hydrocarbons or $CCl_4$. (i) Fairly dilute alcohol solutions (at concentrations below 0.5 M) appear to contain, in addition to the monomeric alcohol, at least two associated species.[1-6,8-16,29,32] This conclusion results from the fact that the best fit to the data, whichever the investigated property, is obtained by using at least two equilibrium association constants. (ii) At concentration below 0.5 M the association does not proceed to large aggregates.[4,10-12] Trimers[8] and tetramers[1] are most often invoked for the interpretation of the results. Dimers appear to be present only in small amounts[1,5,8,13] but the authors disagree on whether this amount can be neglected in the mass conservation equation.[1,11] (iii) The presently accepted model, which agrees with the results of the most recent studies by means of various methods, involves cyclic and noncyclic polymers[1,2,5,8,10,15,16,29] according to

$$\text{monomer (A)} \rightleftharpoons \text{small noncyclic polymer } (A_n) \not\rightleftharpoons \text{cyclic polymer } (A_{n' \geq n,C}) \quad (1)$$

Bordewijk[15] recently pointed out that the discrimination between different association models cannot be achieved by investigating properties which vary monotonically with the total alcohol concentration. Indeed the calculated variations of such properties are not very sensitive to the model (for instance to different sets of values of $n$ and $n'$ in reaction 1) as those of properties which show a maximum and/or a minimum as the alcohol concentration is increased. This explains the renewed interest in measurements of apparent dipole moment $\mu_a$ of alcohols in solution. $\mu_a$ goes through a maximum at a concentration which depends on the solvent[15-17] (0.02, 0.04, and 0.4 M for 1-octanol in cyclohexane, $CCl_4$, and benzene, respectively[16]). This maximum has been attributed to the relative variations of concentration of high dipole moment linear (but small) polymers and of low dipole moment cyclic polymers.[15,16] It must be noted that studies of static dielectric constant of alcohol solutions have yielded much more information than dielectric relaxation studies. Indeed, two out of the three relaxation processes found for alcohol solutions are of intramolecular origin and make extremely complicated the study of the third process which results from the intermolecular association of alcohol molecules, in the case of dielectric relaxation.[20]

† Present address: 163 Manoutcheri Ave., Meched, Iran.

Ultrasonic absorption is another property of alcohol solutions which shows a nonmonotonous change with the alcohol concentration.[24-29] At low concentration the absorption of alcohol solutions is close to that of the solvent then increases very rapidly and linearly with concentration, goes through a maximum, and decreases.[24-26,29] As for $\mu_a$ the position of the maximum of ultrasonic absorption is very sensitive to the nature of the solvent and practically independent of the alcohol alkyl chain length. In fact there appears to be a correlation between the changes of $\mu_a$ and of the excess absorption with concentration. This point is examined further in the Discussion. However the changes of absorption are much more pronounced than those of $\mu_a$. They should therefore provide a much more severe test to any postulated model than $\mu_a$ data.

The purpose of the systematic ultrasonic absorption studies that we started a few years ago[26,29] was to obtain information on the values of $n$ and $n'$ in reaction 1 and to check the range of validity of this association mechanism for various alcohols in different solvents.

In previous studies[26,29] we have shown that the association of primary alcohols in non H-bonding solvents must proceed to species larger than dimers (see footnote 33) and that the ultrasonic absorption of alcohol solutions cannot be due to the reversible cyclization of small linear polymers. Attempts were made[29] to account for the position of the absorption maximum essentially in terms of two models. The first one, which has been reported by Fletcher and Heller,[1] assumes the formation of linear and cyclic tetramers ($A_4$ and $A_{4C}$, respectively) according to

$$4A \rightleftharpoons A_4 \rightleftharpoons A_{4C} \qquad (2)$$

In this model, dimers and trimers are assumed to be present in negligible amount and are not taken into account in the mass conservation equation.

The second model proposed by Tucker and Becker[8] assumes the formation of a linear trimer ($A_3$) and of a cyclic multimer. To fit our data we assumed the model[29]

$$4A \rightleftharpoons A_3 + A \rightleftharpoons A_{4C} \qquad (3)$$

When using the equilibrium constants reported by Fletcher and Heller,[1] and Tucker and Becker[8] the values calculated for the concentration where the maximum of ultrasonic absorption occurs were found to be too large with respect to the experimental results.[29] A choice between reactions 2 and 3 was therefore not possible on the basis of these calculations.

The purpose of this second part of our work is to report the results of measurements of ultrasonic absorption performed on solutions of primary alcohols and of three isomeric octanols in cyclohexane, as a function of the alcohol concentration c, and the ultrasonic frequency. These data have permitted us to obtain new information on the association behavior of alcohols in solution.

Cyclohexane was used as solvent throughout the present investigation for the following reasons. (i) It has been extensively used in investigations of alcohols by means of a variety of methods.[7,14,16,24,27-29] (ii) Its interaction with alcohols is quite weak, and probably comparable with that between normal alkanes and alcohols. The latter is characterized by an enthalpy of about −0.2 kcal/mol,[13,22] as compared with −0.5 and −2 kcal/mol for the interaction between alcohols and $CCl_4$ and toluene, respectively.[2,6,13] These values are to be compared with the intrinsic enthalpy of formation of an H bond, about −5 kcal/mol.[1,2,5,6,21-23] (iii) The ultrasonic absorption of pure cyclohexane ($\alpha_0/f^2 = 195 \times 10^{-17}$ cm$^{-1}$ s$^2$, where $\alpha_0$ is the cyclohexane absorption coefficient and $f$ the ultrasonic frequency) is in the medium range.[26,29] The introduction of small amounts of alcohols in cyclohexane results in a small change of $\alpha_0/f^2$. This change can be evaluated to a good approximation by measuring the absorption of a cyclohexane solution of the saturated hydrocarbon with an alkyl chain identical with that of the alcohol.[29] (iv) Finally, the excess ultrasonic absorption of alcohol solutions in cyclohexane is quite large, even at concentration down to 0.05 M.[24,26-29] This allows measurements to be performed in a range of concentrations where nonideality effects other than those due to association are small and can be neglected.

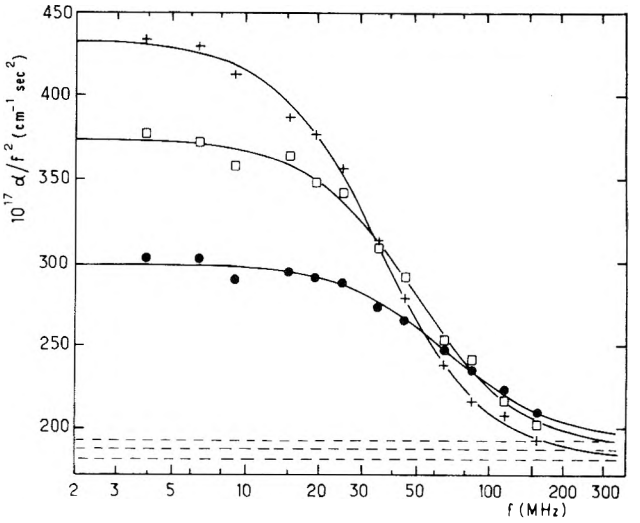


**Figure 1.** Ultrasonic relaxation spectra of 0.012 M solutions of ethanol (●), 1-octanol (□), and 1-hexadecanol (+) in cyclohexane at 25 °C. The solid curves have been obtained by a weighted least-squares fitting of the experimental results to the eq 4. The broken lines give the values of $B$ for the three solutions.

## II. Experimental Section

The ultrasonic absorptions ($\alpha/f^2$ values) of alcohol solutions were measured using the same equipment as in previous studies, in the frequency range 3.94–250 MHz.[26,29]

The various alcohols (ethanol, 1-butanol, 1-octanol, 1-dodecanol, 1-hexadecanol, 3-octanol, 2-methyl-3-heptanol, and 2,4-dimethyl-3-hexanol) were purchased from Fluka (Switzerland). The first five alcohols were of purissimum grade and the other three were of purum grade. All these compounds were used without further purification. The cyclohexane was freshly double distilled before use.

The solutions were prepared by weighing in both the alcohol and the solvent required to prepare 100 or 150 cm$^3$ of solution.

## III. Results

For the sake of illustrating the results we have shown in Figure 1 the ultrasonic absorption spectra of solutions of ethanol, 1-octanol, and 1-hexadecanol in cyclohexane. The absorption $\alpha/f^2$ is plotted against the frequency in a semilogarithmic plot. The values of $\alpha/f^2$ for all of the investigated solutions are available as supplementary material (see paragraph at end of text regarding supplementary material). In all instances the experimental results could be fitted very satisfactorily to the eq 4 which

$$\frac{\alpha}{f^2} = \frac{R}{1 + f^2/f_R^2} + B \qquad (4)$$

holds for a single relaxation frequency process.

For each alcohol solution the constant $B$ was set equal to the $\alpha/f^2$ value of an equimolecular solution of the alkane

with an alkyl chain identical with that of the alcohol. (In all instances these $\alpha/f^2$ values were found to be independent of $f$ in the frequency range investigated.) The validity of this procedure has been demonstrated in a previous study.[29]

In fitting the $\alpha/f^2$ vs. $f$ data to eq 4 a two-parameter weighted least-squares fitting procedure was adopted, where the parameters $R$ and $f_R$ are determined by minimization of the quantity

$$\sigma^2 = \Sigma\left[\frac{(\alpha/f^2)_{calcd} - (\alpha/f^2)_{exptl}}{(\alpha/f^2)_{exptl}}\right]^2 \qquad (4')$$

where $(\alpha/f^2)_{calcd}$ is the value of the absorption calculated by means of eq 4 for a given set of $R$ and $f_R$ values.

In Figure 1 the solid lines have been obtained as just described. In all instances the root mean square deviation $[\sigma^2/p]^{1/2}$ where $p$ is the number of experimental points was about 1% or less, and therefore smaller than the experimental uncertainty on $(\alpha/f^2)_{exptl}$, estimated to be about 2%. This result provides convincing evidence that the ultrasonic relaxation spectra of alcohol solutions in cyclohexane are characteristic of a single relaxation time. The values of $R$, $f_R$, and $B$ for the various systems investigated are listed in Table I. It can be seen that $f_R$ increases and that $R$ goes through a maximum as the alcohol concentration is increased except for the hindered isomer 2,4-dimethyl-3-hexanol, in agreement with observations made in other studies.[24,25,27-29]

The errors on $f_R$ and $R$ have been evaluated by changing at random and by a relative amount between 2 and −2% the $(\alpha/f^2)_{exptl}$ values found for a given alcohol solution, and fitting each of the sets of $\alpha/f^2$ values so obtained to eq 4, using the above weighted least-squares procedure. The relative error on $R$ is about 7%. The error on $f_R$ is of about 10% for $R > 100 \times 10^{-17}$ cm$^{-1}$ s$^2$ but increases rapidly as $R$ decreases.

As part of this study we have also determined the curves $\alpha/f^2$ vs. c at 9.09 MHz and 25 °C for all of the primary alcohols except 1-octanol. For this alcohol and for its three isomers (3-octanol, 2-methyl-3-heptanol, and 2,4-dimethyl-3-hexanol) the $\alpha/f^2$ vs. c curves were determined at 6.49 MHz in a previous study.[29] Finally, for 1-butanol the $\alpha/f^2$ vs. c curve was also determined at 85.3 MHz. As was emphasized above and as is shown below such results provide a very severe test to any association model which may be postulated for alcohols. Here again the excess absorption due to the association of the alcohol was obtained by taking the difference between the absorptions of equimolar solutions of the alcohol under study and of the corresponding saturated hydrocarbon, for instance, $n$-hexadecane in the case of 1-hexadecanol. The excess absorptions, referred to as $\Delta\alpha/f^2$, are given as supplementary material (see paragraph at end of text).

TABLE I: Values of the Relaxation Frequencies and Amplitudes

| Alcohol | c, M | $10^{17}R$, cm$^{-1}$ s$^2$ | $f_R$, MHz | $10^{17}B$, cm$^{-1}$ s$^2$ |
|---|---|---|---|---|
| Methanol | 0.098 | 94 | 72 | 194 |
| | 0.12 | 90 | 79 | 194 |
| Ethanol, | 0.06 | 70 | 45 | 194 |
| $c_{M,0} = c_{M,f} = 0.120$ M | 0.09 | 107 | 51 | 193 |
| | 0.12 | 106 | 67 | 193 |
| | 0.16 | 100 | 88 | 191 |
| | 0.20 | 90 | 109 | 191 |
| | 0.25 | 79 | 136 | 190 |
| 1-Butanol, | 0.06 | 86 | 41 | 194 |
| $c_{M,0} = c_{M,f} = 0.125$ M | 0.089 | 129 | 50 | 193 |
| | 0.12 | 131 | 66 | 192 |
| | 0.16 | 132 | 75 | 191 |
| | 0.22 | 116 | 106 | 189 |
| | 0.31 | 98 | 126 | 186 |
| 1-Octanol, | 0.047 | 91 | 30 | 192 |
| $c_{M,0} = 0.120$ M, | 0.085 | 170 | 41 | 190 |
| $c_{M,f} = 0.126$ M | 0.12 | 187 | 50 | 188 |
| | 0.19 | 173 | 71 | 184 |
| | 0.276 | 147 | 89 | 179 |
| 1-Dodecanol, | 0.05 | 115 | 25 | 190 |
| $c_{M,0} = 0.117$ M, | 0.087 | 215 | 33 | 187 |
| $c_{M,f} = 0.13$ M | 0.12 | 226 | 40 | 184 |
| | 0.16 | 222 | 52 | 180 |
| | 0.22 | 201 | 68 | 174 |
| | 0.305 | 173 | 76 | 168 |
| 1-Hexadecanol, | 0.04 | 74 | 20 | 190 |
| $c_{M,0} = 0.115$ M, | 0.085 | 138 | 27 | 185 |
| $c_{M,f} = 0.13$ M | 0.118 | 252 | 36 | 182 |
| | 0.16 | 255 | 43 | 177 |
| | 0.21 | 233 | 54 | 172 |
| | 0.27 | 205 | 68 | 165 |
| 3-Octanol, | | | | |
| $c_{M,0} = c_{M,f} = 0.32$ M | 0.07 | 25 | 58 | 191 |
| | 0.14 | 85 | 69 | 186 |
| | 0.22 | 113 | 92 | 182 |
| | 0.30 | 123 | 116 | 177 |
| | 0.45 | 117 | 163 | 169 |
| | 0.60 | 112 | 195 | 161 |
| 2-Methyl-3-heptanol, | 0.15 | 64 | 82 | 186 |
| $c_{M,0} = c_{M,f} = 0.55$ M | 0.25 | 98 | 115 | 180 |
| | 0.40 | 111 | 161 | 171 |
| | 0.80 | 102 | 277 | 153 |
| | 1 | 93 | 329 | 147 |
| 2,4-Dimethyl-3-hexanol | 0.25 | 36 | 144 | 183 |
| | 0.40 | 56 | 187 | 176 |
| | 0.65 | 68 | 215 | 164 |
| | 0.90 | 72 | 242 | 154 |

## IV. Discussion

1. *The Association Model.* The following general reaction mechanism, derived from that postulated by Fletcher and Heller,[1] was adopted for the purpose of fitting the results of Table I and the $\Delta\alpha/f^2$ data

$$nA \rightleftharpoons A_n \rightleftharpoons A_{nC} \qquad (5)$$

However, in contradistinction with these workers, we do not assume that the noncyclic species $A_n$ is linear. Rather, $A_n$ is believed to adopt a conformation intermediate between the linear and cyclic conformations, owing to steric hindrance of the alkyl chain which may favor a bending of the successive ···OH···OH···OH bonds. Because of this bending there may be a certain aggregation number for which the two ends of the polymer are fairly close to each other. The probability for these two ends to H bond together may then be larger than for H bonding with a free alcohol molecule, thereby resulting in a cyclization of the noncyclic species. The general mechanism 5 has been favored with respect to the one which could be derived from the model of Tucker and Becker[8] because it is difficult to explain why stable noncyclic species would still have to incorporate one or several additional monomeric alcohol molecules to give stable cyclic species.

2. *The Equations.* It has been previously[29] pointed out that the excess absorption of alcohol solutions is very likely due to the perturbation by the sound waves of the association–dissociation equilibrium in reaction mechanism 5. In this mechanism all species intermediate between the monomer and $A_n$ are assumed to be present in the solution only in very small amount. It is understood, however, that $A_n$ is formed by the following series of bimolecular reactions:

$$A + A \underset{k_{-1}}{\overset{k_1}{\rightleftharpoons}} A_2 \qquad K_1 = k_1/k_{-1}$$

$$A_2 + A \underset{k_{-2}}{\overset{k_2}{\rightleftharpoons}} A_3 \qquad K_2 = k_2/k_{-2} \qquad (6)$$

$$A_{n-1} + A \underset{k_-}{\overset{k}{\rightleftharpoons}} A_n \qquad K = k/k_-$$

As far as kinetics goes the Bodenstein approximation can be used for $A_2$, $A_3$, ..., $A_{n-1}$. Writing $d[A_2]/dt = d[A_3]/dt = \ldots = d[A_{n-1}]/dt = 0$ leads to the equation

$$[A_{n-1}] = \frac{K_1K_2\cdots K_{n-3}K_{n-2}[A]^{n-1} + k[A_n]\mathfrak{A}}{k_{-(n-2)} + k_-[A]\mathfrak{A}} \qquad (7)$$

where

$$\mathfrak{A} = 1 + \frac{k_{n-2}[A]}{k_{-(n-3)}}\left[\left(1 + \frac{k_{n-3}[A]}{k_{-(n-4)}}\left(1 + \cdots\left(1 + \frac{k_3[A]}{k_{-2}}\left(1 + \frac{k_2[A]}{k_{-1}}\right)\right)\right)\right)\right] \qquad (8)$$

Inserting $[A_{n-1}]$ into the rate equation

$$d[A_n]/dt = k[A][A_{n-1}] - k_-[A_n] \qquad (9)$$

results in

$$\frac{d[A_n]}{dt} = \frac{K_1K_2\cdots K_{n-2}k[A]^n - k_-[A_n]}{1 + [kA/k_{-(n-2)}]\mathfrak{A}} \qquad (10)$$

We have previously shown that[29]

$$k_1 > k_2 \approx k_3 \approx \cdots \approx k \qquad (11a)$$

Moreover, since reaction mechanism 5 assumes, in agreement with the experimental observations, that all intermediate species are present only in very small amount, we have

$$K_1 \approx K_2 \approx \cdots << K = k/k_-$$

The combination of this equation with eq 11a results in

$$k_{-1} \approx k_{-2} \approx \cdots \gg k_- \qquad (11b)$$

On the other hand, since there is only a very small amount of dimer one has

$$[A_2]/[A] = k_1[A]/k_{-1} \ll 1 \qquad (12)$$

Finally, since $k_1 > k_2$ it results that the ratios $k_2[A]/k_{-1}$, $k_3[A]/k_{-2}$, $k_{n-2}[A]/k_{-(n-3)}$, and $k[A]/k_{-(n-2)}$ are all much smaller than 1. Therefore $\mathfrak{A} \approx 1$ and

$$\frac{d[A_n]}{dt} = \prod_{i=1}^{n-2} K_i k[A]^n - k_-[A_n] \qquad (13)$$

The relaxation time is readily obtained as

$$1/\tau_R = 2\pi f_R = k_-(K_T n^2[A]^{n-1} + 1) \qquad (14)$$

where $K_T$ is the total equilibrium constant for the formation of the noncyclic $n$-mer, given by

$$K_T = \prod_{i=1}^{n-1} K_i = [A_n]/[A]^n \qquad (15)$$

This expression of $\tau_R$ is the same as the one which can be derived for the one-step $n$-molecular reaction

$$nA \underset{k_-}{\overset{k_-K_T}{\rightleftharpoons}} A_n \qquad (16)$$

However the above derivation shows that $k_-$ represents the rate constant for the dissociation of *one* monomer from the aggregate $A_n$ in the case of the series of bimolecular reactions 6, rather than the rate constant for the dissociation of $A_n$ in $n$A, as one would think when considering reaction 16.

The relaxation amplitude, obtained following the usual calculations,[29] is given by

$$R = \frac{2\pi^2\rho v}{10^3 RT}\frac{K_T[A](n-1)^2}{k_-(n^2K_T[A]^{n-1} + 1)^2} \times \left(\Delta V^\circ - \frac{\theta}{\rho C_p}\Delta H^\circ\right)^2 \qquad (17)$$

where $\rho$, $v$, $\theta$, and $C_p$ are the density, ultrasonic velocity, expansion coefficient, and specific heat capacity of the alcohol solution in cyclohexane. For the dilute solutions used in this study, these quantities can be taken as equal to those for cyclohexane. At 25 °C we found $2\pi^2\rho v/10^3RT = 7.78 \times 10^{-8}$ cgs and $\theta/(\rho C_p) = 3.55$ cm$^3$/kcal when the concentrations are expressed in mol/L and the average volume change $\Delta V^\circ$ and enthalpy change $\Delta H^\circ$ for the formation of one H bond in cm$^3$/mol and kcal/mol, respectively. In this study we have assumed that $\Delta V^\circ$ can be neglected with respect to the enthalpy term in eq 17. Indeed $|\Delta V^\circ|$ is probably less than 3 cm$^3$/mol.[34] On the other hand, $|\Delta H^\circ|$ is larger than 5 kcal/mol.[1,2,5,6,21-23] Thus $\Delta V^\circ$ represents less than 15% of the enthalpy term and may be neglected when considering the errors resulting from the approximations involved in the derivation of eq 14, 17, 19, and 20 (see below), particularly the assumed absence of species other than A, $A_n$, and $A_{nC}$.

$R$ is related to the excess absorption $\Delta\alpha/f^2$ by the equation

$$\frac{\Delta\alpha}{f^2} = \frac{R}{1 + \omega^2\tau_R{}^2} \qquad (18)$$

It can be shown that at a given frequency $f$, $\Delta\alpha/f^2$ goes through a maximum at a concentration $c_{M,f}$ given by

$$c_{M,f} = [A]_{M,f} + nK_T(1 + K_C)[A]_{M,f}{}^n \qquad (19)$$

where

$$[A]_{M,f} = \left\{\frac{1 + (n-1)\left[1 + \frac{n(n-2)}{(n-1)^2}\left(\frac{\omega}{k_-}\right)^2\right]^{1/2}}{n^2K_T(n-2)}\right\}^{1/(n-1)} \qquad (20)$$

and

$$K_C = [A_{nC}]/[A_n] \qquad (21)$$

$K_C$ is the cyclization constant for the $n$-mer. At low frequency, where $(\omega/k_-)^2 << 1$, eq 20 reduces to

$$[A]_{M,0} = [n(n-2)K_T]^{-1/(n-1)} \qquad (22)$$

The insertion of $[A]_{M,0}$ into eq 19 gives the concentration $c_{M,0}$ where $R$ goes through a maximum. Note that $K_T$ can be expressed in terms of $n$, $K_C$, and $c_{M,0}$ according to

$$K_T = \frac{(K_C + n - 1)^{n-1}}{n(n-2)^n c_{M,0}{}^{n-1}} \qquad (23)$$

3. *Analysis of the Data.* The available experimental data are the values of $f_R$ and $R$ at various $c$'s, the value of $c_{M,0}$ obtained from the plot of $R$ vs. $c$, the values of $\Delta\alpha/f^2$

TABLE II: Effect of a Change in the Value of $c_{M,0}$ on the Calculated Values of $K_C$, $K_T$, $k_-$, $k'$, and $\Delta H°$ Best Fitting the Results for 1-Butanol at 25 °C

| $c_{M,0}$, M | $K_C$ | $K_T$, $M^{-3}$ | $10^{-8}k_-$, $s^{-1}$ | $10^{-9}k'$, $M^{-1}\,s^{-1}$ | $\Delta H°$, kcal/mol |
|---|---|---|---|---|---|
| 0.115 | 0.8 | 564 | 1.23 | 1.02 | −4.4 |
| 0.125 | 1.2 | 593 | 1.34 | 1.13 | −4.7 |
| 0.135 | 1.5 | 579 | 1.44 | 1.20 | −4.8 |

at various $c$'s and 6.49 or 9.09 MHz (supplementary Material), and the values of $c_{M,f}$ at those frequencies, given in Table I. On the other hand, the quantities of interest are $n$, $K_C$, $K_T$, $k_-$, and $\Delta H°$. The following procedure was adopted. Reasonable values of $n$ and $K_C$ were chosen ($n$ = 3 and $K_C$ = 0 are the initial values for all of the alcohols investigated), and used to calculate $K_T$ by means of eq 23. The mass conservation equation (eq 19 where the subscript $M$ is removed) then permits the calculation of [A] as a function of $c$. These data, together with $K_C$, $K_T$, and $n$ are then used for a least-squares fit to the $f_R$ against $c$ data, with $k_-$ as an adjustable parameter. Finally the $n$, $K_C$, $K_T$, and $k_-$ results are used for a least-squares fit to the $\Delta\alpha/f^2$ vs. $c$ data and/or the $R$ vs. $c$ data, with $|\Delta H°|$ as an adjustable parameter. This procedure is then repeated at a given $n$ value, for different $K_C$ to obtain a series of sets of $K_C$, $K_T$, $k_-$, and $\Delta H°$ fitting the experimental results. (Since reactions of formation of a H bond are always exothermic,[1,2,5,6,21-23] we have used in the rest of this paper $\Delta H°$ with its proper sign rather than $|\Delta H°|$.) Finally, $n$ is changed and the calculations are repeated.

The value of $c_{M,0}$ is usually not as accurately determined as $c_{M,f}$ because many more experimental results determine the $\Delta\alpha/f^2$ vs. $c$ curve at 6.49 or 9.09 MHz than the $R$ vs. $c$ curve. However, for ethanol and butanol one can write, to a good approximation

$$c_{M,0} \cong c_{M,f} \tag{24}$$

because $(\omega/k_-)^2 << 1$ (see below). For long-chain primary alcohols (octanol, dodecanol, hexadecanol), this approximation introduces an error of 5–15% on the position of the absorption maximum, which results in a large error on $K_T$. This error was largely reduced by the following procedure. Once the $k_-$ values had been determined in the approximation $c_{M,0} = c_{M,f}$, the values of $k_-$, $K_T$, $K_C$, and $n$ were inserted into eq 19 and 20 to obtain a new value $c'_{M,f}$ of $c_{M,f}$ with $c'_{M,f} > c_{M,f}$. The value of $c_{M,0}$ was then calculated as

$$c_{M,0} = {c_{M,f}}^2/c'_{M,f} \tag{25}$$

This value was used to recalculate $K_T$ and $k_-$ for various sets of $n$ and $K_C$ values. The values of $c_{M,0}$ and $c_{M,f}$ are given in Table I.

The calculations have been performed for $n$ = 3, 4, and 5. Indeed although most of the models reported in the literature involve the first two values of $n$, the value $n$ = 5 cannot be discarded. For instance, the results reported by Aveyard et al.[11] (IR absorption and vapor pressure osmometry) and Anderson et al.[21] (calorimetry) are not inconsistent with such an association behavior although the deviations from the experimental results would then be slightly larger than for $n$ = 4.

Finally, it must be emphasized that the above calculation procedure relies very much on the values of $c_{M,0}$ and $c_{M,f}$. The actual calculations have shown that the values of $K_C$ and $K_T$ are rather sensitive to the values of $c_{M,f}$. However $k_-$ and $\Delta H°$ are only slightly dependent on this quantity and even on the value of $n$. An example of calculations showing the effect of a change of $c_{M,0}$ equal to the maximum uncertainty on this quantity (±0.01 M) on the values

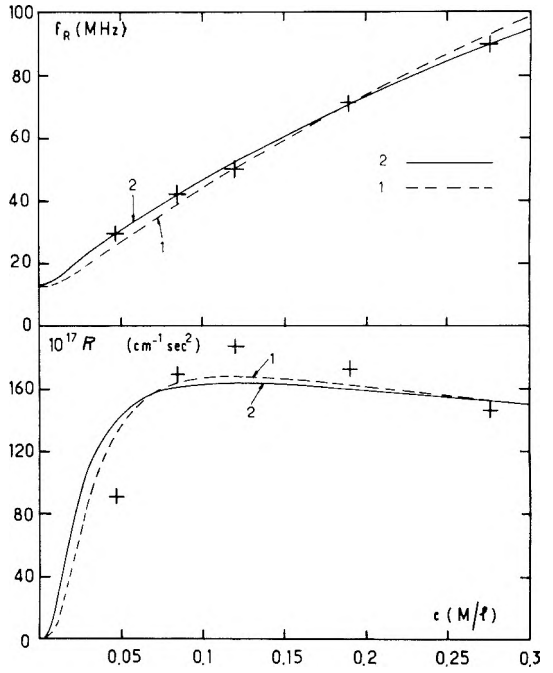


**Figure 2.** Fittings to the $f_R$ vs. $c$ data and to the $R$ vs. $c$ data for 1-butanol solutions in cyclohexane at 25 °C, assuming $n$ = 3: (curve 1) $K_C$ = 0; $K_T$ = 92.6 $M^{-2}$; $k_-$ = 7.9 × $10^7$ $s^{-1}$, and $\Delta H°$ = −5.2 kcal/mol; (curve 2) $K_C$ = 1; $K_T$ = 208 $M^{-2}$; $k_-$ = 8.2 × $10^7$ $s^{-1}$, and $\Delta H°$ = −6.3 kcal/mol.

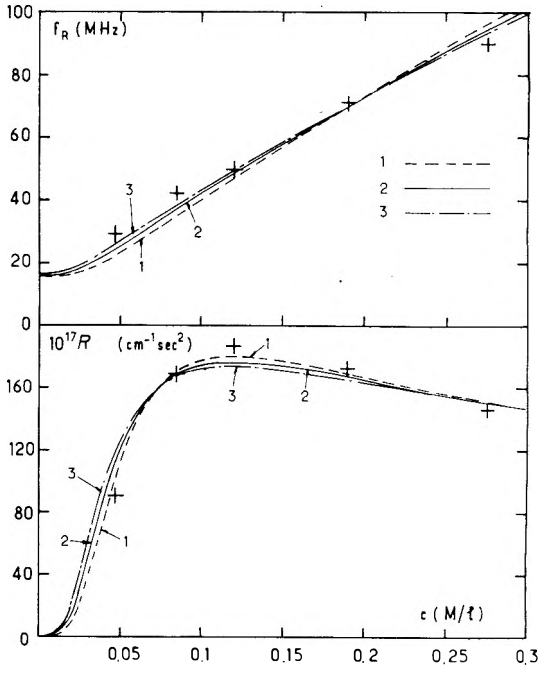


**Figure 3.** Fittings to the $f_R$ vs. $c$ data and to the $R$ vs. $c$ for 1-butanol in cyclohexane at 25 °C, assuming $n$ = 4: (curve 1) $K_C$ = 0.5; $K_T$ = 388 $M^{-3}$; $k_-$ = 9.8 × $10^7$ $s^{-1}$, and $\Delta H°$ = −4.6 kcal/mol; (curve 2) $K_C$ = 1; $K_T$ = 579 $M^{-3}$; $k_-$ = 1.02 × $10^8$ $s^{-1}$, and $\Delta H°$ = −4.9 kcal/mol; (curve 3) $K_C$ = 1.5; $K_T$ = 824 $M^{-3}$; $k_-$ = 1.04 × $10^8$ $s^{-1}$, and $\Delta H°$ = −5.3 kcal/mol.

of $K_C$, $K_T$, $k_-$, and $\Delta H°$ best fitting the results is given in Table II.

4. *Results for Primary Alcohols.* We have shown in Figures 2–4 some examples of curve fittings, using the values $n$ = 3, 4, and 5, respectively, for 1-butanol. Similar curves were calculated for the other primary alcohols. The calculated variations of $f_R$ with $c$ closely follow the experimental results for the three values of $n$ tested in this work. The residual mean squares ${S_{f_R}}^2$ of $f_R$ corresponding to all the calculated curves of Figures 2, 3, and 4 (see Table

TABLE III: Residual Mean Squares[a] $S_{f_R}^2$ (in $MHz^2$) and $S_R^2$ (in $10^{34}$ $cm^{-2}$ $s^4$) Corresponding to the Calculated Curves of Figures 2-4

| Figure | $n$ | Curve | $S_{f_R}^2$ [b] | $S_R^2$ [c] |
|---|---|---|---|---|
| 2 | 3 | 1 | 9.7 | 525 |
| | | 2 | 1.7 | 769 |
| 3 | 4 | 1 | 39 | 38 |
| | | 2 | 20 | 133 |
| | | 3 | 10 | 235 |
| 4 | 5 | 1 | 31 | 10 |
| | | 2 | 16 | 61 |
| | | 3 | 8.4 | 142 |

[a] Defined as the sum of the squared deviations divided by the difference between the number of experiments and the number of parameters (K. Hyunyong, *J. Chem. Educ.*, 47, 120 (1970)). [b] Maximum value 50. [c] Maximum value 152.

III) are smaller than the value of this quantity calculated from the estimated error on $f_R$ (10%). This finding constitutes a good illustration of the Bordewijk[15] statement, namely, that a property which shows a monotonous change with concentration is not a good criteria to test an association mechanism. On the contrary, the calculated variations of $R$ with $c$ clearly show that for $n = 3$ there are no values of $K_C$ which yield a reasonable fit to the data, while about equally good fits are obtained for $n = 4$ and 5, with appropriate $K_C$ values. This is further substantiated by comparing the residual mean squares $S_R^2$ of $R$ corresponding to the curves of Figures 2–4, to the maximum value of this quantity calculated from the estimated error on $R$ (see Table III). Thus, trimers cannot be the predominant species in primary alcohol solutions at $c <$ 0.3 M.

The ranges of $K_C$ values and the corresponding ranges of $K_T$, $k_-$, and $\Delta H°$ values best fitting the results are compiled in Table IV for $n = 4$ and 5. For each alcohol, the listed range of $K_C$ values corresponds to the common part of the two ranges of $K_C$ values best fitting the $f_R$ vs. $c$ and $R$ vs. $c$ data, with more weight being given to the $K_C$ values best fitting the $R$ vs. c data. In all instances the $K_C$ values differ from zero. Thus, the ultrasonic absorption studies confirm the conclusions of other investigations,[1,2,5,8,10,15,16,29] namely, that cyclic and noncyclic species are at equilibrium in alcohol solutions in nonpolar solvents. This finding provides an explanation for the observation of Musa and Eisner.[24] In their ultrasonic study of *tert*-butyl alcohol in cyclohexane these authors interpreted the results on the basis of the reaction $4A \rightleftharpoons A_4$ but could not account for the amount of alcohol in the solution when inserting in the mass conservation equation the tetramerization constant evaluated from the ultrasonic data. The difference obviously arises from the fact that the cyclic tetramer, which is not involved in the kinetics of the association process but must be considered in the stoichiometry, is not taken into account.

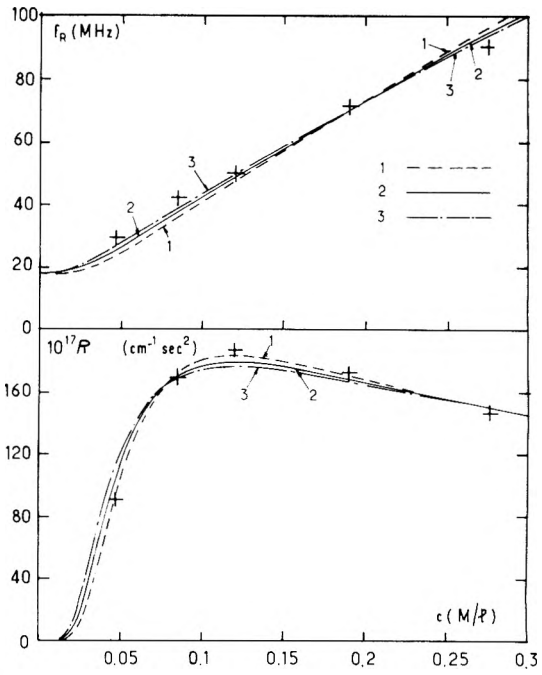


**Figure 4.** Fittings to the $f_R$ vs. c data and to the $R$ vs. c data for 1-butanol in cyclohexane at 25 °C, assuming $n = 5$: (curve 1) $K_C = 1.9$; $K_T = 4810$ $M^{-4}$; $k_- = 1.12 \times 10^8$ $s^{-1}$, and $\Delta H° = -4.8$ kcal/mol; (curve 2) $K_C = 2.7$; $K_T = 8000$ $M^{-4}$; $k_- = 1.15 \times 10^8$ $s^{-1}$, and $\Delta H° = -5.1$ kcal/mol; (curve 3) $K_C = 3.5$; $K_T = 12560$ $M^{-4}$; $k_- = 1.17 \times 10^8$ $s^{-1}$, and $\Delta H° = -5.4$ kcal/mol.

The results of Table IV show that for both $n = 4$ and 5 the value of $K_C$ appears to decrease slightly upon increasing length of the alkyl chain, particularly for long chain alcohols. This result may indicate that steric hindrance introduced by the alkyl chain has an increasing destabilizing effect on the cyclic structures as the chain grows. In fact, for 1-hexadecanol the $K_C$ values best fitting the $f_R$ and $\Delta\alpha/f^2$ data overlap only very little for $n = 4$.

TABLE IV: Values of $K_C$, $K_T$, $k_-$, $k'$, and $\Delta H°$ Best Fitting the Ultrasonic Absorption Data for Primary Alcohols at 25 °C[a]

| | $n = 4$ | | | | | $n = 5$ | | | | |
|---|---|---|---|---|---|---|---|---|---|---|
| | $K_C$ | $K_T$, $M^{-3}$ | $10^{-8}k_-$, $s^{-1}$ | $10^{-9}k'$, $M^{-1}$ $s^{-1}$ | $-\Delta H°$, kcal/mol | $K_C$ | $K_T$, $M^{-4}$ | $10^{-8}k_-$, $s^{-1}$ | $10^{-9}k'$, $M^{-1}$ $s^{-1}$ | $-\Delta H°$, kcal/mol |
| Ethanol | 0.5 | 387 | 1.48 | 1.08 | 4 | 2 | 5144 | 1.68 | 1.42 | 4.2 |
| | 0.8 | 496 | 1.50 | 1.19 | 4.2 | 2.5 | 7085 | 1.70 | 1.56 | 4.4 |
| | 1.2 | 670 | 1.53 | 1.34 | 4.4 | 3 | 9529 | 1.72 | 1.7 | 4.5 |
| Butanol | 0.7 | 405 | 1.31 | 0.97 | 4.4 | 2.3 | 5310 | 1.48 | 1.27 | 4.6 |
| | 1.2 | 593 | 1.35 | 1.13 | 4.7 | 3 | 8094 | 1.51 | 1.43 | 4.8 |
| | 1.7 | 831 | 1.37 | 1.29 | 5 | 3.7 | 11850 | 1.54 | 1.60 | 5.1 |
| Octanol | 0.5 | 388 | 0.98 | 0.72 | 4.5 | 1.9 | 4809 | 1.12 | 0.93 | 4.8 |
| | 1 | 578 | 1.02 | 0.85 | 4.9 | 2.7 | 7998 | 1.15 | 1.09 | 5 |
| | 1.5 | 824 | 1.04 | 0.98 | 5.2 | 3.5 | 12558 | 1.17 | 1.24 | 5.3 |
| Dodecanol | 0.2 | 320 | 0.75 | 0.51 | 4.4 | 1.5 | 4019 | 0.87 | 0.69 | 4.6 |
| | 0.7 | 494 | 0.79 | 0.63 | 4.8 | 2 | 5692 | 0.89 | 0.77 | 4.9 |
| | 1.2 | 723 | 0.82 | 0.73 | 5.2 | 2.5 | 7840 | 0.91 | 0.85 | 5.1 |
| Hexadecanol | 0 | 277 | 0.65 | 0.42 | 4.2 | 1 | 2941 | 0.75 | 0.55 | 4.4 |
| | 0.5 | 440 | 0.69 | 0.53 | 4.7 | 1.5 | 4306 | 0.77 | 0.63 | 4.6 |
| | 1 | 657 | 0.72 | 0.62 | 5 | 2 | 6098 | 0.79 | 0.70 | 4.9 |

[a] In this table, for each alcohol the second line gives the best fitting values. The first and third lines give data which still fit the results within the experimental uncertainty, but with a much larger total root mean square deviation.

TABLE V: Number and Weight Average Aggregation Numbers for 1-Butanol in Cyclohexane at 25 °C

| | $\bar{n}_n$ | | | $\bar{n}_w$ | | |
|---|---|---|---|---|---|---|
| c, M | a | b | c | a | b | c |
| 0.1 | 1.3 | 1.5 | 1.7 | 2.1 | 2.4 | 3.0 |
| 0.2 | 1.8 | 1.9 | 2.2 | 3.3 | 2.9 | 3.8 |
| 0.3 | 2.1 | 2.2 | 2.6 | 4.2 | 3.2 | 4.1 |
| 0.4 | 2.5 | 2.4 | 2.9 | 4.9 | 3.3 | 4.3 |
| 0.5 | 2.8 | 2.6 | 3.1 | 5.3 | 3.4 | 4.4 |
| 0.7 | 3.3 | 2.8 | 3.4 | 5.8 | 3.6 | 4.5 |

[a] From ref 14. [b] Calculated from the results of Table III for $n = 4$ and $K_T(1 + K_C) = 1300$ M$^{-1}$. [c] Calculated from the results of Table III, for $n = 5$ and $K_T(1 + K_C) = 8100$ M$^{-4}$.

For $n = 5$, however, the listed $K_C$ values provide a much better overall fit to the data than in the case for $n = 4$. It thus appears as if the steric hindrance due to a long alkyl chain resulted in the formation of larger noncyclic and cyclic species than in the case of alcohols with shorter alkyl chain. On the other hand, the results listed in Table IV seem to indicate that for both $n = 4$ and 5, $K_T$ increases in going from ethanol to 1-octanol, in agreement with the finding of Fletcher and Heller.[1,2] However, for longer alcohols, $K_T$ shows a small decrease. To our knowledge there has not been any detailed investigations of the association of long chain alcohols by other methods. For this reason it cannot be said whether the observed changes of $K_T$ and $K_C$ found in this work indicate a real trend in the association behavior of primary alcohols or result from the various approximations involved in the calculations. The values of $K_T$ and $K_C$ found in this investigation may be compared to the results reported by other workers. For 1-octanol in *n*-decane, Fletcher and Heller[1] reported $K_T = 235$ M$^{-3}$ and $K_C = 2.2$. For the same alcohol in cyclohexane we have obtained $K_T = 578 \pm 200$ M$^{-3}$ and $K_C = 1 \pm 0.5$. The difference between the two sets of values is fairly large. Nevertheless, since the errors on the individual values are large, particularly in ultrasonic absorption (the uncertainty in the IR measurements[1] could not be estimated), the two sets of results may still be considered as consistent. On the other hand, Meeussen and Huyskens[14] have calculated the number and weight average association numbers $\bar{n}_n$ and $\bar{n}_w$ of 1-butanol in cyclohexane as a function of c from measurements of partition coefficients between water and cyclohexane. With the $K_T$ and $K_C$ values found for 1-butanol in this study we have calculated $\bar{n}_n$ and $\bar{n}_w$ for $n = 4$ and 5. The results are listed in Table V. It can be seen that in the concentration range investigated in our work the ultrasonic values of $\bar{n}_n$ for $n = 4$ agree fairly well with those of Meeussen and Huyskens.[14] The agreement is less satisfactory for $\bar{n}_w$. If it is assumed that only one associated species is present the results of Meeussen and Huyskens suggest that the aggregation number of this species slowly increases with concentration. Note that the values of $\bar{n}_w$ and $\bar{n}_n$ are only slightly decreased when dimerization is taken into account, with a dimerization constant of 1 M$^{-1}$ (see below).

The values of $\Delta H°$ are all around $-4.8 \pm 0.2$ kcal/mol, except for ethanol where a somewhat smaller value has been found. These values are about 10–15% smaller than those determined by other methods. The complete neglecting of the dimers is partly responsible for these small values of $\Delta H°$. Indeed, calculations where dimers are taken into account (see below) have yielded values of $|\Delta H°|$ larger by about 0.2 kcal/mol. However, most of the difference between the ultrasonic values of $\Delta H°$ and those obtained by means of IR[1,2] or calorimetry[11,21] probably arise from the assumption made above, namely, that the $\Delta V°$ term in eq 17 is negligible with respect to the enthalpy term. If we use the value $\Delta H° = -5.6$ kcal/mol[1,2,11,21] and insert this result in the eq 17, the volume change $\Delta V°$ is found to be of about $-2 \pm 1$ cm$^3$/mol. This value is of the same order as that found by other workers from pressure studies.[34] Note that the $\Delta H°$ values do not appear to constitute a valuable test of the goodness of a model. Fletcher and Heller[1] pointed out that all of the association models that were tested in their IR study consistently yielded values of $\Delta H°$ around $-5$ kcal/mol.

For a given alcohol, the values of $k_-$ (see Table IV) obtained for $n = 4$ and 5 show surprisingly small differences: about 15% for ethanol and 10% for 1-hexadecanol. These values which decrease only by a factor of about 2 in going from ethanol to hexadecanol, are all of the order of $10^8$ s$^{-1}$. Similar values for the dissociation rate constants of a number of H-bonded dimers have been reported in several kinetic studies of H bonding in nonpolar solvents, including cyclohexane.[35-37]

From the values of $k_-$ and $K_T$ it becomes possible to evaluate a lower bound $k'$ for $k$ (see reaction 6). For instance, for $n = 4$, we have

$$k = k_- \frac{k_{-1}}{k_1} \frac{k_{-2}}{k_2} K_T \tag{26}$$

We know that $k_- << k_{-1}, k_{-2}$ and that $k_1 > k_2 \approx k$, therefore

$$k > k_- K_T^{1/3} = k' \tag{27}$$

Likewise, for $n = 5$ we have

$$k > k_- K_T^{1/4} = k' \tag{28}$$

The values of $k'$ given in Table IV are all close to $10^9$ M$^{-1}$ s$^{-1}$, and show a decrease by a factor of about 2 in going from ethanol to hexadecanol. The value of the diffusion controlled association rate constant of one alcohol molecule A to an alcohol trimer $A_3$ may be calculated by means of the equation[38]

$$k_{dif} = 4\pi a p \frac{N}{1000}(D_A + D_{A_3}) \tag{29}$$

where $N$ is Avogadro's number, $D_A$ and $D_{A_3}$ are the diffusion coefficients of the alcohol monomer A and trimer $A_3$ in cyclohexane, $a$ is the reaction distance taken as 0.5 nm, and $p$ a steric factor, accounting for the fact that the H-bonding sites on $A_3$ are hindered with respect to the monomer. We have assumed that $p = 0.75$ for the unhindered primary alcohols. For 1-octanol in cyclohexane $D_A = 1.25 \times 10^{-5}$ cm$^2$ s$^{-1}$ [39] and we may assume that $D_{A_3} \sim D_A/3^{1/3} = 1.08 \times 10^{-5}$ cm$^2$ s$^{-1}$. Inserting these numerical values in eq 29 yields $k_{dif} = 5.8 \times 10^9$ M$^{-1}$ s$^{-1}$ for 1-octanol. This value is only a factor of 7 larger than $k'$, the lower bound of $k$. One can therefore safely conclude that the rate of association of alcohol molecules through a H bond is close to its diffusion controlled limit. This conclusion is further substantiated by the correlation which can be seen in Figure 5 between the values of $k'$ and $k_-$ for $n = 4$ and 5 and the diffusion coefficients of primary alcohols in benzene.[40] (A similar plot should be obtained when using the $D_A$ values in cyclohexane but these values could not be found in the literature for long-chain alcohols.) Note that such a conclusion agrees with the results of a number of kinetic studies of association of small molecules through H bonds in organic solvents.[35-37] It is at variance, however, with the conclusions of Rassing and coworkers[27,28] who investigated the association of benzyl alcohol and *tert*-butyl alcohol in cyclohexane by means of ultrasonic absorption. The stepwise association model

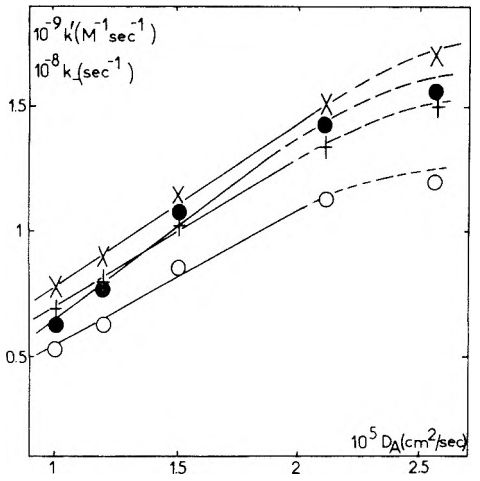


**Figure 5.** Correlation between the rate constants $k'$ and $k_-$ of primary alcohols in cyclohexane for $n = 4$ (O and +) $n = 5$ (● and ×) and their diffusion coefficients in benzene.[40] The experimental results correspond to ethanol, butanol, octanol, dodecanol, and hexadecanol.

adopted by these workers yielded association rate constants of $5 \times 10^8$ $M^{-1}$ $s^{-1}$ for the dimerization reaction and $10^8$ $M^{-1}$ $s^{-1}$ for the subsequent association steps. These values result from the assumptions underlying the Rassing et al.[27,28] model which are equivalent to assuming that dimers are the predominant species in alcohol solutions.

In the above calculations the effect of dimerization on the kinetics of alcohol association has been completely neglected (dimers were assumed to be in a stationary state). However, evidence for the existence of a small amount of open dimers has been reported in several papers.[5,11,15,16,21] For this reason, on the basis of the calculated values of $K_C$, $K_T$, $k_-$, and $\Delta H°$ we shall first evaluate the eventual contribution of dimers to the excess absorption of primary alcohols. Then, as a further assessment of the effect of dimerization, we shall examine how the values of $K_C$, $K_T$, and $k_-$ are modified when dimerization is taken into account in the case of 1-octanol. The following association model is now considered

$$2A \overset{k_D}{\rightleftharpoons} A_2 \tag{30a}$$

$$(n-2)A + A_2 \underset{k_-}{\overset{k}{\rightleftharpoons}} A_n \tag{30b}$$

$$A_n \rightleftharpoons A_{nC} \tag{30c}$$

In the calculations, the dimerization is assumed to be very fast with respect to the subsequent association steps leading to $A_n$, and the intermediate species $A_3$, ..., $A_{n-1}$ are assumed to be in a stationary state. The dimerization constant $K_D$ is taken as 1 $M^{-1}$ throughout the calculations. (Values of this order or smaller have been reported in several studies.[5,11,16,21]) The excess absorption for the dimerization step is given by

$$\frac{\Delta\alpha_D}{f^2} = 9.83 \times 10^{-7} \Delta H_D^2 \times \frac{K_D^2[A]^2}{k_D(4K_D[A] + 1)^2[1 + f^2/f_{R,D}^2]} \tag{31}$$

with

$$f_{R,D} = k_D K_D^{-1}(4K_D[A] + 1)/2\pi \tag{32}$$

where [A] is obtained by solving the mass conservation equation

$$c = [A] + 2K_D[A]^2 + 4K_T(1 + K_C)[A]^4 \tag{33}$$

with $k_D = k' \approx 10^9$ $M^{-1}$ $s^{-1}$, $K_D = 1$ $M^{-1}$, $K_T(1 + K_C) = 1150$ $M^{-3}$ (case of 1-octanol) and $\Delta H_D = -5$ kcal/mol. The calculated values of $\Delta\alpha_D/f^2$ where found to be below 2 and $10 \times 10^{-17}$ $cm^{-1}$ $s^2$ at c = 0.05 and 0.35 M, at frequencies below 100 MHz. Note that these values represent *maximum* estimates. If $k_D$ is taken as $k_{dif}$ rather than $k'$ the values of $\Delta\alpha_D/f^2$ would instead be 0.2 and $2 \times 10^{-17}$ $cm^{-1}$ $s^2$. Thus, for our purpose, the contribution of dimerization to the excess absorption of unhindered alcohols may safely be neglected at low frequencies where the absorption due to the other association steps is almost two orders of magnitude larger. At higher frequencies the absorption due to dimerization may introduce some errors in the determination of the value of $B$ from the plot of $\alpha/f^2$ vs. c. This difficulty was avoided in our work by determining $B$ as described above.

We now examine reaction 30b which gives rise to the observed excess absorption. The expressions of $f_R$ and $R$ for this reaction derived using the general equations for coupled equilibria are given by

$$f_R = k_-[1 + n^2K_T[A]^{n-1}/(4K_D[A] + 1)]/2\pi \tag{34}$$

and

$$R = 9.83 \times 10^{-7} \Delta H^2 \times \frac{K_T[A]^n[2K_D[A](n-2) + n - 1]^2}{k_-(4K_D[A] + 1 + n^2K_T[A]^{n-1})^2} \tag{35}$$

where $\Delta H$ is the average enthalpy for the formation of one H bond. The fit to the data was made using the procedure described above with $K_D = 1$ $M^{-1}$. The calculations showed that for $n = 5$, simultaneous fits to the $f_R$ vs. $c$ values and $R$ and $\Delta\alpha/f^2$ vs. $c$ values are obtained for 1-octanol in a narrower range of $K_C$ values than if dimerization was neglected. In fact, the two ranges of $K_C$ values fitting the two sets of data hardly overlapped. A better overlapping would be obtained for $n = 6$. The $k_-$ values (and thus the $k'$ values) were very close to those when $K_D = 0$. On the other hand, the $|\Delta H°|$ value best fitting the results was larger by about 0.2 kcal/mol, which makes it closer to the values obtained by other methods. Finally, although $K_T$ and $K_C$ are respectively increased and decreased, the product $K_T(1 + K_C)$ is only slightly increased when dimerization is taken into account. Since the $K_D$ value used in this calculations represents an upper limit, the overall effect of dimers and of the other species assumed to be in a stationary state appears to be relatively small.

5. *Results for 3-Octanol and 2-Methyl-3-heptanol.* For these two alcohols the curves $\Delta\alpha/f^2$ vs. $c$ still show a maximum which indicates that, as for primary alcohols, association proceeds beyond the dimer stage. We have however no indication whether cyclic and noncyclic species are at equilibrium, as for primary alcohols. At any rate we have performed on the results of Table I and on the $\Delta\alpha/f^2$ vs. $c$ data the same calculations as for primary alcohols on the basis of reaction mechanism 5. For 3-octanol the results could not be fitted with $n = 3$ but good fits were obtained for $n = 4$ and 5. For 2-methyl-3-heptanol a good fit to the data could be obtained with $n = 3$ and $K_C$ close to zero. A fairly good fit was also obtained for $n = 4$ but the data could not be fitted with $n = 5$. The data listed in Table VI show much smaller values of $K_T$ and larger values of $k_-$ than for the unhindered 1-octanol. Thus, the noncyclic $n$-mers formed by hindered alcohols such as 3-octanol and 2-methyl-3-heptanol have a much lower stability than those formed by 1-octanol. This decreased stability shows essentially through the larger dissociation rate constants.

TABLE VI: Results for 3-Octanol and 2-Methyl-3-heptanol at 25 °C

| | 3-Octanol | | 2-Methyl-3-heptanol | |
|---|---|---|---|---|
| | $n = 4$ | $n = 5$ | $n = 3$ | $n = 4$ |
| $K_C$ | 1 | 3 | 0 | 1.5 |
| $K_T$, $M^{-3}$ or $M^{-4}$ | 30.5 | 188 | 4.4 | 8.6 |
| $10^{-8}k_-$, $s^{-1}$ | 2.5 | 2.8 | 3.3 | 4.3 |
| $\Delta H^\circ$, kcal/mol | −3.9 | −4.2 | −3.9 | −3.9 |
| $10^{-8}k'$, $M^{-1}$ $s^{-1}$ | 7.8 | 10.4 | 7 | 8.8 |

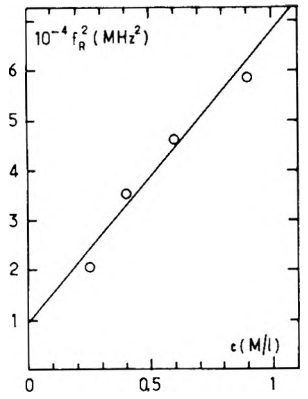


**Figure 6.** Plot of $f_R^2$ vs. $c$ for 2,4-dimethyl-3-hexanol in cyclohexane at 25 °C.

It is well understood, however, that the results of Table VI have only a semiquantitative character because the dimerization step was not taken into account. This step is expected to largely affect the results of Table VI owing to the smaller $K_T$ values for the two hindered octanols with respect to 1-octanol. Approximate calculations using $K_D = 1\ M^{-1}$, $\Delta H = -4.7$ kcal/mol of H bond and $k = 10^9\ M^{-1}\ s^{-1}$ have yielded for 2-methyl-3-heptanol values of $\Delta\alpha/f^2$ of 24 and $34 \times 10^{-17}\ cm^{-1}\ s^2$ at $c = 0.35$ and 0.7 M, respectively. These values represent upper limits. Nevertheless, they show that for 2-methyl-3-heptanol the assumption that the dimerization step can be neglected is hardly justified. This assumption holds much better in the case of 3-octanol where the value of $K_T(1 + K_c)$ is three times larger than for 2-methyl-3-heptanol.

6. *Results for 2,4-Dimethyl-3-hexanol.* The $\Delta\alpha/f^2$ and $R$ vs. $c$ curves show only a sigmoidal increase (Figure 2 in ref 29). Moreover, the plot of $f_R^2$ vs. $c$ is practically linear (Figure 6). These two results indicate that the association of 2,4-dimethyl-3-hexanol is essentially limited to dimerization. Larger aggregates than dimers are likely to be present only in fairly small amounts. Using eq 30–33 with $K_T = 0$ we found $k_- = 6.3 \times 10^8\ s^{-1}$, $k = 4.6 \times 10^8\ M^{-1}\ s^{-1}$, $K_D \approx 0.7\ M^{-1}$, and $\Delta H_D = -4.5 \pm 0.2$ kcal/mol. Note that the value of $k_-$ is much larger than for 1-octanol. A somewhat smaller value is found for the association rate constant, owing to strong steric hindrance about the OH group of 2,4-dimethyl-3-hexanol.

7. *Comparison between Dipole Moment Data at Low Frequency and Ultrasonic Absorption Data.* We have shown in Figures 7 and 8 the concentration dependence of the square of the apparent dipole moment $\mu_a^2$ at 2 MHz (from the data in ref 16) and of $\Delta\alpha/f^2$ at 6.49 MHz for 1- and 3-octanol in cyclohexane and 1-octanol in $CCl_4$. The maximum or the end of the plateau of the $\mu_a^2$ vs. $c$ curves occurs at the concentration corresponding to the onset of absorption on the $\Delta\alpha/f^2$ vs. $c$ curves. It must be recalled that the maximum or the plateau on the $\mu_a^2$ vs. $c$ curves was attributed to the antagonistic effects associated with the formation of high-dipole moment open dimers which predominate at low c's, and low dipole moment cyclic trimers and tetramers.[15,16] Our results and calculations

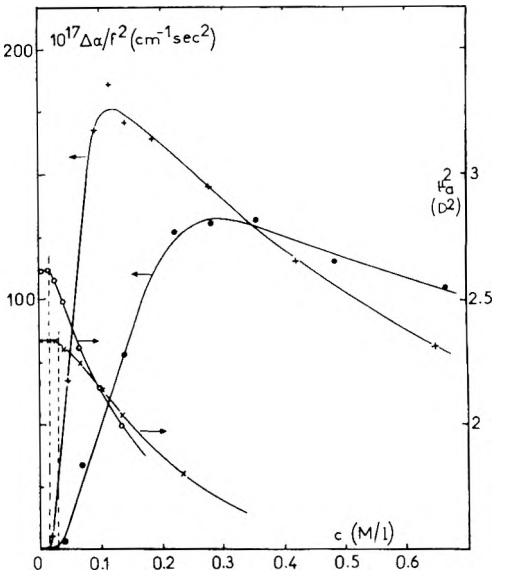


**Figure 7.** Concentration dependence of the square of the apparent dipole moment and of $\Delta\alpha/f^2$ for 1-octanol (O and +) and 3-octanol (× and ●) in cyclohexane at 25 °C. The onset of excess absorption occurs at the same concentration as the end of the plateau or the small maximum in $\mu_a^2$.

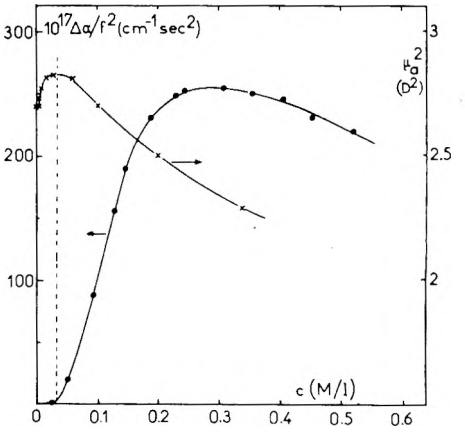


**Figure 8.** Concentration dependence of the square of the dipole moment (×) and of the excess absorption (●) of 1-octanol in $CCl_4$ at 25 °C.

agree with this interpretation. Indeed the calculations performed with $K_D = 1\ M^{-1}$ and $K_T(1 + K_C) = 700\ M^{-3}$ show that the change of $\Delta\alpha/f^2$ with $c$ closely follows that of the concentration of $A_4$ (or $A_5$) with c. The two curves show similar changes of slope at $c \approx 0.02$ M. At $c < 0.02$ M the dimer is largely predominant but the dimerization yields only a negligible excess absorption because $K_D$ and $c$ are too small.

In addition to kinetic information the ultrasonic absorption results also provide two important additional information with respect to dipole moment data. First, they clearly show that for primary alcohols, tetramers are the smallest associated species which account for the results while in dipole moment studies a choice could not be made between trimers and tetramers (no consideration was given to larger species).[15,16] Second, they indicate that the word cyclic used in the interpretation of the dipole moment measurements must not taken too literally. Indeed the ultrasonic results indicate that the alcohol solutions contain, in addition to a very small amount of dimers, true cyclic species where the two ends are H bonded together in equilibrium with the noncyclic species. As pointed out in section 1 of the Discussion, these noncyclic species are likely to adopt a somewhat folded conformation. Thus they would contribute much less to

the apparent dipole moment of the alcohol in solution than linear species and, in this type of measurement, may be looked at as cyclic species although this is not true in the chemical meaning of the word cyclic.

## Conclusion

The ultrasonic absorption data relative to primary alcohols support the association model proposed by other workers on the basis of studies by means of various techniques. The results indicate that the aggregated species giving rise to the excess ultrasonic absorption are noncyclic tetramers or pentamers and that cyclic species are present in solution. Pentamers may be favored with respect to tetramers in solution of long chain alcohols such as 1-hexadecanol.

The results have been analyzed on the basis of a reaction mechanism which assumes a simultaneous formation of cyclic and noncyclic tetramers or pentamers. For hindered alcohols the results clearly show a decreased stability of the tetramers and pentamers with respect to unhindered alcohols. The association of 2,4-dimethyl-3-hexanol leads essentially to dimers.

The results indicate that the rate of association of alcohol molecules through the H bond in cyclohexane is close to its diffusion-controlled limit for primary alcohols, and only slightly smaller (by a factor of 3–5) for a very hindered alcohol such as 2,4-dimethyl-3-hexanol. On the other hand, the rate of dissociation of one alcohol molecule from a noncyclic species (tetramer, pentamer, or even longer aggregates) depends only slightly on the alkyl chain length of the alcohol. This result establishes a clear difference between this reaction and the dissociation of one amphiphilic ion from micelles in aqueous solutions. The latter process is very strongly dependent on chain length and its kinetics is controlled by the hydrophobic free energy gained by the chain in the course of the dissociation.[41] It is likely however that in the case of solutions of detergent in organic solvents where associated species commonly referred to as inverted micelles are found, the dependence of $k_-$ on the chain length of detergent will be small, as in the case of alcohol solutions.

*Supplementary Material Available:* Tables of raw ultrasonic absorption data (6 pages). Ordering information is given on any current masthead page.

## References and Notes


(1) (a) A. Fletcher and C. Heller, *J. Phys. Chem.*, **71**, 3742 (1967); (b) *ibid.*, **72**, 1841 (1968).
(2) A. Fletcher, *J. Phys. Chem.*, **73**, 2217 (1969).
(3) R. Hammaker, R. Clegg, L. Patterson, P. Ridder, and S. Rock, *J. Phys. Chem.*, **72**, 1837 (1968).
(4) J. Dos Santos, P. Pineau, and M. Josien, *J. Chim. Phys. Physicochim. Biol.*, **62**, 628 (1965).
(5) A. Fletcher, *J. Phys. Chem.*, **76**, 2562 (1972).
(6) H. Van Ness, J. Van Vinkle, H. Richtol, and H. B. Hollinger, *J. Phys. Chem.*, **71**, 1483 (1967).
(7) W. D. Dixon, *J. Phys. Chem.*, **74**, 1396 (1970).
(8) E. Tucker and E. Becker, *J. Phys. Chem.*, **77**, 1783 (1973).
(9) M. Servanton-Gadouleau, J. Biais, and B. Lemanceau, *J. Chim. Phys. Physicochim. Biol.*, **72**, 831 (1975).
(10) E. Tucker, S. Farnham, and S. Christian, *J. Phys. Chem.*, **73**, 3820 (1969).
(11) R. Aveyard, B. Briscol, and J. Chapman, *J. Chem. Soc., Faraday Trans. 1*, **69**, 1772 (1973).
(12) V. Cheam, S. Farnham, and S. Christian, *J. Phys. Chem.*, **74**, 4157 (1970).
(13) R. Aveyard and R. Mitchell, *Trans. Faraday Soc.*, **65**, 2645 (1969).
(14) E. Meeussen and P. Huyskens, *J. Chim. Phys. Physicochim. Biol.*, **63**, 845 (1966).
(15) P. Bordewijk, M. Kunst, and A. Rip., *J. Phys. Chem.*, **77**, 548 (1973); M. Kunst, D. Van Duijn, and P. Bordewijk, *Ber. Bunsenges. Phys. Chem.*, **80**, 839 (1976).
(16) C. Campbell, G. Brink, and L. Glasser, *J. Phys. Chem.*, **79**, 660 (1975); **80**, 686 (1976).
(17) B. Singh and J. K. Vij, *Bull. Chem. Soc. Jpn.*, **49**, 1824 (1976).
(18) J. Crossley, *J. Phys. Chem.*, **75**, 1790 (1971).
(19) M. Van Gemert, G. De Loor, P. Bordewijk, P. Quickenden, and A. Suggett, *Adv. Mol. Relaxation Processes*, **5**, 301 (1973).
(20) J. Crossley, L. Glasser, and C. Smyth, *J. Chem. Phys.*, **55**, 2197 (1971); L. Glasser, J. Crossley, and C. Smyth, *ibid.*, **57**, 3977 (1972); C. Campbell, J. Crossley, and L. Glasser, *Adv. Mol. Relaxation Processes*, **9**, 63 (1976).
(21) B. Anderson, J. Rytting, S. Lindenbaum, and T. Higuchi, *J. Phys. Chem.*, **79**, 2340 (1975).
(22) F. Smith and I. Brown, *Aust. J. Chem.*, **26**, 691 (1973).
(23) C. Savini, D. Winterhalter, and H. Van Ness, *J. Chem. Eng. Data*, **10**, 168 (1965).
(24) R. Musa and M. Eisner, *J. Chem. Phys.*, **30**, 227 (1959).
(25) V. Solovyev, C. Montrose, M. Watkins, and T. Litovitz, *J. Chem. Phys.*, **48**, 2155 (1968).
(26) J. Lang and R. Zana, *Trans. Faraday Soc.*, **66**, 957 (1970).
(27) J. Rassing and B. Jensen, *Acta Chim. Scand.*, **24**, 855 (1970).
(28) F. Garland, J. Rassing, and G. Atkinson, *J. Phys. Chem.*, **75**, 3182 (1971).
(29) R. Zana and J. Lang, *Adv. Mol. Relaxation Processes*, 7, 21 (1975).
(30) M. Emara and G. Atkinson, *Adv. Mol. Relaxation Processes*, 6, 233 (1974).
(31) A. Fletcher and C. Heller, *J. Catal.*, **6**, 263 (1966).
(32) N. Coggeshall and E. Saier, *J. Am. Chem. Soc.*, **73**, 5414 (1951).
(33) In a recent report Emara and Atkinson[30] have reinterpreted the results of Solovyev et al.[25] (ethanol in ethyl halides) in terms of a monomer–dimer equilibrium. On the basis of this model the authors accounted satisfactorily for the monotonous increase of $f_R$ with alcohol concentration $c$. However, this model did not permit to account, even on a qualitative basis, for the maximum found in the variation of the excess ultrasonic absorption with $c$. For this reason the monomer–dimer equilibrium cannot be responsible for the excess absorption of ethanol solutions and, therefore, must be discarded.
(34) E. Fishman and H. G. Drickamer, *J. Chem. Phys.*, **24**, 548 (1956).
(35) G. G. Hammes and A. C. Park, *J. Am. Chem. Soc.*, **91**, 956 (1969); G. G. Hammes and P. J. Lillford, *ibid.*, **92**, 7578 (1970); G. G. Hammes and H. O. Spivey, *ibid.*, **88**, 1621 (1966).
(36) L. De Maeyer, M. Eigen, and J. Suarez, *J. Am. Chem. Soc.*, **90**, 3157 (1968).
(37) R. W. Hopmann, *Ber. Bunsenges. Phys. Chem.*, **77**, 52 (1973).
(38) I. Amdur and G. G. Hammes, "Chemical Kinetics", McGraw-Hill, 1966, p 63.
(39) M. A. Gillot, Thèse de 3ème cycle, University of Montpellier, 1970.
(40) E. Rossi, E. Bianchi, and A. Rossi, *J. Chim. Phys. Physicochim. Biol.*, **58**, 90 (1958).
(41) E. A. G. Aniansson, S. N. Wall, M. Almgren, H. Hoffmann, I. Kielmann, W. Ulbricht, R. Zana, J. Lang, and C. Tondre, *J. Phys. Chem.*, **80**, 905 (1976).

# Ultrasonic Absorption in Relation to Hydrogen Bonding in Solutions of Alcohols. 3. Effect of Temperature on the Kinetics of Self-Association in Solutions of 1-Octanol in Cyclohexane

**A. Djavanbakht,† R. Zana,* and J. Lang**

*CNRS, Centre de Recherches sur les Macromolécules 6, rue Boussingault, 67083 Strasbourg, Cedex, France* *(Received March 23, 1977)*

*Publication costs assisted by CNRS*

The ultrasonic absorption relaxation spectra of solutions of 1-octanol in cyclohexane have been determined at temperatures ranging from 8 to 43 °C. The results have been interpreted on the basis of a reaction mechanism which assumes the formation of noncyclic and cyclic tetramers or pentamers. The equations derived in a previous paper give a good account of the results over the whole temperature range. The results of the calculations confirm that in cyclohexane the association reaction of alcohol molecules through H bond is essentially diffusion controlled. The activation entropy and enthalpy for the dissociation of one alcohol molecule from an alcohol *n*-mer have been determined for the first time and found to be both positive. Finally, the entropy and enthalpy changes for the formation of noncyclic and cyclic species obtained in this study are in good agreement with the values determined by means of various equilibrium methods.

## I. Introduction

This paper is the third of a series dealing with the investigation of H bonding in alcohol solutions by means of ultrasonic absorption.[1,2]

In a previous paper[2] we have reported a study of the relaxational behavior of the ultrasonic absorption of solutions of five primary alcohols and of three isomeric octanols in cyclohexane at 25 °C. These results have been interpreted on the basis of the reaction mechanism

$$nA \rightleftharpoons A_n \rightleftharpoons A_{nC} \qquad (1)$$

(noncyclic species) (cyclic species)

where all species intermediate between the monomeric alcohol A and the *n*-mer $A_n$ are assumed to be present in negligible amount. The excess ultrasonic absorption is attributed to the association step. For primary alcohols and 3-octanol, the experimental results could be fitted to expressions of the relaxation frequency $f_R$ and amplitude $R$ derived on the basis of reaction mechanism 1, in the case where $n = 4$ or 5. For hindered alcohols such as 2-methyl-3-heptanol and 2,4-dimethyl-3-hexanol, the best fits to the data were obtained for $n = 3$ and 2, respectively. The calculations showed that in all instances the rate of association of alcohol molecules through H bonding in cyclohexane is close to its diffusion-controlled limit.[2] On the other hand, the dissociation rate constant $k_-$ of one alcohol molecule, from the *n*-mer $A_n$, is only slightly dependent on the alkyl chain length, for primary alcohols. This rate constant increases with the degree of steric hindrance about the OH group, reflecting the decreased stability of associated species with respect to unhindered alcohols.

In this paper, we report the results of a study of the temperature dependence of $f_R$ and $R$ for 1-octanol in cyclohexane. This study was undertaken in order to gain informations on the temperature dependence of the kinetics of association through H bonding, and to try to assess the range of temperatures where reaction mechanism 1 is valid.

† Present address: 163 Manoutcheri Ave., Meched, Iran.

## II. Experimental Section and Results

The ultrasonic absorption $\alpha/f^2$ (where $\alpha$ is the ultrasonic absorption coefficient and $f$ the frequency) was measured using the same equipment as in previous studies,[1,2] in the frequency range from 3.94 to 250 MHz. The measurements have been performed at 8, 17, 25, 34, 39, and 43 °C. The temperature was kept constant to better than 0.1 °C in the course of the measurements. The ultrasonic relaxation spectra of a series of 1-octanol solutions in cyclohexane were determined at each temperature. The values of $\alpha/f^2$ are given as supplementary material (see paragraph at end of text regarding supplementary material). In all instances, as in our previous studies[1,2] the experimental results could be fitted to the eq 2, which

$$\frac{\alpha}{f^2} = \frac{R}{1 + f^2/f_R^2} + B \qquad (2)$$

characterizes a process with a single relaxation frequency.

The values of the constant $B$ were obtained from the measurement of the values of $\alpha/f^2$ for *n*-octane solutions in cyclohexane at the same temperatures as 1-octanol solutions.[1,2] These values were found to be independent of frequency and are given in Table I.

The values of $R$ and $f_R$ listed in Table I were obtained by fitting the values of $\alpha/f^2$ (supplementary material) to eq 2, using a two-parameter weighted least-squares procedure to minimize the quantity $\sigma^2$ given by eq 4′ in ref 2. In all instances the value of $(\sigma^2/p)^{1/2}$ (see ref 2) was smaller or at most equal to the experimental error on the $\alpha/f^2$ values (about 2% in the whole temperature range). The error on $R$ is always less than 10%. The error on $f_R$ may be larger, mostly for the solutions characterized by values of $R$ below $50 \times 10^{-17}$ cm$^{-1}$ s$^2$ and temperatures above 25 °C where the experimental results are usually more scattered than at lower temperatures. In those instances the error on $f_R$ may reach 20–30%.

At each temperature, $f_R$ increases with alcohol concentration c and $R$ goes through a maximum at a concentration $c_{M,0}$ which increases with $T$. These observations are quite similar to those made in our previous study. At 43 °C the value of $c_{M,0}$ could not be accurately determined from the $R$ vs. c plot. For this reason we have plotted the $\Delta\alpha/f^2$ vs. $c$ curve at 43 °C and 9.09 MHz ($\Delta\alpha/f^2$ represents

TABLE I: Values of the Relaxation Amplitude $R$ and Frequency $f_R$ for 1-Octanol Solutions in Cyclohexane at Various Temperatures[a]

| | $c$, M | $10^{17}R$ cm$^{-1}$ s$^2$ | $f_R$, MHz | $10^{17}B$ cm$^{-1}$ s$^2$ |
|---|---|---|---|---|
| 8 °C, | 0.04 | 343 | 12.3 | 176 |
| $c_{M,0}$ = 0.076 M | 0.08 | 381 | 20.1 | 174 |
| | 0.13 | 337 | 28.9 | 171 |
| | 0.19 | 285 | 37.9 | 168 |
| | 0.25 | 241 | 48.5 | 164 |
| 17 °C, | 0.04 | 143 | 20.4 | 184 |
| $c_{M,0}$ = 0.1 M | 0.08 | 252 | 28.4 | 182 |
| | 0.128 | 249 | 40.2 | 179 |
| | 0.188 | 223 | 52.9 | 175 |
| | 0.248 | 193 | 65.4 | 171 |
| 34 °C, | 0.04 | 11 | 49.6 | 201 |
| $c_{M,0}$ = 0.15 M | 0.79 | 74 | 56 | 199 |
| | 0.127 | 116 | 72.5 | 196 |
| | 0.183 | 119 | 99.6 | 192 |
| | 0.243 | 112 | 122.2 | 188 |
| 39 °C, | 0.071 | 33 | 60.2 | 206 |
| $c_{M,0}$ = 0.18 M | 0.12 | 71 | 83.6 | 202 |
| | 0.178 | 95 | 106.2 | 198 |
| | 0.217 | 97 | 108.7 | 196 |
| 43 °C, | 0.078 | 23 | 81.4 | 211 |
| $c_{M,0}$ = 0.22 M | 0.126 | 58 | 91.2 | 208 |
| | 0.181 | 73 | 115.7 | 204 |
| | 0.241 | 77 | 131.7 | 200 |

[a] The results at 25 °C are given in the preceding paper.

the difference between the absorptions of equimolecular solutions of 1-octanol and $n$-octane). This curve goes through a maximum at a concentration very close to $c_{M,0}$ (see ref 2). The values of $c_{M,0}$ are listed in Table I.

The $f_R$ and $R$ data were analyzed by means of eq 14, 17, and 19–23 given in ref 2. These equations assume that dimerization may be neglected both in the stoichiometry and kinetics. This approximation is supported by the results reported in the previous paper[2] for unhindered alcohols.

The fitting procedure was the same as previously.[2] The goodness of the fits to the $f_R$ and $R$ vs. $c$ data were characterized by the values of the residual mean squares $S_{f_R}^2$ and $S_R^2$ of $f_R$ and $R$, respectively (see ref 2). These values show that whatever the temperature and the value of $K_C$, the assumption of an association number equal to 3 always leads to values of $S_R^2$ larger than the maximum value of this quantity calculated from the estimated error on $R$ (see ref 2). Thus, over the whole temperature and concentration ranges investigated in this work, trimers cannot be the species giving rise to the observed excess absorption.

On the contrary, values $n$ = 4 and 5 permit a satisfactory account of the experimental results. We have shown in Figures 1–4 some examples of curve fittings for $n$ = 4 and 5 at the two extreme temperatures investigated in this work. While the fits are very satisfactory at 8 °C, the agreement between the calculated curves and the experimental results is not as good at 43 °C. At this high temperature, however, the errors on $f_R$ are rather large as can be seen in Figures 3 and 4. As a result, the range of $K_C$ values which fit the $f_R$ data within the experimental error is very large. However the range of $K_C$ values which reasonably fit the $R$ data is much more narrow and overlaps the first range only in its very lower part. It must also be pointed out that the comparison of the results relative to $n$ = 4 and 5 at 34, 39, and 43 °C seems to indicate that the overall fit to the data obtained with $n$ = 5 is better than with $n$ = 4 Note that for long chain

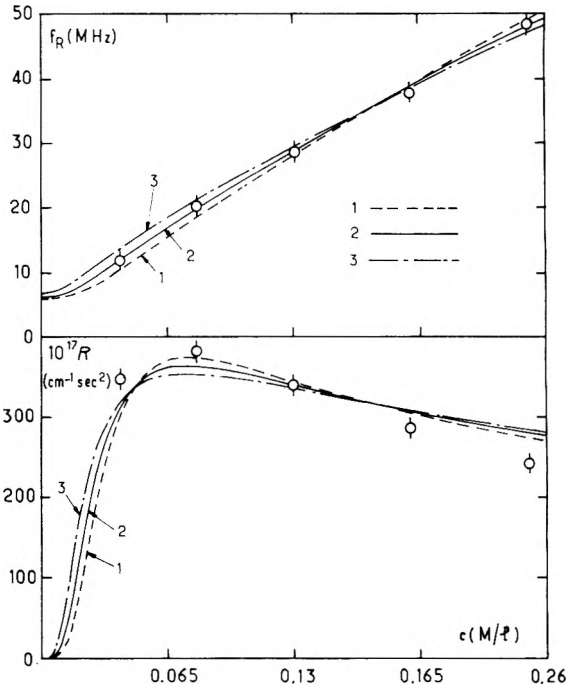


**Figure 1.** Fittings to the $f_R$ and $R$ data for 1-octanol in cyclohexane at 8 °C, with $n$ = 4: (curve 1) $K_C$ = 0.5; (curve 2) $K_C$ = 1.3; (curve 3) $K_C$ = 3. The corresponding values of $K_T$, $k_-$, and $\Delta H°$ are listed in Table II. The errors bars on $f_R$ and $R$ have been obtained from the fittings of the $\alpha/f^2$ vs. $f$ values of Appendix I to eq 2. For this purpose, the $\alpha/f^2$ values found for a given solution at a given temperature were changed at random by a relative amount between −2 and 2%. Each of the sets of $\alpha/f^2$ values obtained in this manner was then fitted to eq 2 and the $R$ and $f_R$ values obtained by means of a weighted least-squares procedure. About 50 sets of $\alpha/f^2$ values were used to obtain the error bars.

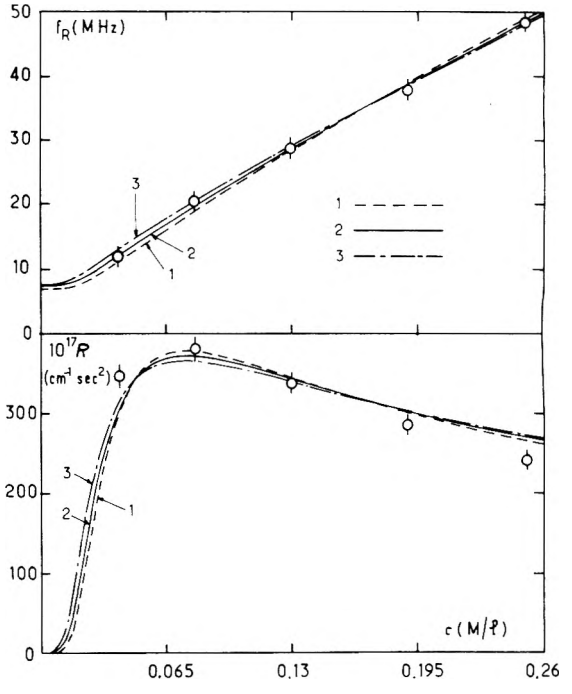


**Figure 2.** Fittings to the $f_R$ and $R$ data for 1-octanol in cyclohexane at 8 °C, with $n$ = 5: (curve 1) $K_C$ = 2; (curve 2) $K_C$ = 2.8; (curve 3) $K_C$ = 4. The corresponding values of $K_T$, $k_-$, and $\Delta H°$ are listed in Table II.

alcohols, a better account of the results was obtained with $n$ = 5 than with $n$ = 4, while equally good fits were obtained for shorter alcohols.

In Table II are listed the values of $K_C = [A_{nC}]/[A_n]$, $K_T = [A_n]/[A]^n$, $k_-$, $k' = k_- K_T^{1/(n-1)}$, the lower bound of the

TABLE II: Values of $K_C$, $K_T$, $k_-$, $k'$, and $\Delta H°$, Best Fitting the Ultrasonic Absorption Data for 1-Octanol in Cyclohexane, at Different Temperatures[a]

| | | $n = 4$ | | | | | $n = 5$ | | | | |
|---|---|---|---|---|---|---|---|---|---|---|---|
| $t$, °C | $c_{M,0}$, M | $K_C$ | $K_T$, $M^{-3}$ | $10^{-7}k_-$, $s^{-1}$ | $10^{-8}k'$, $M^{-1}s^{-1}$ | $-\Delta H°$, kcal/mol | $K_C$ | $10^{-3}K_T$, $M^{-4}$ | $10^{-7}k_-$, $s^{-1}$ | $10^{-8}k'$, $M^{-1}s^{-1}$ | $-\Delta H°$, kcal/mol |
| 8 | 0.076 | 0.5 | 1530 | 3.7 | 4.3 | 4.7 | 2 | 32 | 4.2 | 5.7 | 4.9 |
| | | 1.3 | 2830 | 4.0 | 5.6 | 5.3 | 2.8 | 52.7 | 4.4 | 6.7 | 5.3 |
| | | 3 | 7690 | 4.3 | 8.4 | 6.4 | 4 | 101 | 4.6 | 8.2 | 5.8 |
| 17 | 0.10 | 0.5 | 670 | 6.5 | 5.7 | 4.6 | 2 | 10.7 | 7.5 | 7.6 | 4.9 |
| | | 1 | 1000 | 6.8 | 6.8 | 5.0 | 2.8 | 17.6 | 7.7 | 8.9 | 5.2 |
| | | 2 | 1950 | 7.1 | 8.8 | 5.6 | 4 | 33.7 | 7.9 | 10.7 | 5.7 |
| 25 | 0.120 | 0.5 | 390 | 9.8 | 7.1 | 4.5 | 1.9 | 4.8 | 11.2 | 9.3 | 4.8 |
| | | 1 | 580 | 10.2 | 8.5 | 4.9 | 2.7 | 8 | 11.4 | 10.9 | 5.1 |
| | | 1.5 | 820 | 10.4 | 9.7 | 5.2 | 3.5 | 12.6 | 11.7 | 12.4 | 5.3 |
| 34 | 0.15 | 0 | 125 | 17.1 | 8.6 | 4.2 | 1 | 1 | 19.4 | 11 | 4.4 |
| | | 0.2 | 150 | 17.4 | 9.3 | 4.4 | 1.6 | 1.6 | 19.8 | 12.5 | 4.6 |
| | | 0.4 | 180 | 17.6 | 10 | 4.5 | 2.5 | 2.9 | 20.1 | 14.8 | 5.0 |
| 39 | 0.18 | 0 | 70 | 21.7 | 9 | 3.9 | 0.5 | 0.32 | 24.4 | 10.3 | 3.9 |
| | | 0.2 | 90 | 21.8 | 9.7 | 4.0 | 1 | 0.49 | 24.4 | 11.5 | 4.0 |
| | | 0.5 | 115 | 21.8 | 10.6 | 4.2 | 2 | 1.02 | 24.4 | 13.8 | 4.3 |
| 43 | 0.22 | 0 | 40 | 28.6 | 9.7 | 3.8 | 1 | 0.22 | 32 | 12.3 | 3.9 |
| | | 0.3 | 53 | 28.4 | 10.7 | 3.9 | 1.4 | 0.30 | 31.8 | 13.2 | 4.0 |
| | | 1 | 94 | 27.9 | 12.7 | 4.2 | 2 | 0.45 | 31.6 | 14.6 | 4.1 |

[a] At each temperature, the second line gives the best fitting values. The first and third lines give data which still fit the results within the experimental uncertainty, but with a much larger total root mean square deviation.

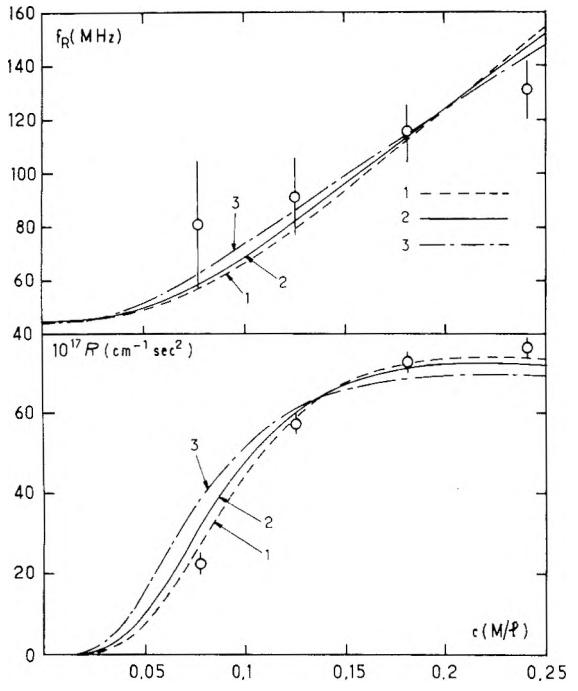


**Figure 3.** Fittings to the $f_R$ and $R$ data for 1-octanol in cyclohexane at 43 °C, with $n = 4$: (curve 1) $K_C = 0$; (curve 2) $K_C = 0.3$; (curve 3) $K_C = 1$. The corresponding values of $K_T$, $k_-$, and $\Delta H°$ are listed in Table II. The errors bars have been obtained as explained in the caption of Figure 1.

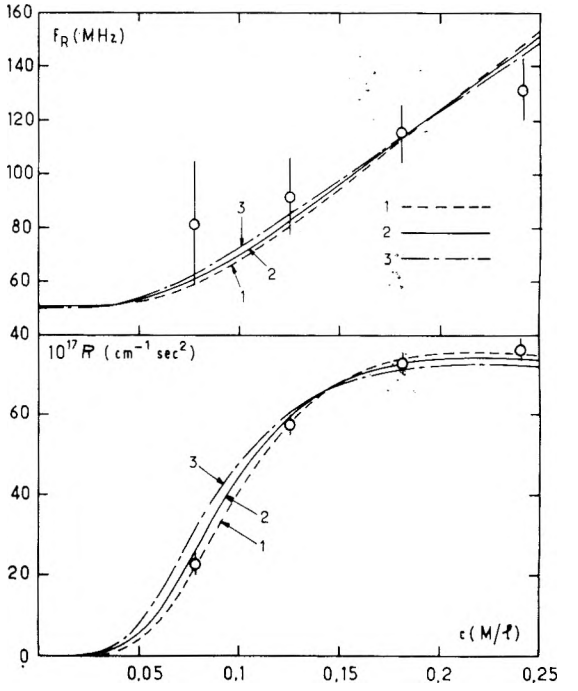


**Figure 4.** Fittings to the $f_R$ and $R$ data for 1-octanol in cyclohexane at 43 °C, with $n = 5$: (curve 1) $K_C = 1$; (curve 2) $K_C = 1.4$; (curve 3) $K_C = 2$. The corresponding values of $K_T$, $k_-$, and $\Delta H°$ are listed in Table II.

rate constant $k$ of association of A to $A_{n-1}$, and $\Delta H°$, the enthalpy change for the formation of one H bond. While the $K_C$ and $K_T$ values which fit the results within the experimental uncertainty are only approximately determined, the $k_-$ values are not sensitive to these errors and are fairly accurate. Moreover, the $k_-$ values increase by only 10% in going from $n = 4$ to 5, i.e. a variation comparable to that observed for an increase of temperature by 1–2 °C. The values of $k'$ and $\Delta H°$ are also practically independent of the value of $n$, but those of $K_T$ and $K_C$ strongly depend on this quantity.

## Discussion

1. *Dissociation Rate Constant.* $k_-$ shows a significant increase with temperature. The plots of ln $(k_-/T)$ vs. $1/T$ for $n = 4$ and 5 are shown in Figure 5. The two lines run parallel and yield $\Delta H_-^{\ddagger} = 9.1$ kcal/mol and $\Delta S_-^{\ddagger} = 8.4$ cal/deg mol.

To our knowledge, these values represent the first ones ever reported for the average activation enthalpy and entropy for the breakage of a single hydrogen bond between alcohol molecules in cyclohexane. (The word average has been used because this breakdown is likely to affect any of the two H bonds which are at the two ends of alcohol tetramers or pentamers in cyclohexane.) However, there have been reports[3,4] of $\Delta H_-^{\ddagger}$ and $\Delta S_-^{\ddagger}$ values for the dissociation of a closed dimer of benzoic acid into two monomers, in a number of solvents, including cyclohexane.[4] Although the process involved in these studies as well as the type of H bond involved differs from the corresponding ones in alcohol solutions, the results 7

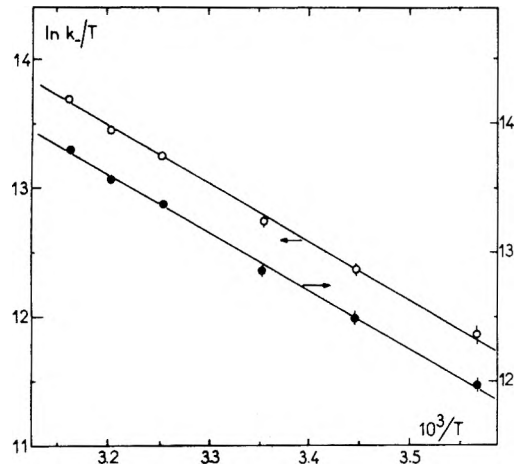


**Figure 5.** Temperature dependence of ln ($k_-/T$) using the $k_-$ values for $n$ = 4 (O) and $n$ = 5 (●).

kcal/mol and 6.8 cal/deg mol of H bond dissociated do not significantly differ from those found for alcohols. The difference is probably within experimental uncertainty because in benzoic acid studies the relaxation spectra involved measurement at only four or five frequencies.

The positive value of $\Delta S_-^\ddagger$ can be readily explained on the basis of the general scheme for a hydrogen bonding equilibrium between an acceptor A and a donor D, which can be written[5]

$$\underset{\text{encounter complex}}{A + D \rightleftharpoons AD} \rightleftharpoons \underset{\text{H-bond complex}}{A\text{-}D} \qquad (3)$$

In such a scheme the freedom of the two reactants is restricted in the H-bonded complex with respect to the encounter complex. This of course explains the positive $\Delta S_-^\ddagger$. It must be kept in mind, however, that in the case of alcohol solutions, the H-bonded complex is in fact a tetramer or a pentamer whose stability with respect to smaller associated species (dimers, trimers) may be the result of a cooperative effect in H bonding, owing possibly to electron delocalization and/or H-bond conjugation.[6] Moreover, we have pointed out in part 2 of this series that the tetramer or pentamer may adopt a somewhat "bent" or folded conformation. This conformation may be necessary in order to achieve the postulated electron delocalization and/or H-bond conjugation. Thus an additional step

$$A\text{-}D \rightleftharpoons (A\text{-}D)' \qquad (3a)$$

must be added to reaction mechanism 3, where the species (A–D)′ has an increased stability with respect to A–D because of the above postulated effects. As far as entropy goes, two antagonistic effects may be at play in going to (A–D)′: an increase of entropy due to the electron delocalization and a decrease of entropy of conformational origin. These two effects may cancel each other.

2. *Equilibrium Association Constant $K_T$ and Average Entalpy Change $\Delta H°$ for the Formation of One H Bond.* The $\Delta H°$ values listed in Table II are practically independent of $n$ and of the temperature in the range 8–25 °C and equal to −5.1 ± 0.2 kcal/mol. As previously[2] pointed out, the difference between this value and those obtained in a number of other investigations[6-11] (−5.4 to −5.6 kcal/mol) is likely to arise from the assumptions that dimerization can be neglected in reaction 1 and that $\Delta V°$ is negligible in eq 17 of ref 2. As the temperature is increased above 25 °C, $\Delta H°$ shows an increase to a value of about −4 kcal/mol. We do not believe, however, that this variation represents a real trend. More likely, it is due to

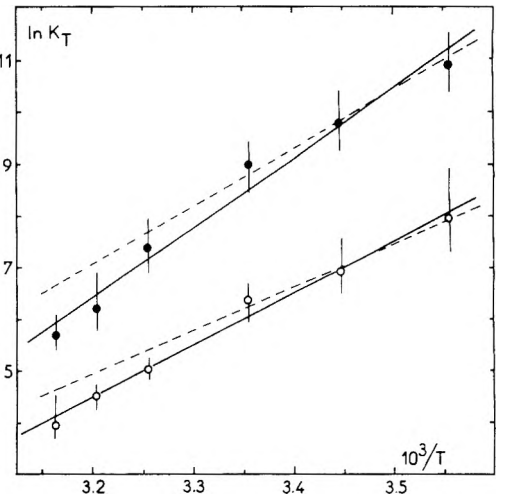


**Figure 6.** Temperature dependence of ln $K_T$. The solid lines have been obtained using a least-squares procedure. The dotted lines give more weight to the low temperature values: (O) $n$ = 4; (●) $n$ = 5.

the approximations involved in the derivation of the equations used for the analysis of the ultrasonic data (particularly, the neglecting of the dimers at high temperature) as well as to the large errors involved in the $f_R$ data at high temperature.

$K_T$ shows a large decrease as the temperature is increased. The ln $K_T$ vs. $1/T$ plots shown on Figure 6 are linear and yield, both for $n$ = 4 and 5, $\Delta H°$ = −6.7 kcal/mol and $\Delta S°$ = −18.2 cal/deg mol. Thus, the $\Delta H°$ values calculated from the $K_T$ data are significantly smaller than those listed in Table II. The difference comes from the fact that the latter are obtained from the fittings to the $R$ vs. $c$ data while the former are really obtained from the fittings to the $f_R$ vs. $c$ data which yield $K_T$ values. As pointed out above the relative error on $R$ is much smaller than on $f_R$. The values of $\Delta H°$ in Table II are therefore likely to be more accurate than those derived from the $K_T$ data. In fact the two sets of results at temperature up to 25 °C are in very close agreement. Indeed, if we give more weight to the low temperature data of Figure 6 (dotted lines) we obtain $\Delta H°$ = −5.6 kcal/mol for both $n$ = 4 and 5. On the contrary the high temperature results yield too small values of $\Delta H°$ when using the $f_R$ vs. $c$ data and too large values with the $R$ vs. c data. This suggests some kind of systematic error in the measurements or in their analysis. In the following we shall use the average value $\Delta H°$ = −5.4 kcal/mol.

The negative value found for $\Delta S°$ is comparable to those reported by other workers. For instance, Fletcher and Heller[8] give a value −14.7 cal/deg mol for the average entropy change for the formation of one H bond of the noncyclic tetramer of 1-octanol in $n$-decane on the basis of the temperature dependence of IR spectra. Aveyard and Mitchell[10] found almost the same result by calorimetric measurements. Note that the difference between these results and ours is completely eliminated if, as for the $\Delta H°$ values, more weight is given to the low temperature data. For instance, the dotted lines on Figure 6, which have been drawn through the low temperature data, yield $\Delta S°$ = −14.2 cal/deg mol. The average value −16.2 cal/deg mol will be used in the rest of the discussion.

3. *Activation Enthalpy $\Delta H^\ddagger$ and Entropy $\Delta S^\ddagger$ for the Reaction of H Bond Formation.* These quantities calculated from

$$\Delta H° = \Delta H^\ddagger - \Delta H_-^\ddagger \qquad (4)$$

$$\Delta S° = \Delta S^\ddagger - \Delta S_-^\ddagger \qquad (5)$$

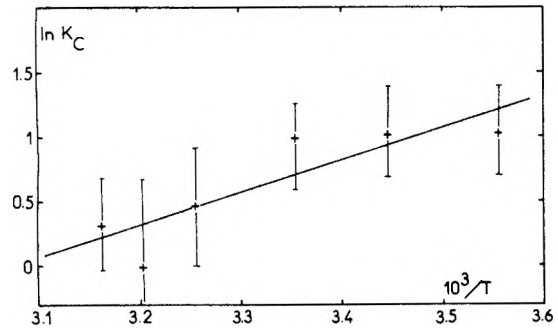


**Figure 7.** Temperature dependence of ln $K_C$ using the values for $n = 5$. The solid line has been obtained using a least-squares procedure.

have been found to be $\Delta H^{\ddagger} = 3.7$ kcal/mol and $\Delta S^{\ddagger} = -7.8$ cal/deg mol. These values are to be compared with those for the viscous flow of cyclohexane $\Delta H_{\eta}^{\ddagger} = 3$ kcal/mol and $\Delta S_{\eta}^{\ddagger} = -10.2$ cal/deg mol. The closeness of values of the activation enthalpies and entropies leaves no doubt that the association reaction of one alcohol molecule to an alcohol $n$-mer is diffusion controlled.

4. *Temperature Dependence of the Cyclization Constant* $K_C$. The ln $K_C$ vs. $1/T$ plot is shown in Figure 7. For $n = 4$, the values of $K_C$ are too close to zero to obtain any significant information. For $n = 5$, however, a least-squares fitting of the data yields $\Delta H°_C = -5 \pm 1$ kcal/mol and $\Delta S°_C = -15 \pm 5$ cal/deg mol. Somewhat similar values would be found for $n = 4$ if the low temperature results were given more weight than high temperature ones.

Fletcher and Heller[7] reported for the cyclization of the 1-octanol tetramer is $n$-decane $\Delta H°_C = -3.8$ kcal/mol and $\Delta S°_C = -11.2$ cal/deg mol. The agreement between the two sets of data is within the experimental uncertainty.

## Conclusions

The results obtained in this study confirm the assignment made in our previous works, namely, that the excess ultrasonic absorption of alcohol solutions in cyclohexane is due to the formation of noncyclic tetramers or pentamers. The values of the activation enthalpy and entropy for the association of one alcohol molecule to an $(n - 1)$-mer confirm that this reaction is diffusion controlled. The activation enthalpy and entropy for the dissociation of an alcohol molecule from the stable noncyclic $n$-mer have been obtained for the first time. These two quantities are positive. The equilibrium thermodynamic quantities for the formation of noncyclic and cyclic species have also been obtained. They are in agreement with those determined by "equilibrium" measurements.

*Supplementary Material Available:* Tables of raw ultrasonic absorption data (3 pages). Ordering information is given on any current masthead page.

## References and Notes

(1) R. Zana and J. Lang, *Adv. Mol. Relaxation Processes*, **7**, 21 (1975).
(2) A. Djavanbakht, J. Lang, and R. Zana, *J. Phys. Chem.*, preceding paper in this issue.
(3) W. Maier, *Z. Elektrochem.*, **64**, 132 (1960).
(4) L. Borucki, *Ber. Bunsenges. Phys. Chem.*, **71**, 504 (1967).
(5) G. G. Hammes and A. C. Park, *J. Am. Chem. Soc.*, **90**, 4151 (1968).
(6) L. De Maeyer, *Isr. J. Chem.*, **9**, 351 (1971), and references therein.
(7) A. Fletcher and A. Heller, *J. Phys. Chem.*, **71**, 3742 (1968); **72**, 1841 (1968).
(8) A. Fletcher, *J. Phys. Chem.*, **73**, 2217 (1969); **76**, 2562 (1972).
(9) H. Van Ness, J. Van Vinkle, H. Richtol, and B. Hollinger, *J. Phys. Chem.*, **71**, 1483 (1967).
(10) R. Aveyard and R. Mitchell, *Trans. Faraday, Soc.*, **65**, 2645 (1969).
(11) B. Anderson, J. Rytting, S. Lindenbaum, and T. Higuchi, *J. Phys. Chem.*, **79**, 2340 (1975).

# Plastic Phases in Globular Phosphorus Compounds. A New Structural Criterion for Plastic Behavior

**Michèle Postel and Jean G. Riess***

*Laboratoire de Chimie Minérale Moléculaire, Equipe de Recherche Associée au CNRS, Parc Valrose, 06034 Nice Cedex, France*
*(Received April 8, 1977)*

The search into plastic phase behavior of globular phosphorus compounds (oxides, sulfides, and imides) led us to question globularity of molecules as a valid structural criterion of plastic crystals. The parameter $R = d_m/D_M$ = (minimum distance between molecular centers)/(maximum diameter of the molecule), which expresses the degree of molecular interlocking in the solid, has been tested for a variety of inorganic and organic derivatives; all compounds which show $R$ values higher than 0.81 have plastic phases, while compounds which have lower $R$ values do not. Therefore the parameter $R$ is proposed as a structural criterion for plasticity.

## Introduction

The existence of plastic crystals, i.e., highly disordered rotatory phases where the molecules actually tumble rapidly in the solid while maintaining their positional order in the lattice, was first recognized by Timmermans,[1] who defined two criteria for this behavior, one on thermodynamic, the other on structural grounds.

As far as thermodynamics is concerned, he noted that plastic crystals exhibit a low entropy of fusion, and he proposed as an arbitrary but convenient upper limit of $\Delta S_m = 5$ eu. This value, although it turned out to be satisfactory in most cases, suffers some exceptions; thus, both sulfur hexafluoride and hexachloroethane have been shown to exhibit plastic phases, although their $\Delta S_m$ are equal to 5.4 and 5.5 eu, respectively.[2] Furthermore, one should remember that $\Delta S_m$ is not an absolute measure of the degree of disorder in the solid state, but a measure of the *difference* in organization between the liquid and the solid. Thus, 2-methyl-2-propanol, on the basis of its low entropy of fusion ($\Delta S_m = 4.70$ eu),[3] was first classified as a globular compound having a plastic crystal phase;[4] in fact, neutron transmission measurements showed that its small entropy of fusion originates essentially in the ordering of the liquid through hydrogen bonds more than from a high degree of

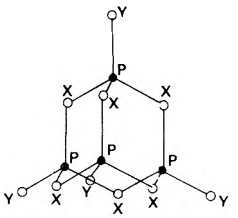


**Figure 1.** Structure of some closo phosphorus derivatives; $P_4O_6$ (X = O); $P_4O_{10}$ (X = Y = O); $P_4(NCH_3)_6$ (X = $NCH_3$); $P_4S_{10}$ (X = Y = S).

freedom in the solid.[5] The same situation is probably valid for methanol, which was initially thought to have a plastic phase on the basis of its low $\Delta S_m$ (4.6 eu).[6]

From a structural viewpoint, on the other hand, Timmermans pointed out that plastic behavior was characteristic of globular, i.e., nearly spherically shaped, molecules.[1] This globularity has commonly been considered as the structural feature which causes a molecule to exhibit plastic phase behavior. It has been stated that "plastic crystals are the high-temperature form of solids based on nearly spherical molecules".[7] It has also been suggested that "plastic crystals" would be better called "crystals with globular molecular".[8] That globularity is essential has been well-illustrated by Miller and Smyth,[9] who examined a series of ten different tetrasubstituted methane derivatives; departure from globularity caused plasticity to disappear, or at least significantly slowed down the molecular motions in the solid. However, it has been shown in a few cases that not all molecules that are globular give rise to plastic crystals. Thus, while methane, silane, germane, and carbon tetrachloride all form plastic crystals, silicon tetrachloride does not.[10] Another striking exception is hexamethylenetetramine $N_4(CH_2)_6$, which, although it has the same basic molecular structure as adamantane, shows no rotational transition.[11]

Plastic phases arouse considerable interest, and many reviews concerning them are available.[12] Yet little progress seemed to have been made toward the definition of better criteria allowing the prediction of which globular compounds are plastic and which are not, and why.

In this connection, we undertook a search into plastic phase behavior of globular phosporus-based compounds, most of which are similar in structure to adamantane, a well-documented plastic compound. We then realized that, whereas $P_4(NCH_3)_6$ and $P_4S_{10}$ exhibit plastic behavior over a large range of temperatures, some other equally symmetrical and globular molecules, such as $P_4O_6$ and $P_4O_{10}$, do not. This led us to question globularity as a valid structural criterion, and investigate which other structural parameters might provide a more reliable way of predicting plastic phase behavior.

## Results and Discussion

(1) *Plastic Behavior of Phosphorus Closo Compounds.* Since phosphorus chemistry has many globular "cage" or closo structures (Figure 1), it seemed appropriate to undertake a systematic search for data revelant to the existence of plastic phase behavior.

White phosphorus, $P_4$, itself, is well known to exhibit this property in its $\alpha$ cubic form between 196.6 and 317.6 K,[13] and the two extreme terms of the series of molecular phosphorus sulfides, $P_4S_3$ and $P_4S_{10}$, were also known to have a plastic phase;[14] the rigid/plastic phase transition has been well characterized in the case of $P_4S_3$ ($T_t$ = 313.9 K, $T_m$ = 447 K, $\Delta S_m$ = 5.0 eu), while the observation of a very sharp single line in the $^{31}P$ spectrum of solid $P_4S_{10}$ leaves no doubt that at room temperature rapid reorientation of the molecules occurs in the solid, and further implies a very large range of plastic behavior, since $T_m$ = 561 K.

We also recently reported the plastic behavior of tetraphosphorus hexa-*N*-methylimide, $P_4(NCH_3)_6$, in the 329–395 K temperature range, and of the structurally related arsenimide, $As_4(NCH_3)_6$, between 346 and 393 K.[15] Concerning the tetraphosphorus hexa-*N*-methylimide tetrasulfides and tetraoxides, $P_4(NCH_3)_6S_4$ and $P_4(NCH_3)_6O_4$, no plastic phases were detected up to 423 K; unfortunately both compounds start decomposing around this temperature, thus precluding any investigation nearer to the melting points (519 and 448 K, respectively). Likewise, significant measurements were made impossible in the case of the intermediate thioimides, $P_4(NCH_3)_6S_n$, where $n$ = 1 to 3, because of the existence of an interconversion process among these thiophosphorimides through scrambling of the peripheral sulfur atoms,[16] even in the solid.

On the other hand, the thermodynamic data available on the phosphorus oxides indicate that these compounds lack such plastic phase behavior; the entropies of melting for $P_4O_6$ and $P_4O_{10}$ are respectively 11.4[17] and 9.0[18] eu, i.e., they have values sufficiently high to preclude the existence of plastic phases with reasonable certainty. The intermediate oxides $P_4O_7$, $P_4O_8$, and $P_4O_9$, whose molecular symmetry is lower, and whose structures depart from globularity, are even less likely present as plastic phases.

The striking feature is thus that $P_4S_{10}$ and $P_4(NCH_3)_6$ exhibit plastic phases, while $P_4O_6$ and $P_4O_{10}$ do not, although all four compounds have isoglobular molecules of same $T_d$ symmetry. Several factors are likely to contribute to this difference in behavior; first, the hydrogen–hydrogen interactions, which are known to have a determining influence on the packing in many crystals, should contribute to the separation of molecules such as $P_4(NCH_3)_6$, and thus favor free rotation in the solid. Indeed, due to its six protubing methyl groups, $P_4(NCH_3)_6$ can be envisioned as being almost perfectly spherical and "coated" with hydrogen atoms, as is the case for adamantane. On the other hand, the location and local polarity on the oxygen atoms in $P_4O_6$ and $P_4O_{10}$ probably contribute to increasing molecular interlocking as the molecules are not so perfectly spherical and therefore hinder the rotation in the solid. Thus, the way the $P_4O_{10}$ molecules pack together in the crystal is of much interest; each molecule has four spikes and four recesses, and the spikes of each molecule fit into the recesses of the four nearest neighbors, leading to a close packing with considerable interlocking. The structural data[19,20] show that such an interpenetration does not exist in $P_4S_{10}$, the peripheral sulfur atoms being too large to fit into the niches of the neighboring molecules. This leads to a considerable increase in the minimum distance $d_m$ between molecular centers; thus if one takes the experimental $d_m$ value found for $P_4O_{10}$ (6.05 Å) to evaluate what the $d_m$ should be for $P_4S_{10}$ in the hypothesis that the same packing occurs in both compounds, one is led to predict that $d_m$ = 7.66 Å for $P_4S_{10}$, while the experimentally found value is 9.50 Å.

(2) *A New Structural Criterion for Predicting the Existence of Plastic Phases.* There is little doubt that the existence of a plastic phase is related to the degree of molecular interlocking, whatever the origin of this interlocking is. Indeed, molecular motion in plastic crystals, and even in liquids, is seldom, if ever, entirely free.[21] Plastic behavior implies that the interlocking is sufficiently weak not to obstruct the rapid correlated movements of neighboring molecules. When this interlocking becomes too strong, plastic phase behavior is prevented. We

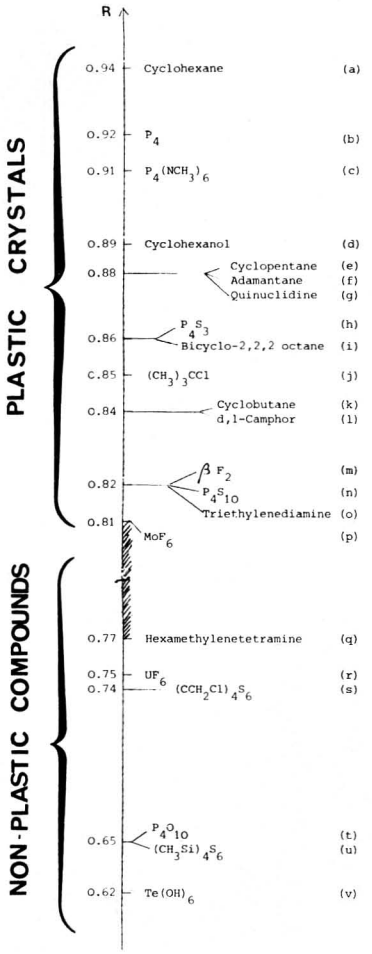


**Figure 2.** *R* Scale. For each compound the references listed account first for the structural data, second for the plastic behavior: (a) 12b; T. Sugawara, Y. Sakamoto, and E. Kanda, *Sci. Rep. Res. Inst. Tokyo Univ., Ser. A*, **1**, 29 (1949); (b) 13; (c) F. A. Cotton, J. M. Troup, F. Casabianca, and J. G. Riess, *Inorg. Chim. Acta*, **11**, L 33 (1974); 15; (d) 12b; (e) 12b; (f) 12b; (g) 12b; I. Darmon and C. Brot, *Mol. Cryst.*, **1**, 417 (1966); (h) Y. C. Leung, J. Waser, S. Van Houten, A. Vos, G. A. Wiegers, and E. H. Wiebenga, *Acta Crystallogr.*, **10**, 574 (1957); (i) I. Darmon and C. Brot, *Mol. Cryst.*, **1**, 417 (1966); (j) 12b; (k) 12b; (l) 12b; (m) T. H. Jordan, W. E. Strieb, and W. N. Lipscomb, *J. Chem. Phys.*, **41**, 760 (1964); 12b; (n) M. G. Gibby, A. Pines, W. K. Rhim, and J. S. Waugh, *J. Chem.* Phys., **56**, 991 (1972); (o) J. K. Nimmo and B. W. Lucas, *Acta Crystallogr. Sect. B*, **32**, 348, 597 (1976); 12b; (p) J. H. Levy, P. L. Sanger, J. C. Taylor, and P. W. Wilson, *Acta Crystallogr., Sect. B*, **31**, 1065 (1974); J. H. Levy, J. C. Taylor, and P. W. Wilson, *Acta Crystallogr., Sect. B*, **31**, 398 (1974); 24; (q) P. A. Shaffer, *J. Am. Chem. Soc.*, **69**, 1557 (1947); 22; (r) J. C. Taylor and P. W. Wilson, *J. Solid State Chem.*, **14**, 378 (1975); (s) S. Aleby, *Acta Crystallogr., Sect. B*, **30**, 2877 (1974); (t) D. W. S. Cruickshank, *Acta Crystallogr.*, **17**, 677 (1964); B. Beagley, D. W. J. Cruickshank, and T. B. Hewitt, *Trans. Faraday Soc.*, **63**, 836 (1976); (u) J. C. J. Bart and J. J. Daly, *J. Chem. Soc., Dalton Trans.*, 2063 (1975); (v) O. Lindquist, *Acta Chem. Scand.*, **24**, 3178 (1970).

therefore sought a way of expressing the degree of molecular interlocking, or in other words an absolute measurement of the density of molecular packing. This in turn was expected to reflect the ability of a given substance to undergo plastic behavior.

Such a clue is provided by the parameter $R$ defined as follows:

$$R = d_m/D_M = \text{(minimum distance between molecular centers)/(maximum diameter of the molecule)}$$

where $D_M$ is the diameter of the sphere that will just circumscribe the freely rotating molecule ($d_m$ and $D_M$ have been introduced by Dunning).[12b] Any intermolecular repulsion such as the hydrogen–hydrogen interactions will increase $d_m$, and therefore $R$. For example, $R$ is equal to 0.91 for $P_4(NCH_3)_6$ and falls to 0.65 for $P_4O_{10}$ where, on the contrary, polar effects are expected to lower $d_m$ and consequently $R$. Likewise while $R = 0.86$ for *tert*-butyl chloride, a well-known plastic crystal, it falls to 0.62 for teluric acid, for which, although its shape is perfectly globular, there exists a strong network of hydrogen bonds.

As a consequence, we calculated the value of $R$ for various inorganic and organic globular compounds from the available crystallographic data. These results are given in Figure 2, in the form of an $R$ scale.

This scale clearly shows that plasticity is indeed related to the value of $R$; here all the compounds which show $R$ values higher than 0.81 have plastic phases, while the compounds which have lower $R$ values do not. The limit can be situated between $R = 0.77 \pm 0.02$ on the basis that hexamethylenetetramine has definitely been shown not to have a plastic phase,[22] although it possesses some molecular freedom below the melting point,[23] and $R = 0.81 \pm 0.01$, calculated for $MoF_6$, which was shown to be plastically crystalline in its cubic phase.[24] The highest $R$ value was found for cyclohexane, which is indeed a very soft solid in its plastic phase. Similarly $P_4(NCH_3)_6$ appears from its $R$ value (0.91) to be "very plastic", in agreement with its large domain of plasticity and its very narrow $^1H$ NMR line, even 50 °C below its melting point.[15]

Thus we propose to take parameter $R$ as a structural criterion for plasticity. It is essential to note that each time that $R$ could be evaluated for both rigid and plastic phases it was found to have the same value within experimental error. For example, $R = 0.81$ for $MoF_6$ both in its rigid orthorhombic and plastic cubic phases. This is understandable since the physical properties, which induce the plastic behavior, already exist in the rigid phase. However, the disposition of molecules in this phase opposes the correlated movements of neighboring molecules; this disposition is modified when the crystalline transition occurs, so that rotation becomes possible.[25] For example, the latter arrangement for adamantane is changed by only a 9° twist in the molecules about the $c$ axis at the rigid to plastic transition.[26] Furthermore $R$ shows almost no temperature dependence in the examples studied. Thus a value of $R$ calculated in any solid phase and at any temperature may be taken as significant for the prediction of plastic behavior.

*Acknowledgment.* The authors are grateful to the donors of the Petroleum Research Fund, administered by the American Chemical Society, for partial support of this work, and to NATO for Grant No. 1062.

## References and Notes

(1) J. Timmermans, *J. Chim. Phys.*, **35**, 331 (1938).
(2) P. A. Winsor, "Liquid Crystals and Plastic Crystals", Vol. I, G. W. Gray and P. A. Winsor, Ed., Wiley, New York, N.Y., 1974, p 48.
(3) F. L. Oettig, *J. Phys. Chem.*, **67**, 2757 (1963).
(4) J. Timmermans, *J. Phys. Chem. Solids*, **18**, 1 (1961).
(5) L. Q. Amaral, R. Fulfaro, and L. A. Vinhas, *J. Chem. Phys.*, **63**, 1312 (1975).
(6) H. G. Carlson and E. F. Westrum, Jr., *J. Chem. Phys.*, **54**, 1464 (1971).
(7) E. F. Westrum, Jr., *Phys. Chem., Ser. One*, **10**, 231 (1972).
(8) G. W. Smith, *Int. Sci. Technol.*, **61**, 72 (1967).
(9) R. C. Miller and C. P. Smyth, *J. Am. Chem. Soc.*, **79**, 20 (1957).
(10) L. A. K. Staveley, *Annu. Rev. Phys. Chem.*, **13**, 351 (1962).
(11) S. S. Chang and E. F. Westrum, Jr., *J. Phys. Chem.*, **64**, 1547 (1960).
(12) See, for example, ref 1, 2, 4, 7, 10, and (a) C. Brot and M. Renaud, *Bull. Soc. Fr. Miner. Cristallogr.*, **95**, 183 (1972); (b) W. J. Dunning, *J. Phys. Chem. Solids*, **18**, 21 (1961); (c) P. Rigny, Thesis, Report CEA-R-3464 (1967).
(13) H. W. Spiess, R. Grosescu, and U. Haeberlen, *Chem. Phys.*, **6**, 226 (1974).

(14) M. G. Gibby, A. Pines, W. K. Rhim, and J. S. Waugh, *J. Chem. Phys.*, **56**, 991 (1972).
(15) M. Postel, F. Casabianca, and J. G. Riess, *Inorg. Chim. Acta*, **17**, L23 (1976).
(16) J-C. Elkaim, A. Wolff, and J. G. Riess, *Phosphorus*, **2**, 249 (1973).
(17) O. Kubaschewski and E. L. Evans, "La Thermochimie en Métallurgie", Gauthiers-Villars, Paris, 1964.
(18) A. D. F. Toy, "Comprehensive Inorganic Chemistry", Vol. II, Pergamon, Oxford, 1973, p 389.
(19) D. W. J. Cruickshank, *Acta Crystallogr.*, **17**, 677 (1964).
(20) A. Vos and E. H. Wiebenga, *Acta Crystallogr.*, **8**, 217 (1955).
(21) C. Brot and B. Lassier-Govers, *Ber. Bunsenges. Phys. Chem.*, **72**, 31 (1976).
(22) C. A. Fyfe and D. Harold-Smith, *Can. J. Chem.*, **54**, 769 (1976).
(23) G. W. Smith, *J. Chem. Phys.*, **36**, 3081 (1962).
(24) P. Rigny and J. Virlet, *J. Chem. Phys.*, **51**, 3807 (1969).
(25) G. B. Guthrie and J. P. McCullough, *J. Phys. Chem. Solids*, **18**, 53 (1961).
(26) E. F. Westrum, Jr., *J. Chim. Phys.*, **62**, 46 (1966).

# The Kinetic Isotope Effect in Dehydration of Ionic Solids. 2. The Kinetics of Dehydration of Calcium Oxalate Monohydrate

**Emanuel P. Manche***

*Department of Natural Sciences, York College of the City University of New York, Jamaica, New York 11451*

**and Benjamin Carroll**

*Department of Chemistry, Rutgers—The State University, Newark, New Jersey 07102* *(Received July 11, 1977)*

The kinetics of the isothermal dehydration of the protonated and deuterated monohydrate of calcium oxalate has been investigated at 120, 150, and 170 °C. The rate of dehydration for these salts were found to be $k_H/k_D = 1.025 \pm 0.012$. This result rules out the enormous kinetic isotope effect as given in the literature. An isotope effect of a few percent is not ruled out; this magnitude is in keeping with that found by Heinzinger in other dehydration processes. An estimated difference of about 150 cal/mol between the heat of desorption for $H_2O$ and $D_2O$ should have led to a ratio, $k_H/k_D = 1.20$. The smaller observed ratio has been explained on the basis of a compensation effect and may be considered an example of the Barclay–Butler correlation.

## Introduction

A number of papers have appeared on the kinetic hydrogen isotope effect for the dehydration of the pentahydrate of copper sulfate,[1] the monohydrate of calcium oxalate,[2] in addition to several other types of inorganic salts.[3] Without exception all of these papers have dealt with the activation energies, comparing the temperature coefficients of the rates usually for fully protonated and fully deuterated hydrates.

Some of these reported effects have been dramatic. Values for calcium oxalate monohydrate have been observed as 12 and 31 kcal/mol for the $H_2O$ and $D_2O$ salts, respectively. In the case of copper sulfate pentahydrate, values of 19 and 33 kcal/mol have been reported for the protonated and deuterated hydrates, respectively, in the initial stages of the dehydration process and 30 as compared to 53 kcal/mol for the monohydrate salts. Yet the investigators in this work obtained identical thermodynamic values for the enthalpy for the dehydration reaction, their results being reported to the nearest kilocalorie.

The kinetic isotope effect in every case has been determined by means of the so-called dynamic or nonisothermal procedure. Recently, we have repeated the work for the calcium oxalate monohydrate[4] using a thermogravimetric method that we considered the most accurate of the dynamic procedures. Here we found the activation energy ratio $E_D/E_H = 1.07$. However, the departure of the ratio from unity could not be considered significant since the experimental error inherent in dynamic procedures is about 5–10%. Since a similar percentage error in the isothermal rates of reaction is equivalent to a fraction of a kilocalorie in the activation energy, we have investigated the ratio of the dehydration of calcium oxalate monohydrate for the protonated and deuterated salts at 120, 150, and 170 °C.

The isothermally determined rates were compared at the same degree of progress of the reaction. Further, care was taken so that sample size, particle size, and container geometry were kept the same. These factors appear to be significant for heterogeneous reactions particularly for reversible reaction.

Reactions of the type A(solid) → B(solid) + C(gas), where the reaction is reversible, present the problem of removing the gas component rapidly from the locus of reaction. Previous work of Dollimore, Jones, and Spooner[5] has shown that the presence of water vapor will give rise to a Smith–Topley effect.[6] Whereas it is usually assumed that the reaction rate is a maximum when the pressure of the gaseous products is zero and decreases continuously to a zero rate at the equilibrium pressure, the dehydration reaction of calcium oxalate monohydrate was an exception to this generalization.

Here Dollimore et al. found that the rate was accelerated by the presence of water vapor within a certain defined range, and the activation energy increased more than twofold over that obtained when the dehydration was carried out in vacuo.

We found it more convenient to carry out the dehydration reaction in an atmosphere of dry nitrogen at a fixed flow rate. In this range of flow an activation energy for the protonated calcium salt was found to be practically identical with the Dollimore value of 16.4 kcal/mol that was obtained in vacuo.

Solid state kinetics carried out isothermally present the problem of attaining the temperature of interest in a time interval that is small as compared to the lifetime of the reaction. We found that discarding the first 10% of the degree of conversion, $\alpha$, to the anhydrous state was ade-

TABLE I: Dehydration Rates for $CaC_2O_4 \cdot H_2O$ and $CaC_2O_4 \cdot D_2O$ and Their Relative Values at 120 °C

| $\alpha$ | $(\Delta\alpha/\Delta t)_H$ | $(\Delta\alpha/\Delta t)_D$ | $k_H/k_D$ |
|---|---|---|---|
| 0.2 | 0.050 | 0.052 | 0.962 |
| 0.3 | 0.051 | 0.053 | 0.962 |
| 0.4 | 0.050 | 0.051 | 0.980 |
| 0.5 | 0.048 | 0.050 | 0.960 |
| 0.6 | 0.046 | 0.048 | 0.958 |
| 0.7 | 0.044 | 0.045 | 0.978 |
| 0.8 | 0.041 | 0.043 | 0.953 |
| 0.9 | 0.034 | 0.034 | 1.000 |

quate for obtaining kinetic information at the specified temperature. Since reaction parameters may vary with the progress of the reaction we have compared rates at the same degree of conversion using thermogravimetry to obtain this fractional weight loss.

## Experimental Section and Results

The salts used in these studies were prepared from Fisher Scientific Co. reagent grade calcium oxalate monohydrate powder, lot no. 751593. The powder was sieved with a sonic sifter and the fines passing the 37-$\mu$m screen were collected and used for all the experiments described in this paper. The powder was divided into two parts and placed in an oven, set at 200 °C, for 24 h. The two samples were transferred to two previously prepared chambers, one saturated with water and the other with $D_2O$. After equilibration the samples were transferred to $P_2O_5$ desiccating chambers.

The identity of the $CaC_2O_4 \cdot H_2O$ and $CaC_2O_4 \cdot D_2O$ salts was made from absorption spectra taken on a Beckman 4240 infrared spectrophotometer as well as from stoichiometric considerations based on thermogravimetric measurements.

Thermogravimetric curves were obtained using a Perkin-Elmer TGS-1 thermobalance. The balance furnace was calibrated at each temperature, in a flow of nitrogen, using small gauge chromel–alumel thermocouples referenced to a 0 °C ice bath. Temperature control was achieved with a Perkin-Elmer UU-1 temperature programmer.

For each analysis, 5.00 mg of sample was weighed in a platinum crucible using a Cahn G-2 microbalance. The sample was transferred to the stirrup of the thermobalance that was previously flushed with dry nitrogen and set to flow at a rate of 25 mL/min, a value found to be adequate to prevent a reverse reaction.

Dehydration experiments were carried out isothermally at 120, 150, and 170 °C. After the sample was introduced into the balance, the furnace was ballistically heated to the desired preset temperature. A check was made of the rate of temperature rise of the furnace. It was determined for example that, when the controller was set at 150 °C, the temperature of the furnace reached a value of $1 - 1/e$ of the set temperature in 12 s. The rapid furnace temperature equilibration was due mainly to its very low mass. The fractional weight loss, $\alpha$, which is a measure of the progress of the reaction was calculated from the time-based strip chart.

Since the slopes were almost linear, particularly for the first half-life of the reaction, we have listed the values for the rates, $\Delta\alpha/\Delta t$, taken directly from the unsmoothed normalized weight loss curve, the value for $\Delta\alpha$ listed at $\alpha_i$ being that for $\alpha_i - \alpha_{i-0.1}$. The rates are in units of minutes$^{-1}$ and their ratios listed as $k_H/k_D$ are given in Tables I–III for 120, 150, and 170 °C, respectively.

## Discussion

The average of all the values for $k_H/k_D$ for all temperatures, i.e. 120, 150, and 170 °C, is $1.02_5$. If the values

TABLE II: Dehydration Rates for $CaC_2O_4 \cdot H_2O$ and $CaC_2O_4 \cdot D_2O$ and Their Relative Values at 150 °C

| $\alpha$ | $(\Delta\alpha/\Delta t)_H$ | $(\Delta\alpha/\Delta t)_D$ | $k_H/k_D$ |
|---|---|---|---|
| 0.2 | 0.222 | 0.228 | 0.974 |
| 0.3 | 0.228 | 0.219 | 1.041 |
| 0.4 | 0.215 | 0.204 | 1.054 |
| 0.5 | 0.204 | 0.197 | 1.036 |
| 0.6 | 0.194 | 0.192 | 1.010 |
| 0.7 | 0.179 | 0.183 | 1.077 |
| 0.8 | 0.165 | 0.170 | 0.971 |
| 0.9 | 0.127 | 0.130 | 0.977 |

TABLE III: Dehydration Rates for $CaC_2O_4 \cdot H_2O$ and $CaC_2O_4 \cdot D_2O$ and Their Relative Values at 170 °C

| $\alpha$ | $(\Delta\alpha/\Delta t)_H$ | $(\Delta\alpha/\Delta t)_D$ | $k_H/k_D$ |
|---|---|---|---|
| 0.2 | 0.549 | 0.528 | 1.040 |
| 0.3 | 0.570 | 0.552 | 1.033 |
| 0.4 | 0.620 | 0.548 | 1.131 |
| 0.5 | 0.572 | 0.520 | 1.100 |
| 0.6 | 0.524 | 0.492 | 1.065 |
| 0.7 | 0.476 | 0.432 | 1.102 |
| 0.8 | 0.400 | 0.370 | 1.081 |
| 0.9 | 0.336 | 0.294 | 1.143 |

for only the first half of the reaction are taken, where the rates approximate that for a zero-order reaction, the average remains about the same viz., $1.02_3$. The averages appear to be reliable to ±0.01. In view of this experimental error the departure of $k_H/k_D$ from unity cannot be taken as significant. However, the magnitude of this effect is in keeping with the findings of Heinzinger and co-workers in their mass spectrometric equilibrium studies of the dehydration of copper sulfate pentahydrate where the hydrate was formed from natural water.[7-9] These workers have reported isotope effects of only a few percent.

In a previous paper,[4] using transitions-state theory, we estimated that a primary isotope (if it existed) would yield a difference in activation energy of about 0.5 kcal, this value being based on the difference in the zero point energies of the $H_2O$ and $D_2O$ molecules.[10] An upper limit of 1 kcal could be obtained if a diffusion mechanism were employed. However regardless of the mechanisms used, they would have to involve a final step, the desorption of the water molecule from the surface of the solid. Here we have estimated a difference of about 150 cal in the molar heat of vaporization.[4] In view of the fact that the measurements in the tables for the 120–170 °C range of temperature yield an average value of 16.2 ± 0.2 kcal/mol, which is practically identical with the enthalpy of this reaction,[11] one would expect a difference of 150 cal in the activation energy between the two hydrates. Using the Arrhenius equation for the rate constants and assuming that the frequency factors are the same for both hydrates, a value of $k_H/k_D = 1.20$ is obtained. That this ratio has been found close to unity would suggest that the frequency factors are not the same but exhibit a compensating effect. This may be seen using transition state theory in thermodynamic terms, viz.

$$k_H/k_D = e^{(\Delta S_H^{\ddagger} - \Delta S_D^{\ddagger})/R} e^{-(\Delta H_H^{\ddagger} - \Delta H_D^{\ddagger})/RT}$$

or

$$\ln (k_H/k_D) = \Delta(\Delta S^{\ddagger})/R - \Delta(\Delta H^{\ddagger})/RT$$

where $\Delta(\Delta S^{\ddagger})$ and $\Delta(\Delta H^{\ddagger})$ are the differences in entropy and enthalpy of activation. With $k_H/k_D$ being close to unity, we then have $T\Delta(\Delta S^{\ddagger}) \simeq \Delta(\Delta H^{\ddagger})$.

This relation may be considered a kinetic expression for the Barclay–Butler correlation which has found wide application in the thermodynamic hydration studies of

solvent–hydrogen isotope effects.[12]

## References and Notes


(1) H. Oki, E. Kyuno, and R. Tsuchiya, *Bull. Chem. Soc. Jpn.*, **43**, 3263 (1970).
(2) H. G. Wiedemann and A. van Tets, *Naturwissenschaften*, **54**, 442 (1967).
(3) N. R. Chaudhuri and G. K. Pathak, *Thermochim. Acta*, **12**, 71 (1975). Also see N. R. Chaudhuri, G. K. Pathak, and S. Mitra in "Thermal Analysis", I. Buzás, Ed., Heyden & Sons, New York, N.Y., 1974, p 615.
(4) E. P. Manche and B. Carroll, *Thermochim. Acta*, in press.
(5) D. Dollimore, T. E. Jones, and P. Spooner, *J. Chem. Soc. A*, 2809 (1970).
(6) M. I. Smith and B. Topley, *J. Chem. Soc.*, 321 (1935).
(7) K. Heinzinger and T. S. Rao, *Z. Naturforsch. A*, **22**, 2111 (1967).
(8) K. Heinzinger and B. Maiwald, *Bull. Chem. Soc. Jpn.*, **45**, 2237 (1972).
(9) B. Maiwald and K. Heinzinger, *Z. Naturforsch. A*, **27**, 819 (1972).
(10) J. Bigeleisen, *J. Chem. Phys.*, **17**, 675 (1949).
(11) F. Rossini et al., *Natl. Bur. Stand., U.S., Circ.*, **No. 500** (1952).
(12) H. L. Friedman and C. V. Krishnam, *Water, Comp. Treatise*, **3**, 1 (1973).


# Homogeneous Nucleation and Glass Formation in Aqueous Alkali Halide Solutions at High Pressures


**H. Kanno and C. A. Angell***

*Department of Chemistry, Purdue University, West Lafayette, Indiana 47907*


*(Received July 26, 1977)*

*Publication costs assisted by the National Science Foundation*



The limit of supercooling determined by homogeneous nucleation has been investigated as a function of pressure for aqueous solutions of the common alkali halides LiCl, NaCl, KCl, CsCl, and KI for dilute solutions. The pressure dependence of the homogeneous nucleation temperature follows the pattern established earlier for $H_2O$, $T_H$ decreasing curvilinearly until crystallization of ice III becomes favored at ~2 kbar pressure and $T$ < −90 °C. For 1 *m* solutions the $T_H$ vs. pressure plots are indistinguishable for these salts, implying that the $T_H$ depression, like the freezing point depression, is a colligative property. More concentrated solutions, containing 1 or more mol of salt per 20 mol of water (30 in the case of LiCl), fail to crystallize above ~1.5 kbar and glassy phases may be obtained below −120 °C. The glass transition temperature shows a small positive pressure dependence. At constant alkali chloride concentration and pressure the glass transition temperature is a maximum for NaCl.


## Introduction

Recently it was demonstrated that imposition of pressure on "clean" water rapidly depresses the homogeneous nucleation temperature, a limit of −92 °C being reached at 2.09 kbar when the nucleation of ice III becomes favored.[1] Having previously observed the suppression of nucleation in concentrated solutions of highly soluble salts,[2] we became interested in the extent to which supercooling and consequent vitrification could be enhanced by the combination of pressure and solutes. In particular, we were attracted to the possibility of vitrifying solutions of common salt and KCl which always crystallize during cooling under normal conditions. The present short paper reports the results of an investigation of this question and the conditions under which vitrification of these solutions can be accomplished.

## Experimental Section

As in the pure water study, the emulsification technique of Rasmussen and MacKenzie[5] was utilized to avoid heterogeneous nucleation. The only modification was the replacement of heptane as the dispersant phase by a 1:1 by volume mixture of methylcyclohexane MCH and methylcyclopentane MCP in order to avoid dispersant crystallization on cooling to low temperatures ($T_m$(heptane) = −90.6 °C at 1 atm). Solutions in distilled water were prepared by weighing vacuum-dried analytical grade salts (Mallinkrodt). The emulsions contained 30–40% aqueous solution, the richer preparations being used where vitrification occurred and detection of the glass transition phenomenon was desired.

Small samples (~0.04–0.08 mL), contained in thin glass tubes of 2.0–3.2-mm i.d., were pressurized hydraulically and the thermal effects associated with crystallization, glass → liquid transition, eutectic melting, or redissolution were detected by DTA using a collinear sample thermocouple–reference thermocouple arrangement employing fine stainless steel-sheathed Cr/Al thermocouples. Details of the technique have been described in earlier publications.[4] Detection of the glass transition, which is registered as a change of heat capacity rather than of enthalpy, required the use of the larger sample tube size. Glass transition temperatures were always measured during heating because the hysteresis in thermal properties then assists its detection (see Figure 3, inset). Pressures were determined using a calibrated Heise Bourdon guage, readable to ±2 bar.

Measurements of $T_H$ were made using both increasing and decreasing pressure sequences and results were reproducible to within the precision of any individual measurement (±0.5 °C at low pressures and ±2 °C at high pressures where crystallisation is slower and the exotherm by which $T_H$ is defined (Figure 1 inset) is more spread out).

## Results

A plot of the pressure effect on the homogeneous nucleation temperatures obtained during cooling at different pressures, and of melting–dissolution transitions obtained during reheating at the same pressures, is shown in Figure 1 for the case of a 1 *m* NaCl solution. Apart from the striking depression of $T_H$ with increase of pressure up to 2 kbar, there are two interesting features of Figure 2 to

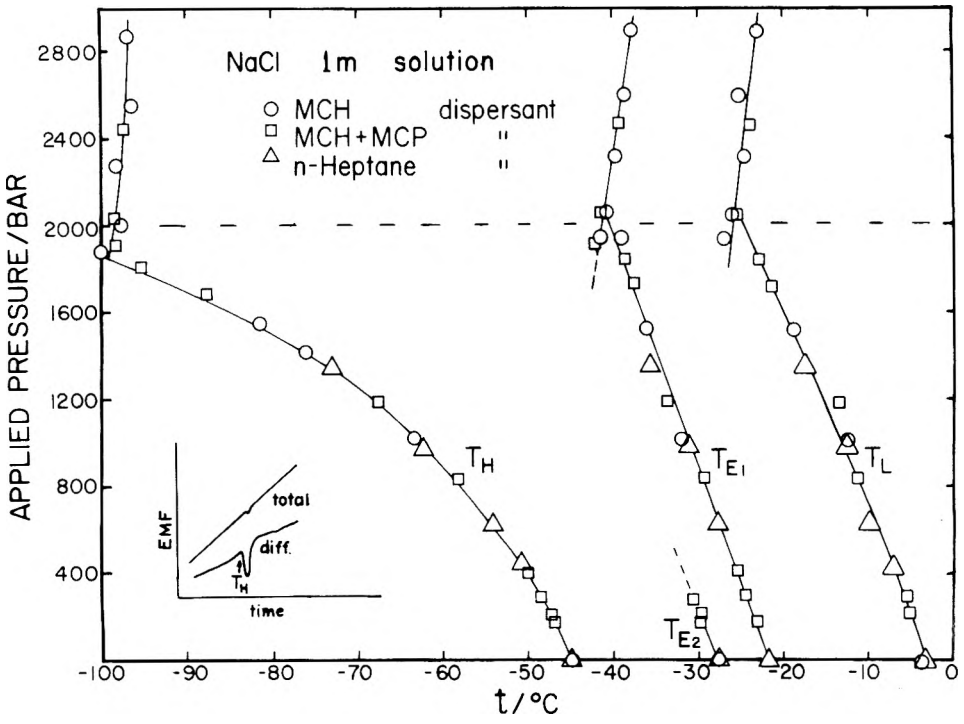


**Figure 1.** Homogeneous nucleation and remelting eutectic and liquidus points for 1 *m* NaCl emulsified solutions. For definition of points from the DTA traces, see insets to Figures 3 and 4.

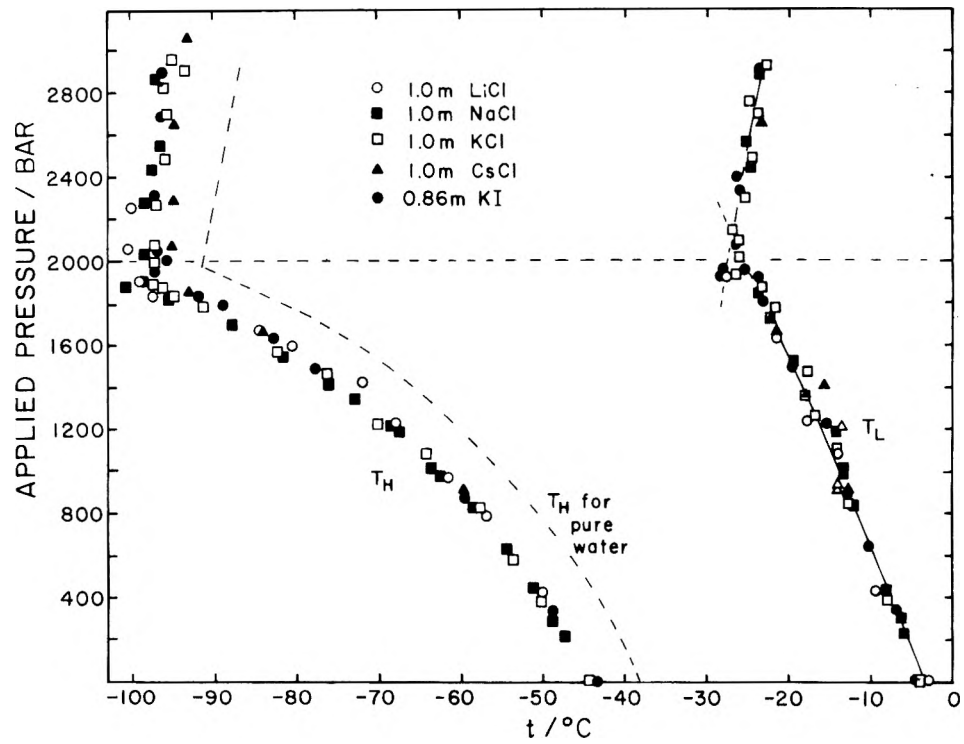


**Figure 2.** Homogeneous nucleation and liquidus temperatures for emulsified 1 *m* alkali halide solutions (0.86 *m* in case of KI).

which some attention should be given here.

The short line of melting transitions between 0 and 500 bar pressure was observed for solutions in which reheating was commenced immediately following observation of $T_H$. The reheating DTA trace for an equilibrium mixture of freezing products should show only two features: a sharp heat absorption corresponding to eutectic (stable hydrate + ice → eutectic solution) melting and a more gradual heat absorption terminating sharply as the last ice crystals redissolve at the liquidus temperature. Thus the observation of three absorptions in the low (0–500 bar) pressure range is anomalous. From the known equilibrium diagram for NaCl at 1 atm, the curves marked $T_{E_1}$ and $T_L$ represent the expected behavior. The short curve marked $T_{E_2}$ must therefore represent the eutectic melting of an ice + metastable hydrate mixture formed in the freezing of a fraction of the emulsion droplets. Separate experiments showed that this transition is the only one observed in samples reheated immediately after observation of $T_H$. This implies that the metastable hydrate, which remains unidentified, is characterized by fast crystallization kinetics presumably because its short range order resembles that of the solution remaining after removal of excess water at $T_H$. To observe $T_{E_1}$, samples had to be cooled initially

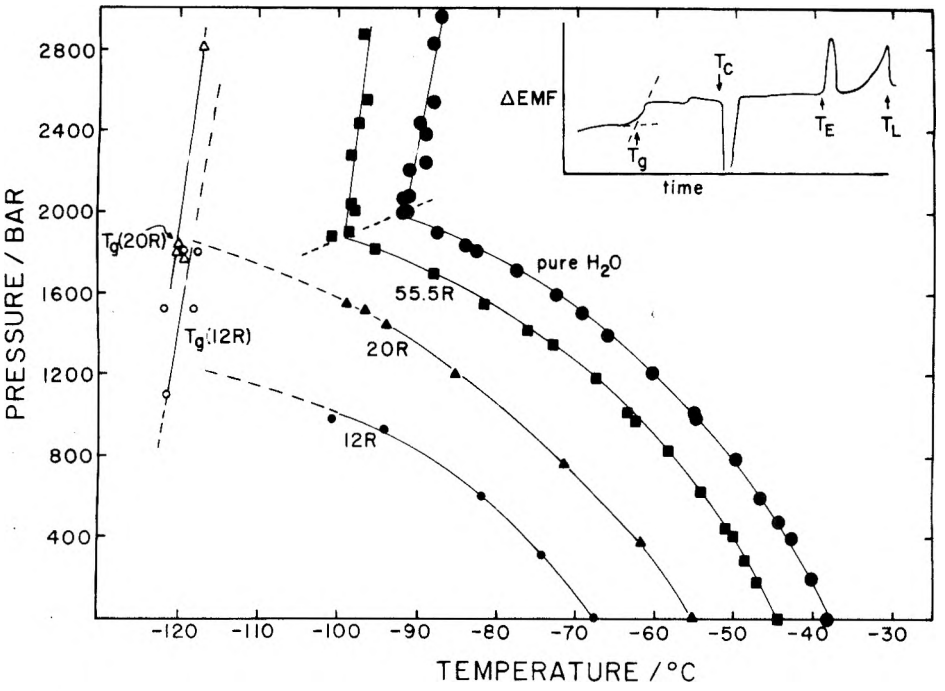


**Figure 3.** Homogeneous nucleation temperatures and glass transition temperatures for emulsified NaCl solutions of various concentrations. The inset is an illustrative DTA trace showing transitions observed during warm-up of 20 R NaCl solution initially vitrified: $T_g$ (glass transition), $T_c$ (crystallization or devitrification), $T_E$ (ice + salt eutectic melting), $T_L$ (liquidus temperature, defined by a drop in the apparent solution heat capacity associated with disappearance of last ice crystal). The second bump above $T_g$ is commonly seen in warm-up DTA traces of high pressure vitreous aqueous solution, but is not discussed in this paper (see ref 5).

below −55 °C. The fact that $T_H < -55$ °C above 500 bar, therefore accounts for the absence of $T_{E_2}$ above this pressure.

The other feature of Figure 1 which must be noted is the occurrence of anomalous melting transitions in the vicinity of 2 kbar. This is the pressure at which earlier studies[1] showed the occurrence of a changeover from homogeneous nucleation of ice I to homogeneous nucleation of ice III in the case of pure water. This changeover is responsible for the break in the $T_H$ vs. pressure plot for the solution at 1 kbar in Figure 1. The origin of the extra melting transition is clearly therefore the presence of a distribution of ices I and III between the frozen droplets and thus the presence of both (ice I + stable hydrate) and (ice III + stable hydrate) eutectic meltings. Evidently there is a range of pressures over which local order fluctuations in the directions of ice I and ice III topologies are of similar probability. Such overlap was not observed for pure water.

The freezing–remelting vs. pressure plots for 1 *m* KCl, CsCl, and KI solutions are qualitatively the same as for NaCl except that the $T_{E_2}$ feature (metastable hydrate + ice eutectic melting) is absent, and the extension of the ice III $T_{E_1}$ curve to lower pressures is more pronounced (details below). These differences are probably due to the poorer water-coordinating abilities of the larger cations, and the generally more destructured nature of the solutions. The $T_H$ vs. pressure curves for 1 *m* solutions of LiCl, NaCl, KCl, and CsCl are indistinguishable within experimental uncertainty (see Figure 2). Within this same uncertainty a KI solution, inadvertently prepared at 0.86 *m* instead of 1 m, gives the same $T_H$ curve (though these points are considered less reliable because of some iodide decomposition). The liquidus curves for these solutions are also indistinguishable although more accurate measurements would reveal displacements resulting from the different activity coefficients at these concentrations. The suggestion of Figure 2 is that the $T_H$ depression, $T_H$(pure water) − $T_H$(solution), in sufficiently dilute solutions may, like the freezing point depression, be a colligative property of the solution.

The main distinctions between the Figure 1 type plots for 1 *m* solutions lie in the $T_{E_1}$ curves which reflect the difference in high concentration solution behavior. In the case of 1 *m* LiCl the eutectic melting transitions are not observed. This is because the concentrated LiCl–$H_2O$ which remains after the crystallization of the excess $H_2O$ at $T_H$ is very resistant to crystallization.[2] Above 2.5 kbar the primary (ice III) crystallization exotherm which defines $T_H$ becomes very diffuse and is not easily detected, implying slow crystallization kinetics and probably vitrification of the entire solution on fast cooling. This latter possibility was not investigated for the emulsified sample though an extensive study of the glass transition phenomenon in more concentrated unemulsified LiCl solutions at high pressures has been performed and will be reported separately.[5]

The effect of salt concentration on the $T_H$ vs. pressure plot is shown in Figures 3 and 4 for the cases of NaCl and KCl solutions. Concentrations are marked in R units (R = moles water:moles salt = 55.5/*m*) because R units are the more direct indicators of the solution constitution and of the associated high concentration solution properties. As expected from earlier normal pressure studies by Rasmussen[3b] and Xans,[3c] increasing concentration produces an accelerating depression of $T_H$ which is more pronounced the higher the pressure (see Figure 5). Figures 3 and 4 include the $T_H$ vs. *p* plots for pure water[1] and for the 1 *m* (i.e., 55.5 R) solutions already seen in Figures 1 and 2. The effect of concentration on the nucleation of ice III in KCl solutions is interesting. At low concentrations $T_H$ has a positive pressure dependence in the ice III nucleation regime but at the increased concentration of 35 R the plot develops a negative slope (Figure 4). This implies that even the denser ice III has a larger molar volume than that ($V_m$) of the water in the solution.

The changing probability of ice I vs. ice III nucleation in the vicinity of 2 kbar was studied carefully in the case

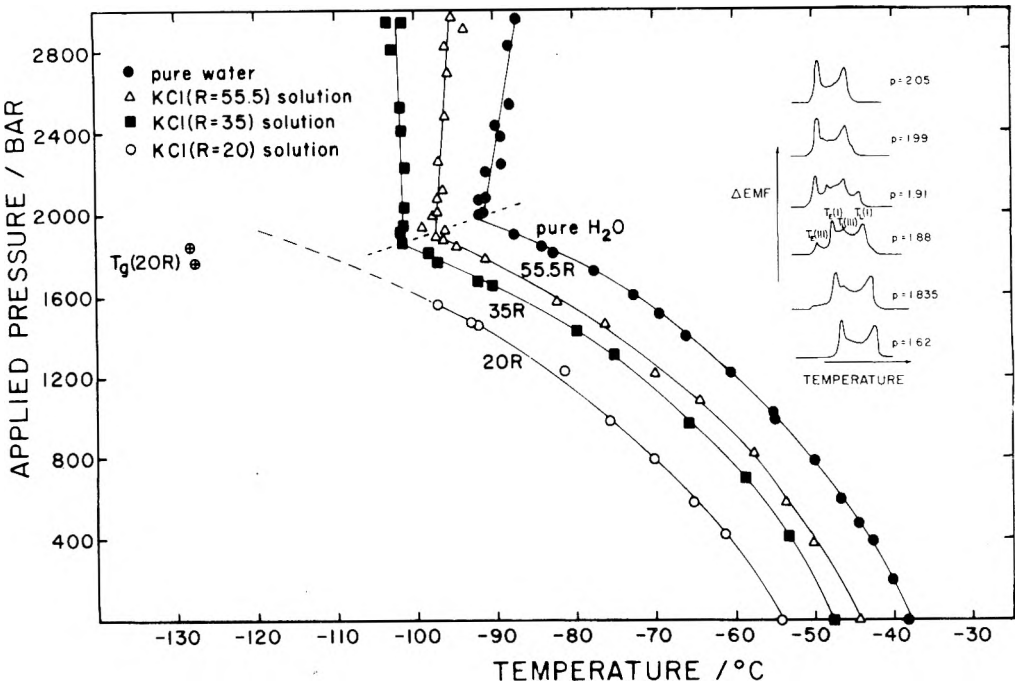


**Figure 4.** Homogeneous nucleation temperatures and glass transition temperatures as a function of pressure for emulsified KCl solutions of different concentrations. The inset contains DTA traces showing remelting behavior in vicinity of 2 kbar due to presence of both ice I- and ice III-containing emulsion droplets.

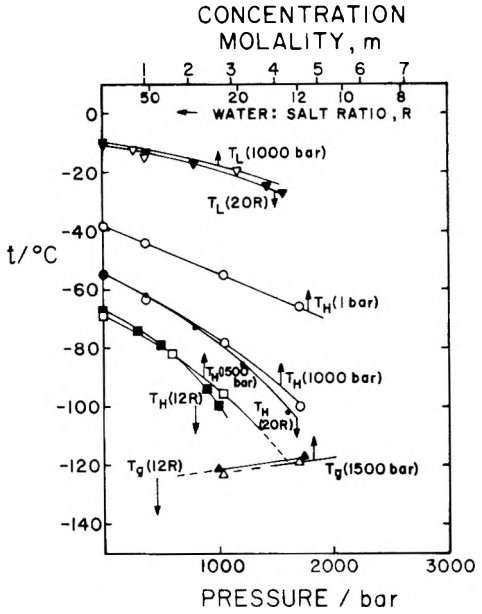


**Figure 5.** Isomolal and isobaric plots of $T_L$, $T_H$, and $T_g$ for NaCl solutions showing approximate equivalence of pressure and composition variables.

of 1 *m* KCl. The remelting behavior for emulsions frozen at successively increasing pressures is shown in Figure 4, inset. At 1.62 kbar only the ice I + salt eutectic $T_E$(I) and subsequent dissolution of excess ice I absorptions are seen. At $p$ = 1.835 kbar a small absorption occurs at a lower temperature corresponding to the metastable extension of the ice III + salt eutectic $T_E$(III), implying that a small fraction of the droplets homogeneously nucleated ice III rather than ice I during cooling. The probability of ice III nucleation, judged by the magnitude of the low temperature absorption, increases progressively with increasing pressure until above 2 kbar this is the only ice formed. The pressure range of comparable polymorph nucleation probabilities is thus 0.16 kbar.

At 20 R, the $T_H$ exotherm is not observed above 1600 bar for either NaCl or KCl solutions, and studies with larger samples in a modified pressure cell confirmed that continued cooling to −190 °C produced vitrified forms of these solutions. Glass transition temperatures for samples vitrified at 1900 bar (a limit imposed by a leaking seal in this apparatus) were found to be −120 °C for NaCl and −127 °C for KCl. A single value obtained subsequently at 2800 bar establishes a positive pressure dependence for $T_g$ in this pressure range.

Emulsion studies were performed at higher concentrations only for the NaCl system (Figure 3). As expected, the pressure necessary to suppress ice crystallization in a 12 R solution is lower than for the 20 R solution. Glass transition temperatures were determined between 900 and 1900 bar and show a small positive pressure dependence (Figure 3). In separate experiments using *bulk* solutions it was earlier concluded that NaCl solutions could be vitrified in a narrow range of concentrations between 12 and 16 R at pressures above 2 kbar, but that KCl solutions could not be vitrified in any range. The lower viscosity of KCl solutions which is observed at high temperatures, and is implied at low temperatures by their lower $T_g$, must favor heterogeneous nucleation in this system.

## Discussion

Homogeneous nucleation occurs when a critical size subset of the molecules in the system under study spontaneously reorganizes itself in real space from a packing characteristic of the amorphous region of phase space to one characteristic of the crystalline region of phase space.[6] It must be expected that, for a given thermodynamic driving force (degree of supercooling), such improbable fluctuations will occur more readily in systems in which the short-range packing topologies in the two regions of phase space are similar. Factors which cause topological distinctions between fluid and crystalline regions of phase space to increase should, accordingly, reduce the probability of nucleation at the same supercooling or, equivalently, should increase the degree of supercooling necessary to cause observable nucleation during cooling at a given rate.

The effect of pressure on $T_H$ in both pure water and aqueous solutions is probably best understood in the above

terms. Increases of pressure cause progressive decreases in the average O–H---O bond angle[7,8] shifting the local order progressively away from that of linear OH---O bond angle ice I structure until, at ~2 kbar, fluctuations toward the ice III bend–bond topology become equally probable. In pure water the break in the $T_H$-pressure plot associated with change from ice I to ice III nucleation occurs at ~0.1 kbar lower pressure than the intersection of the ice I and ice III melting curves. In the solutions the $T_L$ intersections continue to fall at ~2.09 kbar while the $T_H$ breaks occur at progressively lower pressures as concentration increases (see e.g., Figure 4). These observations suggest that ice III-like bent bond topologies are somewhat favored in the liquid state[9] and that this tendency is enhanced in the presence of solute. In the solutions it would further seem that the solvent structure is generally less sharply defined than in the case of pure water because, in the latter, the changeover from ice I nucleation to ice III nucleation occurs quite abruptly whereas in 1 *m* KCl solution the two nucleation probabilities (which reflect topology fluctuations) are of comparable magnitude over a 160-bar pressure range (Figure 4 inset).

Second components depress $T_H$ for essentially the same reason they depress the liquidus temperature (freezing point) $T_L$, i.e., because the chemical potential of water in the liquid phase is lowered while that of ice is unaffected. The $T_H$ depression constant is evidently (Figure 2) greater than the freezing point depression constant. This should hold true for any solution in which the heat capacity of the pure liquid solvent substantially exceeds that of the crystal, because then $\Delta H$ for the phase transition will be lower at the lower temperatures ($K_f \propto 1/\Delta H$). The pressure-induced and composition-induced depressions of $T_L$ and $T_H$ have the same curvilinear character such that, for suitably chosen pressure and composition scales, the functions are approximately equivalent. Figure 5 shows that when constant pressure or constant composition conditions are chosen such that $T_L$ is the same at zero solute concentration or zero pressure, respectively, then the entire isobaric concentration and isomolal pressure plots for $T_L$, $T_H$, and also $T_g$ almost superimpose. For these properties, pressure and concentration can be treated as equivalent variables. There are limitations on the usefulness of this observation, however, since it is known from other studies[10] that the effect of solutes on derivative properties of the solution (e.g., heat capacity) is strongly solute dependent.

Some insight into the time scales for order fluctuation leading to nucleation can be gained from the observation that vitrification, i.e., the freezing-in of a particular solution structure at the temperature $T_g$, can be achieved even though $T_H > T_g$. At $T_H$ the probability of crystal-forming order fluctuations occurring within the solution becomes large. If the fluctuation fails to occur during cooling it must be because it requires a growth time which is long relative to the time necessary to rearrange the molecules in the liquid into lower energy but still fully amorphous configurations. Ultimately, with decreasing temperature, this latter time itself becomes long with respect to the observation time scale and the amorphous phase configuration, as well as any embryonic nuclei it may contain, becomes arrested, producing the "glassy" state. The differences in time scale reflect the difference in system subspace which must be explored in order to substantially achieve the respective local equilibrium structures. Other studies presently being reported[11] suggest this is of the order of 10 Å for the amorphous structure relaxation.

In general, the closer $T_H$ approaches $T_g$ the less probable it is that crystals will be observed to develop at a given cooling rate. Figures 3 and 4 show that for R = 20 increase of pressure causes $T_g$ to approach $T_H$, rapidly in the ice I crystallization region, so that vitrification evidently becomes more probable as pressure increases.

Having now achieved vitrification of three alkali halide solutions, it is of interest, finally, to observe the cation effect on the glass transition temperature at constant concentration and pressure. At 1.9 kbar and R = 20 we find $T_g(Li^+) = -130$ °C, $T_g(Na^+) = -120$ °C, and $T_g(K^+) = -127$ °C. The maximum in $T_g$ for sodium salts, which has previously been observed in the alkali acetate series,[12] is evidently maintained in even the simplest alkali metal salt solutions hence must be a cation hydration effect. The maximum at $Na^+$ is anomalous in the face of the known systematic increases in ambient temperature solution viscosities as the alkali cation radius decreases.[1]

*Acknowledgment.* It is a pleasure to acknowledge support of this work by the National Science Foundation under Grant DMR 73-02632-A01.

## References and Notes

(1) (a) H. Kanno, R. J. Speedy, and C. A. Angell, *Science*, **189**, 880 (1975); (b) P. Xans and G. Barnaud, *C. R. Acad. Sci., Paris, Ser. B*, **280**, 25 (1975).
(2) C. A. Angell and E. J. Sare, *J. Chem. Phys.*, **52**, 1058 (1970).
(3) (a) D. H. Rasmussen and A. P. MacKenzie, *J. Chem Phys.*, **59**, 5003 (1973); (b) D. H. Rasmussen and A. P. MacKenzie in "Water Structure at the Water-Salt Interface", H. H. G. Jellinek, Ed., Plenum Press, New York, N.Y., 1972, p 126; (c) P. Xans, *C. R. Acad. Sci., Paris, Ser. B*, **277**, 321 (1973).
(4) E. Williams and C. A. Angell, *J. Phys. Chem.*, **81**, 232 (1977).
(5) H. Kanno and C. A. Angell, to be published.
(6) D. Turnbull and J. C. Fisher, *J. Chem. Phys.*, **17**, 71 (1949).
(7) G. E. Walrafen, *J. Solution Chem.*, **2**, 159 (1973).
(8) C. A. Angell and H. Kanno, *Science*, **193**, 1121 (1976).
(9) S. A. Rice, *Top. Current Chem.*, **60**, 109 (1975). The shift in favor of ice III nucleation at lower temperatures cannot be due to an increased bulk free energy difference driving force for ice III nucleation because $\Delta S$ for ice I → ice III is positive (though small) [F. Franks in "Water a Comprehensive Treatise", Vol. I, F. Franks, Ed., Plenum Press, New York, N.Y., Chapter 4]. This implies that of the three $G$ vs. $T$ curves which intersect at $P = 2.09$ kbar, $T = 250$ K, the curve for ice I has the smallest slope; hence for any supercooled state at the triple point pressure, $\Delta G_{(\text{water}\rightarrow\text{ice I})} > \Delta G_{(\text{water}\rightarrow\text{ice III})}$.
(10) C. A. Angell and W. Sichina, to be published.
(11) A. Barkatt and C. A. Angell, *J. Chem. Phys.*, submitted for publication.
(12) E. J. Sare, Ph.D. Thesis, Purdue University, 1970.
(13) R. A. Robinson and R. H. Stokes, "Electrolyte Solutions", Academic Press, New York, N.Y., 1955.

# Charge-Transfer Complexes. Influence of Nonideality of Solution (Solvent Competition) on Complexation

**M. H. Litt* and Jasmina Wellinghoff**

*Department of Macromolecular Science, Case Western Reserve University, Cleveland, Ohio 44106* *(Received September 17, 1977)*

The effect of solvent on weak charge-transfer complex formation is reexamined. Ultraviolet absorption data are presented from the styrene–fumaronitrile complex in carbon tetrachloride, chlorobenzene, 1,2-dichloroethane, and ethanol. In all cases, the peak maximum is slightly dependent on donor concentration, showing a red shift of 8 to 13 nm with increasing styrene concentration. Benesi–Hildebrand analyses of the data lead to curved lines; extrapolation of the linear portions give apparent negative values of $K$ and $\epsilon$ for the studies in dichloroethane and ethanol. [Similar trends were noted in our NMR data (not discussed).] This peculiarity is analyzed in terms of various theories from the literature and none succeed in rationalizing the data. A new theory is presented here which is based on the reasonable model that the interaction of the acceptor occurs in two sequential processes: competitive solvation of the acceptor by donor and solvent in the nearest neighbor cage, where the molecules rotate freely, and subsequent true complexation of donor and acceptor where they maintain fixed relative positions. The mathematics of the derivation are presented. The resulting equation can be shown to fit the data using reasonable values for the four parameters. The theory is applied to some literature data also.

## Introduction

Difficulties in determining the concentration of weak charge-transfer complexes using the Benesi–Hildebrand (B–H) equation[1] and its modifications[2] have been frequently discussed in the literature. Zero[3] and even negative[4] intercepts were reported implying zero and negative formation constants for the complex. Polar solvents such as methanol and acetonitrile tend to make any numerical determination of the equilibrium constant uncertain.[5,6]

Person[7] pointed out that the B–H plot would give zero intercept despite a moderately large equilibrium constant if the equilibrium concentration of the complex is not of the same order of magnitude as the equilibrium concentration of the more dilute component. Deranleau[8] and Guidry and Drago[9] came essentially to the same conclusion.

Some authors considered solution nonideality as the main reason for the encountered troubles,[10-13] while higher-order complexes[14,15] were postulated to complicate the situation in some cases.

In our preliminary work we noticed the strong effect the solvent had on the formation constant of the complex and decided to investigate the problem further, accounting for the solvent effect. We chose styrene as the donor and fumaronitrile as the acceptor and observed the behavior of this system in four solvents.

## Experimental Section

*Fumaronitrile* was obtained from Baker Chemical Co., melting point 95–97 °C. It was used as received.

*Styrene* was twice distilled under vacuum and used fresh after distillation.

*Solvents* were all spectroscopic quality.

*UV absorption experiments* were run on a Cary 14 spectrophotometer with 1-cm quartz cells. Absorbances were read to ±0.005 accuracy.

Solutions were made in the following way. Both fumaronitrile and styrene were weighed in separate flasks on a balance with ±0.0002 g accuracy, resulting in a 2% error in concentration determination of the more dilute component. Styrene was diluted to the mark with desired solvent and this mixture used to dissolve fumaronitrile and dilute to the chosen concentration. During the UV absorption experiment the sample cell contained the latter solution, with all three components (donor, acceptor, solvent), while the reference cell contained the solution of donor/solvent, the same one used for preparing the sample cell solution. This procedure was adopted to eliminate any possible, small absorption due to styrene at high styrene concentrations. The acceptor absorption does not interfere. The UV absorption measurements were run at room temperature (22 ± 2 °C). The errors in absorbance and concentration are included as the minimum error in the presentation of data.

## Results

The charge transfer spectrum consisted of a slope with a small peak superimposed on it. (The curve could be observed down to 300 nm at low styrene concentrations, but only to ~310 nm at high styrene concentrations.) It was felt that the absorption consisted of two superimposed bands, probably charge transfer bands; the larger one had its peak below 300 nm and the smaller band had a peak ($\lambda_{max}$) which varied from 304 to 317 nm depending on solvent and donor concentration. As the small band varied in $\lambda_{max}$, we felt that the large peak would do so also. Therefore, data taken at a constant $\lambda$ would probably be meaningless. This supposition was confirmed when the ratios of optical densities at 310 and 320 nm were taken. They varied considerably with styrene concentration. The data are given in Table AI in Appendix I (see paragraph at end of text regarding supplementary material). Repeat determinations from scratch are given as duplicate data points, showing the reproducibility of the experimental technique.

Since $\lambda_{max}$ was changing with donor concentration, it was felt that the best procedure was to assume that both bands varied in a similar manner. Therefore, the absorption at the $\lambda_{max}$ of the observable peak should be proportional to the complex concentration; this value was measured and used in subsequent calculations.

The spectral data are listed in Table I. Figure 1 shows the change in normalized absorbance of the complex between fumaronitrile and styrene in four solvents, $CCl_4$, $C_6H_5Cl$, $C_2H_4Cl_2$, and $C_2H_5OH$, with dielectric constants of 2.2, 5.7, 10.5, and 24.3, respectively. The plots curve slightly (except for $C_2H_4Cl_2$) at low styrene concentrations and start diverging considerably from linearity above [D]

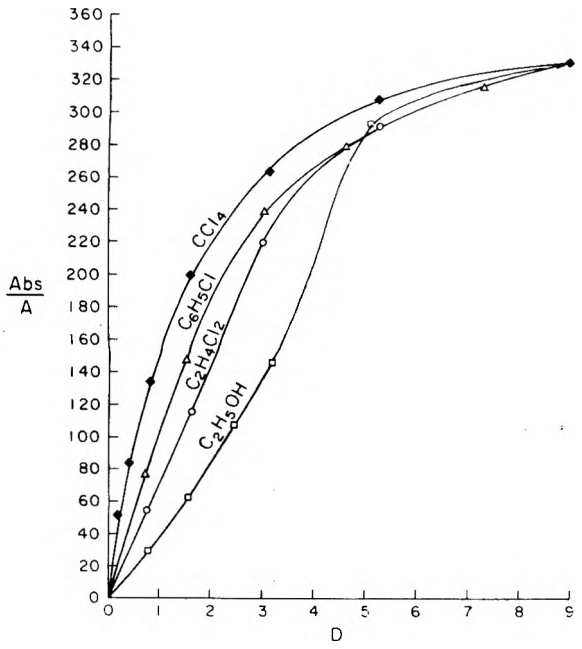


**Figure 1.** Normalized absorbance of the fumaronitrile [A]–styrene [D] complex vs. donor concentration in various solvents. See Table I for exact concentrations. [A] and [D] are the concentration of the acceptor and donor, respectively, and are given in moles/liter.

≈ 2–3 mol/L. Whatever the shape of the curves, it is evident that a finite complex concentration exists in all four solvents. Figure 2 shows the same data plotted according to the B–H equation. As can be seen the lines are curved at very high donor concentration. Extrapolation of the linear portions results in negative intercepts for two sets of data, these in dichloroethane and ethanol. In Figure 3 the data for the ethanol system are plotted according to Drago's method[9] for testing the usefulness and credibility of the data according to his definition. The system appears to be a well defined one, but the intersection point is negative, implying a negative formation constant. This method was devised assuming 1:1 complexes and ideal solutions and therefore shows the same weaknesses as the B–H treatment when these conditions are not met.

## Discussion

From the B–H plots shown in Figure 2, values for the formation constants ($K$) and molar absorptivities ($\epsilon$) of the system in all solvents were determined, Table I. In two cases, zero and negative intercepts and formation constants were observed, which is not physically reasonable.

Also, the plots are not really straight lines. There is curvature at high donor concentrations. As mentioned in the Introduction there are several possible explanations for the difficulties we are encountering.

*Higher-Order Complexes.* It has been argued that second-order complexes could be responsible for the deviation from a straight line of the B–H plots[15] as shown in Figure 2. (The B–H plot of data for iodine/benzene, etc.[1] is also curved when plotted carefully. They too cover the whole range of [D].) According to this theory although negative and zero intercepts would be found, their interpretation would be different and the constants determined from them would be meaningful. The 1:1 complex, DA, is supposed to exist in dilute solution of donor, while 2:1 complexes, $D_2A$, will also be present at high donor concentration.

The treatment[15] shows that a negative intercept for the lower donor concentration portion of the plot will be found when the product, $K_2\epsilon_2$, for the $D_2A$ complex is larger than $K_1\epsilon_1$, for DA. In the case of the styrene–fumaronitrile system and other $\pi$ charge-transfer complexes, $K_2$ could only be considerably smaller then $K_1$. Due to the planar nature of both the acceptor and the donor molecule, the most likely configuration for the most stable complex is the "stack" arrangement. Crystal structure studies on aromatic complexes with various acceptors ($\pi$–$\pi$ complexes) have demonstrated this.[2] Once a DA complex is formed, the electron density of the acceptor is significantly increased, its electron affinity consequently decreased, and the formation of DAD must be characterized by a smaller constant both energetically and entropically. If $K_2$ is bound to be smaller, then only an increase in $\epsilon_2$ can make the product of $K_2\epsilon_2$ larger than $K_1\epsilon_1$. That this does not happen was shown by Litt and Summers[16] in a study of a series of complexes, both free in solution, and with the donors fixed in position in polymer side chains. All measurements were done at low concentrations of both donor and acceptor and in one solvent, chlorobenzene. Under these conditions the probability for $D_2A$ to form is much larger when the acceptor can be sandwiched between two donors attached to the polymer chain and separated by a fixed, favorable, distance. In all cases the molar absorptivity dropped going from free donors in solution to donors fixed on polymer chains. (Here, the constant was higher due to the geometry of the polymeric donors, which forces the acceptors into the most favorable configuration for complexing.)

One case was found in the literature where a normal donor–acceptor pair might have formed a higher order complex, tetracyanoethylene–hexamethylbenzene.[17] Here as the pressure was raised, the initial red shift of $\lambda_{max}$ changed to a blue shift at 1000 atm and the oscillator

TABLE I: Charge Transfer Band Maximum ($\lambda$) and Its Normalized Absorbance (Abs/[A]) for the Fumaronitrile [A]-Styrene [D] System in Four Solvents

| Solvent | $\lambda$, nm | [D], M | Abs/[A] | [A], M |
|---|---|---|---|---|
| $CCl_4$ | 304 | 0.208 | 52 ± 2 | 0.0060 ± 0.00012 |
| | 305 | 0.404 | 85 ± 3 | |
| | 307 | 0.807 | 135 ± 4 | |
| | 308 | 1.58 | 200 ± 5 | |
| | 310 | 3.16 | 263 ± 6 | |
| | 311 | 5.25 | 308 ± 8 | |
| | 317 | 8.70 | 333 ± 8 | |
| $C_6H_5Cl$ | 308 | 0.680 | 78 ± 4 | 0.0030 ± 0.00006 |
| | 310 | 1.505 | 148 ± 5 | |
| | 311 | 2.99 | 240 ± 7 | |
| | 313 | 4.63 | 278 ± 8 | |
| | 317 | 7.32 | 316 ± 9 | |
| | 317 | 8.70 | 333 ± 9 | |
| $C_2H_4Cl_2$ | 308 | 0.80 | 57 ± 2 | 0.0060 ± 0.00012 |
| | 310 | 1.58 | 117 ± 3 | |
| | 313 | 3.00 | 220 ± 5 | |
| | 314 | 5.18 | 292 ± 6 | |
| | 317 | 8.70 | 333 ± 8 | |
| $C_2H_5OH$ | 309 | 0.80 | 29 ± 2 | 0.0060 ± 0.00012 |
| | 309 | 1.59 | 63 ± 3 | |
| | 309 | 2.43 | 108 ± 3 | |
| | 310 | 3.16 | 147 ± 4 | |
| | 312 | 5.06 | 294 ± 7 | |
| | 317 | 8.70 | 333 ± 8 | |

**$K$ and $\epsilon$ Calculated by Benesi-Hildebrand Equation[a]**

| Solvent | $K$, $M^{-1}$ | $\epsilon$ |
|---|---|---|
| $CCl_4$ | 1.1 | 310 |
| $C_6H_5Cl$ | 0.25 | 560 |
| $C_2H_4Cl_2$ | −0.013 | −5000 |
| $C_2H_5OH$ | −0.08 | −420 |

[a] Reference 1.

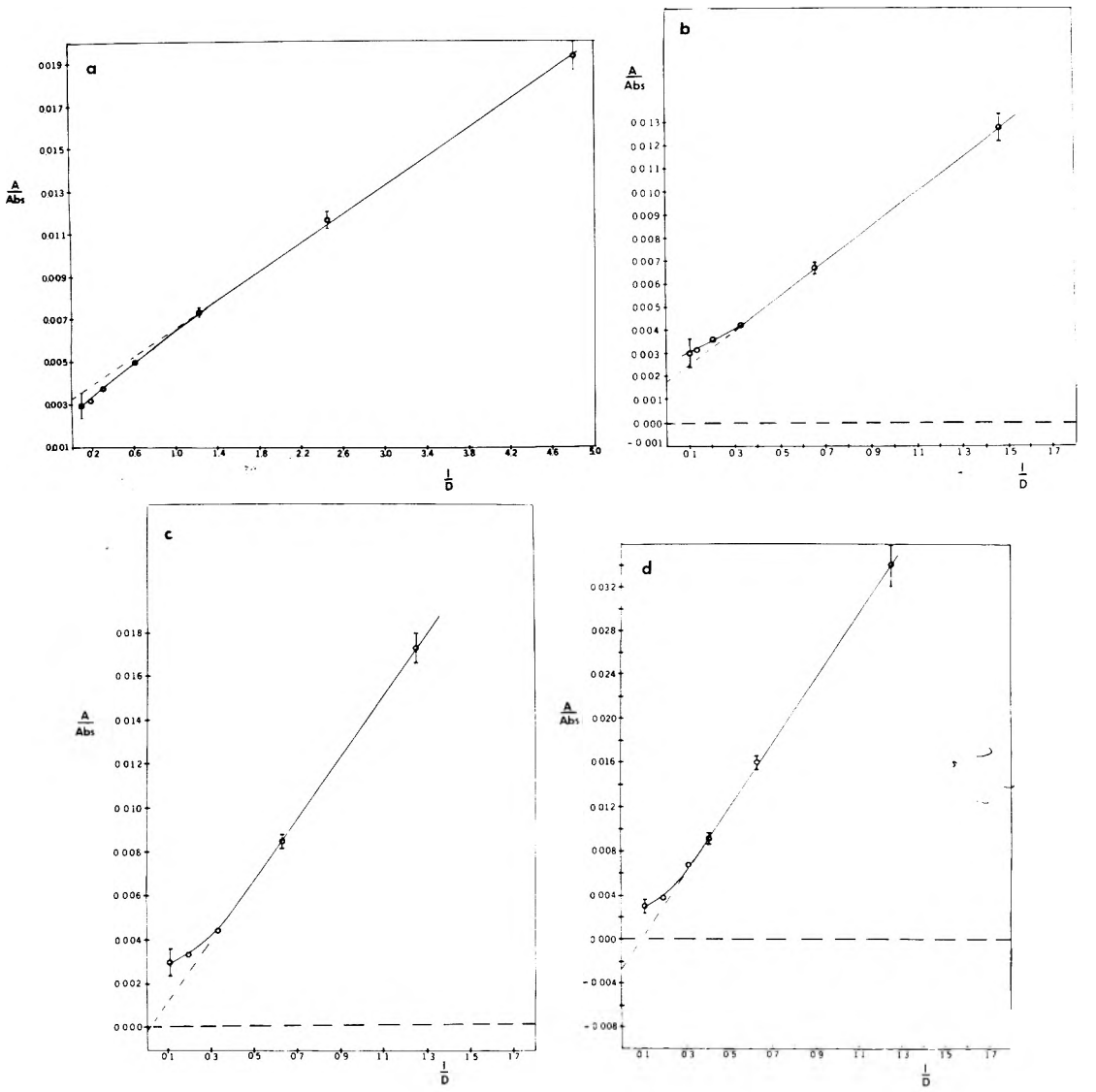


**Figure 2.** Benesi–Hildebrand plots for the fumaronitrile–styrene complex: (a) in $CCl_4$; (b) in $C_6H_5Cl$; (c) in $C_2H_4Cl_2$; (d) in $C_2H_5OH$. [A] and [D] are in M. Where graph extends below the origin, [A]/Abs = 0 is indicated by the dotted horizontal line. Errors are shown as error bars when they are larger than the point diameter.

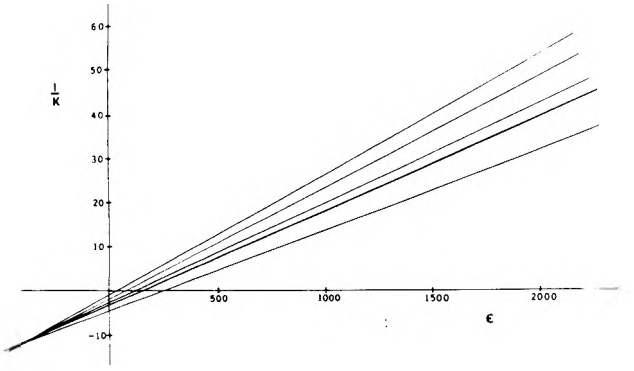


**Figure 3.** Drago's plot for the fumaronitrile–styrene system in $C_2H_5OH$.

strength, $\epsilon$, started to decrease above 2000 atm. This fits the expectations for a $\pi$–$\pi$–$\pi$ complex. Other, weaker complexes showed only a red shift and increased absorption with increasing pressure.

Another possible indication of second-order complexes could be found in the spectra themselves, if a considerable shift of the absorption is observed. Litt and Summers,[16] for example, found a red shift in two cases. However, for the other "$D_2A$" complexes there was no shift from the wavelength of the DA absorption. As can be seen from Table I the position of the absorption for the fumaronitrile–styrene system shifts slightly toward lower energy as the concentration of donor is increased. We feel that this shift is due to changes in the solvent, as more and more donor alters the original medium. This phenomenon[18] is generally observed and is caused by the differential effect of the environment on the excited and/or ground state of the absorbing entity. In $CCl_4$ the effect is the strongest. Styrene is more polarizable than $CCl_4$ and probably a slight polarization is induced by the dipole of the complex. The increase in polarization due to the increased dipole moment of the complex upon excitation results in the excited state being more stabilized relative to the ground state with increasing styrene content. In ethanol where the solvent tends to solvate acceptor strongly, as will be shown later, the initial wavelength is higher than with $CCl_4$, as the solvent is more polar, and there is almost no change in $\lambda$ until [D] > 3 M. From this discussion it seems that the presence of $D_2A$ cannot be used to rationalize our results.

*Nonideality of Solutions.* Drago and co-workers[19] found that the B–H $K$ for the DMA–$I_2$ system decreases from 6.9 $M^{-1}$ in $CCl_4$ to 2.6 in benzene and 1.4 in $CH_2Cl_2$. The decrease of $K$ with polarity of the solvent is also seen from the data for tetrachlorophthalic anhydride–hexamethylbenzene[20] (see Table II). Evans[3] found that B–H plots

TABLE II: Comparison of Experimental Abs/[A] with the Values Calculated using Carter's Method ($C_2H_4Cl_2$ Results)

| (Abs/[A])$_{obsd}$ | (Abs/[A])$_{calcd}$ | % error |
|---|---|---|
| 57 | 59.5 | +4.3 |
| 117 | 117 | 0.0 |
| 220 | 222 | +0.9 |
| 292 | 384 | +31.5 |
| 333 | 666 | +100.0 |

for the $I_2$–*n*-heptane system pass exactly through the origin ($K = 0$). Zeegers and Butler[5,6] had difficulties assigning values for constants for divinyl ether–maleic anhydride and divinyl ether–fumaronitrile complexes in acetonitrile and methanol, respectively. Hanna and Asbaugh,[4] using NMR, found negative and zero intercepts for the systems TCNQ with benzene and toluene, respectively, in dioxane. More highly methylated benzenes gave positive intercepts. As shown, our own data produced negative intercepts in some cases.

Several authors, therefore, have tried to account for the sharp changes in formation constants and molar absorptivities by recognizing solvation effects. Mulliken and Person[21] give a treatment which is essentially a summary of many others.

The B–H equation is based on two essential assumptions: (1) solutions are ideal, (2) both donor and acceptor concentrations are low. Considering that real solutions are usually not ideal, Mulliken and Person derived a thermodynamic equilibrium constant related to the B–H or apparent constant through a quotient of activity coefficients:

$$K_a = K(\gamma_C/\gamma_A\gamma_D) = K\Gamma$$

They then calculate $\Gamma$ from solubility parameters assuming it depends linearly on donor concentration. In doing so they are using the regular solution theory[22] and assume that the solubility parameter of the complex can be expressed as the geometric average of the solubility parameters of the components. Since solubility parameters themselves depend on solvent there still could be considerable uncertainty about the value of $\Gamma$, so that this theory is not particularly helpful.

Similarly Carter et al.[10] assume that all species are solvated. They write

$$AS_n + DS_m \rightleftarrows DAS_p + qS$$

where $q = n + m - p$, and derive the following equation:

$$\frac{[A]}{Abs} = \frac{1}{[D]K\epsilon} + \frac{1}{\epsilon}\left(1 - \frac{q(m+1)}{K[S_0]}\right)$$

where $[S_0]$ is the concentration of solvent when $[D] = 0$. They estimate $K = 2.27$ for the iodine–heptane case for which the B–H plot passed through the origin. (The latter implies an infinite $\epsilon$ and $K$.)

We have applied Carter's procedure to our data in $C_2H_4Cl_2$ which gives a B–H plot with a very slightly negative intercept. We were not able to obtain the same correction factor, $q(m + 1)$, from all experimental points if the criterion of the graph, $\epsilon$ vs. $K$ passing through zero, was satisfied. As [D] increased, $q(m + 1)$ decreased as is indeed to be expected from Carter's equilibrium. However, when we picked one that seemed to come closest to producing the desired effect ($q(m + 1) = 17$), we determined $K = 1.37$ and $\epsilon = 54$. With these we were able to reproduce well the points on the straight line portion of [A]/Abs vs. 1/[D], but the two points causing the curvature were off by a large amount as shown in Table II. The disagreement in the last two points is such that no experimental error could explain it.

It appears that, although these methods eliminate the problem of zero intercepts, they do not take care of the curvature in the B–H plot. We would like to emphasize that the curving of the B–H plot has been observed by many investigators and does not appear suddenly in our results. Also, our NMR data for the styrene–fumaronitrile system give B–H plots which are totally analogous to the UV plots. However, the data are difficult to rationalize and are not presented here. Possible problems with NMR determinations are mentioned in the conclusions.

More recently Lane, Christian, and Childs[13] proposed a technique by which activity coefficients of all components in the system, including that of the complex, could be determined. Although the important conclusions of their work are generally valid, the method they suggest involves a very long experimental procedure and, what is more serious, appears to be limited to cases where the solubility method can be used.

*Effect of Solvent on K and $\epsilon$.* In principle three possibilities exist: that $\epsilon$ can change with solvent, that $K$ can change while $\epsilon$ remains constant, and that both $K$ and $\epsilon$ change with solvent.

In all previous work the molar absorptivity was assumed constant for a chosen acceptor–donor–solvent system regardless of the actual concentration of the donor, while it was always assumed different for the same acceptor–donor pair if the solvent changes. (The acceptor concentration is always low.) At first glance this seems reasonable. However, as the acceptor concentration is usually low, the acceptor–donor–solvent mixture really contains two solvents, the solvent and the donor.

Benesi's and Hildebrand's report itself[1] is a good example of a case involving the above-mentioned contradictory assumptions. They applied their equation to the iodine–benzene and iodine–mesitylene complex, both in carbon tetrachloride and *n*-heptane. In all cases they assumed a unique molar absorptivity for mixtures of benzene or mesitylene with solvent despite the fact that they increased the donor concentration up to a mole fraction of 1. At the same time they assumed different absorptivities for the same complex in the two solvents. The molar absorptivities for the iodine–benzene complex in the two solvents were found different. Their results, however, show that the molar absorptivity of the stronger iodine–mesitylene complex was virtually independent of the solvent.

In the spectroscopic literature of both regular organic compounds and charge-transfer complexes there are many instances of fairly constant molar absorptivities[1,23,24] as solvent is changed drastically. For example, $\epsilon_{max}$ for the 326-m$\mu$ absorption of vitamin A is 48 310 and 51 000 in cyclohexane and ethanol, respectively. Also, going from hexane, through ether and chloroform, to ethanol did not affect the molar absorptivity of mesitylene oxide.[23]

The complex *o*-xylene–TCNE in $CHCl_3$ was found to have a molar absorptivity of 3820, in $CH_2Cl_2$ 3860, and in $Et_2O$ 4430.[24] The values of the respective constants were 9.46, 6.97, and 2.95. For a generally weaker anisole–TCNE complex, the values of $K$ and $\epsilon$ in $CH_2Cl_2$ and $Et_2O$ were 4.42 and 2080, and 1.55 and 2860, respectively. However, the authors observed that $Et_2O$ forms a complex on its own with TCNE which somewhat blurs the results. Still both systems have relatively high equilibrium constants and relatively constant molar absorptivities, the stronger one showing less variation in $\epsilon$.

TABLE III: Tetrachlorophthalic Anhydride-Hexamethylbenzene Complex in Different Solvents[a]

| Solvent | ε | K, $M^{-1}$ | d[b] |
|---|---|---|---|
| n-Hexane | | 34 | 1.89 |
| $CCl_4$ | 1700 | 14 | 2.24 |
| Benzene | 1950 | 2.3 | 2.28 |
| Dibutyl ether | 1800 | 13 | 3.06 |
| Fluorobenzene | 1750 | 2.7 | 5.42 |
| Benzotrifluoride | 1500 | 6.4 | 9.18 |
| Cyclohexanone | 1800 | 2.4 | 18.3 |

[a] Taken from ref 20. [b] d is the solvent dielectric constant.

The *N,N*-dimethylaniline–1,3,5-trinitrobenzene complex has been studied in five solvents[25] whose dielectric constants vary from 1.89 to 4.81. Although the dielectric constant range is not particularly large it is remarkable that while the formation constants vary greatly, the molar absorptivities remain within the error limits. For example, $K_{n\text{-hexane}} = 8.2\ M^{-1}$ and $K_{CHCl_3} = 1.3\ M^{-1}$, but $\epsilon_{n\text{-hexane}} = 1120$ and $\epsilon_{CHCl_3} = 1140$.

The same was found for naphthalene–*s*-trinitrobenzene complexes[26] which were also studied in five solvents. A more striking example is the tetrachlorophthalic anhydride–hexamethylbenzene complex.[20] Table III lists the values of $K$ and $\epsilon$ for this complex in a series of solvents, the solvent dielectric constant being included.

Again, although $K$ varies considerable, $\epsilon$ stays roughly at 1750 ± 100 with no trend.

The charge-transfer complex formation data, interpreted through the models usually in use, show that in different environments the molar absorptivity for strong complexes tends to be constant, while it changes for weak complexes. The question seems to remain open. When or why does the absorptivity change, and can we explain it through a model in a consistent way?

In view of all the difficulties encountered by us and by others we have conceived of a model that, although incomplete, does specifically include the solvent interaction, and appears to be able to describe the experimental results well.

## Model for Nonideal Solvation and Its Application. The Fumaronitrile–Styrene Complex

The model which we propose assumes a low concentration for the acceptor only. This is the usual assumption since most organic compounds which function as acceptors have poor solubility in the solvents used. Also, since most optical measurements must be made at low concentrations of one component, this is usually the acceptor.

Because solvation is explicitly included, the model can cover the whole range of donor concentration up to 100% donor. Through its postulates, it derives the dependence of the "equilibrium constant" on solvent.

The process of complex formation is viewed as consisting of two separate steps: (1) solvation and (2) complex formation.

(1) An acceptor molecule dissolved in a mixture of solvent and donor is continually exchanging molecules in its solvation shell. The acceptor population will include the whole range of solvated molecules from acceptors with only solvent molecules to acceptors surrounded only by donors. The rate of exchange of a solvent molecule with a donor and vice versa will reflect the general concentration of the two in the solution and also the change in solvation energy of the system as one molecule replaces the other. This determines the equilibrium constant in the solvation step. Thus an equilibrium population of acceptor molecules exists in solution, having varying numbers of donor molecules in the solvation shells, from zero to the coordination number of the acceptor. (We call the coordination number $x$, and have postulated it as 12. The exact value does not matter.) Free or almost free rotation of the acceptor molecule within its cage is assumed. The solvating molecules are also rotating in thermal equilibrium.

(2) If an acceptor molecule has one or more donors in its solvation shell, it can interact with one donor to form a true charge-transfer complex. Here the donor and acceptor are in fixed positions relative to one another. For $\pi$–$\pi$ complexes, the $\pi$ orbitals of the donor and acceptor will overlap. The greater the number of donors in the solvation shell, the better the chance for complex formation. As the complex is in equilibrium, it can also dissociate back to a free acceptor and a solvating donor.

As the donor and acceptor separately have little or no dipole moment, while the complex has a dipole, the complex may possibly be stabilized by a polar environment. Though this postulate is debatable, its consequences are discussed below. Since the formation of complex does not change the nature of the rest of the solvation shell, its polarity can be considered to be the average of the solvent and donor molecules present around that particular complex. This is defined by the solvent and donor molecules present before complex formation. The change in solvation shell polarity due to replacing a molecule of solvent with one of donor will be approximately constant whatever the solvation shell composition. The solvation energy of the complex will also then change by a constant value and the equilibrium constant for complexing will change by a constant factor. If the donor is more polar than the solvent (e.g., $CCl_4$), the equilibrium constant could increase as donor concentration is increased. If the donor is less polar than the solvent, the equilibrium constant could decrease as donor is added, but as there are more donors to potentially complex, the complex concentration rises.

The mathematics for this is worked out in the Appendix (supplementary material). The final equation is given as follows:

$$\frac{[A]}{[C]} = 1 + \left[\frac{1}{K_{2(1)}x} + \frac{1}{K_1K_{2(1)}x}\frac{[S]}{[D]}\right]\left[\frac{1 + K_1[D]/[S]}{1 + aK_1[D]/[S]}\right]^{x-1} \quad (1)$$

where [A] is the total concentration of acceptor (fumaronitrile) in all forms; [C] the concentration of complex; [D] the concentration of donor (styrene), [D] >> [A] or [C] << [A]; [S] the concentration of solvent; $K_1$ the equilibrium constant for replacing a solvent molecule with a donor molecule in the solvation shell of the acceptor; $K_{2(1)}$ the equilibrium constant for collapse to complex of an acceptor molecule with one donor molecule in the solvation shell; $a$ the relative change in $K_2$ due to the change of polarity of the solvation shell when one solvent molecule is replaced by a donor molecule:

$$a = K_{2(i+1)}/K_{2(i)}$$

and $x$ the number of molecules in first coordination shell of acceptor. Under ideal conditions, $K_1$ and $a = 1$.

*Application to Optical Absorption.* Using the UV light absorption technique one measures the absorbance, Abs (optical density), of the charge-transfer band due to the complex. According to Beer's law, Abs = $\epsilon lc$ where $\epsilon$ is the extinction coefficient of the absorbing species, $c$ the concentration, and $l$ the length of the light path, that is,

TABLE IV: Values of $R$, $I_s$/Sl, and $a$

| Solvent | $R$ | $I_s$/Sl[a] | $a$ (first values) |
|---|---|---|---|
| $CCl_4$ | 0.797 | 11.75 | 1.025 |
| $C_6H_5Cl$ | 1.190 | 3.29 | 0.98 |
| $C_2H_4Cl_2$ | 2.160 | 1.24 | 0.88 |
| $C_2H_5OH$ | 4.50 | 0.392 | 0.72 |

[a] Intercept and slope determined by least-squares method.

of the cell. Since in most cases $l = 1$ cm, we can write the relation between the measured absorbance and the constants $K_1$ and $K_{2(1)}$.

$$\frac{[A]}{Abs} = \frac{1}{\epsilon} + \left[\frac{1}{\epsilon K_{2(1)}x} + \frac{1}{\epsilon K_1 K_{2(1)}x}\frac{[S]}{[D]}\right]\left[\frac{1 + K_1[D]/[S]}{1 + aK_1[D]/[S]}\right]^{x-1} \quad (2)$$

For $a = 1$, eq 2 reduces to a form equivalent to the B–H equation, though the coefficients have different meanings. Equation 2 at low donor concentrations and/or $a = 1$ can be simplified to

$$\frac{[A]}{Abs} = \frac{1}{\epsilon} + \frac{1}{\epsilon K_{2(1)}x} + \frac{1}{\epsilon K_1 K_{2(1)}x}\frac{[S]}{[D]} \quad (3)$$

To make a direct comparison with the Benesi–Hildebrand equation we can write $[S] \approx ([D_0] - [D])[S_0]/[D_0]$ where the subscript zero indicates the maximum possible concentration of the solvent or donor. Equation 4 shows the result.

$$\frac{[A]}{Abs} = \frac{1}{\epsilon} + \frac{1}{\epsilon K_{2(1)}x} - \frac{[S_0]/[D_0]}{\epsilon K_1 K_{2(1)}x} + \frac{[S_0]}{\epsilon K_1 K_{2(1)}x[D]} \quad (4)$$

As $[S_0]$ is usually about equal to $[D_0]$, if $K_1K_{2(1)}x \approx 0.5$, the Benesi–Hildebrand treatment will have a near-zero intercept, which has been found experimentally. If $K_1K_{2(1)}x < 0.5$ and $K_1 < 1$, the equation has a negative intercept, which we have demonstrated. This can happen only if both $K_1$ and $K_{2(1)}x$ are relatively small, which means that weak complexes in solvents which preferentially solvate the acceptor are the ones which show complications.

When [A]/Abs is plotted vs. [S]/[D] (Figure 4), no zero or negative intercepts appear. The linear part of the plots is described by eq 3 and the intercept of the extrapolated line, $I_s$, is

$$I_s = \frac{1}{\epsilon}\left[1 + \frac{1}{K_{2(1)}x}\right] \quad (5)$$

It can be seen from Figure 4 that the intercept decreases as the dielectric constant of the solvent increases.

To find the first estimates of the various constants one can proceed as follows, assuming that $\epsilon$ remains constant as solvent is replaced by styrene. If $([A]/Abs)_c$ is any point on the curved portion of the plot of [A]/Abs vs. [S]/[D] and $I_s$ is the extrapolated intercept, then their ratio is

$$\left(\frac{[A]}{(Abs)}\right)_c \Big/ I_s = \left\{K_{2(1)}x + \left[1 + \frac{1}{K_1}\frac{[S]}{[D]}\right]\left[\frac{1 + K_1([D]/[S])}{1 + aK_1([D]/[S])}\right]^{x-1}\right\} \Big/ (1 + K_{2(1)}x) \quad (6)$$

The left side of eq 6 can be determined from the graph, as also the ratio of the intercept, $I_s$, to the slope, Sl, for the linear region of the curve.

$$I_s/Sl = K_1(1 + K_{2(1)}x) \quad (7)$$

The latter allows us to express $K_1$ in terms of known $I_s$ and Sl and $K_{2(1)}x$. If $([A]/Abs)_{s=0}/(I_s)$ is designated by $R$, one can write

$$K_{2(1)}x = \frac{1 - Ra^{x-1}}{a^{x-1}(R - 1)} \quad (8)$$

Now, for any value of $a$, eq 8 can be solved for $K_{2(1)}x$ and then eq 7 solved for $K_1$. These are substituted into eq 6. An acceptable value of $a$ is obtained when the right side of eq 6 equals the experimental value. Table IV lists the values of $R$, $I_s$/Sl, and the calculated values of $a$.

Once $a$ and $K_{2(1)}x$ are known, $\epsilon$ can be easily calculated from eq 5. As mentioned earlier this assumes that $\epsilon$ does not change with increasing donor concentration, an assumption made by virtually all the previous workers in the field.

Starting with the first graphically determined estimates, the best estimate for each constant is obtained by minimizing $\sum\Delta^2$. These are given in Table V. The errors listed in Table V are obtained as the standard deviations of the estimates. No a priori assumption was made concerning $\epsilon$ in the four solvents, but it was found identical for all four cases within error limits.

Table VI (supplementary material) shows the agreement between the experimental and calculated values of Abs/[A]. There is no trend in their differences as a function of styrene concentration and a good fit is found up to 100% styrene for all the solvents used. The average root mean square of the differences ranges between 2 and 5% which is probably within the experimental error of the determination.

As was pointed out earlier only a relatively small part of the acceptor is actually in the complexed state. The exact amount of the complexed fraction can be easily calculated since the complex concentration can be determined at any point from eq 1. The latter can be written more explicitly as

$$[C] = [A]K_1K_{2(1)}x([D]/[S]) \Big/ \left\{K_1K_{2(1)}x[D]/[S] + (1 + K_1[D]/[S])\left[\frac{1 + K_1[D]/[S]}{1 + aK_1[D]/[S]}\right]^{x-1}\right\} \quad (9)$$

TABLE V: Parameters of Eq 2 in Various Solvents for Fumaronitrile–Styrene System at 25 °C

| Solvent | $d$[a] | $a$ | $K_1$ | $K_{2(1)}x$ | $\epsilon$ |
|---|---|---|---|---|---|
| $CCl_4$ | 2.24 | 1.024 ± 0.006 | 9.6 ± 1.1 | 0.165 ± 0.0072 | 1820 ± 60 |
| $C_6H_5Cl$ | 5.7 | 0.979 ± 0.006 | 2.65 ± 0.45 | 0.283 ± 0.0012 | 1850 ± 70 |
| $C_2H_4Cl_2$ | 10.5 | 0.88 ± 0.03 | 0.57 ± 0.08 | 0.895 ± 0.041 | 1850 ± 90 |
| $C_2H_5OH$ | 24.3 | 0.72 ± 0.08 | 0.040 ± 0.0013 | 8.0 ± 0.3 | 1820 ± 70 |

[a] $d$ is the solvent dielectric constant.

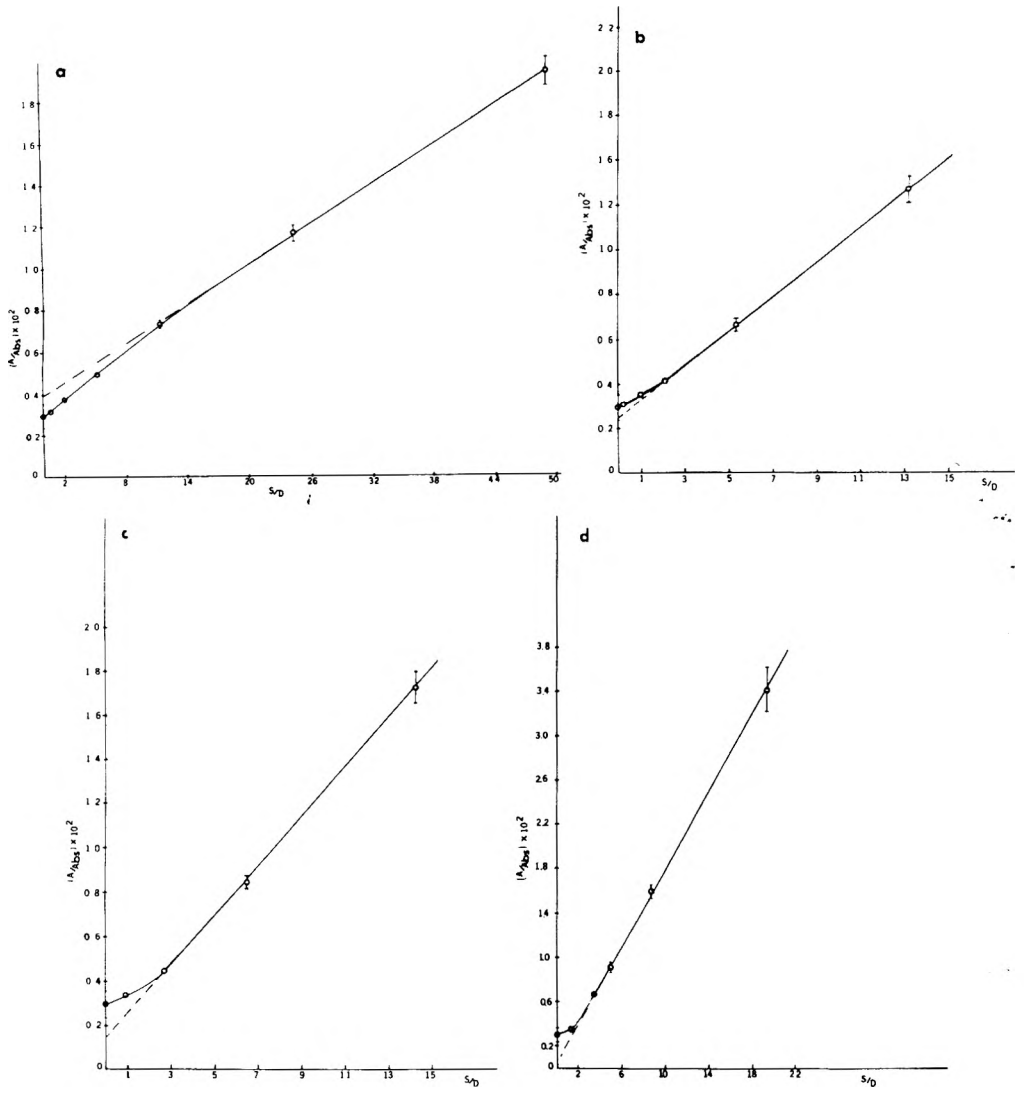


**Figure 4.** [A]/Abs vs. [S]/[D] according to eq 2, where [S] is the solvent concentration: (a) in $CCl_4$; (b) in $C_6H_5Cl$; (c) in $C_2H_4Cl_2$; (d) in $C_2H_5OH$. [A], [D], and [S] are in M. Errors are shown in error bars when they are larger than the point diameter.

**TABLE VII: Complex Concentration for the Fumaronitrile-Styrene System in Different Solvents**

| Solvent | Donor concn, mol/L | % of acceptor in complex |
|---|---|---|
| $CCl_4$ | 1.58 | 11.1 |
| $C_6H_5Cl$ | 1.505 | 8.0 |
| $C_2H_4Cl_2$ | 1.58 | 6.2 |
| $C_2H_5OH$ | 1.59 | 3.6 |

If the absorbance is measured in a particular case, the complex concentration is Abs/$\epsilon$, and the fraction of $A$ complexed is Abs/[A]$\epsilon$. Table VII shows the percent of complexed acceptor in all four solvents, at a relatively low styrene concentration. As can be seen, the highest complex concentration is present in $CCl_4$, the lowest in ethanol. Considering the high value of $K_{2(1)}x$ for the ethanol system, it is clear that the poor solvation of fumaronitrile by styrene compared with ethanol, as shown by the low $K_1$, actually determines the degree of complexation, overcoming entirely the effect of the favorable free energy change for complexation. However, it should be pointed out that even in a solvent as polar as ethanol, a finite, reasonably large concentration of the complex is present.

We have so far emphasized the curvature in the various [A]/Abs vs. 1/[D] and [S]/[D] plots, and have presented a method by which this can be rationalized. As shown before, other methods attempting to solve difficulties in treating the experimental data seem to fail in this aspect. However, one can treat the data with a straight line approximation since the curvature is not large. Here, $a$ = 1 and there is no change in $K_2$ with change in solvent/donor composition. A minimization procedure gives the estimates for the other three constants as shown in Table VIII. Comparison with the experiment is shown in Table IX.

Table VIII contains much of interest; both $k_{2(1)}x$ and $\epsilon$ are constant within the experimental error of the parameters. The only term which varies is the solvation equilibrium term, $K_1$. Here, it probably does not vary enough. For example, fumaronitrile is much more soluble in ethanol than in styrene, implying greater free energy

**TABLE VIII: Parameters of Eq 2 when $a$ = 1 for Fumaronitrile-Styrene System at 25 °C in Various Solvents**

| Solvent | $d$ | $K_1$ | $K_{2(1)}x$ | $\epsilon$ |
|---|---|---|---|---|
| $CCl_4$ | 2.24 | 7.0 ± 1.0 | 0.20 ± 0.03 | 1950 ± 0.0 |
| $C_6H_5Cl$ | 5.7 | 3.74 ± 0.41 | 0.20 ± 0.002 | 1830 ± 45 |
| $C_2H_4Cl_2$ | 10.5 | 3.2 ± 1.0 | 0.23 ± 0.01 | 1850 ± 163 |
| $C_2H_5OH$ | 24.3 | 2.30 ± 0.94 | 0.23 ± 0.002 | 1895 ± 260 |

of interaction ($K_1 < 1$). This was found if $a$ is allowed to vary, Table V, but not if $a \equiv 1$.

Table IX (supplementary material) shows the agreement between experimental and calculated values of Abs/[A]. Here the agreement becomes very poor as the solvent polarity increases. For chlorobenzene and carbon tetrachloride, the agreement is within experimental error. However, for 1,2-dichloroethane, the lowest concentration point is off by 32% and in ethanol, the calculated values of absorbance for the two lowest concentrations deviate by 54 and 35%. The agreement for the rest of the values is not as good as that found in Table VI. Thus in the polar solvents, when $a \equiv 1$, some agreement can be found in the higher styrene concentration range, but there is systematic curvature which cannot be accounted for by any straight line equation. The calculated values for Abs/[A] given in Table VI using the parameters in Table V show a random error around the best line.

However, Table VIII shows constant $K_{2(1)}x$ and $K_1$ values that do not differ as much from each other as those in Table IV. The uncertainty in $\epsilon$ is rather large in the case of ethanol, which was also the case for which the constants in Table IV differed very much from all the others. Possibly ethanol forms a weak complex with fumaronitrile by H bonding, and treatments assuming only one complex will not succeed. We think that the straight line approximation, although not adequate, has the merit of revealing whether a system is one in which the solvent is competing through solvation (then, it should be a relatively good approximation) or through complex formation with one of the other components (bad approximation). In that light the constants in Table V for the $C_2H_5OH$ case might not have realistic magnitudes.

## Remarks and Conclusions

This work, we hope, offers some answers to the questions discussed earlier. Possible curvature in B-H plots is rationalized. It may be due to strong solvent interaction with donor or acceptor.

The problem of "negative constants" is removed. We see however a pronounced dependence of the complex concentration on the solvent/donor mixture, where the changing solvation of acceptor determines the shape of the absorbance/donor concentration curve. The most interesting result is that the overall complex concentration depends mainly on $K_1$, that is, on the ability of the donor to compete with the original solvent in solvating the acceptor.

The usual assumption of constancy of the molar absorptivity with increasing donor concentration seems to be justified. The contradiction implicit in earlier results with different solvents is also resolved, since $\epsilon$ was found constant for all solvents. One can tentatively rationalize this as follows. For a given donor–acceptor pair, the molar absorptivity depends on the transition moment which is proportional to the overlap integral of the complex. The difference in energy between the lowest unoccupied M of the acceptor and the highest occupied MO of the donor in the complex is also partly determined by the overlap integral. If there is greater overlap, the energy difference decreases, $\lambda$ increases, and $\epsilon$ becomes larger. Thus, a constant $\lambda$ when changing solvent implies a constant overlap integral and a constant $\epsilon$.

We now have a reasonable explanation for the many reports that $\epsilon$ sometimes changes with the solvent and sometimes not. From eq 4 it can be seen that if $K_{2(1)}x >> 1$ for the complex in question in a given solvent, the constant terms sum is very close to unity and the intercept of the linear plot is simply $1/\epsilon$. As long as the complex is strong enough ($K_{2(1)}x$ and $K_1$ large in all solvents), $\epsilon$, determined using B–H and related equations, would be a constant. Whenever these conditions are not met, $\epsilon$ would vary.

The model seems to be applicable over the whole range of donor concentration. Experimentally, only simple spectroscopic measurements are required. The theory is thus easy to use. The same basic approach can be applied to NMR data. Here, however, differing solvation of the acceptor and reference make the simple extrapolation suspect. Correction by using a separate reference means that the chemical shift of the free acceptor must by measured and this is also difficult.

*Acknowledgment.* We thank Drs. E. W. Abrahamson and Y. H. Pao for stimulating discussions. We also thank the ARO-D for partial support of this work.

*Supplementary Material Available:* Data showing the agreement between calculated and experimental values of Abs/[A] (Tables VI and IX), absorbance data for charge-transfer solutions of styrene–fumaronitrile (Appendix I), and derivations of charge-transfer complex equations (Appendix II) (7 pages). Ordering information is available on any current masthead page.

## References and Notes

(1) H. A. Benesi and J. H. Hildebrand, *J. Am. Chem. Soc.*, **70**, 2832 (1948).
(2) R. Foster "Organic Charge-Transfer Complexes", Academic Press, New York, N.Y., 1969.
(3) D. F. Evans, *J. Chem. Phys.*, **23**, 1424 (1955).
(4) M. W. Hanna and A. L. Ashbaugh, *J. Phys. Chem.*, **68**, 811 (1964).
(5) B. Zeegers and G. B. Butler, *J. Macromol. Sci.-Chem.*, **A6**(8), 1569 (1972).
(6) B. Zeegers and G. B. Butler, *J. Macromol. Sci.-Chem.*, **A7**(2), 349 (1973).
(7) W. B. Person, *J. Am. Chem. Soc.*, 87, 167 (1965).
(8) D. A. Deranleau, *J. Am. Chem. Soc.*, **91**, 4044 (1969).
(9) R. M. Guidry and R. S. Drago, *J. Am. Chem. Soc.*, **95**, 6645 (1973).
(10) S. Carter, J. N. Murrell, and E. J. Rosch, *J. Chem. Soc.*, 2048 (1965).
(11) S. Carter, *J. Chem. Soc. A*, 404 (1968).
(12) P. J. Tratter and M. W. Hanna, *J. Am. Chem. Soc.*, **88**, 3724 (1966).
(13) E. H. Lane, S. D. Christian, and J. D. Childs, *J. Am. Chem. Soc.*, **96**, 38 (1974).
(14) S. D. Ross and M. M. Labes, *J. Am. Chem. Soc.*, **79**, 76 (1957).
(15) D. A. Deranleau, *J. Am. Chem. Soc.*, **91**, 4050 (1969).
(16) M. H. Litt and J. W. Summers, *J. Polym. Sci.*, **11**, 1359 (1973).
(17) A. H. Ewald, *Trans. Faraday Soc.*, **64**, 733 (1968).
(18) H. Suzuki, "Electronic Absorption Spectra and Geometry of Organic Molecules", Academic Press, New York, N.Y., 1967.
(19) R. S. Drago, T. F. Bolles, and R. J. Niedzielski, *J. Am. Chem. Soc.*, **88**, 2717 (1966).
(20) J. Czekalla and K. O. Meyer, *Z. Phys. Chem. (Frankfurt am Main)*, **27**, 185 (1961).
(21) R. S. Mulliken and W. B. Person, "Molecular Complexes", Wiley-Interscience, New York, N.Y., 1969, Chapter 7.
(22) J. H. Hildebrand and R. L. Scott, "Regular Solutions", Prentice-Hall, Englewood Cliffs, N.J., 1962.
(23) A. E. Gillam "Electronic Absorption Spectroscopy in Organic Chemistry", Edward Arnold Publishers, London, 1954, Chapter 12, Appendix 2.
(24) R. E. Merrifield and W. D. Phillips, *J. Am. Chem. Soc.*, **80**, 2778 (1958).
(25) R. Foster and D. L. Hammick, *J. Chem. Soc.*, 2685 (1954).
(26) C. C. Thompson, Jr., and P. A. D. de Maine, *J. Am. Chem. Soc.*, **85**, 3096 (1963).

# The Effect of Electrolyte on Dipole Layers at Liquid–Air Interfaces

**W. G. Madden,† R. Gomer,***

*James Franck Institute, University of Chicago, Chicago, Illinois 60637*

**and M. J. Mandell‡**

*Department of Chemistry, University of California at Los Angeles, Los Angeles, California 90024* *(Received July 1, 1977)*

*Publication costs assisted by the National Science Foundation and the Advanced Research Projects Agency of the Department of Defense*

Equations describing the effect of electrolyte on the potential of a dipole layer at a liquid–air interface are set up. Their numerical solution is briefly outlined and the results of the calculation are presented. Substantial screening results for potentials ≥0.1 V even at very low electrolyte concentrations ($10^{-4}$ M). The calculated variation of the screened potential with electrolyte concentration for various assumed values of the unscreeened potential (i.e., with no electrolyte present) can be compared with the experimentally obtainable variation and this allows an estimate of the unscreened potential actually present. The latter is estimated to be 50 mV in the case of $H_2O$, the surface being negative with respect to the bulk of the water phase. The disruption of the water dipole layer by reorientation of $H_2O$ molecules by ions is estimated. The effect is important only at high electrolyte concentration (1–0.1 M) where it improves the fit of the experimental data to theory.

## Introduction

In connection with a recent investigation of absolute half-cell emfs[1] it was necessary to estimate the magnitude of the potential difference between the interior and the free surface (in contact with air) of $H_2O$. Such a potential difference has been postulated[2] because tetrahedral charge distribution of $H_2O$ might lead to preferential orientations in the surface region and thus to a dipole layer which would make the mean electrostatic potential at the surface different from that in the bulk. The method used to investigate this possibility and to estimate the sign and size of the potential difference is based on the following argument. If such orientation effects exist, they must persist for some mean distance into the liquid. This coherence length $\lambda$ must be at least 2–3 and probably more molecular diameters, i.e., $\lambda \geq 10$ Å. It is thus possible for electrolyte to penetrate into the dipole layer and partially screen it. The extent to which the dipole layer potential is reduced must be a function of electrolyte concentration. If it is assumed that the presence of electrolyte simply screens the dipole potential without otherwise disrupting the structure that gave rise to it, it is possible to set up and solve numerically an appropriate Boltzmann–Poisson equation and thus to calculate the screening as a function of electrolyte concentration c.

The screened potential difference, $V(0)$, turns out to vary most rapidly with $c$ the greater the unscreened, original potential difference $V^0(0)$ (hereafter $V^0$). It is possible to find experimentally the change of $V(0)$ with c in absolute terms, i.e., the differences between $V(0)$ values for different concentrations of electrolyte, but not the absolute value of any one $V(0)$. By looking for the best fit of the experimental points to curves calculated for various values of $V^0$ it is possible to deduce the magnitude and sign of $V^0$, i.e., the potential difference between bulk and surface of the solution, as indicated in Figure 1. The screening effect calculated as outlined ignores the fact that electrolyte ions may tend to disrupt the preferential orientation of the $H_2O$ molecules giving rise to the dipole layer in the first place, and thus gives a lower limit to screening. In ref 1 only the results of a calculation ignoring this disruption effect were used to estimate $V^0$. In addition to presenting this calculation we include here a rough estimate of the disruption effect and its possible effect on the value of $V^0$. It turns out that the effect is very small at concentrations still high enough to cause substantial screening, so that the estimate obtained in ref 1 is not substantially altered.

## Formulation of the Problem

We start by describing the screening calculation for a given initial distribution of $H_2O$ dipoles which is assumed to remain unchanged by the introduction of electrolyte.

We assume that the water–air interface is flat and that the original unscreened potential at the interface is

$$V^0(z) = V^0 e^{-z/\lambda} \tag{1}$$

where $z$ is the direction normal to the surface and is taken as positive into the interior of the solution. $V^0$ is the potential at the surface, relative to that in the bulk, as already pointed out, and $\lambda$ is the e-folding or coherence length. We shall take $V^0$ as positive, although this is of course arbitrary. If this potential is assumed to be formed (for reasons of mathematical convenience) by a fixed positive surface charge layer and a charge density $\rho^0$ of opposite sign decaying into the interior of the solution, the latter can easily be shown by direct application of Poisson's equation to have the form

$$-4\pi\rho^0 = (V^0/\lambda^2)e^{-z/\lambda} \tag{2}$$

in agreement with the second derivative of $V^0(z)$.

The simplest Poisson–Boltzmann equation which can be written treats the electrolyte ions as point charges and assumes that their heat of solvation is constant up to the liquid–air interface. The resulting equation (for monovalent ions) is

$$d^2V/dz^2 = -(4\pi cq/K)(e^{-Vq/kT} - e^{Vq/kT}) + (V^0/\lambda^2)e^{-z/\lambda} \tag{3}$$

where $q$ is the magnitude of the ionic charge (taken as positive) and $K$ the dielectric constant. We introduce the

† Present address: Dartmouth College, Hanover, N.H. 03755.
‡ Present address: Systems Science and Software, La Jolla, Calif.

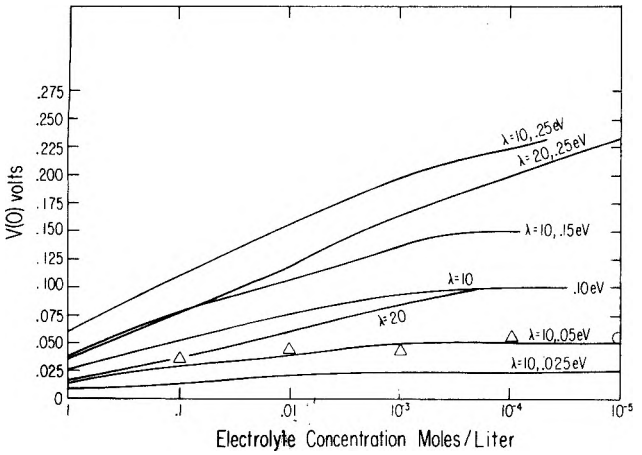


**Figure 1.** Plots of calculated curves of $V(0)$ vs. monovalent electrolyte concentration for various values of the unscreened dipole layer potential $V^0$ at 300 K. The values on the curves indicate the assumed coherence length λ of the layer and the assumed strength of $V^0$. The curves were calculated for anion and cation radii of 2 Å from eq 17. The triangular points represent the experimentally determined[1] variation of $V(0)$, fitted to the λ = 10 Å, $V^0$ = −0.05 V curve by suitable choice of the ordinate zero for the experimental curve.

new variables $\varphi = Vq/kT$, $y = z/L$, and $a = L/\lambda$ where $L$ is the Debye length

$$L = (KkT/8\pi cq^2)^{1/2} = 0.34(K/M)^{1/2}\ \text{Å} \tag{4}$$

with c the concentration in ion pairs/cm$^3$ and $M$ the concentration in moles/liter. This transforms eq 3 into

$$d^2\varphi/dy^2 = \sinh\varphi + \varphi^0 a^2 e^{-ay} \tag{5}$$

where $\varphi^0 = V^0 q/kT$. For sufficiently weak $\varphi$ eq 5 can be linearized by replacing sinh $\varphi$ by $\varphi$, with the straightforward solution

$$\varphi(y)/\varphi^0 = \left(\frac{a}{a^2-1}\right)(ae^{-ay} - e^{-y}) \tag{6}$$

which leads to

$$\varphi(0)/\varphi^0 = V(0)/V^0 = a/(1+a) \tag{7}$$

The nonlinearized form, eq 5 must be solved numerically. Since analytic solution is not possible in any case, both eq 5 and a more sophisticated version were solved. The latter takes into account that the heat of solvation of ions decreases as they approach the air interface because of image effects, i.e., that a potential energy term reflecting this change must be added to $V$. The latter has been shown by Onsager and Samaras[3] to have the form

$$W = A(q^2/4Kz)e^{-2z/L} \tag{8}$$

with $A$ a factor taking the finite size of ion into account:

$$A = e^{r/L}/(1 + r/L) \tag{9}$$

where $r$ is the ionic radius. The effect of including $W$ in the Poisson–Boltzmann equation is twofold. First there will be a tendency for ions to avoid the immediate surface region, thus decreasing the amount of screening, relative to that indicated by eq 5. Second, introduction of electrolyte will produce a surface dipole layer if anion and cation concentrations in the surface region differ. This will be the case if anion and cation radii differ, because of the $A$ term in eq 8. The Poisson–Boltzmann equation now takes the form

$$d^2\varphi/dy^2 = {}^1/_2[e^{\varphi-(W_-/kT)} - e^{-\varphi-(W_+/kT)}] + \varphi^0 a^2 e^{-ay} \tag{10}$$

where the quantities $\varphi$, $y$, and $a$ are defined as before. Equations 5 and 10 must be solved with the boundary conditions

$$d\varphi/dy|_\infty = 0 \tag{11}$$

$$\varphi(\infty) = 0 \tag{12}$$

and the constraint

$$\int_0^\infty \rho_{ion}\, dy = 0 \tag{13}$$

The integral constraint, eq 13, can be rewritten

$$\int_0^\infty [d^2\varphi/dy^2]\, dy - \varphi^0 = 0 \tag{14}$$

or in view of eq 11

$$-d\varphi/dy|_0 = \varphi^0 \tag{15}$$

For purposes of numerical solution it is convenient to introduce the new independent variable

$$x = e^{-ay} \tag{16}$$

whose range is 1 to 0. Equation 10 then takes the form

$$a^2x^2(d^2\varphi/dx^2) + a^2x(d\varphi/dx) + {}^1/_2[e^{-\varphi}e^{\varphi_+ ax^{2/a}/\ln x} - e^{\varphi}e^{\varphi_- ax^{2/a}/\ln x}] - \varphi^0 a^2 x = 0 \tag{17}$$

where

$$\varphi_\pm = A_\pm \frac{q^2}{4KLkT} \tag{18}$$

where the positive subscript refers to cations of radius $r_+$ and the negative subscript to anions of radius $r_-$. Since

$$a\varphi_\pm = A_\pm \frac{q^2}{4KkT}\frac{1}{\lambda} \tag{19}$$

eq 17 goes over into the transform of eq 5 if, for given $a$, λ is allowed → ∞. The constraints eq 11–13 take the forms

$$\varphi(x = 0) = 0 \tag{20}$$

$$x(d\varphi/dx)|_0 = 0 \tag{21}$$

$$\int_0^1 \frac{dx}{x}[e^{\varphi}e^{\varphi - ax^{2/a}/\ln x} - e^{-\varphi}e^{\varphi + ax^{2/a}/\ln x}] = 0 \tag{22}$$

and the analogue of eq 15 becomes

$$d\varphi/dx|_1 = \varphi^0/a \tag{23}$$

## Method of Solution

Numerical solution of eq 17 was carried out by replacing the continuous variable $x$ by a discrete set of $N + 1$ equally spaced points $x_i$ ($i = 0$ to $N$). The derivatives at a given $x_i$ were then evaluated by assuming $\varphi$ to be quadratic in the interval $x_{i-1}$ to $x_{i+1}$, which yields

$$d\varphi/dx|_{x_i} = \frac{\varphi(x_{i+1}) - \varphi(x_{i-1})}{x_{i+1} - x_{i-1}} \tag{24}$$

and

$$d^2\varphi/dx^2|_{x_i} = \frac{\varphi(x_{i+1}) + \varphi(x_{i-1}) - 2\varphi(x_i)}{(x_{i+1} - x_i)^2} \tag{25}$$

The differential equation eq 17 was then evaluated at the interior points $x_1 \ldots x_{N-1}$, generating $N - 1$ nonlinear algebraic equations in the $N + 1$ unknowns $\varphi(x_0) \ldots \varphi(x_N)$. The two additional equations required for the solution were obtained from the boundary conditions eq 20 and either the integral constraint eq 22 or the differential form eq 23. The integral condition was reduced to an algebraic equation in $\varphi(x_i)$ by using Simpson's rule, and the differential boundary condition was evaluated by applying

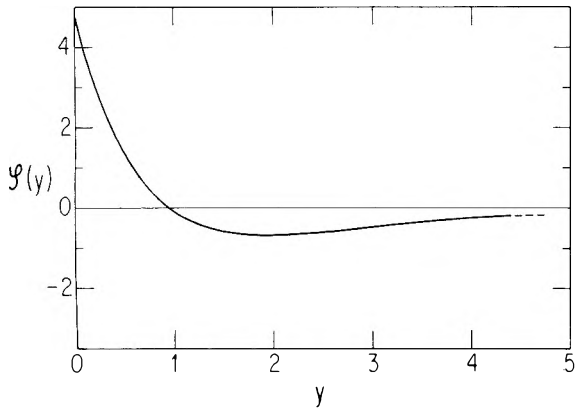


**Figure 2.** Plot of $\varphi(y)$ vs. $y$ based on solution of eq 17 and the following parameter: $\varphi^0 = 10$, $\lambda = 10$ Å, $r_+ = r_- = 2$ Å.

eq 23 to the interval $x_{N-2}$ to $x_N$. The resultant system of $N + 1$ nonlinear equations was solved using Brown's iteration method.[4] The initial guess for the $\varphi(x_i)$ values required for the iteration was obtained either from the solution of the linearized equation, eq 6, or from a previous solution for slightly different parameters.

For $a \leq 1$ and $N = 20$, solutions of eq 17 using the integral and differential boundary conditions were in excellent agreement. At higher values of $a$ the two results diverged badly even with $N = 40$ because of a breakdown in the numerical approximation to the integral boundary conditions. The reason for this is most easily seen by considering the linearized version of eq 5, for which the integral boundary condition becomes

$$\int_0^\infty \varphi \, dy = 0 \tag{26}$$

This condition obviously requires a crossover from a region of positive $\varphi$ to one of negative $\varphi$ and this is found from eq 6 to occur at $y_c$

$$y_c = \frac{\ln a}{a - 1} \tag{27}$$

except for $a = 1$ where $y_c = 1$. The corresponding value of $x$, $x_c$, is

$$x_c = a^{-[a/(a-1)]} \tag{28}$$

which approaches $1/a$ as $a \rightarrow \infty$. Consequently the negative part of the integral corresponding to eq 26 in $x$, $\varphi$ space is compressed into a very narrow range of $x$ values so that numerical integration becomes difficult. In the case of eq 17 the form of the integrand of eq 26 is no longer quite so transparent, but again involves balancing positive and negative regions of integration. Figure 2 shows a plot of $\varphi$ vs. $y$ for a solution of eq 17 with $\varphi^0 = 10$, $\lambda = 10$ Å, and $a = 1$. For this case $y_c = 0.9$, very close to the value for the linearized equation. Thus the same crowding occurs for large values of $a$. Actual calculations were therefore carried out with the integral boundary condition and $N = 20$ for $a \leq 1$, and with the differential boundary condition and $N = 40$ for $a > 1$.

## Results

Figure 2 shows a typical potential distribution in real (normalized) space. The potential varies quite steeply at first, then becomes weakly negative, flattens out, and gradually approaches 0 as $y \rightarrow \infty$. For the particular example picked the crossover point is almost exactly the Debye length; as $\varphi^0$ increases and screening gets stronger, the crossover is shifted to smaller values, but is still of the order of $L$, as expected. Before discussing the dependence of $V(0)/V^0$ on $a$ for various situations, it will be useful to

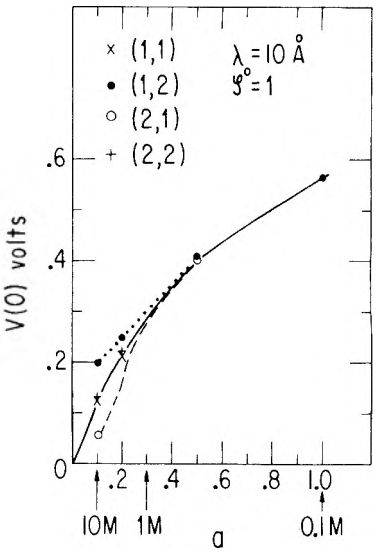


**Figure 3.** Plots of $\varphi(0)$ vs. $a$ (and concentration in moles/liter) for $\varphi^0 = 1$, $\lambda = 10$ Å, and various combinations of $r_+$ and $r_-$, indicated in Å by $(r_+, r_-)$ on the figure.

recall that $a = L/\lambda$ and that $L \propto M^{-1/2}$ so that $M$, the concentration in moles/liter, is proportional to $(a\lambda)^{-2}$. If the dielectric constant of $H_2O$ is taken as 78, we find that

$$M = 9/(a\lambda)^2 \tag{29}$$

for $\lambda$ in Å.

It was pointed out in ref 1 that the assumption of a normal dielectric constant, even in the region of the orientation produced dipole layer, is physically reasonable, since the ion–water interactions are much stronger than the water–water orientation producing interactions. It should also be pointed out that this amounts, in part, to taking the disruption effect into account.

Figure 3 shows plots of $V(0)/V^0$ for $\varphi^0 = 1$ and various combinations of $r_+$ and $r_-$, for $\lambda = 10$ Å, as function of $a$ (and $M$). The variations are in the expected direction: For $r_+ = r_-$ the values of $r$(2 or 1 Å) make very little difference. For $r_+ = 1$ Å, $r_- = 2$ Å, $V(0)$ lies above the value for equal radii, and for $r_+ = 2$ Å, $r_- = 1$ Å the curve lies below those for $r_+ = r_-$ by almost the same amount. These differences correspond to ion concentration differences near the surface. However, the effect is quite small. At $a = 0.1$, corresponding to a 10 M solution, this potential is only $0.075kT$, and as $a$ increases, i.e., the concentration decreases, the curves rapidly converge. For higher $\varphi^0$ the absolute values of these ion caused layer potentials have virtually identical values at the same concentrations. This means, of course, that the $V(0)/V^0$ values will be much closer for various combinations of radii.

Because of the smallness of this effect and the insensitivity to actual values of $r$, we discuss from this point on only curves based on $r_+ = r_- = 2$ Å. Figure 4 shows plots of $V(0)/V^0$ vs. $a$ for a number of $\varphi^0$ values for $\lambda = 10$ Å, and Figure 5 shows similar results for $\lambda = 20$ Å. Also shown are the linearized results and those based on eq 5[5] for two values of $\varphi^0$. Several facts are worth noting. Up to $\varphi^0 = 4$ the linearized result is in quite good agreement with the more exact solutions. For higher values of $\varphi^0$ the nonlinear equation gives much stronger screening, which increases drastically with increasing $\varphi^0$. Equation 5, which neglects the avoidance of the surface by ions, gives stronger screening than eq 17. It has already been indicated that eq 17 goes over into eq 5 (or its transform), as $\lambda \rightarrow \infty$. It is consequently not surprising that the solutions of eq 17 and 5 agree more closely for $\lambda = 20$ Å than for $\lambda = 10$ Å.

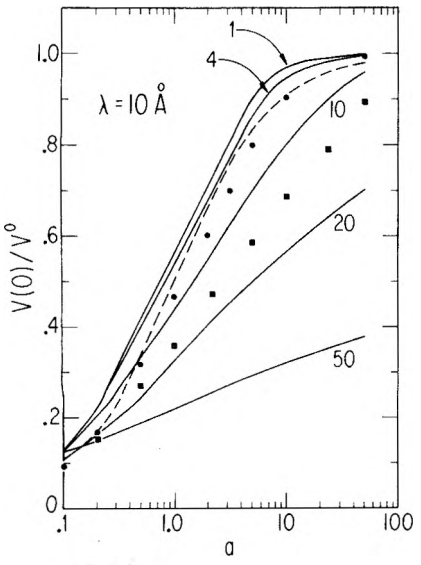


**Figure 4.** Plots of $\varphi(0)/\varphi^0 = V(0)/V^0$ vs. $a$ for various values of $\varphi^0$ for $\lambda$ = 10 Å, $r_+ = r_- = 2$ Å, based on eq 17. $\varphi^0$ values indicated by numbers next to curves. Dashed curve represents solution of linearized version of eq 5. (●) and (■) are solutions of eq 5 for $\varphi^0$ = 4 and 10, respectively.

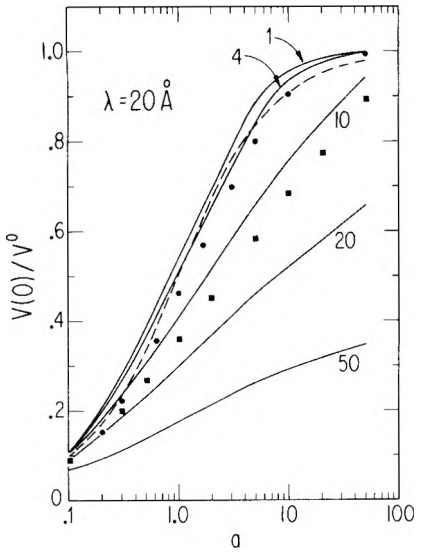


**Figure 5.** Plots of $\varphi(0)/\varphi^0 = V(0)/V^0$ vs. $a$ for various values of $\varphi^0$ for $\lambda$ = 20 Å, $r_+ = r_- = 2$ Å, based on eq 17. $\varphi^0$ values indicated by numbers next to curves. Dashed curve represents solution of linearized version of eq 5. (●) and (■) are solutions of eq 5 for $\varphi^0$ = 4 and 10, respectively.

Further, the disagreement becomes more pronounced for larger $\varphi^0$ as one would expect. The differences between the $\lambda$ = 10 Å and $\lambda$ = 20 Å results are in general quite small, particularly when translated from $a$ to concentrations.

It was stated in the Introduction that the variation of $V(0)$ with concentration became more pronounced the greater $V^0$. It might be thought from the curves of Figures 3 and 4 that the variation decreases with increasing $V^0$. It must be remembered however that these curves show relative variations, $V(0)/V^0$ vs. $a$ (or concentration), while the curves needed for comparison with experiment are absolute variations, $V(0)$ vs. $M$, and these do in fact vary more steeply the stronger $V^0$, as shown in Figure 1.

Finally it should be pointed out that the limits of validity of the present treatment are somewhat different from those of Debye–Hückel theory. We are primarily considering the interaction of ions, not with each other but with an external potential (even $W$ can be considered as such). At high concentrations the Onsager–Samaras approximation to $W$ is undoubtedly poor and the quantitative values of the ion segregation potential are therefore not very reliable, although the order of magnitude of the effect should be correct.

## The Disruption Effect

It was pointed out in the Introduction that the assumption of a fixed orientation produced dipole layer, unaffected by electrolyte, is too naive, since ion–water interactions will tend to reorient $H_2O$ molecules and thus disrupt the preferential orientation giving rise to the dipole layer. We give in this section a rough estimate of this effect. We first calculate the unscreened but disrupted potential remaining at a given electrolyte concentration, and can then proceed to calculate the screening as already outlined. Since the excesses or deficiencies in cation or anion concentration required for screening are exceedingly small, this procedure is adequate.

We start by assuming that each ion reorients a spherical solvent shell of radius $r_0$ and thereby reduces the polarization per unit volume by $(4/3)\pi r_0^3$ so that the original potential $V^0$ is reduced to a value $V^{0\prime}$

$$V^{0\prime} = V^0(1 - 2(4/3)\pi r_0^3 c) = V^0(1 - 0.005Mr_0^3) \quad (30)$$

if $c$ is expressed in moles/liter (M).

We use the following model to estimate $r_0$: Immediately surrounding each ion we assume a rigidly oriented inner hydration shell of thickness $r_0'$. Beyond this shell we calculate the total polarization per ion as follows. The field seen by a water molecule from a given ion is radially outward from the ion and given by

$$E = \frac{-3}{2}\frac{\mathrm{d}}{\mathrm{d}r}\left(\frac{q}{Kr}e^{-r/L}\right) = \frac{-3}{2}\frac{q}{K}\left(\frac{1}{r^2} + \frac{1}{Lr}\right)e^{-r/L} \quad (31)$$

where the factor (3/2) takes into account that the $H_2O$ molecules under consideration must be considered to be in a cavity in the medium. The mean dipole moment of a water molecule in this field is, neglecting $H_2O$–$H_2O$ interactions

$$\langle\mu\rangle = \frac{1}{3}\frac{\mu^2 E}{kT} \quad (32)$$

so that an upper limit to the total polarization per ion, $P$, (beyond the rigid shell up to $r_0'$) is

$$P = \int_{r_0'}^{\infty} \frac{q\mu^2}{2KkT}\left(\frac{1}{r^2} + \frac{1}{Lr}\right)e^{-r/L}\,4\pi r^2\,\mathrm{d}r = \frac{3q\mu^2}{2KL^2kT}\left(\frac{4\pi L^3}{3}\right)e^{-r_0'/L}(2 + r_0'/L) \quad (33)$$

The effective volume polarized per ion is $P/\mu$. Since the ion–dipole interaction energy divided by $kT$ is of order

$$\frac{3}{2}\frac{q\mu}{Kr^2kT} = \frac{2.7}{r_A^2} \ll 1 \quad \text{for } r \geq 5 \text{ Å} \quad (34)$$

the approximation inherent in eq 32 for $\langle\mu\rangle$ is adequate for our purposes, since we shall take $r_0' \geq 5$ Å. Thus the total volume of water $v$ reorganized per ion is

$$v = \frac{4}{3}\pi r_0'^3 + \frac{q\mu 2\pi L}{KkT}e^{-r_0'/L}(2 + r_0'/L) \quad (35)$$

If eq 4 is used to express $L$ as a function of concentration $M$ we obtain for the analogue of eq 30

$$V^{0\prime}/V^0 = 1 - 0.005Mr_0'^3 - 0.122M^{1/2}e^{-Mr_0'^{3/2}/3}(1 + 0.167r_0'M^{1/2}) \quad (36)$$

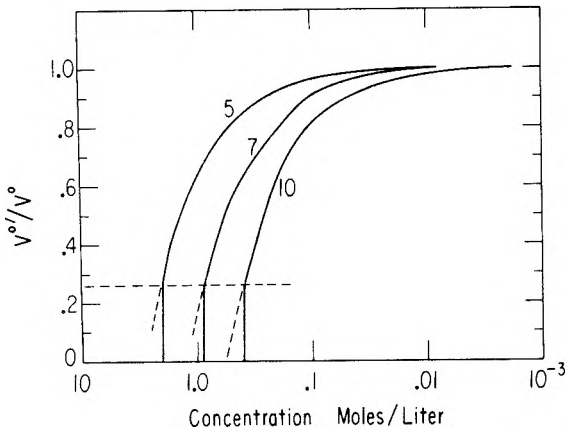


**Figure 6.** Plots of $V^{0\prime}/V^0$ vs. $M$ for various values of $r_0$, indicated on figure, based on eq 39. Dashed curves are continuation of eq 39 beyond $V^{0\prime}/V^0 = 0.26$.

Thus the disruption effect appears linear in $M$ at high, and roughly square root in $M$ at low concentrations. However, for $r_0' \geq 5$ Å the total effect is negligible at concentrations where the third term in eq 36 dominates so that we are justified in using only the second term, i.e., in using eq 30 with $r_0 \approx r_0'$. In other words, the dominant effect is the creation of a rigid hydration shell, with reorientation beyond this shell essentially negligible. Thus the calculation of the reorientation effect is insensitive to the details of the ion–$H_2O$ interaction beyond the rigid hydration shell. At very high concentrations this equation gives an incorrect behavior since $V^{0\prime}/V^0$ cannot become negative, but should approach 0. Somewhat arbitrarily we assume that eq 30 describes the disruption up to a concentration corresponding to the touching of the hydration shells, which corresponds to

$$0.005Mr_0^3 = 0.74 \tag{37}$$

since the volume fraction occupied by close packed spheres is 0.74, so that eq 30 holds for

$$M \leq 148/r_0^3 \tag{38}$$

For higher concentrations we take $V^{0\prime}/V^0 = 0$.

It is possible to refine the model slightly by taking into account that the potential $W$ reduces the ion concentration near the surface, that an ion near the surface disrupts a truncated sphere, and finally that the polarization of the orientation dipole layer decreases exponentially rather than linearly. When these effects are included one obtains, for the hard-shell model

$$V^{0\prime}/V^0 \cong 1 - 0.005M\int_0^{r_0}[r_0^3 + {}^1/_4(r_0 - z)^3 - {}^3/_4r_0(r_0 - z)^2]e^{-W(z)/kT}e^{-z/\lambda}dz/\lambda - 0.005Me^{-r_0/\lambda} \tag{39}$$

Equation 39 was solved numerically for several values of $r_0$, taking $\lambda = 10$ Å. The results are shown in Figure 6. We assume that $V^{0\prime}/V^0$ is represented by eq 39 until $V^{0\prime}/V^0 = 0.26$ according to eq 39. We take this as the point where the hydration shells effectively touch and assume $V^{0\prime} = 0$ for higher concentrations. This procedure is of course crude but cannot make a great deal of difference, since, for $r_0 \geq 7$ Å, $V^{0\prime}/V^0$ is $\ll 1$ at $M = 1$ even if eq 39 is used while at $M = 0.1$, $V^{0\prime}/V^0$ is already close to unity. Thus disruption effect is essentially an off–on effect: Nearly total disruption at $M \geq 1$ and very little disruption at $M < 0.1$.

We consider $r_0 = 7$ Å the most reasonable choice on physical grounds, since it amounts approximately to two

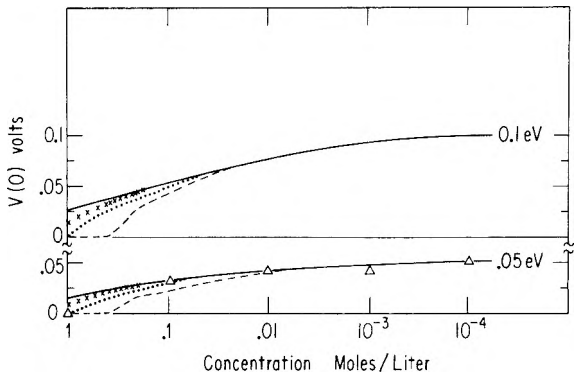


**Figure 7.** Plots of screened disrupted surface potential vs. $M$ for two values of $V^0$, indicated on figure. Solid lines, $V(0)$, uncorrected for disruption; dashed curve, $r_0 = 10$ Å; dotted curve, $r_0 = 7$ Å; crosses, $r_0 = 5$ Å. Also shown are the experimental variations in surface potential,[1] which can be superimposed by suitable adjustment of ordinates on the $V^0 = -0.05$ V curve. Best fit at high concentration is obtained by assuming $r_0 = 7$ Å in eq 39 and $\lambda = 10$ Å in eq 17.

$H_2O$ "layers" around each ion, and also averages the size differences between $K^+$ and $Cl^-$, the ions used in the experiments of ref 1 to investigate the effect of electrolyte concentration on layer potential. Curves of net remaining potential (disruption and then screened) vs. electrolyte concentration based on various $r_0$ values are shown in Figure 7, together with the experimental points taken from ref 1. The fit of the experimental points to the corrected curve for $V^0 = -0.05$ eV, $\lambda = 10$ Å, and $r_0 = 7$ Å is fortuitously good.

## Discussion

It is worthwhile to consider the validity of the approximations in the present treatment of the surface potential screening with particular emphasis on the determination of absolute half-cell emfs. In the problem considered here we are primarily concerned with the screening of an effectively external potential by electrolyte ions. For this situation the Poisson–Boltzmann equation is a far less drastic approximation than it is for ion–ion interaction since the screening arises essentially from the variation in singlet density (i.e., ionic concentration) resulting from the external field. The fact that the ion–ion interaction cannot be treated accurately by the Debye–Hückel limiting law at high concentrations is not relevant, except to the extent that it modifies the form and value of $W$, the repulsive potential seen by ions as they approach the surface.

The Onsager $W$ used here is certainly a crude approximation because it assumes symmetrical screening of ions, which implies that there are other ions between the reference ion and the surface, which is not true for ions very near the surface. This defect will only be important at high concentrations, since at low concentrations the attenuation implied by the Debye length is unimportant for an ion close to the surface. Support for the adequacy of the Onsager treatment comes from the fact that it predicts very substantial exclusion from the surface region (0–20 Å) at low concentrations, and correctly calculates the increase in surface tension with electrolyte concentration, when applied to the Gibbs adsorption equation.[3]

At high concentrations the Onsager $W$ becomes dubious as already indicated. While the *screening* calculated at high concentrations may therefore be in some error, the *net* effective potential resulting from the combination of screening and disruption will not be in serious error because disruption destroys the orientation layer at high concentrations. Disruption will be effective even if the distance of closest approach of an ion is only $r_0$, the radius

of the inner hydration shell.

We conclude then that at low concentration ($M \leq 0.01$) our model is reasonably quantitative, both for screening and disruption, while for $M \geq 1$ screening and disruption combine to make $V(0) \simeq 0$. Thus the difference in experimental values of $V(0)$ at $M = 1$ and at $M = 0.0001$ alone should suffice to fix $V^0$. In addition the fit of the data to the theoretical curve for $M \leq 0.1$ should also be quite good. As Figure 7 indicates this also serves to fix $V^0$, although not as accurately, since the variation of the theoretical curves in the range $M = 0.1$ to $10^{-4}$ is of course less, although still appreciable for $V^0 \geq 0.05$ V. Thus the present work confirms the assignment of $V^0 = -0.05$ V made in ref 1 and consequently the absolute value of the standard hydrogen half-cell emf obtained there, -4.73 V.

*Acknowledgment.* It is a pleasure to acknowledge stimulating discussions with Professor Howard Reiss during the early stages of this work. This work was supported in part by the Advanced Research Projects Agency of the Department of Defense under Contract MDA 903-76-C-0250 with the University of Michigan and in part by NSF Grant DMR 73-07589-A01.

### References and Notes

(1) R. Gomer and G. Tryson, *J. Chem. Phys.*, **66**, 4413 (1977).
(2) N. H. Fletcher, *Phil. Mag.*, **18**, (156), 1287 (1968).
(3) L. Onsager and N. N. T. Samaras, *J. Chem. Phys.*, **2**, 528 (1934).
(4) K. M. Brown, *SIAM J. Numer. Anal.*, **6**(4), 560 (1969).
(5) The values shown in Figures 4 and 5 differ slightly from those shown in Figure 7 of ref 1, which were based on the integral constraint only for all values of $a$, while the curves shown here used this only for $a \leq 1$, and the differential condition for $a > 1$.

# Preparation of a Totally Ordered Monolayer of a Chromophore by Rapid Epitaxial Attachment

**G. R. Bird,* G. Debuch, and D. Möbius**

*Max Planck Institut für Biophysikalische Chemie, Göttingen, D3400, Bundesrepublik Deutschland and Department of Chemistry, Rutgers, The State University of New Jersey, New Brunswick, New Jersey 08903* *(Received May 18, 1977)*

In a study of the specific surface interaction between anisotropic substrates and surfactant chromophores, we have prepared one totally ordered monolayer of chromophores and one partially ordered layer from a trial array of two substrates and five surfactant chromophores. The ordering results from some structural coincidence (epitaxial attachment) between the substrate and the chromophore. Thus the comparison of successes and failures is informative, particularly when the difference turns about the addition of an ethyl group to a nonorienting molecule. This is a new method, based on the formation of a compressed monolayer at the water–air interface in a surface balance. This monolayer is lifted onto a solid substrate, but here the substrate is selected to have a preferred atomic arrangement in one direction lying in the surface. When a dimensional coincidence exists between host and guest, the production of order is very rapid, occurring at lifting rates of 1 cm/20 s. Orientation is observed as polarized absorption of light incident normal to the film surface. The substrate–chromophore combinations which gave orientation were gypsum + 3,3′-dioctadecyl-9-ethylthiacarbocyanine$^+$ (total orientation) and gypsum + 3,3′-dioctadecyloxacyanine$^+$ (partial orientation). The first dye is an analogue of a class of useful photographic sensitizing dyes, and its success as compared to 3,3′-dioctadecylthiacarbocyanine$^+$ parallels the behavior of the thiacarbocyanine sensitizers. A structural hypothesis is proposed for the spectrum of the highly oriented aggregate. Once an epitaxial pair has been discovered, the ordered attachment is found to be highly insensitive to conditions of film deposition.

The first identifiable scientific study of monolayer spreading was performed by Benjamin Franklin[1] in 1774. The preparation of close-packed monolayers on a water surface can be traced back to the work of Raleigh,[2] Pockels,[3] and Langmuir,[4] and Blodgett.[5] The more recent application of this technique to surfactant molecules containing chromophores has facilitated a whole new class of experiments in luminescence and energy transfer.[6,7] The most recent advance in this art is the successful transfer of such monolayers from one solid substrate to another without the intervention of a solvent phase.[8]

The monolayers prepared in this way have a high degree of internal order. In the more common case, the chromophore long axes all lie parallel to the layer plane, and in undiluted films the molecular short axes of the generally planar chromophores stand perpendicular to the layer plane. The long axes of near neighbor molecules usually lie parallel in the plane, giving structures similar to the red-shifted "J" aggregates[9] so useful in the technology of sensitizing silver halide photographic emulsions to long wavelength radiation.

The present experiments were initiated in order to remove the last degree of disorder from these systems. Even with the ordered arrangement described above, the monolayer film presumably exists as an array of microscopic domains or islands of complete order, but with the stacking axes of adjacent islands in random distribution. One comes naturally to this hypothesis of complete order within islands from viewing electron micrographs of other cyanine dye aggregates showing free-standing linear structures with complete order over thousands of angstroms of length. This is quite unlike the local order and long-range "axis-wander" experienced in liquid crystals. The observable consequence of this island-to-island disorder is the absence of polarization effects in the absorption of light incident perpendicular to the layer plane. Polarized light absorption has been observed in the case of chemisorbed dye aggregates on anisotropic crystal faces.[10–12] However, this type of orientation is produced only slowly and requires special treatment of the host face. We have sought to combine the ease, speed, and control

* Address correspondence to this author at Rutgers, the State University of New Jersey, New Brunswick, N.J. 08903.

of monolayer spreading with directional control by an anisotropic substrate. The need for this type of control is indicated precisely by the absence of polarization effects in the formation of close-packed monolayer films and in the lifting of these monolayers onto isotropic substrates such as glass or arachidic acid coated on glass. Polarization effects can be seen with spread films, but only when the critical film pressure is exceeded and the monolayer is collapsed[13] or buckled. This collapse can be observed through the appearance of jagged dark lines across the film, and these lines indicate both multilayer formation and the existence of anisotropic forces in the region of collapse. No such irregularities should be present when a totally ordered monolayer is prepared.

The selection of a substrate was the most critical step in this experiment. The anisotropic silver halide faces, AgCl (110) and AgBr (111) (isotropic, but having extended and narrow terraces), were excluded because of the long adsorption times required to secure orientation.[11,12] Mica was excluded upon noting Skerlak's observation that the historical sensitizer 1,1′-diethyl-2,2′-cyanine$^+$ adsorbed on mica without exhibiting polarized light absorption.[14] In general, one seeks a crystal face which is chemically and electrically anisotropic, but which will not bind the chromophores too strongly to permit reorganization and ordering of the initial monolayer.

At precisely this point in our thinking, the problem of a directing substrate was posed to Professor Laves of the Crystallographic Institute of the E.T.H. in Zurich. Professor Laves was asked to suggest some common minerals having the following properties: (1) transparent in the visible and near ultraviolet regions; (2) easily cleaved along well-defined faces; (3) having anisotropy in the cleavage face; (4) slightly soluble in water; (5) inexpensive. He required all of 1 min to suggest gypsum, $CaSO_4 \cdot 2H_2O$, as a first candidate, and another minute to produce and cleave the large sample of gypsum[30] which was used in all of the successful experiments to be described. We are happy to acknowledge his contribution to the experiment and his donation of the key material.

Requirement (4) may seem enigmatic, since the cleavage face ought not to be destroyed during the coating operation. However, recent experiments on adsorption of dyes to NaCl[15] have impressed on us the desirability of some slight facial reorganization and reordering. To extend the usual logic of surface science, there are clean surfaces, real (contaminated) surfaces, and self-reorganizing surfaces. Of these, the last seem far easiest to study.

A second, synthetic substrate was on hand and was also tested for possible orientation effects. This was a sample of 5× stretched polyvinyl alcohol, a highly anisotropic material used in the production of retardation plates and polarizers. This material was a gift from Mr. Albert S. Makas of the Polaroid Corp. Polyvinyl alcohol is readily soluble in water unless held in the stretched state, so our experiments were executed on films held under spring tension.

With one exception, the surfactant dyes used in these experiments were materials existing from prior syntheses and investigations in this laboratory. The exception is the dye 1,1′-diethyl-3,3′-dioctadecyl-5,5′,6,6′-tetrachlorobenzimidazolocarbocyanine$^+$ *p*-toluenesulfonate$^-$, a gift from Dr. D. F. O'Brien of Eastman Kodak Co.[16] The other dyes and their associated anions are *N,N′*-dioctadecyloxacyanine$^+$ perchlorate$^-$ (Figure 2), *N,N′*-dioctadecyloxacarbocyanine$^+$ perchlorate$^-$ (Figure 3), *N,N′*-dioctadecylthiacarbocyanine$^+$ *p*-chlorobenzenesulfonate$^-$ (Figure 3), and *N,N′*-dioctadecyl-9-ethylthiacarbocyanine$^+$ perchlorate$^-$ (Figure 4). We do not believe that the anions exerted any significant effect, since the concentration of dissolved $CaSO_4$ in the lifted meniscus can approach saturation: $Ca^{3+} = SO_4^{2-} = 0.014$ M. $CdCl_2$ ($3 \times 10^{-4}$ M) and $NaHCO_3$ ($5 \times 10^{-5}$ M) were present in the water substrate except when $MgSO_4$ was present.

The surface balances and the high sensitivity differential spectrometer (single beam optics, oscillating sample, and phase-sensitive detection) have been described.[7] Monolayers were spread on water and also on 1.0 M $MgSO_4$ solution. Both temperature and pressure of spreading were varied. The most common set of spreading conditions was as follows: water, 15 °C, 30 dyn/cm pressure. In all cases, the dyes were dissolved in $CHCl_3$ and spread as the organic solvent evaporated.

Since maximal interaction between dye and substrate was desired, the spread monolayers were lifted in the "Z" mode[17] to place the chromophoric end of the surfactant molecule against the substrate. "Z" spreading was accomplished by excluding a small area of the total water surface with a ring cut from large glass tubing, spreading the dye film, lowering the substrate (gypsum) through the ring and into the water phase, dropping the ring below the surface to allow film–substrate contact, and finally raising the substrate out of the water and through the surface film. Lifting rates were of the order of 0.05 cm/s. Only half of the substrate crystal was immersed, so that the coated and uncoated sections could be compared in the differential spectrometer. Most of the monolayer coatings were photosensitive, so samples were stored in the dark and examined in the spectrometer shortly after coating. The photosensitivity was not so great as to require exclusion of oxygen from the spectrometer sample compartment.

Gypsum is a monoclinic crystal, cleaving naturally in the *ac* plane.[18] Thus there is no ambiguity as to the location of the *b* axis perpendicular to the cleavage plane. Unfortunately, all six possible permutations of the (100), (101), (102), and (001) directions have appeared in the literature as unit cell edges. The axes of DeJong and Bouman[19] give the shortest unit cell edges and so correspond to the present convention. However, this designation of axes is also arbitrary, and one cannot in general predict the preferred direction for attachment of molecular long axes. In fact, orientation did occur along the *a* axis of DeJong and Bouman for the molecules examined here. It could perfectly well occur along some other axis for some other surfactant chromophore. The relative orientations of the more common published axes are represented in Figure 1.

For propagation of light along the *b* axis in a gypsum crystal there are two perpendicular directions corresponding to the maximum and minimum indices of refraction. These directions are easily located by finding the directions for extinction with the crystal between crossed polarizers, as in a petrographic microscope. As shown in Figure 1, neither of these null-rotation directions corresponds to any of the possible crystal axes.[18] This introduces an optical complication, since the crystal will act as a partial depolarizer when one attempts to measure the degree of polarization of absorption using a crystal coated on both sides. To avoid this difficulty, we cleaved the dyed crystals and examined the final sample with the single monolayer-dyed face toward the calcite polarizer. While the grating monochromator had very appreciable internal polarization,[20] this was completely overridden by the essentially perfect polarization of the calcite polarizer.

## Results

Since the results of this type of orientation experiment

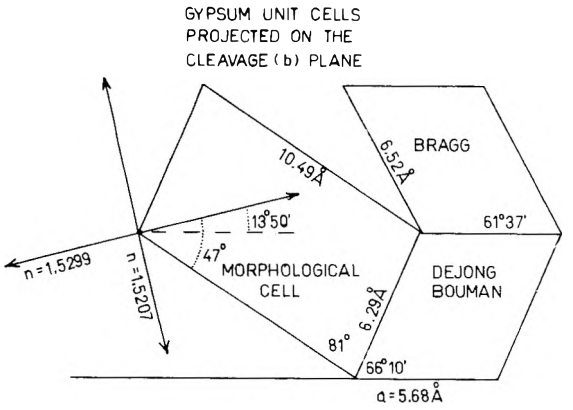


**Figure 1.** Some of the various unit cells which have been used to describe the crystal structure of gypsum: $CaSO_4 \cdot 2H_2O$. The monoclinic *b* axis, being perpendicular to any chosen *a* and *c* axes, is uniquely defined, but there is an element of arbitrary choice in the designation of the nonperpendicular axes. The cell of DeJong and Bouman conforms to the convention of choosing the shortest possible axes, and the a axis of this cell corresponds to the direction for successful orientation of long axes of adsorbed dye molecules. The large gypsum crystal used to prepare samples for this investigation exhibited natural striations along the *a* and c axes, so orientation of the crystal was accomplished by comparing the striations with the direction for nondepolarization of transmitted light, as shown by the perpendicular arrows.

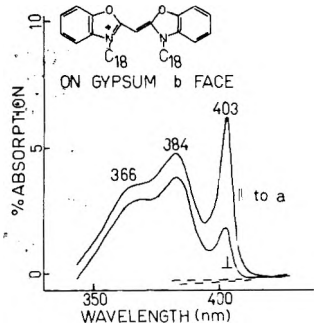


**Figure 2.** Partial orientation of the dye 3,3′-dioctadecyloxacyanine$^+$ on the gypsum cleavage face. The absorption band at 403 nm arises from a surface aggregate of the dye, presumably having a "brickstone" structure with the molecular long edge (0–0) on the gypsum surface. The dichroic ratio shown here is about 3:1, the highest obtained with this dye. The broader absorption bands at 384 and 366 nm resemble the solution spectrum, and are presumably associated with chromophores adsorbed flat-on to the gypsum surface. The aggregate and monomer systems can be further distinguished by the relatively rapid photobleaching of the aggregate absorption. The polarization of the bands at 384 and 366 nm is apparent only, resulting from unequal zero-absorption baselines (dashed lines) caused by multiple internal cleavages within the crystal sample.

are not easily predicted from one surfactant dye to another, we shall report the results in the order obtained, to illustrate the interplay of confusion and understanding. The very first dyeing with 3,3′-octadecyloxacyanine$^+$ produced highly significant polarization at 403 nm, as shown in Figure 2. The two shorter wavelength absorption bands of this molecule at 384 and 366 nm are characteristic of the isolated molecule and the dimer, respectively, and showed no polarization at any time. The slight apparent polarization of these bands results from shifting zero absorption baselines, as indicated by the dashed lines. This baseline shift is associated with the optical effects of internal cleavages in the particular gypsum sample.

The long wavelength absorption at 403 nm is assigned to an aggregate of the dye with chromophores in a "brickstone" geometry.[21] This aggregate has a primitive unit cell (one molecule) and a single absorption band. Ratios of absorbances as high as 3.0 were obtained, and with this initial success in hand, it seemed an easy matter to alter the conditions of spreading to raise the ratio of

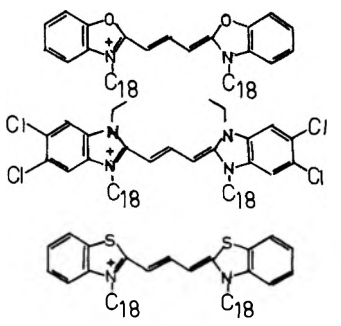

**Figure 3.** Structures of three 3,3′-dioctadecylcarbocyanines which gave no significant dichroism upon attachment of a compressed monolayer to the gypsum face. The negative result for the third of these dyes, 3,3′-dioctadecylthiacarbocyanine$^+$, is especially significant, since it resembles so closely the dye of Figure 4.

aggregate/monomer coverage and simultaneously to improve the dichroic ratio (ratio of parallel/perpendicular absorbances in polarized light). In fact, we were unable to improve the dichroic ratio of the initial result. The spreading of a film of 1:1 M octadecane/dye produced layers with almost all dye in the aggregate form, but destroyed all significant polarization. Changes aimed at improved monolayer order included spreading at reduced temperature, spreading at increased film pressure, and spreading over a 1.0 M $MgSO_4$ solution, the last to fix a negative charge on the substrate by the common ion effect,[31] and so increase the attractive forces between cationic dye and gypsum substrate. When none of these steps proved to be effective, we were forced to conclude that the packing structure of the aggregate of this dye was not closely commensurate with any major parameter of the gypsum surface.

The next three dyes were chosen for examination on the basis of similarity to known photographic sensitizing materials, and are shown in Figure 3. None of the three gave any significant polarization of absorption on attachment to gypsum. The first dye, 3,3′-dioctadecyloxacarbocyanine$^+$, gave a broad absorption band with equal peaks at 470 and 496 nm, suggestive of a "herringbone" packing structure[22] with molecular long axes arranged in a nonparallel geometry.

The second dye, 1,1′-diethyl-3,3′-dioctadecyl-5,5′,6,6′-tetrachlorobenzimidazolocarbocyanine$^+$, has the chromophoric backbone of a class of favorite photographic research materials. The parent compound of this class, the 1,1′,3,3′-tetraethyl derivative, has given strongly polarized absorption when adsorbed to anisotropic faces of AgBr and AgCl.[11,12] O'Brien has investigated the 3,3′-dioctadecyl derivative extensively[16] and shown that it forms a relatively unique structure on well-ordered AgBr faces with absorption at 577 nm. This matches almost perfectly with the absorption of the tetraethyl derivative, and can be attributed to an ordered, epitaxial attachment to AgBr, like that identified from the observations of polarized absorption.[11] O'Brien also observed that the surfactant dye absorbed at 592 ± 2 nm on a wide variety of disordered substrates including evaporated AgBr. On this basis we expected to observe polarized absorption on gypsum surfaces, and were considerably disappointed. The absorption maximum on gypsum was blue-shifted from O'Brien's 592-nm value, varying from 564 to 582 nm. On gypsum this material is certainly packing with chromophoric long axes parallel (the J-aggregate structure) but with a wide variation of aggregate sizes and with island-to-island disorder.

The last of these unsuccessful dyes is 3,3′-dioctadecylthiacarbocyanine$^+$. The chromophore of this molecule

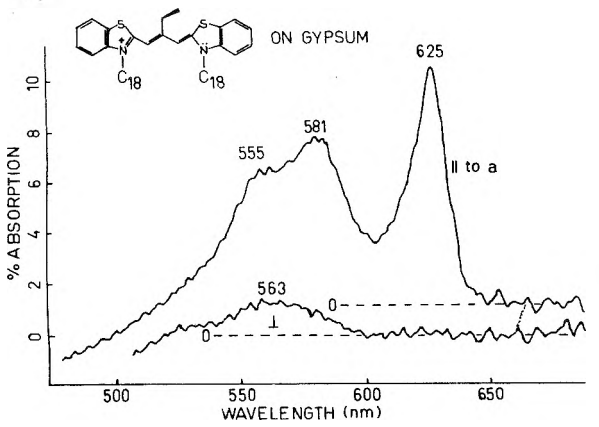


**Figure 4.** Successful orientation of the dye 3,3′-dioctadecyl-9-ethylthiacarbocyanine$^+$. This dye was spread from $CHCl_3$ solvent onto pure water at 15 °C, and the monolayer film was compressed to a pressure of 30 dyn/cm. A gypsum crystal was then lifted through the film from water to air (Z deposition) at a rate of approximately 0.05 cm/s. This crystal was then cleaved to remove one of the two dye monolayers, and was examined with polarized light in a differential absorption spectrometer. The three absorption bands at 625, 581, and 555 nm are assigned to a single aggregate structure in which all molecular long axes lie parallel to each other and to the gypsum *a* axis. The weak perpendicular absorption at 563 nm is assigned to isolated molecules adsorbed with chromophore planes flat-on to the gypsum surface, and with molecular long axes either isotropically distributed or approximately perpendicular to the *a* axis. The absorption spectrum for electric vector parallel to the gypsum *a* axis is displaced upward 1.0%. Note the very similar patterns of irregular structure beyond 640 nm. These result from superimposed thin film interference patterns of several internal cleavages. As connected by the dotted line, the parallel and perpendicular patterns are identical except for a slight wavelength displacement. Except for the flat-on monomeric absorption component, the dye attached to this surface may be said to be totally oriented.

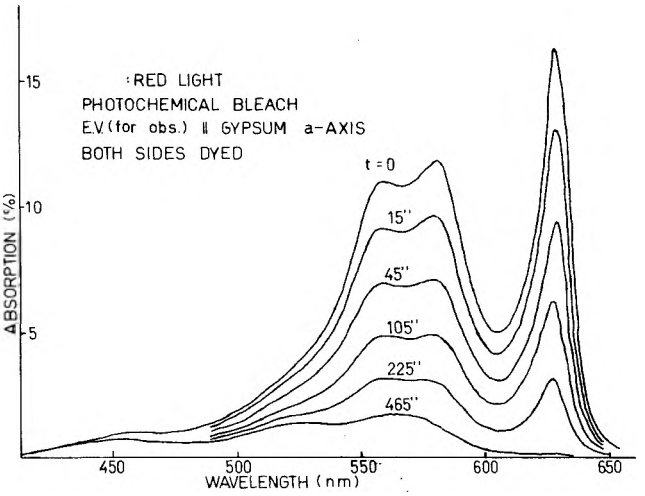


**Figure 5.** Photobleaching of a double monolayer of 3,3′-dioctadecyl-9-ethylthiacarbocyanine$^+$ with "white" light (tungsten lamp) passed through a piece of Schott RG610 glass, a sharp-cut red filter material having approximately 20% transmission at 610 nm and 1% at 600 nm. Irradiation is concentrated in the longest wavelength absorption band, but the three parallel absorption bands show proportional decay of absorption. This indicates that the three absorptions are assignable to a single aggregate structure. On the basis of decreasing absorptions, one would expect pseudo-first-order kinetics for the time dependence of bleaching. Instead, pseudo-second-order kinetics are observed. We have no simple explanation for this observation, but a generalized mechanism of energy transport within aggregates followed by bleaching at localized active (impurity?) sites suggests itself.

is the basis for a useful class of red sensitizing dyes, but this molecule is not configured to form a red-shifted, parallel aggregate. Like the oxacarbocyanine it gave a broad, flat-topped absorption band from 465 to 580 nm, suggestive of a herringbone structure.[22]

Totally different results were obtained with the last dye tested, 3,3′-dioctadecyl-9-ethylthiacarbocyanine$^+$, as shown in Figure 4. This material, which differs from the prior dye only by the addition of the 9-ethyl group, gave strongly polarized absorption in every case of spreading on water and Z-coating on gypsum. The three strong absorption peaks at 625, 581, and 555 nm were always polarized parallel to the gypsum *a* axis. The polarization ratios were highest for the 625-nm band, being unmeasurable and certainly greater than 20 in the spectrum of Figure 4. The weak perpendicular band at 563 nm represents the only significant disorder on the surface, and we assign it to isolated molecules lying perpendicular to the *a* axis, probably with the chromophores lying flat against the gypsum surface. The shoulder of this band at about 525 nm had the expected separation of 1200–1300 $cm^{-1}$ observed as the dominant vibrational progression in many monomeric cyanine dyes. By contrast the aggregate bands at 555 and 581 nm have a separation of 806 $cm^{-1}$.

After numerous efforts to suppress the absorption bands at 555 and 581 nm in favor of the 625-nm absorption had failed, it was noted that these three bands were appearing with constant intensity ratios and might be assignable to a single aggregate structure. To settle this point, the system was photobleached in air with filtered red light obtained from a tungsten lamp. The filter was a Schott RG610 sharp cut red glass which blocked substantially all radiation shorter than 610 nm from the sample. The absorbance changes at the three maxima were in simple proportion, indicating that we were dealing with a single packing structure. The partially bleached absorption spectra are shown in Figure 5.

The invariance of an absorption system to minor perturbations is a helpful test of ordered, epitaxial attachment of the monolayer to the crystal substrate. The absorption of this last dye on gypsum was found to be invariant to the change from pure surfactant dye to a 1:1 M mixture with *n*-octadecane, retaining both the location of absorption maxima and the high dichroic ratio in the mixed monolayer. This is to be contrasted with the behavior of the same monolayer deposited directly on glass or on glass coated with layers of arachidic acid. The substantially continuous absorption shifts of these irregularly attached systems are shown in Table I. The pure monolayer on glass and on arachidic acid shows an absorption system similar to the gypsum monolayer (structurally similar?), but the long wavelength absorption disappears and the other two bands shift on addition of octadecane to the layer.

At high monolayer pressures and at octadecane/dye ratios greater than 1:1, the absorption of a second aggregate is seen, mixed with the dominant spectrum. This second spectrum is also polarized, with at least one perpendicular band at 564 nm and a parallel band at 600–602 nm. We were unable to obtain this spectrum free from strong admixture with the dominant spectrum, and therefore simply note that this dye–substrate combination has the capability of forming more than one ordered, epitaxial structure.

None of the attempts to secure spreading of polarizing monolayers on the stretched polyvinyl alcohol were successful. This identical sample of polymer had been used at Rutgers to study the polarized absorption of isolated molecules incorporated into the bulk PVA phase from nonsolvents for the polymer, and dichroic ratios as high as 10 had been observed.[22] The birefringence tint of the film was compared before and after contact with water in the surface balance, and no significant change of tint

TABLE I: Absorption Peaks and Polarization of Monolayers of 3,3'-Dioctadecyl-9-ethylthiacarbocyanine[a]

| Coating conditions | Absorptions max (nm) and polarization | Remarks |
|---|---|---|
| | (a) Coatings on Gypsum | |
| (1) Fresh cleavage: $H_2O$, 30 dyn/cm, 16 °C | 555 (∥), 581 (∥), 625 (∥), 563 (⊥) | Highly polarizing $R_D > 20$ at 625 nm |
| (2) Crystal etched with (1) HCl, (2) $NaCH_3COO$ (3) $H_2O$, coated at 30 °C | As above | Lower polarization $R_D = 3.5$ |
| (3) Fresh cleavage: $H_2O$ 40 dyn/cm, 1:1 $n$-$C_{18}H_{38}$ | As above | $R_D = 10$ |
| (4) As (3), 1:1 $C_{18}H_{38}$, but spread for 0.25 h | As above, but new parallel band at 602, stronger than 625 and 582 bands | $R_D = 5$ at 625 nm<br>$R_D = 3.5$ 0602 nm |
| (5) 30 dyn/cm at 16 °C: $H_2O$, 1 dye:2 $C_{18}H_{38}$ | 617 (∥), 602 (∥), 566 (⊥), 518 sh(⊥) | 625 → 617-nm shift and broadening suggests breaking of large parallel aggregate.<br>$R_D(\perp) = 1.3$ at 566 implies perpendicular orientation of monomeric dye. |
| | (b) Coatings on Glass Unpolarized Except as Noted | |
| (1) Aracidic acid 4× subcoat on glass, 15 °C, 30 dyn/cm | 477 w, 545, 572, 626 m | Some resemblance to spectrum on gypsum. No dichroism. |
| (2) Aracidic acid 4× on glass, 15 °C, 40 dyn/cm: 1.0 M $MgSO_4$ | 472, 545, 568 sh | No dichroism. No long wavelength shifted absorption. |
| (3) Attempted repeat of (2) | 526, 553, 572, 616, 623(∥) | Repeat film is frosted, suggesting film rupture, or crystallization of $MgSO_4$. |
| (4) Glass, no arachidic acid, 15 °C, 40 dyn/cm: 1.0 M $MgSO_4$ | 527 w, 556, 576, 623 | No dichroism. |
| (5) Attempted repeat of (4) | 540, 556 | Strong doublet |
| (6) Glass, no arachidic acid, 15 °C, 40 dyn/cm, 1:1 $C_{18}H_{38}$ | 527, 569 | Strong doublet |
| (7) Glass, aracidic acid 4×, 15 °C, 40 dyn/cm, 1:1 $C_{18}H_{38}$ | 534, 582 | Strong doublet |
| (8) Glass, no arachidic acid, 15 °C, 40 dyn/cm, 1:2 $C_{18}H_{38}$ | 526, 562 | Strong doublet |
| (9) Aracidic acid 4× on glass, 15 °C, 40 dyn/cm 1:2 $C_{18}H_{38}$ | 528 m, 578, 602 | Strong triplet |

[a] An underline indicates dominant band(s) of the spectrum. All bands seen on coatings over glass or glass + aracidic acid are broad and overlapping, except for the 623-626-nm band. The notation arachidic acid 4× indicates three compressed monolayers picked up in X mode, then one in Z mode (hydrophobic end outward) on the glass slide before the compressed dye film is lifted.

(decrease of internal order) was seen. The simplest interpretation of these negative results could be that the immediate surface of the polyvinyl alcohol film is disordered by contact with water, in spite of the film tension.

## Conclusions

A dominant motive for these experiments was to establish a quick and reliable method for constructing totally ordered monolayers. If monolayer computer elements or energy processing devices should ever come into use, this level of order may be demanded. With five trial dyes and two substrates, one such case of total order and one case of partial order have been obtained. Given the availability of a vast number of surfactant dyes and anisotropic substrates, we can expect that many similar cases will exist. However, the present knowledge of structural dimensions and attractive forces is *not quite* adequate to permit confident prediction of successful combinations. It should be possible to make astute guesses from the existing fragmentary data.

To realize the full utility of a totally ordered monolayer, it should be possible to lift and transfer the monolayer to a new substrate,[8] using the established techniques of casting polystyrene or polyvinyl alcohol over the ordered monolayer. While it has not yet been possible to lift this completely ordered layer off the gypsum surface, more recent experiments[23] employing diluted layers of the oxacarbocyanine$^+$ (dye II in this manuscript) in a fatty acid/ester mixture have demonstrated the successful transfer of monomeric orientation (as polarized light absorption) from gypsum to glass substrates. The transfer of orientation to a second layer of nonidentical chromophore has also been accomplished. It would appear to be only a matter of time, patience, and finesse to accomplish the successful transfer of a fully ordered monolayer.

While the detailed structure of the totally oriented monolayer cannot be determined at this time, some conditions can be set, and a structural hypothesis can be proposed. The long axes of all molecules in the structure are aligned along the $a$ axis. If this were not so, a strong perpendicular absorption band would have to be present. Further, there are at least two and possibly more chromophores in the unit cell of the monolayer, since there are at least two absorption systems in the aggregate. It is not clear whether the 555-nm band is a vibrational satellite of the stronger 581-nm band. The interval is 800 $cm^{-1}$, considerably smaller than the vibrational interval of 1200–1300 $cm^{-1}$ seen in the solution spectra of closely related dyes. A superficially similar absorption structure is found in the solution aggregates of 1,1'-diethyl-2,2'-cyanine$^+$, and there the two shorter wavelength absorption peaks have been identified as 0–0 and 0–1 vibrational

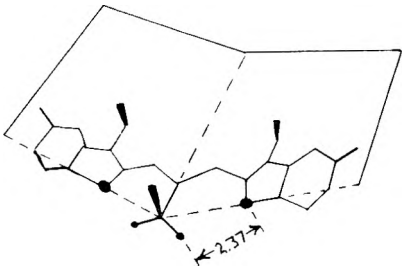


**Figure 6.** The dihedral distortion of a 9-ethylthiacarbocyanine$^+$ cation similar to the dye of Figures 4 and 5. In the crystal structure of 3,3′,9-triethyl-5,5′-dichlorothiacarbocyanine$^+$, bromide$^-$ (1:1 acetic acid solvate), the repulsive contact between sulfurs and 9-methylene protons shown as 2.37 Å distorts the chromophore into two half-planes with an 8.6° dihedral angle between planes. We believe that this dihedral distortion is crucial to an understanding of the very different behavior of dyes with and without the 9-ethyl substituent. This difference of behavior applies to the present investigation and to the behavior of these dyes as photographic sensitizers.

components.[24] However, that aggregate has a totally different structure, with the long wavelength absorption at 576 nm having polarization parallel to the long axis of the helical aggregate while the 496- and 534-nm diad is polarized perpendicular to the long axis. In general, vibrational splitting of one particular absorption band of an aggregate is to be expected whenever that band is only slightly shifted from the absorption of the parent monomer.[25]

The structure of the present totally ordered aggregate on gypsum could best be settled by low energy electron diffraction methods (LEED), but in related investigations the destruction of dyes by the electron beam has prevented successful analysis.[26] The development of a structural hypothesis to fit the data on this particular dye–substrate combination required full use of the data from a crystal structure determination[27] on a closely related dye, 3,3′,-9-triethyl-5,5′-dichlorothiacarbocyanine$^+$ bromide$^-$. The molecular backbone of this dye is identical to that of the oriented surfactant dye. The 9-ethyl group has long been recognized for its importance as a small substituent projecting out of the aromatic plane. Groups such as this are crucial to the performance of photographic sensitizing dyes,[28] and have been referred to as tabs, indexing groups, knobs, or nubbly groups. A single such indexing group can prevent the formation of some undesirable surface structure and thus favor some other more desirable structure.[23] However, the recent x-ray structure has established that the 9-ethyl group also deforms the entire framework from a planar structure to a dihedral structure reminiscent of an airplane wing. The distortion of 8.6° between molecular half-planes[27] results from a repulsion between the heterocyclic sulfurs and the 9-methylene protons, as shown in Figure 6. We cannot be sure that this distortion persists in the monolayer structure on gypsum, but suspect that it does.

This dihedral distortion leads to a packing of alternately strongly bound and weakly bound neighbors in the crystal. The weakly bound neighbors are packed plane-to-plane, but have the ethyl groups facing inward, so that only a weak van der Waals contact can be made at the ends of the molecules. The average separation is thus much greater than the 3.4–3.5-Å spacings found for planar cyanine dyes and many other aromatic systems. The strong contact is between half-planes of staggered molecules packed at just this preferred distance.

To accomodate this structure to the gypsum host, we note that in the monolayer all 9-ethyl groups must lie downward, toward the inorganic face, rather than in the

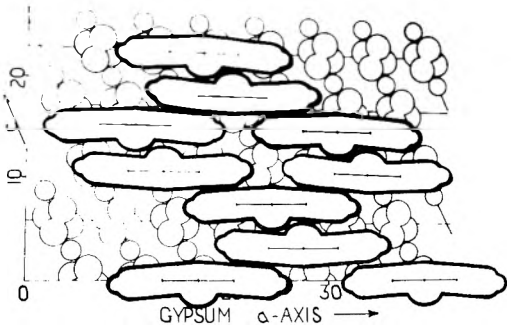


**Figure 7.** Proposed hypothetical structure for the monolayer aggregate of 3,3′-dioctadecyl-9-ethylthiacarbocyanine$^+$ on the cleavage face of gypsum. The horizontal and diagonal lines mark the *a* axis and *c* axis, respectively, following the unit cell of DeJong and Bouman. There is a sulfate sulfur at each intersection of *a* and *c* axes, and the four large circles mark the location of the sulfate oxygens surrounding the sulfur. The upper, more complete circles mark the upper oxygen atoms, lying 0.864 Å above the sulfur. The small circles on the *c* axes mark the location of $Ca^{2+}$ ion, which lie 0.045 Å below the sulfate sulfurs. In constructing this diagram, we effectively assume that no major movement of the ionic $CaSO_4$ sheet occurs on cleavage, with the cleavage breaking only an array of hydrogen bonds by which the waters of hydration bind the parallel sheets together. This surface must be considered as having chemisorbed water molecules attached at some positions. The surfactant chromophores stand with long edge (sulfurs) against the gypsum face, and with chromophore short axes nearly vertical. The cross sections of these aromatic planes are represented by the paper cutout models, with the central bulge on each of these marking the extension of the 9-ethyl group out of the aromatic plane. The solid bars on the molecular cut-outs mark the location of the N–N axis, the center of gravity of the chromophore. Note that the chromophores make both weak attachments (ethyl-groups facing) and strong van der Waals contacts between unhindered half-planes. This structure is proposed to account for the present observations, but cannot be proven to be the actual structure existing on the gypsum surface.

alternating up, down, up, down arrangement in the crystal. This change requires that the weakly bound neighbors be offset just far enough to clear the two 9-ethyl groups, but allows the strong contacts to be preserved. The resulting arrangement is consistent with the epitaxial attachment shown in Figure 7. In this structure each molecule occupies a length of $3.5a$ = 19.88 Å, and on the perpendicular to the *a* axis, the average occupancy of a molecular plane is $(^2/_3)c \sin \beta$ = 3.836 Å. The occupancy on a fully covered and fully ordered surface is thus 76.26 Å$^2$. This hypothetical structure is in accord with all present observations including a semiquantitative estimate of surface concentration of $7.7 \times 10^{13}$ molecules/cm$^2$. This estimate was made by integrating the dipole strength[15] of the parallel and perpendicular absorptions of Figure 4 and is uncertain to the extent that some artistry enters into the location of the curved zero absorption baselines for integration. Some 20% of the total absorption is contributed by isolated molecules absorbing in the perpendicular direction and presumably attached with aromatic planes against the inorganic surface. For these the surface occupancy is estimated to be 166 Å$^2$ from Corey–Pauling–Koltun molecular models. This area is derived for a structure in which the chromophoric group lies flat on the gypsum surface and the hydrophobic octadecyl groups stand perpendicular to the surface.

The packing structure shown in Figure 7 is an hypothetical structure, and is not here defended as THE structure. However, we believe that a quantum mechanical calculation of the absorption bands of this structure will agree with the observed spectrum.

The preparation of a totally ordered monolayer of a surfactant dye has been accomplished by lifting in Z-mode a compressed monolayer of the dye from a water surface onto a gypsum surface. The success of this method re-

quires some structural coincidence between the dimensions of the host crystal and the monolayer stacking structure. Once such a coincidence has been discovered, the preparation of totally ordered monolayers is quick, easy, and subject to subtle control through changes of temperature, film pressure, film strengthening additives (octadecane), and added salts in the water phase.

*Acknowledgment.* The grant of a fellowship to G. R. Bird from the John Simon Guggenheim Memorial Foundation facilitated this investigation, and is gratefully acknowledged. We reiterate our thanks to Professor Dr. F. Laves of the Crystallographic Institute of the Eidengenossische Technische Hochschule, Zurich, for his suggestion of the successful substrate material. Professor Joseph Potenza of the School of Chemistry, Rutgers University, has given a most helpful guided tour through the many representations of the crystallographic structure of gypsum and through the packing behavior of aromatic materials. The authors are deeply indebted to Professor Dr. Hans Kuhn for his helpful advice and encouragement of this work.

## References and Notes

(1) (a) B. Franklin, *Phil. Trans. R. Soc.*, **64**, 445 (1774): For historical analysis of Franklin's experiments, see (b) C. H. Giles, *Chem. Ind., (London)*, 1616 (1969). This article is one of six in an historical series by Giles and Forrester. See also ref 3b.
(2) Lord Raleigh, *Phil. Mag.*, **48**, 337 (1390).
(3) (a) A. Pockels, *Nature (London)*, **43**, 437 (1891); (b) C. H. Giles and S. D. Forrester, *Chem. Ind. (London)*, 43 (1971). This historical study gives a perspective on the remarkable correspondence between Pockels and Lord Raleigh concerning her development of the modern surface balance at home.
(4) I. Langmuir, *J. Am. Chem. Soc.*, **39**, 1848 (1917).
(5) (a) K. B. Blodgett, *J. Am. Chem. Soc.*, **57**, 1007 (1935); (b) *Phys. Rev.*, **55**, 391 (1939).
(6) For a review of results on assembled monolayer systems see H Kuhn and D. Möbius, *Angew. Chem., Int. Ed. Engl.*, **10**, 620 (1971).
(7) For a general article on both results and methods for monolayer systems see H. Kuhn, D. Mobius, and H. Bucher, "Spectroscopy of Monolayer Assemblies" in "Physical Methods of Chemistry", Part IIIB, A. Weissberger and B. W. Rossiter, Ed., Wiley, New York, N.Y., 1972, Chapter VII.
(8) (a) D. Möbius, *Photogr. Sci. Eng.*, **18**, 413 (1974); (b) O. Inacker, D. Möbius, H. Kuhn, and G. Debuch, *ibid.*, in press.
(9) G. R. Bird, K. S. Norland, A. E. Rosenoff, and H. B. Michaud, *Photogr. Sci. Eng.*, **12**, 196 (1968).
(10) W. West and V. I. Saunders, "Wissenschaftliche Photographie" (Proceedings of a conference held in 1956 in Cologne) Verlag Dr. O. Helwich, Darmstadt, 1958.
(11) W. E. Gray, W. R. Brewer, and G. R. Bird, *Photogr. Sci. Eng.*, **14**, 316 (1970).
(12) W. D. Pandolfe, doctoral thesis, Rutgers University, New Brunswick, N.J., 1974 (Section II-C).
(13) R. Steiger, R. Kitzing, and P. Junod, *J. Photogr. Sci.*, **21**, 107 (1973).
(14) T. Skerlak, *Kolloid Z.*, **95**, 265 (1941).
(15) W. D. Pandolfe and G. R. Bird, *Photogr. Sci. Eng.*, **18**, 340 (1974).
(16) D. F. O'Brien, *Photogr. Sci. Eng.*, **17**, 226 (1973)
(17) Reference 7, p 595.
(18) W. A. Wooster, *Z. Kristallogr.*, **94**, 375 (1936).
(19) W. F. deJong and J. Bouman, *Z. Kristallogr.*, **100**, 275 (1938).
(20) J. E. Stewart and W. S. Galloway, *Appl. Opt.*, **1**, 421 (1962).
(21) (a) H. Bucher and H. Kuhn, *Chem. Phys. Lett.*, **6**, 183 (1970); (b) V. Czikkely, H. D. Forsterling, and H. Kuhn, *ibid.*, **6**, 207 (1970).
(22) (a) R. Eckert and H. Kuhn, *Ber. Bunsenges. Phys. Chem.*, **64**, 356 (1960); (b) C. Reich, doctoral thesis, Rutgers University, New Brunswick, N.J., 1977; *Photogr. Sci. Eng.*, **18**, 335 (1974).
(23) D. Möbius and G. Debuch, *Ber. Bunsenges. Phys. Chem.*, **80**, 1180 (1976).
(24) (a) S. F. Mason, *Nature (London)*, **199**, 139 (1963); (b) J. K. Maurus and G. R. Bird, *J. Phys. Chem.*, **76**, 2982 (1972).
(25) T. Kurucsev and U. P. Strauss, *J. Phys. Chem.*, **74**, 3081 (1970).
(26) W. Bottoms, unpublished investigations.
(27) (a) J. Potenza and D. Mastropaolo, *Acta Crystallogr., Sect. B*, **30**, 2353 (1974); (b) D. Mastropaolo, J. Potenza, and G. R. Bird, *Photogr. Sci. Eng.*, **18**, 450 (1974).
(28) W. West, private communication.
(29) A. E. Rosenoff, V. K. Walworth, and G. R. Bird, *Photogr. Sci. Eng.*, **14**, 328 (1970).
(30) A sample from Agrigent, Sicily.
(31) One of the referees has called our attention to the possibility of creating a larger common ion effect by using $Na_2SO_4$ rather than $MgSO_4$. We agree with his comment, and will so proceed in future experiments. Given the difference in solubility of $MgSO_4$ vs. $CaSO_4$ and the difference in ionic radii (0.78 Å vs. 0.99 Å) of the divalent cations, it seems likely that $SO_4^{2-}$ will be more strongly adsorbed to a $CaSO_4 \cdot 2H_2O$ surface than will $Mg^{2+}$, so that some local negative charge must have been imparted to the crystal surface in the experiment reported here.

# The Raman Spectrum of Chemisorbed Methanol on Silica. A Comparison with the Infrared Technique

**B. A. Morrow**

*Department of Chemistry, University of Ottawa, Ottawa, Ontario, Canada K1N 6N5* *(Received July 19, 1977)*

*Publication costs assisted by Imperial Oil Limited*

The Raman spectrum of surface methoxyl groups on silica ($SiOCH_3$) formed as a result of the dissociative chemisorption of methanol is compared with the infrared spectrum. The geometrical conditions for obtaining a maximum in the Raman scattering intensity are discussed. Under favorable conditions the signal-to-noise ratio is comparable to that which can be obtained using infrared spectroscopy although slower scan speeds and larger spectral slit widths have to be employed. Raman scattering associated with the low frequency modes of the Si–O–C unit were not observed and possible reasons for this are discussed.

Although infrared spectroscopy has been routinely used for over 20 years to obtain the vibrational spectrum of adsorbed species on dispersed oxide surfaces the Raman spectroscopic technique has only recently been similarly applied.[1,2] The most successful Raman studies have been carried out using adsorbates which are expected to exhibit a large change in polarizability during one or more normal modes of vibration such as $CCl_4$,[3,4] pyridine,[5-9] or acetylene.[10] In spite of this, the signal-to-noise ratio has generally been considerably lower than can now be achieved using infrared spectroscopy. However, the major difficulty with the infrared technique is that all oxides are opaque below about 1000–1350 $cm^{-1}$ due to the intense absorption associated with the oxide lattice modes and one can rarely observe bands associated with adsorbent–adsorbate stretching modes. This opacity arises because of

the necessity of using sufficient material so that the spectrum of surface species can be detected, usually 5–40 mg/cm$^2$. Conversely, oxides are relatively poor Raman scatterers and, in spite of well-documented problems associated with background fluorescence,[1,2,8,11] one can in principle observe spectra of surface species within the range of about 50–4000-cm$^{-1}$ Raman shift from the exciting line. The present paper compares the problems associated with obtaining the Raman and infrared spectrum of chemisorbed methanol on silica.[12] To the author's knowledge this is the first published account of the Raman spectrum of a surface species which has been formed by a dissociative chemisorption process, that is

$$SiOH + CH_3OH \rightarrow SiOCH_3 + H_2O$$

## Experimental Section

The silica used in this work was Cab-O-Sil HS-5 (BET $N_2$ surface area of 320 m$^2$ g$^{-1}$) which had been heated in air at 600 °C for 24 h prior to use in order to oxidize hydrocarbon impurities. For the infrared work the methylation was carried out by allowing gaseous $CH_3OH$ to react with silica at 400 °C and the spectra obtained have been described in detail elsewhere.[12] For the Raman work the methylation was best carried out by refluxing silica in excess methanol for 24 h followed by filtering and removing excess $CH_3OH$ under vacuum. Both methylation procedures have been described by Morterra and Low[13] and no differences were noted using either procedure with either spectroscopic technique. The refluxing technique was preferable for the Raman work because of a lower fluorescence background.

In the infrared work a 200-mg sample disk 2.5 cm in diameter was mounted in an evacuable quartz cell[14] whereas for the Raman work a 100-mg 12.5-mm diameter disk was either mounted in a suitable holder so that the spectra were recorded with the sample in air or it was placed in an evacuable cell containing a 25-mm diameter Pyrex flat against which the sample rested. No significant differences were noted in the Raman spectra and, with the methylated sample exposed to the laboratory atmosphere for up to 2 weeks, no apparent hydrolysis of the methyl groups occurred, nor did the fluorescent background change. The optimum sample geometry employed will be discussed in the Results section.

Infrared spectra were recorded using a Perkin-Elmer Model 13G filter-grating instrument. Raman spectra were recorded using a Jobin-Yvon HG2 double monochromator with a Control Laser Corp. Model 552 argon ion laser capable of producing up to 2.4 W of power in the 488.0-nm line. This line was used for all experiments unless otherwise stated. Raman scattering was detected with a cooled ITT FW-130 photomultiplier tube and a Princeton Applied Research Model 1105 photon counting system. Scan speeds and spectral slit widths are given where appropriate.

## Results

*Sample Geometry.* In a double beam infrared spectrometer the peak intensity of an *absorption* band (i.e., the optical density) is given by log $(I_0/I)$ where $I_0$ is the percent transmission relative to the baseline of the band and $I$ is the percent transmission at the peak maximum. One generally tries to adjust the quantity of sample so that an average band of interest may have an optical density in the range 0.1–1.0. In order to obtain a suitable signal-to-noise ratio such variables as the energy reaching the detector (which is proportional to the square of the slit width for constant source intensity), the response time constant of the amplifier, the scan speed, and the amplifier gain are adjusted. As long as the spectral slit width is less than or equal to the band half-width then, in the absence of electronic distortion, the peak absorbance depends essentially on the quantity of sample.

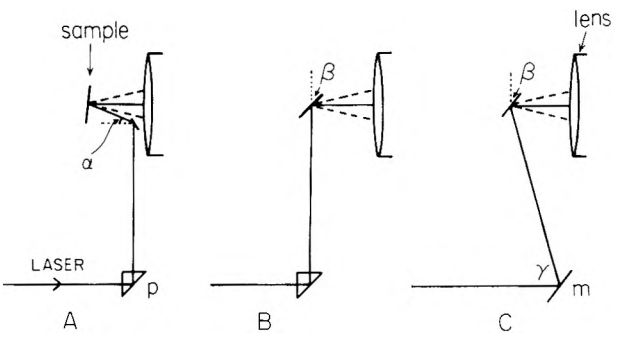


**Figure 1.** Schematic drawings illustrating various illumination geometries. The laser beam strikes either a prism (p) or a mirror (m) and is directed upward toward the sample. The "lens" is the collection lens of the spectrometer. See text for further description.

Raman scattering is measured with a single beam detection system and the light intensity at a given wavelength depends on the number of photons per second reaching the detector. With a photon counting detection system, this is usually referred to as the number of counts per second (cps). This depends (for a given system) on the number of scattering centers reached by the exciting radiation, on the intensity of the exciting radiation, and on the spectrometer slit width. For spectral slit widths comparable to natural band widths, the intensity increases approximately linearly with slit width.[15] Hence for solids (and this applies to adsorbed species on solids) the intensity depends not so much on the quantity of sample above a certain minimum but more on the efficiency with which the scattered light can be collected. In principle the ideal illumination geometry would be one in which a sample was perpendicularly illuminated and the 180° back-scattered light was collected within as large a solid angle as possible.

A practical arrangement which has a small number of reflecting surfaces is shown in Figure 1A. The laser beam (filter and focusing lens not shown) was directed upward after striking a prism on to a small mirror which was slightly larger in diameter than the laser beam. This mirror was situated 10 mm above the base of the 40-mm diameter collection lens of the spectrometer and the beam was directed with near normal incidence on to the slightly inclined sample (10° from the vertical) such that the reflected beam and the Raman scattered radiation was directed horizontally toward the instrument. The 12.5-mm diameter sample disk was 25 mm from the collection lens of the spectrometer and the optimum angle $\alpha$ for direct reflection into the center of the focusing lens was 20°. In the work to be described below this arrangement gave the maximum intensity in the Raman scattered light. The J-Y Raman spectrometer has horizontal slits and the small mirror apparently blocked very little of the scattered light. Any attempt to raise the mirror toward the center of the lens so as to achieve normal impact on the sample always resulted in a decrease in the signal.

An alternative arrangement which has one less reflecting surface is shown in Figure 1B. The laser beam was directed vertically upward toward the sample which was inclined at an angle $\beta$ to the vertical. For $\beta$ = 45° the reflected beam was directed to the center of the lens. The maximum intensity that could be achieved with this arrangement was never more than two-thirds of that which could be achieved with the arrangement of Figure 1A.

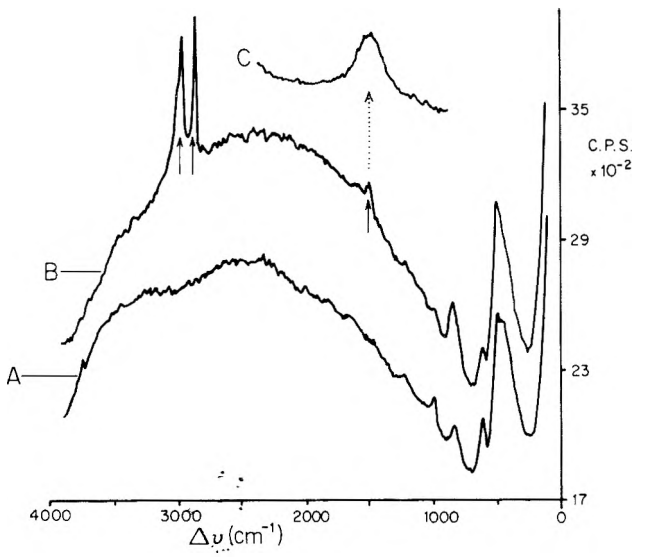


**Figure 2.** (A) Raman spectrum of a silica disk. (B) Raman spectrum of a methylated silica disk. New bands are marked with a vertical arrow. For scan conditions see text. (C) Expanded spectrum of the weak 1465-$cm^{-1}$ feature in B. The wavenumber scale is 10-fold expanded relative to B and the counting scale is 3.3-fold expanded.

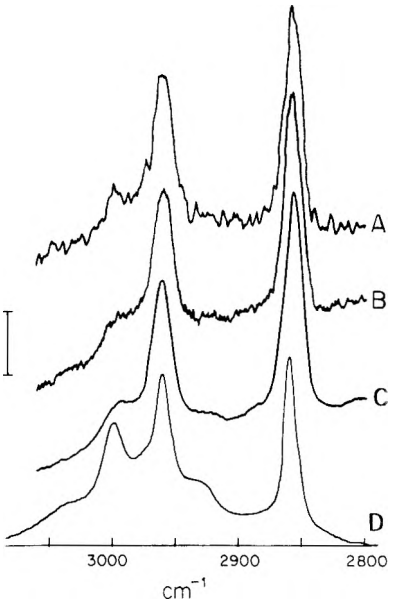


**Figure 3.** Scale expanded Raman spectra (A–C) of methylated silica from 2800- to 3150-$cm^{-1}$ shift. (D) Infrared spectrum of methylated silica. See text for scan conditions. For the intensity scale, the vertical bar to the left represents 3000 cps for the Raman spectra or a transmittance of 0.20 for the infrared spectrum on a linear transmittance scale.

However, this intensity could equally be achieved when the angle $\beta$ was in the range 45–30°. A similar arrangement is shown in Figure 1C. The laser beam was directed upward at an angle $\gamma$ by mirror m. This geometry is a compromise between those shown in Figures 1A and 1B in that we are attempting to approach a more normal incidence using only one reflecting surface. Due to our particular orientation of the laser and the spectrometer, $\gamma$ was about 75° and $\beta$ was varied between 45 to 20° for maximum intensity which was again no more than two-thirds of that achieved with Figure 1A geometry.

For the detection of strong lines the arrangements shown in Figures 1B or 1C were convenient in that the adjustment of the angle $\beta$ was not too critical. However, when the sample rested against an optical flat (in a vacuum cell or using a microscope cover glass) the maximum intensity achieved using the geometry of Figure 1A was always a factor of 2–2.5 greater than could be obtained using the other arrangements.

*Raman Spectra of Chemisorbed Methanol.* The phenomenon whereby high area oxides exhibit a strong fluorescence has been extensively dealt with in the literature.[1,2,8,11] This problem is more severe for zeolite catalysts, probably due to traces of metal ion impurities, than it is for high purity silica and, in very unfavorable cases, may cause background signals as high as $10^6$ cps whereas some Raman lines may be 4 to 5 orders of magnitude weaker. A typical background spectrum of a pressed silica disk is shown in Figure 2A. The relatively sharp features at 480, 600, 800, and 980 $cm^{-1}$ are due to Raman scattering from the silica and the very broad feature extending from 1000 to 4000 $cm^{-1}$ is the background fluorescence. The maximum of the latter shifts by about 1000 $cm^{-1}$ toward zero shift when the exciting line is changed from 488.0 to 514.5 nm. That is, the maximum remains unchanged on an absolute scale, near 18500 $cm^{-1}$. A similarly recorded spectrum of methylated silica is shown in Figure 2B. New features are indicated by vertical arrows.

The spectra shown in Figures 2A and B were recorded using the geometry depicted in Figure 1B. The scan speed was 100 $cm^{-1}$/min using a time constant ($\tau$) of 10 s, a mechanical slit width of 1600 $\mu$m, and a background zero suppression of 1700 cps. The filtered laser power at the sample was 0.60 W. The inset Figure 2C shows the 1465-$cm^{-1}$ feature recorded with a tenfold abscissa expansion using 1.7 W of unfiltered power at the sample. The peak height was 1000 cps above the base line, the scan speed was 10 $cm^{-1}$/min, the time constant was 10 s, and the spectral slit width was 10 $cm^{-1}$. The background or baseline signal level was 16000 cps so that the true peak height in absolute terms was 17000 cps. Using similar slow scan speeds, no additional features were detected in the range 100–2800 $cm^{-1}$ which were also not present in the background spectrum of silica.

The strong features between 2800 and 3050 $cm^{-1}$ are shown on an expanded scale in Figure 3. These spectra were recorded using an unfiltered beam (1.7 W) with a background signal of about 17000 cps. The scan conditions (spectral slit width 9 $cm^{-1}$) were as follows: Figure 3A, 500 $cm^{-1}$/min, $\tau$ = 0.1 s; Figure 3B, 50 $cm^{-1}$/min, $\tau$ = 1 s; Figure 3C, 10 $cm^{-1}$/min, $\tau$ = 10 s. Figure 3D shows the infrared spectrum of a 40 mg $cm^{-2}$ methylated disk which was recorded using a scan speed of 83 $cm^{-1}$/min and a spectral slit width of 2 $cm^{-1}$. The peak intensity of the strongest line at 2858 $cm^{-1}$ in the Raman spectra was 10500 cps and the geometry of Figure 1B was used. The maximum intensity achieved using the geometry of Figure 1A was 15500 cps. Finally, the Raman spectra shown in Figure 3 could also be produced using the 514.5-nm exciting line (1.5 W) although the intensity was slightly lower considering the lower power level and the red shift of the exciting radiation.

## Discussion

The interpretation of the infrared spectrum shown in Figure 3D has been discussed in detail previously.[12] Briefly, the three main absorption bands at 3000, 2958, and 2858 $cm^{-1}$ have been assigned to the three CH stretching modes of an unsymmetrical surface $SiOCH_3$ group which has one strong and two weak CH bonds. The slightly asymmetric band at 1465 $cm^{-1}$ (of shape similar to that shown in Figure 2C) was assigned to the antisymmetric deformation mode. As with the Raman spectrum, the infrared spectrum of the latter was an order of magnitude less intense than that of the $\nu$(CH) bands and a similar

situation prevails with respect to the Raman and infrared spectrum of liquid methanol. However, the Raman spectrum of liquid methanol has a very strong band at 1060 $cm^{-1}$ due to the C–O stretching mode, a band which is also intense in the infrared spectrum. A similar strong infrared band has been reported at 1082 $cm^{-1}$ in the spectrum of solid $SiH_3OCH_3$.[16] Our failure to detect the equivalent band, or any other low frequency lines, in the case of surface $SiOCH_3$ is puzzling. We suspect that this might be associated with a coupling of the low frequency modes with the lattice modes of silica which produces a broad smeared out profile which is essentially undetectable in the general background at low frequency. We have also similarly noted the absence of low frequency bands following the reaction of some halogen containing hydrogen sequestering agents (e.g., $SiCl_3CH_3$) with silica under conditions which should lead to the formation of surface $Si–O–SiCl_2CH_3$.[17] Bands due to the $\nu$(CH) modes of the methyl group have been detected in the Raman spectrum whereas no evidence for $\nu$(Si–Cl) modes has been observed. [This work is still in a preliminary stage and was carried out before we acquired our present and more sensitive Raman spectrometer. Signal-to-noise ratios were about two orders of magnitude poorer than presently obtainable so the statement above may eventually have to be modified.] Finally, the extreme broadening of low frequency modes is also apparent in several infrared studies of adsorbent–adsorbate modes due to (M = metal) M–N,[18] M–O,[18] and M–C[19,20] modes and due to the hydrogen halides on alkali halide surfaces[21] and this may be a general phenomenon.

Previous Raman spectroscopic studies[1-11] have mainly been concerned with physical adsorption on various high surface area oxides and in many cases the signal-to-noise ratio has been far worse than is routinely obtained using infrared spectroscopy. The adsorption of pyridine has been most extensively studied[5-9] because certain modes give rise to particularly strong Raman scattering and these modes ($\nu_1$ and $\nu_{12}$) shift in well-defined ways depending on the type of site pyridine attaches itself to. None the less in that and other published work the main emphasis has been on detecting small frequency shifts and changes in relative intensities as compared to the free molecule and this has been, for example, correlated with the ionic properties of cation exchanged zeolites.[8-11] The spectra shown in Figure 3 clearly demonstrate that under favorable circumstances, Raman spectra of chemisorbed species can be obtained having a signal-to-noise ratio which is comparable to that obtained using infrared spectroscopy. The sensitivity of the technique is still not as great as the infrared technique in that longer scan times (with long time constants) must be employed in order to achieve comparable spectra. (We note also that the spectral slit width was much greater in the Raman case.) None the less, for strong signals one can scan rapidly (Figure 3B) and relatively satisfactory spectra can be obtained. We anticipate that the Raman technique will prove to be a powerful new spectroscopic tool for studying chemisorbed species.

Finally, the spectra recorded here were obtained using a relatively high laser power, a desirable situation since the signal-to-noise ratio increases as the square root of the total count rate. Such power levels might not be possible with weakly chemisorbed species where local heating may become a factor, although this problem can be reduced by rotating the sample. None the less, if the photon counting system is capable of high levels of zero suppression then it is always desirable to direct as much scattered light as possible into the spectrometer. If both the fluorescence background count rate and the Raman scattering count rate increase then the signal-to-noise ratio is bound to increase. The PAR counting system used in this work is capable of suppressing background signals as high as $10^6$ cps.

*Acknowledgment.* Financial support for this work was provided by the National Research Council of Canada and by Imperial Oil Limited. The author also thanks Mary Klemes for advice concerning the experimental aspects of this work and Dr. A. H. Hardin for discussion concerning the interpretation of the low frequency portion of the spectrum.

## References and Notes

(1) T. A. Egerton and A. H. Hardin, *Catal. Rev.*, **11**, 1 (1975).
(2) R. P. Cooney, G. Curthoys, and N. T. Tam, *Adv. Catal.*, **24**, 293 (1974).
(3) P. J. Hendra and E. J. Loader, *Trans. Faraday Soc.*, **67**, 828 (1971).
(4) H. Jeziorowski and H. Knözinger, *Chem. Phys. Lett.*, **43**, 37 (1976).
(5) P. J. Hendra, I. D. M. Turner, E. J. Loader, and M. Stacey, *J. Phys. Chem.*, **78**, 300 (1974).
(6) R. O. Kagel, *J. Phys. Chem.*, **74**, 4518 (1970).
(7) M. Fleischmann, P. J. Hendra, and A. J. McQuillan, *Chem. Phys. Lett.*, **26**, 163 (1974).
(8) T. A. Egerton, A. H. Hardin, Y. Koziorovski, and N. Sheppard, *J. Catal.*, **32**, 343 (1974).
(9) T. A. Egerton, A. H. Hardin, and N. Sheppard, *Can. J. Chem.*, **54**, 586 (1976).
(10) N. T. Tam, R. P. Cooney, and G. Curthoys, *J. Chem. Soc., Faraday Trans. 1*, **72**, 2577, 2592 (1976).
(11) H. Jeziorowski and H. Knözinger, *Chem. Phys. Lett.*, **42**, 162 (1976).
(12) B. A. Morrow, *J. Chem. Soc., Faraday Trans. 1*, **70**, 1527 (1974).
(13) C. Morterra and M. J. D. Low, *Ann. N.Y. Acad. Sci.*, **220**, 135 (1973).
(14) B. A. Morrow and P. Ramamurthy, *J. Phys. Chem.*, **77**, 3052 (1973).
(15) H. J. Bernstein and G. Allen, *J. Opt. Soc. Am.*, **45**, 237 (1955).
(16) G. S. Weiss and E. R. Nixon, *Spectrochim. Acta*, **21**, 903 (1965).
(17) M. L. Hair and W. Hertl, *J. Phys. Chem.*, **77**, 2070 (1973).
(18) G. Blyholder and M. C. Allen, *J. Phys. Chem.*, **70**, 352 (1966); **69**, 3998 (1965).
(19) G. Blyholder and R. Sheets, *J. Phys. Chem.*, **74**, 4335 (1970).
(20) J. K. A. Clarke, G. M. Farren, and H. E. Rubalacave, *J. Phys. Chem.*, **72**, 327 (1968).
(21) R. St. C. Smart and N. Sheppard, *Proc. R. Soc. London, Ser. A*, **320**, 417 (1971).

# Isocyanate Formation During the Reaction of NiNO and CO on Silica-Supported Nickel

**B. A. Morrow* and L. E. Moran**

*Department of Chemistry, University of Ottawa, Ottawa, Canada K1N 6N5* *(Received August 8, 1977)*

*Publication costs assisted by Imperial Oil Limited*

Adsorbed NO on silica-supported nickel reacts at 20 °C to give NiNCO and gaseous $CO_2$. Using $C^{18}O$, the products were $NiNC^{18}O$ and a 1:2:1 mixture of $C^{16}O_2$, $C^{16}O^{18}O$, and $C^{18}O_2$, regardless of the proportions of $C^{18}O$ and $N^{16}O$ used. We postulate that the final step in carbon dioxide formation occurs when CO interacts with a surface carbonate complex which contains two oxygen atoms from the original NO.

Isocyanate intermediates have been widely reported in high temperature reactions between NO and CO over various group 8 metal catalysts.[1-6] Only over Ru has such a species been reported as a result of a reaction carried out at 20 °C.[7] Few details are available concerning the mechanism of isocyanate formation or of it's role in the possible formation of HCN or $NH_3$ in the reaction of these species over solid catalysts.[1-6]

Results are reported here of an infrared and mass spectrometric study of the reaction at 20 °C between chemisorbed NO on silica-supported nickel and CO. Adsorbed nickel isocyanate and gaseous carbon dioxide are the only reaction products and the overall reaction stoichiometry appears to be as follows:

$$2[NiNO + 2CO \rightarrow NiNCO + CO_2] \quad (1)$$

Product identification was confirmed by use of $^{13}C$, $^{15}N$, and $^{18}O$ labeled reactants and we have suggested that the final step in $CO_2$ formation occurs when CO interacts with a surface carbonate species. Our results are compared with brief earlier studies by Blyholder and Allen[8] and by Batychko et al.[9] both of whom suggested that an activated form of NiNO or $Ni(NO)^+$ was formed rather than NiNCO.

The reaction cell (volume 300 mL) and the method of catalyst preparation have been described elsewhere.[10] Catalyst sample disks were 25 mm in diameter weighing 200 mg and contained 9.2 wt % of Ni. Infrared spectra were recorded on a Perkin-Elmer Model 13G spectrometer and mass spectra were run under high resolution conditions on an A.E.I. MS902S instrument. Carbon monoxide containing 99.0% oxygen-18 was supplied by Prochem.

Following the chemisorption of a saturation dose of NO on silica-supported Ni (at least 2 Torr was added and evacuated for 30 min) only a single strong band at 1864 $cm^{-1}$ was observed as previously reported by Blyholder and Allen[8] and this was assigned to linear neutral NiNO (Figure 1A). When excess gaseous CO (>2 Torr) was subsequently added, the intensity of the 1864-$cm^{-1}$ band slowly decreased and new bands appeared at 2191 and 2082 $cm^{-1}$ (Figure 1B, C). After 3 h of CO contact time the intensity of the 1864-$cm^{-1}$ band was about halved, that of the 2191-$cm^{-1}$ band (now shifted to 2201 $cm^{-1}$) had reached its maximum intensity, and the weak band at 2082 $cm^{-1}$ remained virtually unchanged (Figure 1E). Following evacuation for 10 min the 2082-$cm^{-1}$ band disappeared whereas no changes were observed elsewhere even after 24-h evacuation.

The 1864-$cm^{-1}$ band shifted to 1829 $cm^{-1}$ when $^{15}N^{16}O$ was used whereas the 2201-$cm^{-1}$ band shifted downward by 13 $cm^{-1}$ with $^{15}N^{16}O/^{12}C^{16}O$, by 63 $cm^{-1}$ with $^{14}N^{16}O/^{13}C^{16}O$, and by 19 $cm^{-1}$ with $^{14}N^{16}O/^{12}C^{18}O$. The 2082-$cm^{-1}$ band shifted downward by 47 $cm^{-1}$ with $^{14}N^{16}O/^{12}C^{18}O$, by 52 $cm^{-1}$ with $^{14}N^{16}O/^{13}C^{16}O$, and no shift was observed with $^{15}N^{16}O/^{12}C^{16}O$.

The above isotopic shifts indicate that the species responsible for the 2201-$cm^{-1}$ band contains C, N, and O atoms and the magnitude of the shifts is comperable to that which has been reported for various surface isocyanates.[3,4,7,11] Similarly, the shifts in the 2082-$cm^{-1}$ band (and its absolute position) are consistent with the formation of linear adsorbed CO, either on Ni or NiO.[12-14] (Using our catalyst we found that when CO alone was adsorbed on bare hydrogen free Ni, the NiCO band was at 2033 $cm^{-1}$ which is close to that reported by Primet and Sheppard,[12] but when the Ni had been pretreated with $O_2$ at 20 °C then the band was at 2082 $cm^{-1}$.) It would appear that the band observed at 2180 $cm^{-1}$ by Blyholder and Allen[8] and at 2190 $cm^{-1}$ by Batychko et al.[9] after the interaction of adsorbed NO with gaseous CO is not due to an "activated" form of adsorbed NO or to $Ni(NO)^+$ but is also due to surface nickel isocyanate. (These groups did not use isotopically labeled reactants.)

In the above reaction, the bands mentioned were also generated when a less than saturation dose of NO was allowed to react with any dose of gaseous CO. The intensity of the 1864-$cm^{-1}$ band was correspondingly weaker initially and the ultimate intensity of the NiNCO band after CO was added was also weaker but in all cases about 3 h was required before the reaction apparently stopped. In all cases, regardless of the relative proportions of NO or CO used, *only* $CO_2$ plus residual CO was detected in the gas phase (there was no $N_2$, $N_2O$, $NO_2$, or $O_2$) and if $C^{18}O$ was used, in *all* cases a 1:2:1 mixture of $C^{16}O_2$, $C^{16}O^{18}O$, and $C^{18}O_2$ was detected along with $C^{18}O$ only. There was no evidence of isotopic mixing among the surface species, only $NiN^{16}O$, $NiNC^{18}O$, and adsorbed $C^{18}O$ were detected.

The generation of the 1:2:1 mixture of carbon dioxide molecules of mass 44, 46, and 48 regardless of the proportions of $C^{18}O$ and $N^{16}O$ used can most easily be rationalized if we assume that the final step in $CO_2$ formation involves the statistical decomposition of a surface complex which always contains two carbon atoms, two oxygen-16 atoms, and two oxygen-18 atoms. El Shobaky et al.[15] proposed that the interaction between adsorbed $CO_3$ and CO played an important role in the oxidation of CO to $CO_2$ over some nickel oxide catalysts and we propose that in the present case a similar mechanism applies in that $C^{18}O$ interacts with $C^{16}O_2{}^{18}O$ such that the 1:2:1 mixture of labeled $CO_2$ molecules are produced. Although the total stoichiometry could be represented by eq 1, the intermediate step might be as follows:

$$Ni + 2NiN^{16}O + 3C^{18}O \rightarrow 2NiNC^{18}O + NiC^{16}O_2{}^{18}O \quad (2)$$

$$NiC^{16}O_2{}^{18}O + C^{18}O \rightarrow Ni + 2CO_2\ [1:2:1] \quad (3)$$

The processes illustrated in eq 1-3 are only intended to indicate how a precursor $NiC^{16}O_2{}^{18}O$ species and subse-

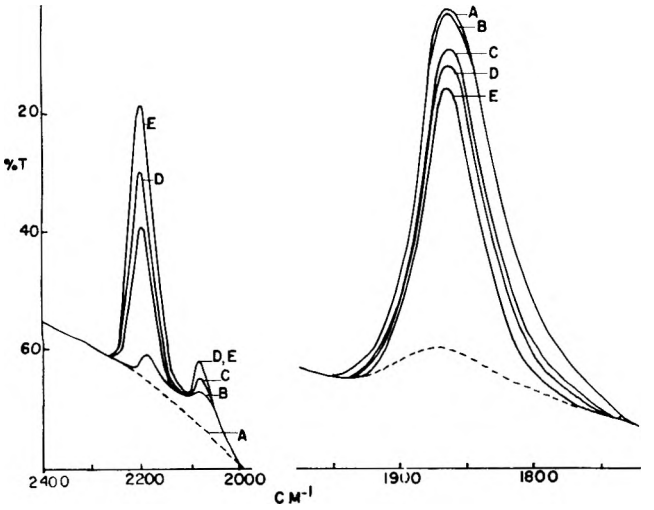


**Figure 1.** The dashed line indicates the background infrared spectrum of a $Ni/SiO_2$ sample. A compensating $SiO_2$ disk was placed in the reference beam in order to partially cancel out strong bands due to silica. The break in the spectrum at 2000 $cm^{-1}$ arises because of a grating change which requires new instrument settings: (A) after adding 10 Torr of NO and evacuating for 30 min; (B) after adding 10 Torr of CO, immediate scan. (C, D, E) after 15, 45, and 180 min, respectively.

quently $CO_2$ [1:2:1] might be generated. At this point we do not know if we should have written $NiC^{18}O$ in place of $C^{18}O$ in any of these equations, nor whether isocyanate formation only occurs after NiNO has decomposed into NiN and NiO. The latter process has been reported in the literature [8,16-18] and it is possible to devise a large number of schemes involving NiN, NiO, or NiCO which will produce the same result. The important point is that if eq 3 represents the final step leading to $CO_2$ formation, then the two oxygen-16 atoms must have come from the original $N^{16}O$ and that this was true regardless of the proportions of $N^{16}O$ and $C^{18}O$ used.

Finally, although stable metal carbonates are reported to have infrared bands in the 1500–1300-$cm^{-1}$ spectral region[19] no such bands were observed in this work. This may indicate that in excess CO reaction 3 occurs rapidly or more probably it may indicate that our proposed carbonate type intermediate has absorption bands below the silica cutoff at 1350 $cm^{-1}$.

*Acknowledgment.* Financial support for this research was provided by the National Research Council of Canada and by Imperial Oil Ltd.

## References and Notes

(1) R. A. Dalla Betta and M. Shelef, *J. Mol. Catal.*, **1**, 431 (1976).
(2) F. Solymosi, J. Sarkany, and A. Schauer, *J. Catal.*, **46**, 297 (1977).
(3) M. L. Unland, *J. Catal.*, **31**, 459 (1973).
(4) M. L. Unland, *J. Phys. Chem.*, **77**, 1952 (1973); **79**, 610 (1975).
(5) A. Hiromichi and H. Tominaga, *J. Catal.*, **43**, 131 (1976).
(6) H. Niiyama, M. Tanake, H. Iida, and E. Echigoya, *Bull. Chem. Soc. Jpn.*, **49**, 2047 (1976).
(7) M. F. Brown and R. D. Gonzalez, *J. Catal.*, **44**, 477 (1976).
(8) G. Blyholder and M. C. Allen, *J. Phys. Chem.*, **69**, 3998 (1965).
(9) S. V. Batychko, M. I. Rossov, and L. M. Roev, *Dokl. Akad. Nauk SSSR*, **191**, 328 (1970).
(10) B. A. Morrow and P. Ramamurthy, *J. Phys. Chem.*, **77**, 3052 (1973).
(11) B. A. Morrow and I. A. Cody, *J. Chem. Soc., Faraday Trans. 1*, **71**, 1021 (1975).
(12) M. Primet and N. Sheppard, *J. Catal.*, **41**, 258 (1976).
(13) R. R. Ford, *Adv. Catal.*, **21**, 103 (1970).
(14) K. Uematsu and W. Komatsu, *J. Catal.*, **17**, 398 (1970).
(15) G. El Shobaky, P. C. Gravelle, and S. J. Teichner, *J. Catal.*, **14**, 4 (1969).
(16) C. R. Brundle, *J. Vac. Sci. Technol.*, **13**, 301 (1976).
(17) H. Conrad, G. Ertl, J. Kuppers, and E. E. Latta, *Surface Sci.*, **50**, 296 (1975).
(18) G. L. Price, B. A. Sexton, and B. G. Baker, *Surface Sci.*, **50**, 506 (1976).
(19) L. H. Little, "Infrared Spectra of Adsorbed Species", Academic Press, London, 1966.

# Evidence on the Isothermal and Warm-Up Luminescence from γ-Irradiated 3-Methylpentane Glass[1,2]

**G. H. Morine and J. E. Willard***

*Department of Chemistry, University of Wisconsin, Madison, Wisconsin 53706* *(Received August 15, 1977)*

*Publication costs assisted by the United States Department of Energy*

The isothermal luminescence of γ-irradiated 3-methylpentane glass at 77 K has been found to grow in proportion to the concentration of trapped electrons to at least $2 \times 10^{19}$ eV $g^{-1}$, in contrast to the implication of reports in the literature. The appearance of luminescence peaks at two different temperatures during warm-up is evidence for neutralization of two types of cation–anion (or radical–radical) pairs, one of which is present in enhanced concentration in samples containing $O_2$. The dose dependence of the integrated warm-up luminescence indicates that the cations and/or anions responsible for the luminescence at doses less than $1 \times 10^{19}$ eV $g^{-1}$ are different from those at considerably higher doses. The extent and limits of knowledge available for assignment of the luminescence peaks to specific elementary processes are discussed.

## Introduction

Following exposure of glassy hydrocarbons to ionizing radiation, trapped electrons ($e_t^-$),[3a] radicals,[3b] and anions[3c] are observable at ≤77 K. Cations equivalent to the $e_t^-$ and anions must also be present, but no optical or definitive ESR spectra have been found for these in pure hydrocarbons, although cations of dilute additives such as olefins, biphenyl, and organic amines with known optical, ESR, or luminescent spectra are identifiable.[3d] The types of trapped cations which may be present in a typical γ-irradiated hydrocarbon glass such as 3-methylpentane (3MP) include $C_6H_{14}^+$, $C_6H_{13}^+$, $C_6H_{15}^+$, $C_{12}H_{28}^+$, and cations of impurities present initially or as the result of radiation-induced decomposition. If the spectroscopy of these species in the glassy state were accurately known, it should be possible to identify them by the spectra of the isothermal, warm-up, and photostimulated luminescence[4] emitted as a result of their neutralization by electrons and

anions in the γ-irradiated samples. Attempts at such identification have been inconclusive because of lack of knowledge of the luminescent spectra. In this paper we extend the information on isothermal and warm-up luminescence from γ-irradiated 3MP glass, and discuss alternative interpretations. We also show that the growth in isothermal luminescence intensity with dose parallels the growth in $e_t^-$ concentration, in contrast to previous[4e,f] evidence.

## Experimental Section

Phillips Pure Grade 3-methylpentane was further purified by passage through a 70-cm column of freshly activated silica gel with collection under dry nitrogen, followed by pumping on the liquid at −75 °C for 10 min and freeze–pump–thaw cycles using liquid nitrogen. It was stored over Na–K alloy, $LiAlH_4$, or Linde 10X molecular sieve freshly activated under vacuum. Following such treatment the optical density at 200 nm was ≤0.08 for a 1-cm path. (Current practice in our laboratory indicates that equal purity is obtained by degassing and exposure to activated molecular sieve without silica gel treatment.) Samples for the luminescence studies (~3.5 mL) were prepared by distillation under vacuum into 1 cm × 1 cm i.d. 5 cm high Suprasil cells.

Measurements of the luminescence intensity were made with the γ-irradiated sample mounted in a quartz Dewar with flat windows. The light was focused by a quartz lens onto the slit of a Bausch and Lomb high intensity monochrometer, or the desired wavelength range was selected by filters. Detection was by means of an RCA 1P28 photomultiplier tube coupled to an electrometer and chart recorder. The warm-up luminescence was determined during spontaneous warming following removal of the liquid nitrogen from the sample Dewar. The temperature of the sample was monitored by a thermocouple attached to the exterior of the cell.

The spectra reported here were determined by scanning the monochrometer by hand, with alternate scan directions to compensate for luminescence growth and decay during scanning. For the isothermal luminescence, the spectrum was scanned in 5-nm steps and the band shape determined. For the warm-up luminescence, only the band maxima was determined.

## Results

*Isothermal Luminescence.* The spectrum of the isothermal luminescence at 77 K from 3MP following γ irradiation at 77 K has been reported[4] to have a small band with $\lambda_{max}$ at 230 nm[4c] and a much more intense broad band for which $\lambda_{max}$ values of 425,[4a,b,f] 415,[4c] and 380 nm[4e] have been given. Our value for the latter band is 420 nm. The samples were quenched in liquid nitrogen immediately before a 5-min $1 \times 10^{19}$ eV $g^{-1}$ γ irradiation and the spectral measurements were made during ~10 min following irradiation.

For determination of the dose dependence of the isothermal luminescence, the luminescence was monitored at 400 nm at 77 K for 1 h starting 6 min after irradiation of the 3MP at 77 K (Figure 1). The samples were quenched to 77 K 25 min before the *end* of their respective irradiations, which varied from ~3 to 13 min. The results (Figure 1) indicate an approximately linear increase in luminescence with dose to $2 \times 10^{19}$ eV $g^{-1}$. To obtain the true relative luminescent intensities, correction has been made for the increase in self-absorption with dose, assuming the following: the average distance traveled by the photons in escaping the 1 cm × 1 cm cell is 0.5 cm; 54% of the $e_t^-$ decay during 1 h over which the luminescence

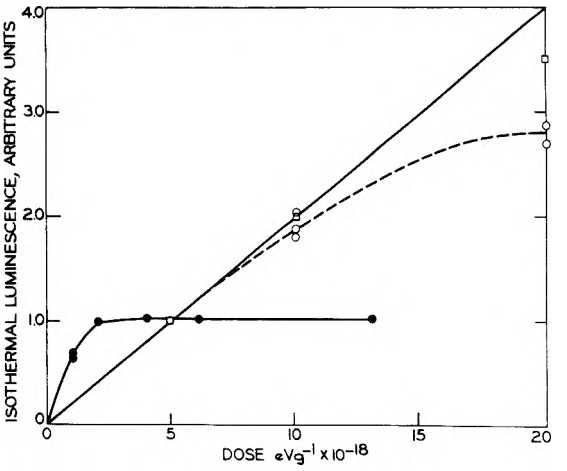


**Figure 1.** Luminescence of γ-irradiated 3MP at 77 K as a function of γ dose. Each point indicates the luminescence integrated over 1 h starting 6 min after the end of γ irradiation at a dose rate of $1.8 \times 10^{18}$ eV $g^{-1}$ $min^{-1}$. The luminescence was viewed through a monochromator set to give a band pass at half-height of about 20 nm centered at 400 nm: (O) relative intensities uncorrected for self-absorption; (□) relative intensities corrected for self-absorption (see text); (O) normalized data of Funabashi et al.[4d]

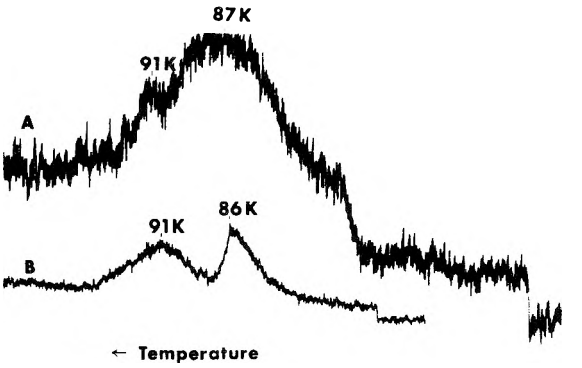


**Figure 2.** Warm-up luminescence from 3MP samples γ irradiated at 77 K. (A) Degassed sample bleached 10 min with 100-W tungsten lamp at 5 cm following $1 \times 10^{20}$ eV $g^{-1}$ γ dose. (B) Sample saturated with air before cooling to 77 K; dose, $5 \times 10^{19}$ eV $g^{-1}$; no photobleaching. The recording of A was done with higher amplification than B. For each plot the cell luminescence was essentially constant in the temperature range directly under the peaks, giving a background intensity at the level of the high temperature end of the plot.

was integrated; $G(e_t^-) = 0.7$; $\epsilon(e_t^-)$ at 1600 nm = $3 \times 10^4$; $\rho$(3MP, 77 K) = 0.87 g $cm^{-3}$; $\epsilon$(400 nm)/$\epsilon$(1600 nm) = 0.08. The average absorption may be estimated from the average of the OD values at 400 nm at the start and end of 1 h over which the luminescence was integrated.

*Warm-Up Luminescence.* Samples of pure degassed 3MP which have been γ irradiated ($5 \times 10^{18}$–$1 \times 10^{20}$ eV $g^{-1}$) at 77 K followed by bleaching the electrons with near-IR light show a broad structureless peak with maximum intensity at 86–87 K when warmed. The temperature and structure of the peak was independent of whether the luminescence was monitored at 360 or 400 nm with a monochromator or by the total light which passed a filter which eliminated wavelengths below 350 nm. The integrated warm-up luminescence intensity was approximately the same as the isothermal luminescence intensity integrated for 1 h starting 6 min after irradiation. Exposure of γ-irradiated samples to light in the 300–700-nm range before warming reduces and, with prolonged exposure, removes the 86 K peak but exposes a much smaller peak with a maximum at ~91 K (Figure 2A), which is only partially bleached on exhaustive illumination. The $\lambda_{max}$ of the spectrum of the 86 K luminescence is at

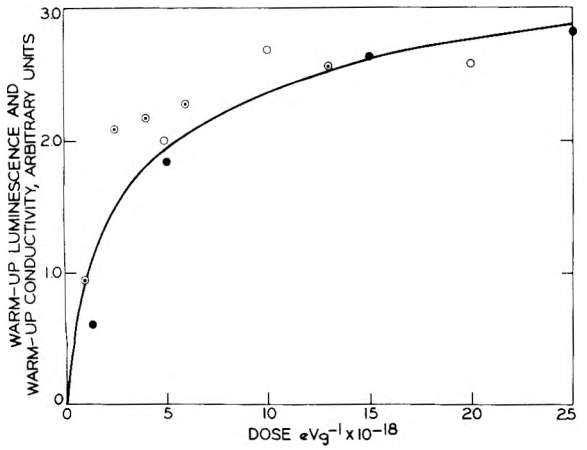


**Figure 3.** Integrated warm-up luminescence and electrical conductivity of γ-irradiated (77 K) 3MP as a function of dose to 2.5 × $10^{19}$ eV $g^{-1}$: (O) luminescence, this work, measured at 400 nm; (⊙) luminescence, ref 4d, measured at 425 nm; (●) electrical conductivity, 85 K peak, ref 19.

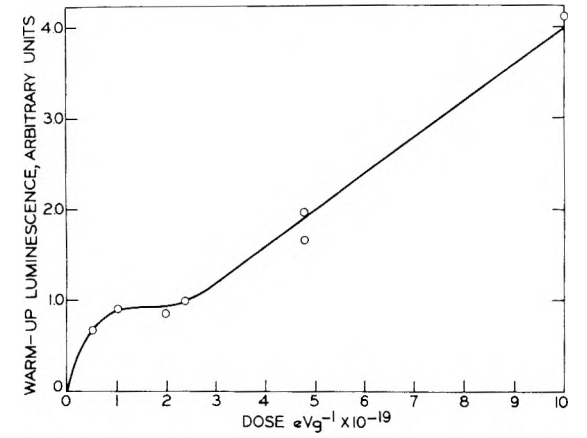


**Figure 4.** Integrated warm-up luminescence of γ-irradiated (77 K) 3MP measured at 400 nm as a function of dose to 1.0 × $10^{20}$ eV $g^{-1}$.

500 ± 20 nm, and that of the 91 K peak 380 ± 20 nm. For samples saturated with air before cooling to 77 K, the integrated warm-up luminescence is greatly increased, and the ratio of the 91 K peak to the 86 K peak is also greatly increased (Figure 2B). (It is worthy of note that the relative intensity of the 91 K peak is enhanced by the decreasing absorption of the luminescence by the sample as the reaction intermediates decay.) The freshly irradiated air-saturated samples are grey or black. This opacity, the 86 K luminescence and part of the 91 K luminescence, can be removed by exposure to light of a medium pressure Hg arc through a Pyrex filter.

The growth in warm-up luminescence of the degassed samples of 3MP with increasing γ dose was linear at doses above ~2 × $10^{19}$ eV $g^{-1}$, but not at lower doses (Figures 3 and 4). For the experiments of Figures 3 and 4 the $e_t^-$ were bleached with 950-nm light prior to warm-up. The warm-up luminescence was monitored at 400 nm at warming rates of 2–4 K $min^{-1}$ and was integrated by weighing the peak cut from the recorder paper. Correction was made for the luminescence from the cell walls. Literature values for warm-up luminescence and warm-up electrical conductivity of 3MP following γ irradiation at 77 K are included in Figure 3.

## Discussion

*Correlation of Dose Dependence of Luminescence and $e_t^-$ Concentration.* The concentration of $e_t^-$ in γ-irradiated 3MP at 77 K measured by ESR or infrared absorption increases linearly with dose at low doses, passes through a maximum at ~1 × $10^{20}$ eV $g^{-1}$, and then decreases.[5,6] By contrast the isothermal luminescence intensity integrated over 15 min following irradiation has been reported to rise to a maximum at 2–4 × $10^{18}$ eV $g^{-1}$ [4d,f] and thereafter remain constant to at least 1.4 × $10^{19}$ eV $g^{-1}$.[4e] If these observations are both correct, the apparent lack of correlation between $e_t^-$ concentration and luminescence intensity implies that the photon yield per electron which combines with a cation decreases dramatically with increasing dose above 2 × $10^{18}$ eV $g^{-1}$ indicating a changing mechanism of neutralization with increasing dose. We have, therefore, determined the growth in integrated isothermal luminescence with dose under conditions similar to those under which the growth in [$e_t^-$] has been studied. The data plotted in Figure 1 show linearity to at least 1 × $10^{19}$ eV $g^{-1}$ and (after correction for the absorption of luminescence by the growing concentration of reaction products[2] and some electron decay during irradiation) near linearity to 2 × $10^{19}$ eV $g^{-1}$, without evidence of the plateau onset at 2–4 × $10^{18}$ eV $g^{-1}$ previously observed. It appears that the plateau observed in the earlier work may have resulted from the competition between the production and decay of $e_t^-$ having reached a steady state at the relatively low dose rate used. The initial half-life for $e_t^-$ decay in 3MP at 77 K varies from ~6 min in unannealed samples in ESR tubes and 25 min for unannealed samples in 1 cm × 1 cm cells to 60 min in well-annealed samples.[7] The dose rates used in the experiments where the plateaus were obtained[4d,f] appear to have been ~2 × $10^{17}$ eV $g^{-1}$ $min^{-1}$, requiring 20 min to reach 4 × $10^{18}$ eV $g^{-1}$. The determinations of growth in $e_t^-$ concentration with dose were made in one case[5] at a 15-fold higher dose rate, requiring a much shorter irradiation time, and in another[6] at 71 K where $e_t^-$ decay is negligible.

Above ~2 × $10^{19}$ eV $g^{-1}$ the rate of growth of $e_t^-$ concentration with dose decreases.[5] This is attributable to prompt capture of a portion of the $e^-$ by the growing concentration of trapped radicals in competition with stable trapping. In this dose region the molar heat of photobleaching of those $e^-$ which are trapped decreases with increasing dose,[8] consistent with the conclusion that the fraction reacting with radicals rather than cations is increasing. It may be assumed that, in this dose region, the isothermal luminescence per mole of $e_t^-$ decaying, measured at 400 nm, would decrease in parallel with the decrease in heat of reaction since the energy of attachment of electrons to radicals is too low (0.5–1 eV)[9] to produce 400-nm photons.

*Warm-Up Luminescence.* The data of Figure 2 show that radiation-produced ions and/or radicals which are quite stable in 3MP at 77 K migrate sufficiently rapidly at higher temperatures so that at a warming rate of ~3 K $min^{-1}$ they all react at ~95 K. At least two discrete populations are indicated by the peaks at 86 and 91 K. The complete elimination of the 86 K peak by exposure of the sample to UV radiation is evidence that it results from reaction of carbanions with cations, the carbanions being removed[3c] by photodetachment when illuminated.

The fact that the 91 K peak is only partially removed by pre-warm-up illumination suggests that it may be the result, in part at least, of radical–radical combination. The difference in photoeffects, the relative enhancement of the 91 K peak by the presence of oxygen, and the difference in $\lambda_{max}$ for the two peaks indicate that they are caused by different species. However, it should be noted that even if all the luminescence were caused by the same species, two peaks might be resolved in the warm-up spectrum, the first resulting from short-range intraspur encounters and

the second resulting from random encounters required for reaction when the spurs are depleted. The contrast between the rates of intraspur reaction and random-encounter reaction is illustrated by these two modes of radical decay in γ-irradiated 3MP glass.[3b] Such spatial control may contribute to the peak separation shown in Figure 2.

Two peaks in the warm-up luminescence of γ-irradiated 3MP, one with $\lambda_{max}$ at ~83 K and one at ~93 K, which are qualitatively similar to those of Figure 2, have been reported[4d] to have different rates of growth with dose. The first increases rapidly with dose below $2 \times 10^{18}$ eV g$^{-1}$ and relatively slowly thereafter. The second peak is negligible below $2 \times 10^{18}$ eV g$^{-1}$ but grows rapidly thereafter up to $1.4 \times 10^{19}$ eV g$^{-1}$, the highest dose tested. A similar feature seems to be reflected in the plot of integrated warm-up luminescence at 400 nm as a function of dose shown in Figure 4 where a rapid initial rise followed by a leveling off is followed by a renewed but slower rise. This suggests that the nature of the cation–anion population formed during the initial stages of irradiation is such as to yield more photons per neutralization event than are produced by the combining species at higher doses. The nature of the predominant cationic or anionic species may change with dose because (1) a charge scavenging impurity is depleted; (2) the concentration of a charge scavenging stable product grows; (3) the solvent radicals, which increase in concentration linearly with dose,[3b] capture progressively more of the electrons or positive charge or both. The latter effect would be expected to become significant only at concentrations high enough for spur overlap to be significant. There is evidence[6] for the onset of such overlap of electron spurs at $<1.2 \times 10^{19}$ eV g$^{-1}$ in 3MP at 77 K.

Sawai has reported that luminescence during warming 3MP to 83 K following γ irradiation at 77 K extends from ~390 to 500 nm with a maximum at ~425 nm. On heating to 90 K, an emission from ~470 to 600 nm with a maximum at 530 nm appeared. The integrated 530-nm luminescence grew linearly with dose to $\geq 7 \times 10^{18}$ eV g$^{-1}$, with no plateau. This dose is in the range which might appear linear on the initial rising portion of Figures 3 and 4.

*Species Which May Be Responsible for the Luminescence.* The only reactions in γ-irradiated organic glasses which are sufficiently exothermic to produce excited species which can luminesce in the visible-UV region are neutralization (of cations by either electrons or anions) and radical–radical reactions. For such luminescence to occur, the product molecule must have excited states available in the appropriate energy region. Both the spectrum and the probability of light emission from these excited states may be different in the glassy phase than in the gas or liquid. The glass provides a dielectric medium which (1) reduces the total energy of neutralization; (2) constrains free rotation, with the result that the excited molecules may luminesce from a geometry characteristic of the cation rather than the lowest excited state of the neutral molecule; (3) may reduce the decomposition of excited molecules, and hence increase the probability of luminescence from the undecomposed form. The influence which these solid state effects may have on the luminescence spectra, and the current lack of knowledge of the identity of the predominant cation in γ-irradiated hydrocarbons, lead to considerable uncertainty in the assignment of the luminescence peaks to specific processes. Also, it is not known whether the luminescence is the product of neutralization of the predominant charged species or only a minor component of the cations and/or anions. There is evidence[10] that only a small fraction of the neutralization events (e.g., $10^{-3}$) result in the emission of photons, but also evidence that for liquid hydrocarbons[11] the low emission yield is due to a low fluorescence yield from the first excited singlet state, rather than to a low $G$ value for the production of this state.

Despite the uncertainities noted above, it is useful to consider what may be concluded from present knowledge about the elementary processes responsible for the luminescence. There is definitive evidence from ESR spectra of γ-irradiated 3MP for the presence of secondary 3-methylpentyl radicals[12] and physically trapped electrons[3a] (produced with $G$ values of 3.0[3b] and 0.7,[13] respectively). Anions, presumed to be predominantly $C_6H_{13}^-$, are indicated by their photodetachment which produces observable electrons[3c] and by their optical absorption.[5] The possible cations include $C_6H_{14}^+$, $C_6H_{13}^+$ (formed in the primary ionization event or by capture of migrating positive charge by $C_6H_{13}$ radicals), $C_6H_{15}^+$ (formed by proton transfer), $C_{12}H_{26}^+$ (formed by $C_6H_{14}^{+*} + C_6H_{14} \rightarrow C_{12}H_{26}^+ + H_2$), and $C_6H_{12}^+$ (formed by capture of positive charge by radiation-produced olefin molecules, or by $C_6H_{14}^{+*} \rightarrow C_6H_{12}^+ + H_2$ where the asterisk indicates an excited state of the cation).

It may be concluded with conviction, based on much evidence, that the isothermal luminescence from γ-irradiated 3MP at 77 K results from neutralization of cations by $e_t^-$ which tunnel and/or diffuse from their traps. As noted above, the 86 K peak of the warm-up spectrum may be assigned with some certainty to the neutralization of cations by anions and it appears that the 91 K peak may involve contribution from both anion–cation and radical–radical combination. These species must be heavier and more slowly diffusing than those responsible for the 86 K peak. The ions may be oxy ions (e.g., $C_6H_{13}O_2^-$ formed by reaction of $O_2^-$ with $C_6H_{13}$ or $C_6H_{13}^-$ with $O_2$) and the radicals may be peroxy radicals (e.g., $C_6H_{13}O_2\cdot$ formed by reaction of $C_6H_{13}\cdot + O_2$), since the peak is greatly enhanced in the presence of $O_2$. In carefully degassed samples the peak is small and is detectable only if a portion of the 86 K peak has been removed by UV exposure at 77 K prior to warm-up. This residual 91 K peak must result from (1) oxy ions or radicals formed from trace $O_2$ remaining even after careful degassing; (2) $C_{12}H_{26}^+$; (3) reactions of cations with anions from different spurs after the spur concentrations have been depleted.

Some assignments of the luminescence peaks from γ-irradiated 3MP glass to specific processes have been suggested in the literature. The 230-nm band observed by Merkel and Hamill[4c] has been attributed by them to fluorescence from the first excited singlet of $C_6H_{14}$ on the basis of the $\lambda_{max}$ of 231 nm reported[14] for the fluorescence from liquid 2-methylpentane when activated by 165-nm radiation. This assignment is plausible but it appears impossible with present knowledge to eliminate alternative possibilities: e.g., the fluorescence of $C_6H_{12}^*$ formed by (1) $C_6H_{14}^+ + e^- \rightarrow C_6H_{14}^* \rightarrow C_6H_{12}^* + H_2$, or (2) $C_6H_{13}^+ + e^- \rightarrow C_6H_{12}^* + H$, or (3) $C_6H_{12}$ + a mobile positive hole $\rightarrow C_6H_{12}^+$, $C_6H_{12}^+ + e^- \rightarrow C_6H_{12}^*$. It has been suggested[4c] that the latter process, involving reaction with a stable radiation product, is ruled out by the observation that the luminescence intensity reaches a saturation level with increasing dose[4d] and by the finding that when a sample is re-irradiated following melting and refreezing the luminescence is not greater than that from the initial irradiation.[4c,10a] As described above, it now appears that the reported saturation of luminescence with dose was simply a result of proportionality of the luminescence intensity

to the $e_t^-$ concentration in experiments where the latter reached a plateau at low doses. Likewise, the re-irradiation tests do not prove that radiation-produced olefins are unimportant since the olefin concentration in the melted and refrozen samples would be much lower than the local olefin concentration in the radiation-produced spurs. Thus the reasons for discarding excited olefins as the source of the observed luminescence do not now appear compelling. It has been reported[10a] that the presence of $10^{-3}$ mole fraction of olefins or diolefins in alkane glasses greatly increases the luminescence observed after $\gamma$ irradiation and, in other work, that $10^{-2}$ mole fraction of 2-methyl-1-pentene in 3MP glass increased the luminescence.[4f] The absorption spectra ($S_0 \rightarrow S_1$) of various olefins show red limits near 200 nm.[15] The 230-nm luminescence of $\gamma$-irradiated 3MP is in the correct energy region to represent olefin fluorescence and has a lifetime <2 ms,[4c] consistent with an allowed transition.

If the 230-nm band is due to fluorescence from an excited olefin, it is plausible that the 420-nm band is the result of phosphorescence from the same molecule. Gas phase electron impact studies show first excited triplet levels of olefins at 4.2–4.3 eV.[16] If the luminescence spectrum is a mirror reflection of the absorption spectrum (hypothetical in this case), the 420-nm (3 eV) band may be olefin phosphorescence rather than the alkane phosphorescence which has been suggested.[4c]

The 86 K warm-up luminescence peak with $\lambda_{max}$ at 480–520 nm which we have observed must include the same species as the integrated luminescence in the 83–90 K range observed by Sawai.[4f] If this luminescence is the result of cation–anion neutralization, it is probable that it comes from the same excited state species as the luminescence from neutralization of the cation by an electron, which gives the 420-nm band of isothermal luminescence. The energy required to remove electrons from the carbanions is not sufficient to reduce the energy of neutralization below that of the first excited triplet of the neutralization product. The red shift of some 0.5 eV for the warm-up luminescence is not inconsistent with this conclusion because of the following: (1) the decreased energy available from neutralization of the cation by a molecular anion rather than an electron may result in emission from a lower vibrational level of the same electronic state; (2) the viscosity of 3MP decreases from $10^{12}$ P at 77 K to $10^8$ P at 86 K.[17] At 77 K the rigidity of the glass may be expected to impede rotation to the equilibrium angle of the excited olefin molecule from that of the cation being neutralized. If such rotation is possible at the lower viscosity at 86 K, the energy of the first excited triplet state and hence of the phosphorescence will be reduced. The principles of such effects have been discussed.[14b,18] Geometric effects may also result in different vibrational levels of the electronic ground state being populated when the excited molecule emits, thus changing the photon energy. The difference in $\lambda_{max}$ for the luminescence from polycrystalline isopentane at 77 K (410 nm) as compared to glassy isopentane (490 nm)[4b] appears to be an example of the results of viscosity related geometric effects.

## References and Notes


(1) This work has been supported in part by the U.S. Energy Research and Development Administration under Contract No. EY-76-S-02-1715.A001 and by the W. F. Vilas Trust of the University of Wisconsin.
(2) Further details of this work are given in the Ph.D. Thesis of G. H. Morine, University of Wisconsin—Madison, 1975.
(3) See for examples and references: (a) J. E. Willard, *J. Phys. Chem.*, **79**, 2966 (1975); (b) M. A. Neiss and J. E. Willard, *ibid.*, **79**, 783 (1975); (c) D. P. Lin and J. E. Willard, *ibid.*, **78**, 1135 (1974); (d) W. H. Hamill, "Ionic Processes in $\gamma$-Irradiated Organic Solids at −196 °C" in "Radical Ions", E. T. Kaiser and L. Kevan, Ed., Wiley, New York, N.Y., 1968, p 321.
(4) (a) M. Burton, M. Dillon, and R. Rein, *J. Chem. Phys.*, **41**, 2228 (1964); (b) O. Janssen and K. Funabashi, *ibid.*, **46**, 101 (1967); (c) P. Merkel and W. Hamill, *ibid.*, **53**, 3414 (1970); (d) K. Funabashi, P. Herley, and M. Burton, *ibid.*, **43**, 3939 (1965); (e) K. Funabashi, C. Herbert, and J. Magee, *J. Phys. Chem.*, **75**, 3221 (1971); (f) T. Sawai, *J. Nucl. Sci. Technol.*, **8**, 431 (1971).
(5) A. Ekstrom, R. Suenram, and J. Willard, *J. Phys. Chem.*, **74**, 1883 (1970).
(6) D. P. Lin and L. Kevan, *J. Chem. Phys.*, **55**, 2629 (1971).
(7) D. Shooter and J. E. Willard, *J. Phys. Chem.*, **76**, 3167 (1972).
(8) S. L. Hager and J. E. Willard, *J. Chem. Phys.*, **63**, 942 (1975).
(9) A. Gaines and F. Page, *Int. J. Mass. Spectrom. Ion Phys.*, **1**, 315 (1968).
(10) (a) B. Brocklehurst and J. Robinson, *Chem. Phys. Lett.*, **10**, 277 (1971); (b) B. Brocklehurst, *Int. J. Radiat. Phys. Chem.*, **6**, 483 (1974).
(11) L. Walter and S. Lipsky, *Int. J. Radiat. Phys. Chem.*, **7**, 175 (1975).
(12) (a) D. Henderson and J. E. Willard, *J. Am. Chem. Soc.*, **91**, 3014 (1969); (b) T. Ichikawa and N. Ohta, *J. Phys. Chem.*, **81**, 561 (1977).
(13) For references see T. Kimura, N. Bremer, and J. E. Willard, *J. Chem. Phys.*, **66**, 1127 (1977).
(14) (a) F. Hirayama, W. Rothman, and S. Lipsky, *Chem. Phys. Lett.*, **5**, 296 (1970); (b) W. Rothman, F. Hirayama, and S. Lipsky, *J. Chem. Phys.*, **58**, 1300 (1973).
(15) J. G. Calvert and J. N. Pitts, Jr., "Photochemistry", Wiley, New York, N.Y., 1966.
(16) J. H. Moore, Jr., *J. Phys. Chem.*, **76**, 1130 (1972).
(17) A. C. Ling and J. E. Willard, *J. Phys. Chem.*, **72**, 1918 (1968).
(18) J. Simons, "Photochemistry and Spectroscopy", Wiley, New York, N.Y., 1971.
(19) B. K. Dietrich, Ph.D. Thesis, University of Wisconsin—Madison, 1971.


# Optical Absorption Spectrum of Chromium(II) Chloride Single Crystals


**David R. Rosseinsky* and Iain A. Dorrity**

*Department of Chemistry, The University, Exeter, England*

*(Received July 19, 1977)*


The spectra from 5000 to 30 000 $cm^{-1}$ of single crystals of $CrCl_2$ have been examined from 300 to 6 K. In making assignments and estimating energy levels, literature treatments of free-ion levels were examined, and the Racah formalism found inadequate; Ferguson's free-atom method served best. The spin allowed transitions were interpreted for a $D_{4h}$ field giving $Dq$, $Ds$, and $Dt$. Quintet–triplet transitions are interpreted as for $O_h$, for several reasons. Intensities and their temperature dependences were examined.


The spectra of the chromium dihalides have received little attention compared with the other transition metal dihalides and, in general, the electronic spectra of Cr(II) compounds have not been extensively studied, largely because they are so readily oxidized. Most of the work has concentrated on the spin-allowed transition $^5E_g(^5D) \rightarrow$

TABLE I: Observed and Calculated Energies, Relative to the $^5D$ Ground State, of the Triplet Terms of the Free $Cr^{2+}$ Ion

| Term | Obsd energy, $cm^{-1}$ | Calcd energies, $cm^{-1}$ | | | | |
|---|---|---|---|---|---|---|
| $^3H$ | 17064 | 16860 | 16188 | 17040 | 16064 | 17500 |
| $^3P_2$ | 17152 | 19058 | 18934 | 19243 | 17768 | 19884 |
| $^3F_3$ | 18176 | 19388 | 19598 | 19595 | 18461 | 20119 |
| $^3G$ | 20521 | 20935 | 20663 | 21190 | 20559 | 21550 |
| $^3D$ | 25419 | 26640 | 27920 | 27000 | 26852 | 27220 |
| $^3F_4$ | 42952 | 44092 | 45698 | 44695 | 44594 | 45016 |
| $^3P_4$ | 48857 | 44422 | 46362 | 45047 | 45287 | 45251 |
| $B/cm^{-1}$ | | 815 | 895 | 830 | 899 | 810 |
| $C/cm^{-1}$ | | 3400 | 3152 | 3430 | 3117 | 3565 |
| $C/B$ | | 4.17 | 3.52 | 4.13 | 3.47 | 4.40 |
| Ref | 17 | 2 | 5 | 18 | 19 | 20 |

$^5T_{2g}(^5D)$ which is often split by Jahn–Teller (distortion) lowering of the orbital degeneracy of these states,[1-3] and few complete analyses[2,4-6,29] of the spin-forbidden transitions have been reported. Diffuse reflectance[2,3,7] and single crystal[5,8] spectra of $CrF_2$ have been reported and there are considerable differences in their interpretation and assignments. For $CrCl_2$, only diffuse reflectance[7,9] studies have been made, but no attempt has been made to assign the observed broad spin-allowed transitions and weak sharp spin-forbidden transitions.

Recently there has been interest[10-12] in the spin-forbidden transitions in the spectra of ferro- and antiferromagnetic Cr(II) compounds and their anomalous intensities and temperature dependence have been related to the magnetic coupling in these compounds. Since $CrCl_2$ is antiferromagnetic it might thus be expected that its spectrum would show similar behavior.

There have been several studies[13-16] of the crystal structure of $CrCl_2$ and reasonable agreement is found for the orthorhombic unit-cell parameters, the unit-cell containing two molecules. In this structure, each $Cr^{2+}$ ion is at the center of a plane of four $Cl^-$ ions, and an additional two $Cl^-$, at longer distances, are almost at right angles to the planar $CrCl_4$ unit. These tetragonally distorted octahedra share their shortest edges to form densely packed chains parallel to the c axis. This tetragonal Jahn–Teller distortion might be expected to have an appreciable effect on the optical absorption spectrum, giving rise to band splittings from the deviation from $O_h$ symmetry.

Antiferromagnetism sets in at the Néel temperature $T_N$ = 20 K and neutron diffraction studies[13] establish that the magnetic unit cell has $b$ and c values double those of the crystallographic unit cell. The structure consists of ferromagnetic (011) planes of $Cr^{2+}$ ions with parallel spins, with adjacent planes having oppositely orientated spins. (The ferrogmagnetic planes are incorrectly identified as (001) planes in ref 30.) From consideration of the intensities of the magnetic reflections, the magnetic moments of the $Cr^{2+}$ ions were found[13] to be directed along one of the long Cr–Cl bonds.

## Free Ion Spectrum

The experimentally observed energies of the terms of the $d^4$ configuration of $Cr^{2+}$ have been given by Moore.[17] From these, the centers of gravity of the spin–orbit components of the triplet terms can be determined, as by Oelkrug[2] and McPherson et al.[4] There is poor agreement between their respective derived values, and so the energies have now been rederived (Table I). These energies differ considerably from those given by Oelkrug,[2] but are in agreement with those of McPherson et al.,[4] apart from the energies of the $^3P_2$ and $^3P_4$ terms.

Several sets of values of the Racah interelectronic repulsion parameters $B$ and $C$, obtained from fitting to the free ion spectrum, are available in the literature. However, Table I shows that the calculated energies are in poor agreement with the observed. No unique set of values of $B$ and $C$ can fit all the free ion energy levels, since the sum of the energies of the $^3P$ states should equal the sum of the energies of the $^3F$, obviously not the case.

As the theory is inadequate for the free ion, calculations made for the $Cr^{2+}$ ion in a ligand field using the strong field scheme will also be considerably in error. Substitution of the reduced experimentally observed term energies directly into the weak field matrices will allow more accurate calculations and assignments to be made.[1,34]

## Experimental Section

Chromium dichloride (Alfa Inorganics) was sublimed at ≃800 °C in silica tubes sealed under vacuum; the commercial product appeared to be contaminated with traces of violet-colored $CrCl_3$ and possibly $Cr_2O_3$. Attempts were made to grow large crystals from melts, but the resultant boules consisted of numerous crystalline regions rather than one single crystal. Only small crystals ~3 × 2 mm could be cleaved from these boules due to this, and to the frequent cleaving along the $c$ axis to form very small needles.

The spectra were measured at 300, 70, and 6 K, in the range 5000–30 000 $cm^{-1}$, with the incident light propagated perpendicular to the crystallographic $c$ axis, using a Beckman Acta MIV spectrophotometer. The crystals were clamped over ≃1.5 mm circular apertures punched in brass plates, and inserted in the sample chamber of an Oxford Instruments CF200 continuous-flow liquid helium cryostat. Temperatures were determined and controlled to within ±2 K by an Oxford Instruments VC30 temperature controller.

The integrated intensities of the observed absorptions were determined by measuring the band areas with a planimeter, but the corresponding oscillator strengths could not be calculated because of the extraordinary difficulty experienced in measuring the thicknesses of the samples, which were probably about 100 μm. Attempts using a micrometer were unsuccessful due to small size and fragility, and measurements using an optical interference technique[21-24] were not applicable.

Recorded absorbance vs. wavelength spectra in the 7000–15 000-$cm^{-1}$ region were replotted for linearity in wavenumber and resolution into Gaussian components using a Dupont 310 curve resolver.

## Results and Discussion

*Quintet–Quintet Transitions.* In an octahedral ligand field the $^5D$ ground state of the free $Cr^{2+}$ ion is split into two terms $^5E_g$ and $^5T_{2g}$, differing by $10Dq$, and thus only one spin-allowed transition $^5E_g \rightarrow {}^5T_{2g}$ is expected. However, since the $CrCl_6$ units here are tetragonally distorted, the effect of the lower symmetry field must be considered in the assignment of the quintet–quintet transitions in $CrCl_2$. For this assignment, the symmetry at the $Cr^{2+}$ site may be considered to be $D_{4h}$, although the symmetry is less than this, since the $CrCl_6$ octahedra are angularly distorted as well as axially lengthened. In a $D_{4h}$ ligand field the $^5D$ free ion term is split giving rise to four quintet states. As the distortion in $CrCl_2$ takes the form of an axial elongation of the $CrCl_6$ octahedra, the $^5B_{1g}$ term is predicted[3] to be the ground state, and three spin-allowed transitions from this state to the other quintet states are thus expected.

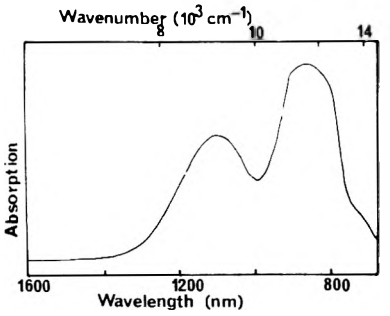


**Figure 1.** Absorption spectrum of $CrCl_2$ in near-IR region at 6 K.

TABLE II: **Assignments and Observed Energies at 6 K of Spin-Allowed Transitions and Ligand Field Parameters for $CrF_2$ and $CrCl_2$**

| Assignment | Theoretical Formula | Obsd energies, cm$^{-1}$ $CrF_2$[a] | $CrCl_2$[b] |
|---|---|---|---|
| $^5B_{1g} \rightarrow {}^5A_{1g}$ | $4Ds + 5Dt$ | 10495 | 9100 |
| $^5B_{1g} \rightarrow {}^5B_{2g}$ | $10Dq$ | 11623 | 11050[c] |
| $^5B_{1g} \rightarrow {}^5E_g$ | $10Dq + 3Ds - 5Dt$ | 14669 | 12250[c] |
| $Dq$/cm$^{-1}$ | | 1162 | 1100 |
| $Ds$/cm$^{-1}$ | | 1934 | 1470 |
| $Dt$/cm$^{-1}$ | | 551 | 640 |

[a] Experimental data for $CrF_2$ from Table II of ref 5. [b] Fackler and Holah[9] observed maxima at 8750 and 12 000 cm$^{-1}$ in diffuse reflectance spectrum at 77 K. [c] Maxima of Gaussian components resolved from band at ≃11750 cm$^{-1}$.

In the spectrum of $CrCl_2$, an intense extremely broad absorption centered at ≃11 000 cm$^{-1}$ was observed at room temperature. On cooling to liquid helium temperatures, the absorption decreased in intensity and revealed two bands at ≃9000 and 11 750 cm$^{-1}$ and a weak shoulder at ≃14 000 cm$^{-1}$, as shown in Figure 1. Gaussian analysis of this absorption enabled the higher-energy band to be resolved into two components centered at 11 050 and 12 250 cm$^{-1}$. By comparison with other Cr(II) spectra,[1-3,9] the three lower-energy bands are assigned to spin-allowed transitions to the $^5A_{1g}$, $^5B_{2g}$, and $^5E_g$ levels, respectively. The shoulder at 14 000 cm$^{-1}$ most probably arises from the presence of a Cr(III) impurity, due to oxidation of the sample. (A broad spin-allowed band, assigned to the $^4A_{2g}(^4F) \rightarrow {}^4T_{2g}(^4F)$ transition, assuming $O_h$ symmetry, is observed[25] at ≃14 200 cm$^{-1}$ in the spectrum of $CrCl_3$ at 4.2 K.) A similar shoulder is also observed in the diffuse reflectance spectrum of $CrCl_2$ reported by Clark.[7]

The ligand field parameters $Dq$, $Ds$, and $Dt$ can be derived empirically from the spectra using the theoretical expressions[3,26] for the transition energies shown in Table II, together with their values at 6 K and the assignments of the spin-allowed transitions. Both $Ds$ and $Dt$ are found to be positive, as expected[3] from consideration of the nature of the distortion in $CrCl_2$. For comparison are presented the corresponding assignments and parameters derived from the 6 K spectrum of $CrF_2$ of Lim and Stout.[5] These values are not Lim and Stout's, since their assignments indicate an unexpectedly small separation between the $^5B_{1g}$ and $^5A_{1g}$ levels, an incorrect sequence of the $^5E_g$ and $^5B_{2g}$ energy levels, and lead to tetragonal splitting parameters $Ds$ and $Dt$ of opposite sign.[34] The assignments given here accord with those of Oelkrug[23] for the room temperature spectrum of $CrF_2$, although he was not able to resolve the $^5B_{1g} \rightarrow {}^5A_{1g}$ transition and thus did not derive values of the parameters $Ds$ and $Dt$.

*Quintet–Triplet Transitions.* A series of sharp bands, which are much less intense than the quintet–quintet transitions, was observed in the spectrum of $CrCl_2$ in the 15 000–22 000 cm$^{-1}$, and corresponds to spin-forbidden transitions. This spectral region is shown in Figure 2 at temperatures of 300, 70, and 6 K.

The Cr site in $CrCl_2$ being tetragonally elongated, the analysis of these transitions should be carried out on the basis of a $D_{4h}$ ligand field, as for the spin-allowed transitions. However, the $D_{4h}$ weak-field matrices have not been formulated, and since, as discussed above, the theoretical formulation of the free ion terms for the $Cr^{2+}$ free ion is inadequate, it is doubtful whether the $D_{4h}$ strong-field matrices[27] provide a basis for the assignment of the spectrum of $CrCl_2$. Furthermore, although this spectral region is complex, it does not appear to be consistent with the presence of the ten transitions which are predicted to occur with the assumption of $D_{4h}$ symmetry. Polarization measurements for interpretation on this basis were not found possible due to the difficulties in cleaving the crystals. The analysis of the visible spectrum of $CrCl_2$ was thus carried out on the basis of an octahedral ligand field. Despite the heavy emphasis above on the tetragonal distortion in $CrCl_2$, especially in the interpretation of the spin-allowed transitions, it nevertheless appears that this approximation is justified by the close similarity of the spectrum to those of Cr(II) chloro complexes,[4,6,12] such as $RbCrCl_3$ and $CsCrCl_3$, in which the $Cr^{2+}$ ion is approximately octahedrally coordinated, and, anticipating the results of this section, by the good agreement between the calculated and observed energies. In the assignment of the spin-forbidden bands of tetragonally distorted Cr(II) complexes[2,8,11] it was noted that the positions of the transitions were almost constant despite the various distortions of the $Cr^{2+}$ environment, and it was concluded[11] that either "the ligand field states retain their cubic symmetry or the lower than cubic symmetry states are insensitive to distortions in the ligand field".

The ligand field calculations of the quintet–triplet transitions were carried out by computer diagonalization of the crystal field energy matrices. The weak field matrices for a $d^4$ ion in an octahedral ligand field, derived by Ferguson et al.,[28] were used and the reduced experimental free-ion term energies were substituted directly into them. Treatment of off-diagonal elements in the free-ion energy matrix follows ref 28.

Table III shows the observed and calculated energies of the quintet–triplet transitions. These calculated energies were obtained by varying the effective free-ion term energies and the best fit was obtained with the percentages of the free-ion values shown in this table, and using a $Dq$ value of 1100 cm$^{-1}$, derived from the energy difference of the $^5B_{1g}$ and $^5B_{2g}$ levels observed in the spin-allowed transitions. The calculated energies were found to be relatively insensitive to the choice of $Dq$, except for the $^5E_g \rightarrow {}^3T_{1ag}(^3H)$ transition, but since this transition was not observed, not much significance can be attached to the $Dq$ value, given here, although it should be noted that $Dq$ is approximately 1100 cm$^{-1}$ for octahedral Cr(II) chloro complexes.

Agreement between the calculated and observed energies is remarkably good, especially considering the nature of the approximation involved in the assumption of octahedral symmetry. The transition to the $^3T_{1g}{}^a(^3H)$ level was calculated to occur at 6620 cm$^{-1}$, but the observed spectrum, recorded down to 5000 cm$^{-1}$, showed no trace of any absorption in this region. A similar failure to observe this transition in the spectrum[2,5] of $CrF_2$, which is also tetragonally distorted, has also been reported, but it has been observed[2,4,6,29] in the spectra of other tetragonally distorted

TABLE III: Observed (6 K) and Calculated Energies Relative to Ground State $^5E_g(^5D)$ and Assignments of Spin-Forbidden Transitions of $CrCl_2$

| Assignment | Energy, $cm^{-1}$ Obsd[a] | Calcd[b] |
|---|---|---|
| $^3T_{1g}{}^a(^3H)$ | | 6450 |
| | 16000 | |
| | 16069 | |
| | 16108 | |
| $^3E_g(^3H)$ | 16129 | 16130 |
| | 16152 | |
| | 16181 | |
| | 16236 | |
| $^3T_{1g}{}^b(^3H)$ | 16281 | 16270 |
| | 16351 | |
| | 16592 | |
| $^3T_{2g}(^3H)$ | 16736 | |
| | 16854 | 16570 |
| | 16941 | |
| | 17109 | |
| | 17352 | |
| | 17421 | |
| $^3A_{2g}(^3F)$ | 17503 | 17600 |
| | 17537 | |
| | 17636 | |
| $^1E_g$, $^1T_{2g}(^1I)^c$ | 17777 | - |
| | 17841 | |
| | 18786 | |
| $^3A_{1g}(^3G)$ | 19036 | 18670 |
| | 19312 | |
| | 20790 | |
| | 20863 | |
| | 20946 | |
| $^3E_g(^3G)$ | 21034 | 21200 |
| | 21132 | |
| | 21331 | |
| $^3T_{1g}(^3P)$ | $\simeq$25300[d] | 25160 |

[a] Fackler and Holah[9] observed bands at 16300, 17500, and 19000 $cm^{-1}$ in the diffuse reflectance spectrum at 77 K. [b] These energies have been calculated with $Dq$ = 1100 $cm^{-1}$ and with the $^3G$, $^3H$, $^3D$, $^3P$, and $^1P$ term energies reduced to 91%, and the $^3F$ and $^1F$ term energies reduced to 88%, of the free ion values (see Table I). [c] Tentative assignment; the energy of this transition has not been calculated, see text. [d] Observed as a shoulder on the onset of charge transfer absorption.

approximately octahedral Cr(II) complexes. Possibly the missing transition is obscured by the low-energy tail of the spin-allowed transitions.

The assignments, given by Alcock et al.[6] for the spectra of $CsCrCl_3$ and $RbCrCl_3$, were made on the basis of calculations using the theoretical Racah formalisms of the free ion energies in the weak field matrices, and differ in some cases from those presented here. From earlier arguments regarding the free ion spectrum of $Cr^{2+}$, the calculations given here are freer of objection and appear to provide a better description of the observed spectrum. The spectra of these chloro complexes lack an equivalent of the absorption centered at $\simeq$17800 $cm^{-1}$ in the 6 K spectrum of $CrCl_2$ (Figure 2) and its assignment to a quintet triplet transition is problematic. Instead it is tentatively assigned to the transitions to the singlet levels $^1E_g$, $^1T_{2g}(^1I)$. Calculation of the energies of these transitions, using the free atom method as employed for the triplet terms, was not possible since the only singlet states that have been observed[17] in the free-ion spectrum are the $^1F$ and $^1G$ terms. However, inspection of the energy level diagram[19] for a $d^4$ ion in an $O_h$ ligand field reveals that these transitions are expected to occur in this region.

The band assigned to the $^5E_g \rightarrow {}^3E_g(^3G)$ transition centered at $\simeq$21100 $cm^{-1}$ appears to lie on top of a very broad, weak absorption. The presence of traces of Cr(III) as an impurity in the sample is the probable cause of this latter absorption, since the absorption spectrum[25] of $CrCl_3$ shows the broad spin-allowed transition $^4A_{2g}(^4F) \rightarrow {}^4T_{1g}(^4F)$ (assuming $O_h$ symmetry at $\simeq$19900 $cm^{-1}$ at 4.2 K). Clark's diffuse reflectance spectrum[7] of $CrCl_2$ shows an intense broad band at $\simeq$20000 $cm^{-1}$, which indicates his sample was severely contaminated with Cr(III).

TABLE IV: Relative Integrated Intensities[a] of Absorptions in $CrCl_2$ Spectrum

| Transition | Relative integrated intensity 300 K | 70 K | 6 K |
|---|---|---|---|
| Spin-allowed absorptions[b] | 1000 | 740 | 630 |
| $^5E_g(^5D) \rightarrow {}^3E_g(^3H)$, $^3T_{1g}{}^b(^3H)$ | 31 | 21 | 14 |
| $^5E_g(^5D) \rightarrow {}^3T_{2g}(^3H)$ | 20 | 19 | 13 |
| $^5E_g(^5D) \rightarrow {}^3A_{2g}(^3F)$ | [c] | 9 | 8 |
| $^5E_g(^5D) \rightarrow {}^3A_{1g}(^3G)$ | 69 | 61 | 33 |
| $^5E_g(^5D) \rightarrow {}^3E_g(^3G)$ | $\simeq$38[d] | 32 | 17 |

[a] Intensities relative to combined intensities of spin-allowed absorptions (= 1000) at 300 K. [b] Combined intensities of spin-allowed transitions to $^5A_{1g}$, $^5B_{2g}$, and $^5E_g$ levels. [c] Not sufficiently resolved at 300 K. [d] Approximate value due to overlapping with charge-transfer absorption.

A considerable amount of fine structure was observed in all the observed bands at 6 K, probably due to the effects of spin–orbit splitting, coupling with phonon and magnon modes, and to the symmetry's being lower than $O_h$. Definite assignments of this structure were not possible.

*Intensities and Temperature Dependence of Spectra.* The difficulties in measuring the thicknesses of the crystals precluded the determination of the oscillator strengths of the observed transitions. However, it is still possible to make some comments of a qualitative nature on their relative intensities, which are given in Table IV. For the spin-allowed quintet–quintet transitions a decrease in intensity as the temperature was lowered was observed. This is as expected and is typical of the behavior of vibronically assisted electronic transitions which show a temperature dependence of the type

$$f(T) = f(0) \coth (h\nu/2kT)$$

The effect of temperature on the spin-forbidden transitions is somewhat different, and although the determination of the integrated intensities of some of the bands is only approximate at 300 K due to the overlapping of adjacent absorptions, Table IV shows that there is only a small decrease in intensity between 300 and 70 K. The exception to this behavior is the band assigned to the $^5E_g(^5D) \rightarrow {}^3A_{2g}(^3F)$ transition, which appears to increase in intensity. At 6 K, however, the spectrum is substantially different, becoming much more complex with the bands showing considerable fine structure. The integrated intensities of all the transitions, with the exception of the transition to the $^3A_{2g}(^3F)$ level, are considerably less at this temperature than at 70 K, and this observed decrease over the 64 K temperature range is much greater than that observed over the 230 K range from 300 to 70 K. In addition, the low-frequency onsets of all the bands, except the manifold attributed to the $^5E_g(^5D) \rightarrow {}^3T_{2g}(^3H)$ transition, become very sharp (see Figure 2).

Anomalously intense spin-forbidden transitions have been observed before in the spectra of various other antiferromagnetic and ferromagnetic Cr(II) compounds,[2,10-12] and the intensities of these bands have been ascribed to the effects of an exchange-induced electron dipole

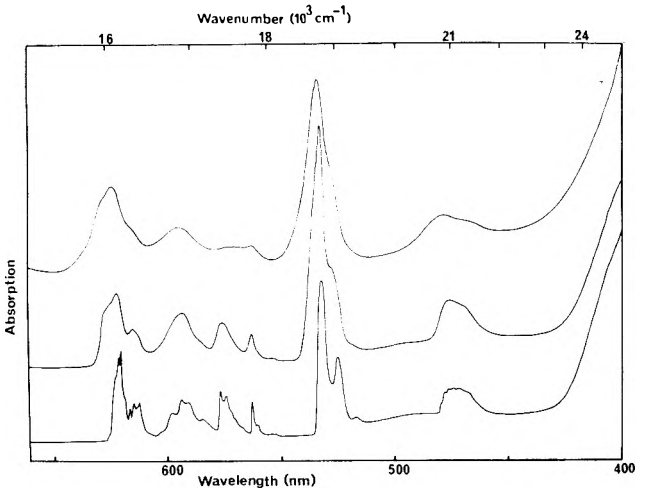


**Figure 2.** Absorption spectrum of $CrCl_2$ in 650–400-nm region: upper trace, 300 K; middle trace, 70 K; lower trace, 6 K.

mechanism, which is related to the magnetic coupling in these compounds. Furthermore, the intensities of the transitions to the $^3E_g(^3H)$ and $^3A_{1g}(^3G)$ levels (octahedral assignments) in the spectrum of ferromagnetic $K_2CrCl_4$ were observed[10] to decrease almost to zero below the Curie temperature, $T_C$ = 65 K, when ferromagnetic ordering set in.

$CrCl_2$ has[13] a Néel temperature of $T_N$ = 20 K and the observed decrease in intensity of the quintet–triplet transitions between 70 and 6 K is most likely related to the onset of antiferromagnetic ordering involving a contribution to the intensities from an exchange-type mechanism. This temperature dependence is in accordance with that experimentally observed and predicted from theoretical considerations,[31,33] for antiferromagnets such as $MnF_2$ and $RbMnF_3$. The spin-forbidden absorptions in these compounds were observed to undergo a sharp decrease in intensity at the Néel temperature, the magnitude of the change being related to the relative contributions from magnon "hot" bands (exciton − magnon), magnon "cold" bands (exciton + magnon), and phonon modes. Further analysis must await detailed studies of the temperature variation of $f$, which to save an immense amount of preparative time should be conducted on a microspectrophotometer requiring much smaller crystals than we found necessary.

## References and Notes


(1) J. Ferguson, *Prog. Inorg. Chem.*, **12**, 159 (1970).
(2) D. Oelkrug, *Ber. Bunsenges. Phys. Chem.*, **70**, 736 (1966).
(3) D. Oelkrug, *Struct. Bonding*, **9**, 1 (1971).
(4) G. L. McPherson, T. J. Kistenmacher, J. B. Folkers, and G. D. Stucky, *J. Chem. Phys.*, **57**, 3771 (1972).
(5) P. E. Lim and J. W. Stout, *J. Chem. Phys.*, **63**, 4886 (1975).
(6) N. W. Alcock, C. F. Putnik, and S. L. Holt, *Inorg. Chem.*, **15**, 3175 (1976).
(7) R. J. H. Clark, *J. Chem. Soc.*, 417 (1964).
(8) W. Holloway and M. Kestigan, *Spectrochim. Acta*, **22**, 1381 (1966).
(9) J. P. Fackler and D. G. Holah, *Inorg. Chem.*, **4**, 954 (1965).
(10) L. F. Larkworthy and A. Yavari, *J. Chem. Soc., Chem. Commun.*, 632 (1973).
(11) P. Day, A. K. Gregson, and D. H. Leech, *Phys. Rev. Lett.*, **30**, 19 (1973).
(12) L. F. Larkworthy, J. K. Trigg, and A. Yavari, *J. Chem. Soc.*, 1879 (1975).
(13) J. W. Cable, M. K. Wilkinson, and E. O. Wollan, *Phys. Rev.*, **118**, 950 (1960).
(14) H. P. Oswalt, *Helv. Chim. Acta*, **44**, 1049 (1961).
(15) L. L. Handy and N. W. Gregory, *J. Chem. Phys.*, **19**, 1314 (1951).
(16) J. W. Tracey, N. W. Gregory, E. C. Lingafelter, J. M. Dunitz, H. C. Mez, R. E. Scheringer, H. Y. Yakel, and M. K. Wilkinson, *Acta. Crystallogr.*, **14**, 927 (1961).
(17) C. E. Moore, *Natl. Bur. Stand. (U.S) Circ.*, **No. 467** (1952).
(18) J. S. Griffith, "The Theory of Transition Metal Ions", University Press, Cambridge, 1961.
(19) E. König and S. Kremer, *J. Phys. Chem.*, **78**, 56 (1974).
(20) Y. Tanabe and S. Sugano, *J. Phys. Soc. Jpn.*, **9**, 753 (1954).
(21) D. S. Martin, Jr., L. D. Hunter, R. Kroening, and P. E. Fanwick, *Inorg. Chem.*, **12**, 301 (1973).
(22) R. F. Kroening, L. D. Hunter, R. M. Rush, D. S. Martin, Jr., and J. C. Clardy, *J. Phys. Chem.*, **77**, 3077 (1973).
(23) R. F. Kroening, R. M. Rush, D. S. Martin, Jr., and J. C. Clardy, *Inorg. Chem.*, **13**, 1366 (1974).
(24) R. M. Rush, D. S. Martin, Jr., and R. G. LeGrand, *Inorg. Chem.*, **14**, 2543 (1975).
(25) C. Limido, G. Pedroli, and G. Spinolo, *Solid State Commun.*, **11**, 1385 (1972).
(26) C. J. Ballhausen, "Introduction to Ligand Field Theory", McGraw-Hill, New York, N.Y., 1962.
(27) J. R. Perumareddi, *J. Phys. Chem.*, **78**, 2678 (1974).
(28) J. Ferguson, H. J. Guggenheim, and E. R. Krausz, *Aust. J. Chem.*, **22**, 1809 (1969).
(29) T. Li and G. D. Stucky, *Acta. Crystallogr., Sect. B*, **29**, 1529 (1973).
(30) R. Colton and J. H. Canterford, "Halides of the First Row Transition Metals", Wiley-Interscience, London, 1969.
(31) K. Shinagawa and Y. Tanabe, *J. Phys. Soc. Jpn.*, **30**, 1280 (1971).
(32) T. Fujiwara and Y. Tanabe, *J. Phys. Soc. Jpn.*, **32**, 912 (1972).
(33) T. Fujiwara, W. Gebhardt, K. Pentanides, and Y. Tanabe, *J. Phys. Soc. Jpn.* **33**, 39 (1972).
(34) D. R. Rosseinsky and I. A. Dorrity, *Coord. Chem. Rev.*, in press.


# Calculated Effects of Distortion on the Electric Field Gradient Parameters of Nitrogen-14 in Pyridinium and Imidazolium Ions


**William L. McCullen and Theodore L. Brown***

*School of Chemical Sciences and Materials Research Laboratory, University of Illinois, Urbana, Illinois 61801*

*(Received July 7, 1977)*


The effects on the electric field gradient parameters of $^{14}N$ of distorting a proton from its equilibrium position have been calculated for pyridinium and imidazolium ions using orbital populations generated by a parameter-free approximate molecular orbital method. The results indicate that small in-plane distortions cause $e^2Qq_{zz}/h$ to decrease by less than 2% while $\eta$ may increase significantly. Small out-of-plane distortions result in increasing $e^2Qq_{zz}/h$ by less than 2% and decreasing $\eta$ by less than 3%.


Utilization of double resonance methods for the detection of $^{14}N$ NQR spectra permits the detection of low frequency quadrupole transitions characteristic of coordinated nitrogen. Accordingly, this technique holds considerable promise for the study of diamagnetic complexes involving nitrogen donor ligands. It has been possible, using a modification of the Townes-Dailey model,[1] to account for the $^{14}N$ NQR spectra of coordinated

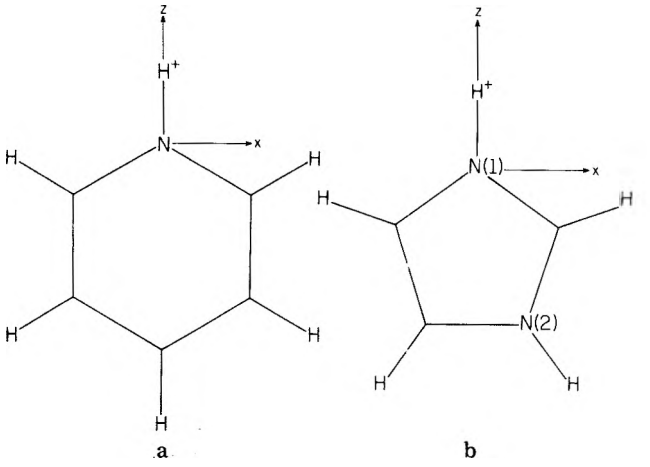


**Figure 1.** Coordinate system for pyridinium (a) and imidazolium (b).

pyridine, phenanthroline, and imidazole.[2-4] In all these cases, the nitrogen is in a quasi-trigonal environment, in which the two N-C bonds and the N-M bond lie in a plane. In applying the Townes-Dailey model to such complexes, we have made the assumption that the metal-nitrogen bond lies along the C-N-C angle bisector, and in the plane of the ligand. However, there are many compounds in which this condition may not hold. For example, in phenanthroline complexes, the metal-nitrogen internuclear axis typically lies 8-10° away from the pseudo-twofold axis through the nitrogen. In addition, packing considerations within the lattice may cause monodentate ligands such as pyridine or imidazole to be displaced so that the metal-nitrogen vector lies away from the in-plane bisector of the C-N-C angle. It is thus important to know the effect of these distortions on the values of the quadrupole coupling constant, $e^2Qq_{zz}/h$, and asymmetry parameter, $\eta$.

We have attempted to evaluate the importance of distortions by calculating the effect of angular distortions on $e^2Qq_{zz}/h$ and $\eta$ at nitrogen in pyridinium and imidazolium ions. These species may be considered to be "complexes" of the neutral ligands, pyridine, and imidazole, respectively, with the proton as Lewis acid. The nitrogen orbital population in the bond to the proton in these species is lower than in the metal complexes of these ligands. In effect, the proton is a stronger Lewis acid than any of the other metal ion species studied. Accordingly, the effects of distortion in pyridinium and imidazolium ions should represent an upper limit to the effects observed in complexes of pyridine and imidazole with metal ions.

## Calculations

The calculations were carried out using a parameter-free approximate molecular orbital method described elsewhere.[5] The geometry employed for pyridine is an idealized structure based on crystal structure data.[6] All C-H bond distances were assumed to be 1.08 Å.[7] An identical geometry is assumed for pyridinium, with addition of a proton to the nitrogen atom, N-H bond distance = 1.08 Å. The geometry assumed for imidazole is that based on a microwave structural study.[8] The geometry for the imidazolium ions is the same as that for imidazole, with the addition of a proton to N(1) with an assumed N-H bond distance of 0.998 Å. The numbering of atoms for pyridinium and imidazolium are shown in Figure 1.

It is important to note that the imidazolium ion is *not* assumed to have $C_{2v}$ symmetry, as is in fact the case for this species. By retaining the ring geometry of neutral imidazole, the amino nitrogen is made to retain an environment which we expect more closely resembles that in metal ion complexes of imidazole.

The molecular orbital calculations provide a set of eigenvectors for the occupied molecular orbitals. Using these the field gradient at nitrogen has been calculated using two levels of approximation. In method I, the field gradient is assumed to arise entirely from the imbalance of nitrogen 2p orbital populations. These are evaluated as the gross atomic orbital populations, assuming a Mulliken population analysis; i.e.

$$N_i = \sum_k N_k(C_{i,k}^2 + \sum_j C_{i,k}C_{i,j}S_{i,j}) \quad (1)$$

where the summation $k$ is over the occupied molecular orbitals of population $N_k$. In method II, additional contributions to the field gradient from charges residing on other atoms are included. These are estimated by computing the net charge in each of the other atoms in the structure, and evaluating the contribution to the field gradient from that net charge in terms of a classical expression for the contribution to the field gradient, i.e.

$$q_{zz}^{\,i} = \sum_\alpha \left(\frac{3\cos^2\theta - 1}{r_{i\alpha}^3}\right)[Z - \sum_m \sum_l N_m(C_{l,m}^2 + \sum_j C_{l,m}C_{j,m}S_{lj})]_\alpha \quad (2)$$

where the summation $\alpha$ is over the other atoms of the molecule. In this expression, $Z$ represents the nuclear charge excluding that balanced by core electrons, and the summation within the bracketed expression represents shielding of that nuclear charge by the electrons occupying the valence atomic orbitals of that atom.

The molecular orbital calculations were carried out for the neutral ligands, pyridine and imidazole, and for the pyridinium and imidazolium ions. For both ions the calculations were repeated with the proton displaced from the in-plane bisector of the CNC angle, in 1° intervals up to 10° displacements. The displacements were made both in-plane and out-of-plane. In the case of the imidazolium ion, the in-plane displacements were carried out in both directions, since these are nonequivalent in that species.

## Results and Discussion

The many attempts which have been made to calculate the quadrupole coupling constant and asymmetry parameter at $^{14}N$ in pyridine, imidazole, and other nitrogen-containing heterocycles have met with varying degrees of success.[8-14] Our method of calculation here does not represent an attempt to improve upon earlier calculations. Our concern is mainly with the changes in the field gradient tensor which occur upon movement of the proton away from the equilibrium position. Thus it is only necessary that the calculations provide a reasonably realistic representation of the field gradient tensor in the neutral ligand and in the ion.

From the population analysis, the diagonal components of the field gradient tensor in the axis systems shown in Figure 1 can be calculated from the following expressions:[15]

$$V_{ZZ} = eq_0[N_{p_z} - {}^1/_2(N_{p_x} + N_{p_y})] \quad (3)$$

$$V_{YY} = eq_0[N_{p_y} - {}^1/_2(N_{p_x} + N_{p_z})] \quad (4)$$

$$V_{XX} = eq_0[N_{p_x} - {}^1/_2(N_{p_y} + N_{p_z})] \quad (5)$$

where $q_0$ is obtained as described below. These diagonal components are relabeled so that $V_{ZZ} \geq V_{YY} \geq V_{XX}$. Then $e^2Qq_{zz}/h = eQV_{ZZ}/h$, and

$$\eta = (V_{XX} - V_{YY})/V_{ZZ} \quad (6)$$

The quantity $q_0$ is calculated using the Clementi SCF atomic wavefunction[16] for the 2p orbital of nitrogen to be

TABLE I: Calculated and Observed Field Gradients

| | Method I | | Townes-Dailey populations | | | Method II | | Exptl | | |
|---|---|---|---|---|---|---|---|---|---|---|
| | $e^2Qq_{zz}/h$, MHz | $\eta$ | $2p_x$ | $2p_y$ | $2p_z$ | $e^2Qq_{zz}/h$, MHz | $\eta$ | $e^2Qq_{zz}/h$, MHz | $\eta$ | Ref |
| Pyridine | −5.827 | 0.0137 | 1.09278 | 1.09875 | 1.75340 | −5.850 | 0.0460 | 4.584 | 0.396 | 14 |
| Pyridinium | −1.750 | 0.4518 | 1.14720 | 1.31492 | 1.08771 | −1.891 | 0.4624 | 1.090 | 0.509 | 2 |
| Imidazole[a] | −5.158 | 0.2407 | 1.09678 | 1.19018 | 1.72563 | −5.146 | 0.2618 | 3.679[b] | 0.022 | 4 |
| Imidazolium[a] | −2.360 | 0.5253 | 1.16166 | 1.38125 | 1.06837 | −2.504 | 0.5833 | 1.451[c] | 0.717 | 4 |

[a] Data for imino nitrogen. [b] Data for *N*-benzylimidazole,[4] chosen because it is free of hydrogen-bonding complications. [c] Data for imidazolium iodide.[4]

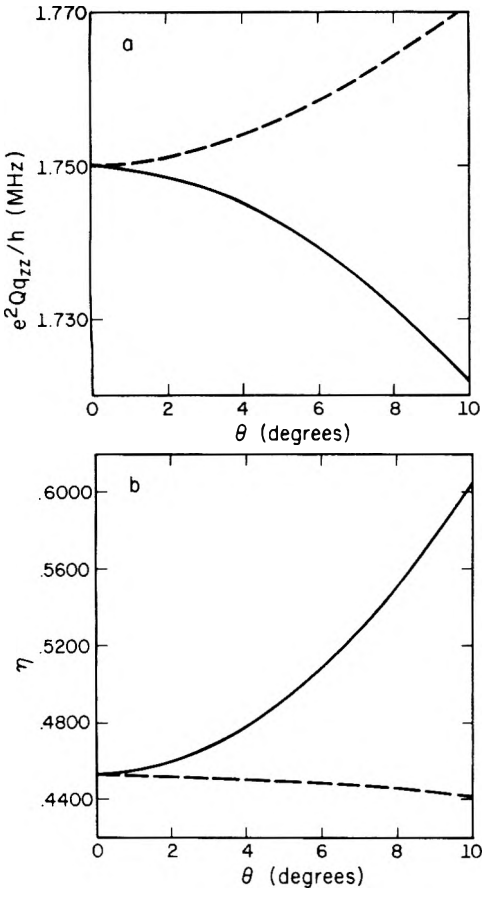


**Figure 2.** Calculated results for pyridinium: (a) graph of $e^2Qq_{zz}/h$ vs. $\theta$ (angle of distortion); (b) graph of $\eta$ vs. $\theta$. The solid curve represents the in-plane results; the dashed curve represents the out-of-plane results.

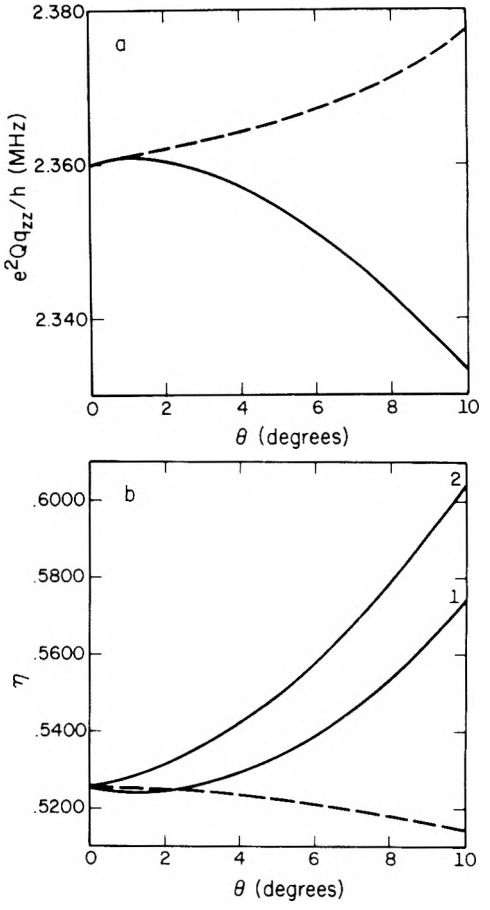


**Figure 3.** Calculated results for imidazolium: (a) graph of $e^2Qq_{zz}/h$ vs. $\theta$; (b) graph of $\eta$ vs. $\theta$. The dashed curve represents the out-of-plane results; curve 1 represents the in-plane distortion toward N(2), and curve 2 represents the in-plane distortion away from N(2).

$1.632 \times 10^{25}$ cm$^{-3}$. The value of $Q$ is chosen so that $e^2Qq_{zz}/h = 8.86$ MHz. This leads to a value of $Q = 0.0156$ b. Using these values, the field gradient parameters for pyridine and pyridinium listed in Table I were obtained, using both method I and method II. As expected the values resulting from these two treatments differ by less than 10%.

Protonation of pyridine radically affects the electronic environment about the nitrogen, in producing a large decrease in $e^2Qq_{zz}/h$. The principal axis system undergoes reorientation, such that the major axis of the field gradient tensor lies normal to the ring. These calculated results are in general agreement with the observations, although the detailed fit with experimental data is not very good. The fact that the major field gradient axis is normal to the plane of the ring suggests that in-plane motions of the proton in the pyridinium ion will have a negligible effect on $e^2Qq_{zz}/h$, whereas out-of plane distortions might be expected to have a larger effect.

Figure 2 shows the changes in $e^2Qq_{zz}/h$ and $\eta$ resulting from *in-plane* distortion of the hydrogen in the pyridinium ion. In keeping with expectations the change in the quadrupole coupling constant is quite small, less than 1.5% as calculated by either method. Such change as does occur results from slightly increased populations of the $2p_x$ and $2p_z$ orbitals, with concurrent reduction in the population of the proton 1s orbital. The asymmetry parameter undergoes comparatively much larger change. This is to be expected, since the asymmetry parameter will depend upon the redistribution of electron density of the $2p_x$ and $2p_z$ orbitals.

Out-of-plane distortion of the proton in pyridinium causes the quadrupolar coupling constant to increase. Surprisingly, the change is again quite small, amounting only to about 1.25% for a 10° distortion. The change in asymmetry parameter, which amounts to a decrease of 2.2% for a 10° distortion, is also quite small.

The results of the calculations for imidazolium are displayed in Table I. As expected, protonation of the unshared electron pair of the imino nitrogen causes a large decrease in $e^2Qq_{zz}/h$ and $\eta$.

The changes in $e^2Qq_{zz}/h$ and $\eta$ for distortions of the hydrogen in imidazolium are displayed in Figure 3. The

values for $e^2Qq_{zz}/h$ were the same for both cases of the in-plane distortions of imidazolium, thus only two curves are shown in Figure 3a. The calculations show than an in-plane distortion in either direction away from the bisector of the C–N–C angle causes a small decrease in the quadrupole coupling constant. When the proton is moved toward N(2), the calculated change in $\eta$ is about 4% for a 10° distortion. On the other hand, $\eta$ changes by about 16% when the proton is moved in the opposite direction in-plane. Just as for pyridinium ion, out-of-plane distortion causes only a small change in either the quadrupole coupling constant or asymmetry parameter. It is noteworthy also that angular distortions of the proton bound to N(1) produce changes of less than 1% in either the quadrupole coupling constant or asymmetry parameter at the amino nitrogen, N(2). These results are consistent with our expectation that the electronic environment at N(2) is virtually insensitive to small changes occurring at N(1).

Results of these calculations show quite clearly that angular distortions in the coordination environment of the ligated nitrogen in coordinated pyridine or imidazole are not likely to have a significant effect on the observed quadrupole coupling constant. On the other hand, in-plane distortions may have somewhat larger effects on the asymmetry parameter, $\eta$. The fact that both in-plane and out-of-plane distortions produce only small perturbations in $e^2Qq_{zz}/h$ suggests that this quantity is likely to be insensitive to distortions regardless of the direction of the principal component of the field gradient tensor. However, the sensitivity of $\eta$ to distortions may vary from one coordination situation to another. The present calculations do lend support to the validity of the approximations made in interpreting the field gradient parameters for $^{14}N$ in the several types of complexes which have already been studied.

*Acknowledgment.* This research was supported by the National Science Foundation through Grant CHE 76-17570. Thanks are due Dennis Lichtenberger and Barbara Jones for development of the molecular orbital program package.

### References and Notes

(1) C. H. Townes and B. P. Dailey, *J. Chem. Phys.*, **17**, 782 (1949).
(2) Y. N. Hsieh, G. V. Rubenacher, C. P. Cheng, and T. L. Brown, *J. Am. Chem. Soc.*, **99**, 1384 (1977).
(3) C. P. Cheng, B. Plankey, J. V. Rund, and T. L. Brown, *J. Am. Chem. Soc.*, in press.
(4) C. I. H. Ashby, C. P. Cheng, and T. L. Brown, to be published.
(5) M. Hall and R. Fenske, *Inorg. Chem.*, **11**, 768 (1972).
(6) F. Durant, J. Verbist, and M. Van Meerssche, *Bull. Soc. Chim. Belg.*, **75**, 806 (1966).
(7) B. Bak, L. Hansen-Nygaard, and J. Tastrup-Andersen, *J. Mol. Spectrosc.*, **2**, 361 (1958).
(8) (a) T. Ha, *Chem. Phys. Lett.*, **37**, 316 (1976); (b) G. Blackman, R. Brown, F. Burden, and I. Elsum, *J. Mol. Spectrosc.*, **60**, 63 (1976).
(9) E. Schempp and P. J. Bray, *J. Chem. Phys.*, **48**, 2381 (1968).
(10) S. Eletr. *Mol. Phys.*, **18**, 119 (1970).
(11) E. Kochanski, J. Lehn, and B. Levy, *Theor. Chim. Acta*, **22**, 111 (1971).
(12) T. Ha and C. O'Konski, *Int. J. Quantum Chem.*, **7**, 609 (1973).
(13) L. Krause and M. Whitehead, *Mol. Phys.*, **26**, 503 (1973).
(14) L. Guibé, *Ann. Phys. (Paris)*, **7**, 177 (1961).
(15) E. Schempp and B. J. Bray in "Physical Chemistry, An Advanced Treatise", Vol. IV, D. Henderson, Ed., Academic Press, New York, N.Y., 1970, Chapter II.
(16) E. Clementi and C. Roetti, *At. Data Nucl. Data Tables*, **14**, 177–478 (1974).

# COMMUNICATIONS TO THE EDITOR

## Spin Exchange and Broadening of Electron Spin Resonance Spectra in Solutions

*Sir:* The study of spin exchange in liquids is a powerful tool in the analysis of the diffusional process in liquids. The widths of individual hyperfine lines of free radicals in liquids are observed to broaden with increasing free radical concentration. This phenomena is due to spin exchange interactions which cause the magnetic environment of an electron spin undergoing magnetic resonance to fluctuate. We are concerned in this communication with the diffusion of free radicals in solution.

Pake and Tuttle[1] first described exchange broadening in terms of radical–radical encounter rate, $\nu$:

$$W = k\nu p + R$$

where $W$ is the ESR line width in gauss, $k$ a constant, $\nu$ the radical–radical encounter rate, and $p$ the probability that exchange will occur upon radical–radical collision. The encounter rate is normally related to the solvent viscosity, $\eta$, and temperature, $T$, through the Stokes–Einstein equation. Hence a plot of line width against $T/\eta$ should be linear. Deviations from this behavior have been reported by Edelstein et al.[2] More recently Povich[3] examined the relationship between line width, viscosity, and temperature using dilute nitroxide free-radical solutions of different viscosities. The results show that broadening is linear with respect to temperature in contrast to the Stokes–Einstein equation. Povich[3] examined the data of Edelstein et al.[2] and showed that similar linear $W$–$T$ behavior is observed for di-*tert*-butyl nitroxide in degassed propane. No explanation was offered for these observations. In this communication we show that these observations can be readily explained by current theories of the liquid state.

Hildebrand[4] showed the similarity between viscous flow and diffusion and presented a new diffusion mechanism where the mean free paths are only small fractions of the molecular diameter. This is in contrast to the well-known rate theory approach where mean free paths equal to the molecular diameter are needed, thereby introducing an activation energy for diffusion. Sridhar and Potter,[5] following the work of Hildebrand,[4] derived an equation for predicting diffusion coefficients in liquids. This equation gives reasonable predictions compared to other available

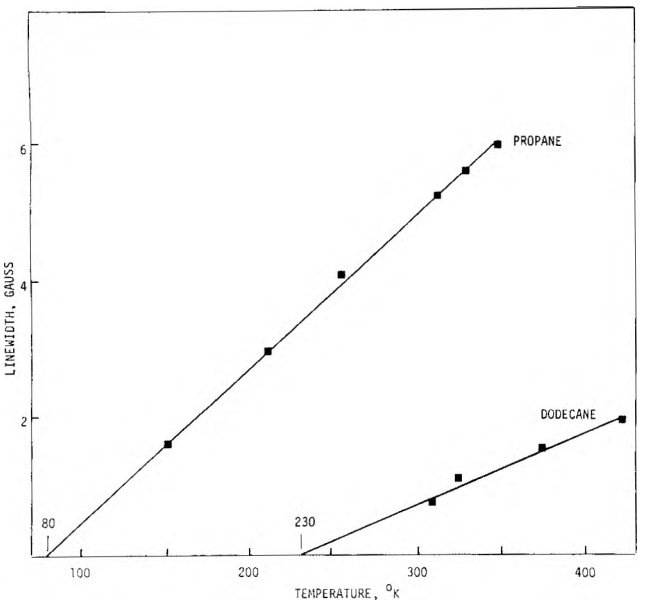


**Figure 1.** ESR line width of propane and dodecane, Data obtained from ref 2 and 3. Extrapolation to zero line width gives the temperature at which the diffusion coefficient is zero.

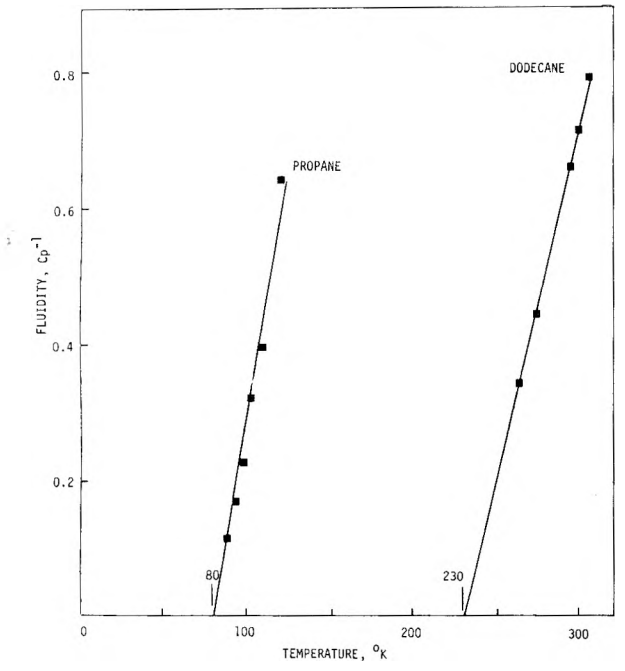


**Figure 2.** Variation of fluidity with temperature. Data obtained from ref 8 and 4. Extrapolation shows that fluidity is zero at the temperature where the line width is zero.

equations. We shall use Hildebrand's mechanism in reexamining the dodecane data of Povich[3] and the propane data of Edelstein et al.[2]

Povich[6] has shown that the relationship between the line width and diffusion coefficient is linear. Sridhar and Potter[7] have used such a relationship to measure oxygen diffusion coefficients in cyclohexane. The data so obtained are consistent with available data on the oxygen–cyclohexane system. We shall assume such a linear dependence of line width on diffusion coefficient in what follows. Line widths in solution will have the same temperature dependence as diffusivities.

According to Hildebrand's mechanism diffusion starts at the same temperature ($T_0$) as fluidity ($1/\eta$) and is linear with temperature. The molal volume at $T_0$ is $V_0$ a corresponding state ratio of the critical volume. In Figure 1 the ESR line width of propane[2] and dodecane[3] is plotted

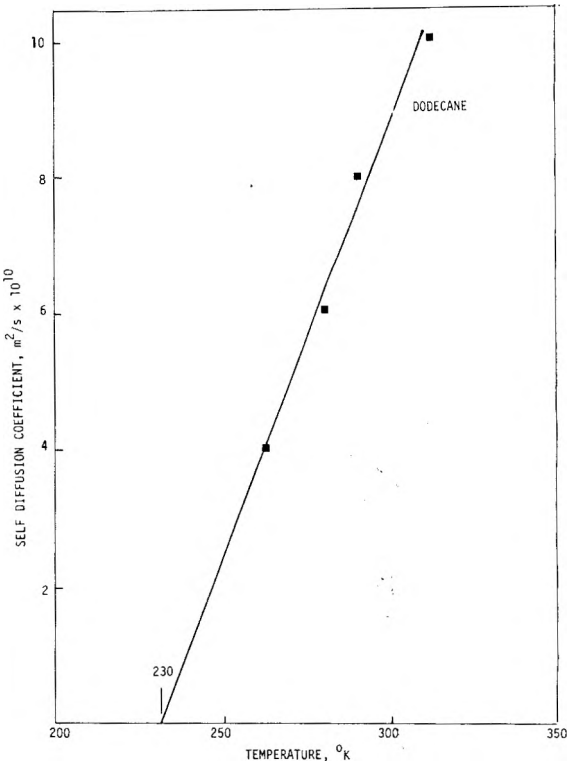


**Figure 3.** Self-diffusion coefficient of dodecane. Data obtained by ref 9 using pulsed NMR technique. The diffusion coefficient is zero at 230 K.

against temperature. Extrapolation of this plot should yield $T_0$ for propane and dodecane due to the above-mentioned relationship between line width and diffusion coefficients. In Figure 2 fluidity is plotted against temperature. The viscosity of dodecane was obtained from the Handbook[8] and for propane from Hildebrand.[4] As seen in Figure 2 both the fluidity lines extrapolate to the same $T_0$ as obtained from Figure 1. In Figure 3 some low temperature self-diffusion data for dodecane are plotted against temperature. These data were obtained using pulsed NMR technique by Ertl and Dullien.[9] Again the data extrapolate to $T_0$, for dodecane, where viscous flow ceases and the diffusion coefficient is zero. Similarly the decrease in line width with increasing pressure reported by Povich[3] based on Edelstein et al.'s[2] data can be explained by a decrease in diffusion coefficient. For example, Benedek and Purcell[10] examined the influence of pressure, at constant temperature, on the self-diffusion coefficient of water. An approximately linear relationship between diffusion coefficient and pressure was noticed with decrease in diffusion coefficient with increasing pressure. Simons and Ponter[11] in a recent review of diffusion in liquid systems comment on the difficulty in relating diffusion coefficient to viscosity alone and conclude that such relationships have marginal utility.

In conclusion we have shown that the observed interactions between free radicals in solution can be explained by available theories of diffusion. At least at low temperatures Hildebrand's[4] theory of diffusion seems to be remarkably supported by available ESR data. Further studies of line broadening, at various temperatures and pressures, should provide valuable insight into the diffusional process in liquids.

## References and Notes

(1) G. E. Pake and T. R. Tuttle, *Phys. Rev. Lett.*, **3**, 423 (1959).
(2) N. Edelstein, A. Kwok, and A. H. Maki, *J. Chem. Phys.*, **41**, 3473 (1964).
(3) M. J. Povich, *J. Phys. Chem.*, **79**, 1108 (1975).

(4) J. H. Hildebrand, *Science*, **174**, 490 (1971).
(5) T. Sridhar and O. E. Potter, *AIChE J.*, **23**, 590 (1977).
(6) M. J. Povich, *Anal. Chem.*, **47**, 346 (1975).
(7) T. Sridhar and O. E. Potter, *Can. J. Chem. Eng.*, submitted for publication.
(8) B. H. Billings and D. E. Gray, Ed., "American Institute of Physics Handbook", McGraw-Hill, New York, N.Y., 1963.
(9) H. Ertl and F. A. L. Dullien, *AIChE J.*, **19**, 1215 (1973).
(10) G. B. Benedek and E. M. J. Purcell, *J. Chem. Phys.*, **22**, 2003 (1954).
(11) J. Simons and A. B. Ponter, *Can. J. Chem. Eng.*, **53**, 541 (1975).

*Department of Chemical Engineering*
*Monash University*
*Clayton, Victoria, 3168 Australia*

**T. Sridhar**
**O. E. Potter***

*Received July 11, 1977*

## Homomolecular Oxygen Isotopic Exchange Reaction on Zinc Sulfide below −80 °C

*Publication costs assisted by Hokkaido University*

*Sir:* Homomolecular oxygen isotopic exchange reactions at −196 or −193 °C have been observed on several oxides such as ZnO, $ZnO/Al_2O_3$, and $TiO_2$.[1-4] So far, the formation of an $O_4^-$ intermediate between $O_2^-$ and $O_2$ was conjectured[2] to account for such an unusual reaction taking place at low temperatures. The authors tried to monitor the $O_2^-$ species during the equilibration reaction on ZnO by using an oxygen-17 isotope, and deduced that the $O_4$ intermediate might be formed instead of $O_4^-$ in low-temperature isotopic exchange reactions.[3,4] This communication shows that the ZnS surface also brings about isotopic equilibration of oxygen at liquid nitrogen temperature, which may be the first observation of this unique exchange reaction over a catalyst other than oxides.

Commercial ZnS (ZnS-I) (99.99%) from Nakarai Chemicals and high purity ZnS (ZnS-II) (99.999%) from Yamanaka Chemicals were used as the catalyst. The sulfide was evacuated for 1 h at 450 °C and treated with 30–50 Torr of $H_2S$ for 1 h at the same temperature. Finally it was evacuated at 450 °C for 2 h. When about 0.5 Torr of a mixture of $^{16}O_2$ and $^{18}O_2$ ($^{16}O_2$ 26% and $^{18}O_2$ 68.7%) was admitted to the reactor at room temperature, evidence of an isotopic exchange reaction was detected to a slight extent on both ZnS-I and ZnS-II. When the temperature of the reactor was lowered, however, isotopic equilibration in the gas phase oxygen was markedly enhanced as shown in Figure 1. From the results shown in Figure 1, the activity for the equilibration reaction has an optimum temperature. If the reaction at −196 °C was stopped at 30 min and the reactor was warmed quickly from −196 °C to room temperature, the isotopic composition of gas phase oxygen changed abruptly as shown in Figure 1. This fact may suggest that the decrease in the activity at a lower temperature than the optimum is caused by the slow desorption of the adsorbed oxygen whose isotopic composition is closer to equilibrium than that in gas phase. That is, the equilibration of gas phase oxygen is controlled by the slow desorption of adsorbed oxygen being more extensively exchanged at a lower than optimum temperature of around −90 °C.

In order to shed light on the active species of this unique isotopic scrambling, a thermal desorption experiment was performed by controlling the nitrogen stream from liquid nitrogen Dewar vessel. A mixture of $^{16}O_2$ and $^{18}O_2$ was admitted to the reactor which had been dipped in liquid nitrogen and kept at that temperature for 15 or 30 min. After that, the reactor was warmed from liquid nitrogen

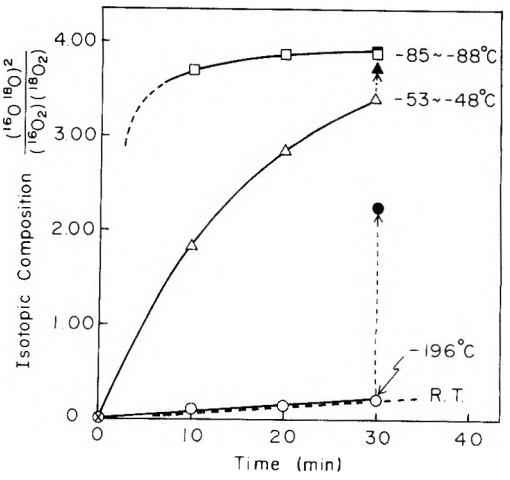


**Figure 1.** Changes in isotopic gas phase (open symbols) composition and of desorbed oxygen (solid symbols) obtained by raising the temperature to room temperature.

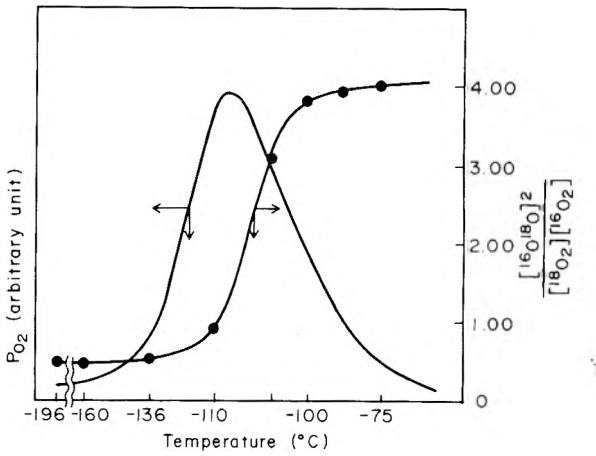


**Figure 2.** Thermal desorption spectrum and isotopic composition of oxygen adsorbed on ZnS at liquid nitrogen temperature for 30 min.

temperature to room temperature. Desorbed oxygen was removed from the reactor by evacuation through a leak, and the pressure change during thermal desorption was monitored by a Pirany gage. The isotopic composition of the desorbed oxygen was simultaneously analyzed by a mass spectrometer. A typical desorption spectrum and its isotopic composition observed on ZnS-I are shown in Figure 2, where a single desorption peak with a maximum at ca. −108 °C is observed. It is obvious that the isotopic composition of the desorbed oxygen depends markedly on the desorption temperature, that is, desorbed oxygen at temperatures lower than −110 °C shows isotopic composition nearly equal to that of the original mixture, while the oxygen desorbing above −100 °C is almost equilibrated. In order to make clear the isotopic equilibration of the adsorbed oxygen at liquid nitrogen temperature, the catalyst was kept at liquid nitrogen temperature for certain intervals, after which the reactor was warmed to room temperature quickly and the average isotopic distribution of the desorbed oxygen was determined by a mass spectrometer. As shown in Figure 3, the average isotopic composition of the desorbed oxygen apparently approaches equilibrium with the contact time at liquid nitrogen temperature. This fact suggests that the active oxygen for isotopic equilibration is held rather strongly on the surface and is miscible with the weakly held inactive oxygen which can desorb below −110 °C because the thermal desorption experiments whose the contact time at liquid nitrogen temperature is varied between 15 and 30 min give quite similar isotopic distributions indicating equilibration of

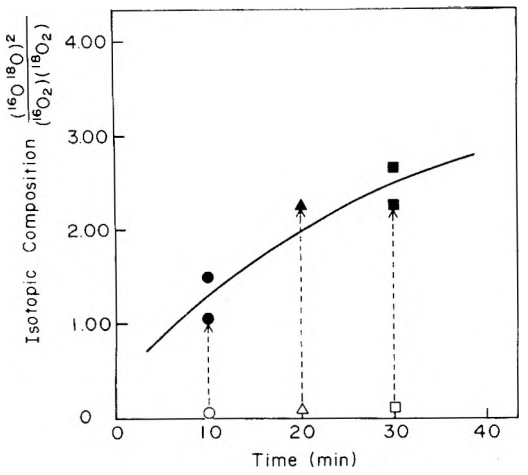


**Figure 3.** Changes of isotopic gas-phase composition and the average desorbed oxygen composition vs. time at liquid nitrogen temperature.

the oxygen desorbing above −100 °C.

A question which arises here is whether the ZnS surface is oxidized by contact with oxygen at liquid nitrogen temperature. To shed light on this problem, an attempt has been made to detect oxygen signals by the Vaccum Generator ESCA-3 instrument with Mg K$\alpha$ or Al K$\alpha$ x-ray excitation. The binding energies of copper signals with respect to the Fermi level were Cu($2p_{3/2}$) = 932.5, Cu(3s) = 122.5, and Cu($L_3M_{4,5}M_{4,5}$) auger = 918.8 eV, and these values were quite in accord with reference data.[5,6] Prior to setting up the sample in the ESCA apparatus, a sample of ZnS-II powder was subjected to evacuation at 450 °C for 1 h followed by treatment with $H_2S$ (48 Torr) for 1 h at the same temperature. After that, it was evacuated at 300 °C for 1 h, and was again treated with 75 Torr of $H_2S$ at 450 °C for 1 h. In a separate experiment, it has been certified that the ZnS undergoing the above treatment is active for the equilibration of oxygen as has been shown in Figure 3.

The ZnS-II sample treated as described above was mounted on a Au mesh plate and heated under evacuation for 2 h at 450 °C in the ESCA chamber. No oxygen signals were observed for this evacuated ZnS-II sample by either Mg K$\alpha$ or Al K$\alpha$. After this premeasurement by ESCA, the sample was cooled to about −150 °C and contacted with oxygen (1 Torr) for 30 min in the apparatus. The manipulator was then warmed to room temperature with the evacuation of oxygen and the sample was subjected to ESCA measurement. A weak O(1s) signal having binding energy of 532.0 eV was observed after an accumulation of 64 times. The binding energy observed in this experiment is undoubtedly higher by about 2 eV than that of ZnO,[7] and is rather close to O(1s) of adsorbed CO.[8] This signal was erased by bombarding with an electron beam for Auger analysis. Accordingly, it may be concluded that the ZnS surface does not change to an oxide upon contact with oxygen at temperatures as low as that of liquid nitrogen, and that the carbon impurity may change to carbon monoxide during the ESCA measurement. It has been known that $SiO_2$, $MoS_2$, and $MoO_3$ show no catalytic activity[11] for such a unique equilibration reaction at low temperatures. Accordingly, ordinal condensed oxygen should be inactive for the exchange reaction, and the isotopic equilibration observed on ZnS surface at rather low temperature is undoubtedly the catalytic process. The fact that no oxygen signals have been detected by ESCA on the ZnS surface after the equilibration reaction may indicate a lack of oxygen dissociation on the surface, which strongly support the $O_4$ intermediate, as has been proposed for ZnO and $TiO_2$.[3,4] However, in remarkable contrast is the fact that ZnS shows no photoeffect on the isotopic equilibration as is observed on ZnO.[1,10]

*Acknowledgment.* We thank professor M. Nagayama and Dr. H. Konno of Hokkaido University for the results of the ESCA experiments and valuable advice, and also Dr. S. Sato for his experimental assistance. This work was supported partly by Science Research Grant No.203001 from the Ministry of Education (Japan).

## References and Notes

(1) T. I. Barry and F. S. Stone, *Proc. R. Soc. London, Ser. A*, **335**, 124 (1960).
(2) K. Hirota and M. Chono, *J. Catal.*, **3**, 196 (1964).
(3) K. Tanaka, *J. Res. Inst. Catal., Hokkaido Univ.*, **23**, 171 (1975).
(4) K. Tanaka and A. Kazusaka, *Chem. Phys. Lett.*, **39**, 536 (1976).
(5) G. Johansson, J. Hedman, A. Berndtsson, M. Klasson, and R. Nilsson, *J. Electron Spectrosc.*, **2**, 295 (1973).
(6) G. Schon, *J. Electron Spectrosc.*, **1**, 377 (1973).
(7) J. Haber, J. Stoch, and L. Ungier, *J. Electron Spectrosc.*, **9**, 459 (1976).
(8) P. R. Norton, *Surface Sci.*, **44**, 624 (1974).
(9) K. Tanaka, *J. Phys. Chem.*, **78**, 555 (1974).
(10) K. Tanaka and K. Miyahara, *J. Phys. Chem.*, **78**, 2303 (1974).
(11) K. Tanaka et al., unpublished data.

*Research Institute for Catalysis*
*Hokkaido University*
*Sapporo, Japan*

**Ken-ichi Tanaka***
**Akio Kazusaka**
**Akiko Yamazaki**
**Koshiro Miyahara**

*Received December 28, 1976; Revised Manuscript Received October 26, 1977*

## Calculation of the Thermodynamic Functions for the Specific Adsorption of Ions on Mercury at the Potential of Zero Charge

*Publication costs assisted by the Consejo Nacional de Investigaciones Científicas y Técnicas (Argentina)*

*Sir:* The specific adsorption of ions plays an important role in the structural theories of the electrical double layer and evaluation of the pertaining thermodynamic data is very useful in interpreting the electrochemical behavior of a metal–ionic solution interface. The electrostatic model for ionic specific adsorption[1] permits an estimation of the thermodynamic data for the adsorption of single charged ions on mercury at the potential of zero charge (pzc) in a relatively simple manner. The model has also been extended by introducing some modifications to cover ionic specific adsorptions at solid electrode/solution interfaces and has been used to calculate the standard free energy change for the adsorption of halides and $OH^-$ ions on gold.[2] This communication reports a revision of the calculation of the thermodynamic data related to the specific adsorption of ions on mercury strictly following the electrostatic model referred to in the literature.[1] These calculations showed some numerical errors in the published results which appreciably alter the values of the standard free energy ($\Delta G_{ad}°$), enthalpy ($\Delta H_{ad}°$), and entropy ($\Delta S_{ad}°$) changes. Results at 25 °C are assembled in Table I. The subscripts o and r refer respectively to the original and corrected data. A straightforward comparison of results shows the following features: (i) The $(\Delta G_{ad}°)_r$ values are actually more negative than those originally reported. (ii) The results now indicate the likely adsorption of $K^+$ ion. (iii) Either the anion or the cation adsorbability order follows their qualitative behavior. (iv) The $(\Delta G_{ad}°)_r$ values

TABLE I: Calculated Thermodynamic Data for Ionic Adsorption at the Mercury/Aqueous Solution Interface[a]

| Ionic species | $(\Delta H_{ad}^{\circ})_o$, kcal/mol | $(\Delta H_{ad}^{\circ})_r$, kcal/mol | $(\Delta S_{ad}^{\circ})_o$, eu | $(\Delta S_{ad}^{\circ})_r$, eu | $(\Delta G_{ad}^{\circ})_o$, kcal/mol | $(\Delta G_{ad}^{\circ})_r$, kcal/mol |
|---|---|---|---|---|---|---|
| $Na^+$ | 18.5 | 16.00 | 16.3 | 20.07 | 13.7 | 10.02 |
| $K^+$ | 6.8 | 0.90 | 13.9 | 11.57 | 2.7 | -2.55 |
| $Cs^+$ | -6.8 | -12.11 | 1.6 | 2.24 | -7.3 | -12.77 |
| $F^-$ | 14.1 | 10.23 | 17.5 | 16.91 | 8.9 | 5.19 |
| $Cl^-$ | -9.6 | -13.73 | -2.1 | -2.03 | -9.0 | -13.12 |
| $Br^-$ | -12.9 | -16.95 | -5.1 | -6.14 | -11.4 | -15.12 |
| $I^-$ | -16.4 | -17.44 | -11.0 | -7.07 | -13.1 | -15.33 |

[a] The standard states for $\Delta S^{\circ}$ and $\Delta G^{\circ}$ are the same as quoted in the literature.[1]

for $Br^-$ and $I^-$ ions are practically equal. (v) The discrepancy between $(\Delta G_{ad}^{\circ})_r$ and that arising from the reported experimental value for the $I^-$ ion[1,3] is somewhat larger than that originally reported.[1]

In spite of the numerical differences already indicated which have to be considered when such data are quoted as reference, it should also be emphasized that the calculated magnitudes are very sensitive to the chosen hydration parameters and the degree of surface coverage by water molecules. Although the electrostatic model approach appears, in the authors' opinion, essentially correct, it involves however several approximations which are open to discussion, as it has been already recognized by Andersen and Bockris.[1] One of them refers to employing experimental primary hydration numbers together with ion-water electrostatic interaction energies which were derived by Eley and Evans[4] for a coordination number equal to 4. Thus $\Delta H_{hyd}$, the calculated hydration enthalpy changes, are in disagreement with the experimental results. Another critical point is the contribution to the total enthalpy change of the difference in the number of hydrogen bonds playing a part in the transfer of ions from the solution to the interface. This number should change depending on whether the process involves an anion or a cation, because of the different orientation of the water dipole in the primary hydration sheath.

As to the structure of water at the metal surface, there is an incongruence between the number of degrees of freedom assigned to the water molecule to evaluate the various thermodynamic contributions and the localized adsorption model which apparently explains the adsorption characteristics of water on mercury at room temperature. Other comments on the electrostatic model have already been indicated by Reeves[5] such as the use of vibrational states for the adsorbed system as if it were a gas phase.

Certainly the electrostatic model for the specific adsorption on ions can be improved with a broader perspective following the more recent advances made both in the structure of water and solutions as well as in the field of the electrical double layer. Therefore, it deserves a further revision as far as the underlying theories on which the model is based.

*Acknowledgment.* The Institute (INIFTA) is sponsored by the following institutions: Universidad Nacional de La Plata, Consejo Nacional de Investigaciones Científicas y Técnicas, and Comisión de Investigaciones Científicas (Provincia de Buenos Aires). This work is partially supported by the Regional Program for the Scientific and Technological Development of the American State Organization. R.G.M. thanks the Organization of American States for the fellowship granted.

## References and Notes

(1) T. N. Andersen and J. O'M. Bockris, *Electrochim. Acta*, **9**, 347 (1969).
(2) D. D. Bodé, *J. Phys. Chem.*, **76**, 2915 (1972).
(3) W. Anderson and R. Parsons, *Proc. Int. Congr. Surf. Act. 2nd*, **3**, 45 (1957).
(4) D. D. Eley and M. G. Evans, *Trans. Faraday Soc.*, **34**, 1043 (1938).
(5) R. M. Reeves in "Modern Aspects of Electrochemistry", Vol. 9, J. O'M. Bockris and B. E. Conway, Ed., Plenum Press, New York, N.Y., 1974, Chapter 4.

*Instituto de Investigaciones Fisicoquímicas Teóricas y Aplicadas División Electroquímica Sucursal 4 La Plata, Argentina*

**R. González Maroto**
**D. Posadas**
**A. J. Arvía***

*Received April 20, 1977*

# AUTHOR INDEX

*Note:* In this Author Index, titles of papers are listed after the name of each author of the paper. Multiple authorship is not indicated. Complete authorship may be ascertained by consulting the original paper.

# KEYWORD INDEX

# Special Centennial Tapes

**4 Historic Symposia! 24 Speakers! Custom Packaging! Special Prices!**

☐ **Milestones in Physical Chemistry**

8 Speakers — 315 Figures
Length: 5 Cassettes — 8 Hours
PRICE: $45 (postpaid)

The Speakers:

- G. T. Seaborg — 40 Years of Transuranium Elements
- D. Hodgkin — Structure of Molecules in Crystals
- G. Porter — Chemistry in Microtime
- P. J. Flory — Thermodynamics of Polymer Solutions
- W. O. Baker — Chemistry of the Solid State
- L. C. Pauling — Perspectives in Chemical Bonding & Structure
- H. Eyring — Reaction Rate Theory
- J. H. Van Vleck — Evolution of Theoretical Chemistry in America

☐ **Structure and Quantum Chemistry**
**+**
**Evolution of Magnetic Resonance**

8 Speakers — 210 Figures
Length: 4 Cassettes — 6 Hours
PRICE: $35 (postpaid)

The Speakers:

- J. A. Pople — Orbital Studies of Molecular Structure & Stability
- H. G. Drickamer — Pressure & Electronic Structure
- F. H. Stillinger — Quantum Chemistry & Eccentric Behavior of Liquid Water
- R. Zwanzig — Molecular Hydrodynamics
- H. S. Gutowsky — 30 Years of Relaxation
- J. S. Waugh — Alchemy of Nuclear Spins
- H. M. McConnell — Spin Labels
- F. A. Bovey — NMR of Macromolecules

☐ **Evolution of Kinetics**

8 Speakers — 140 Figures
Length: 4 Cassettes — 6 Hours
PRICE: $35 (postpaid)

The Speakers:

- B. S. Rabinovitch — Perspectives on Vibration Energy Relaxation in Unimolecular Reactions
- W. A. Noyes, Jr. — Photochemical Kinetics
- R. A. Marcus — Trends in Theoretical Chemical Kinetics
- K. F. Freed — Radiationless Processes in Polyatomic Molecules
- G. B. Kistiakowski — Early Years of Gas Phase Chemical Kinetics
- J. C. Polanyi — Recent Studies of Infrared Chemiluminescence & Fluorescence
- S. Claesson — Diffusion Rates & Chemical Reaction Kinetics
- J. Jortner — Intramolecular Dynamics in Excited Molecular States

## — SPECIAL PRICE —

☐ **BUY ALL THREE SETS — ONLY $85 (postpaid)**

**SAVE $30!**

ORDER FROM:
**American Chemical Society**
1155 Sixteenth St., N.W.
Washington, D.C. 20036
ATTN: DEPT. AP

Name _____

Address _____

City _____ State _____ Zip _____

(allow 4 to 6 weeks for delivery)

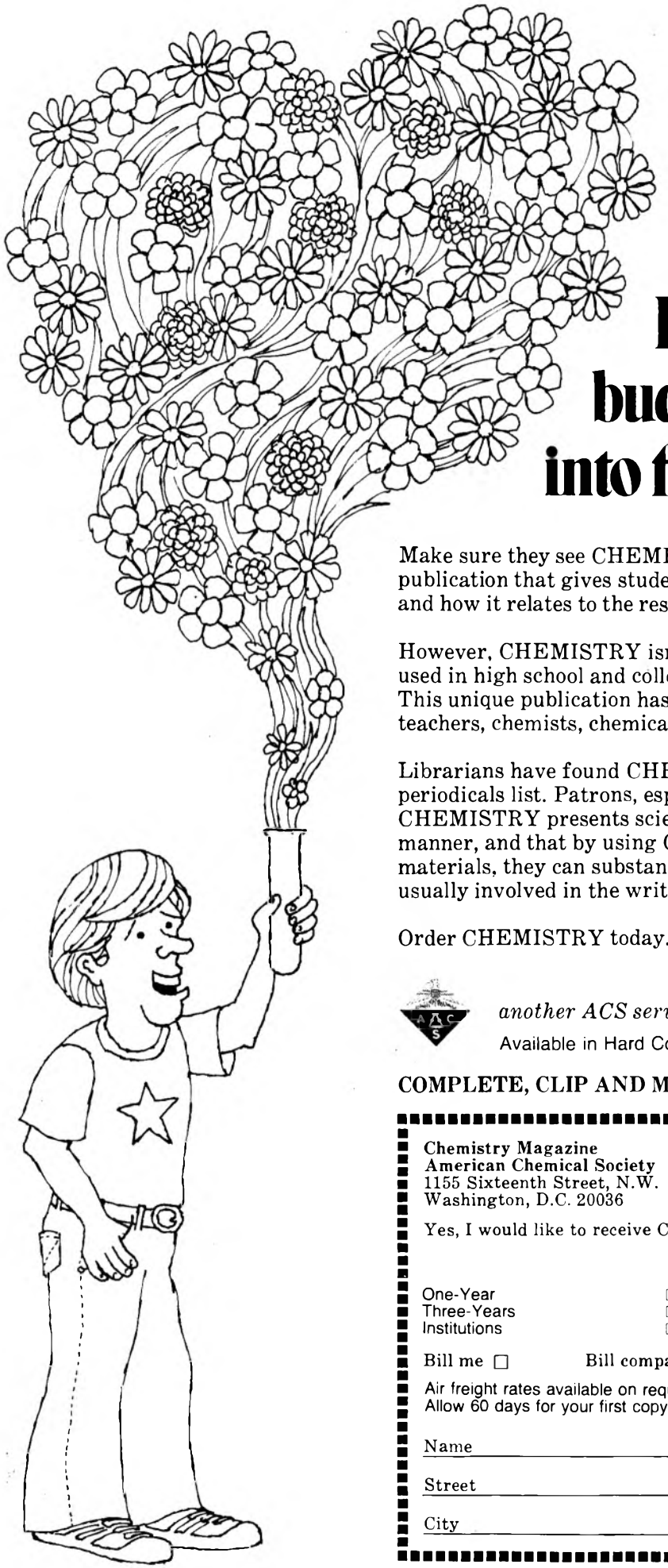

# How to bring budding scientists into full bloom:

Make sure they see CHEMISTRY magazine—an enjoyable, colorful publication that gives students an understanding of chemistry and how it relates to the rest of the world.

However, CHEMISTRY isn't *just* for students, although it's widely used in high school and college courses as an effective teaching aid. This unique publication has found a great deal of acceptance among teachers, chemists, chemical engineers, and laymen.

Librarians have found CHEMISTRY a popular addition to their periodicals list. Patrons, especially students, have discovered that CHEMISTRY presents scientifically sound information in a lively manner, and that by using CHEMISTRY as one of their source materials, they can substantially reduce the amount of drudgery usually involved in the writing of a report.

Order CHEMISTRY today. You'll be happy you did.

*another ACS service*

Available in Hard Copy or Microfiche.

**COMPLETE, CLIP AND MAIL THIS COUPON TODAY**

**Chemistry Magazine**
**American Chemical Society** **1978**
1155 Sixteenth Street, N.W.
Washington, D.C. 20036

Yes, I would like to receive CHEMISTRY at the rate checked below:

| | U.S. | All Other Countries |
|---|---|---|
| One-Year | ☐ $8.00 | ☐ $9.00 |
| Three-Years | ☐ $20.00 | ☐ $23.00 |
| Institutions | ☐ $10.00 | ☐ $11.00 |

Bill me ☐ Bill company ☐ Payment enclosed ☐

Air freight rates available on request.
Allow 60 days for your first copy to be mailed.

Name _____

Street _____ ☐ Home ☐ Business

City _____ State _____ Zip _____